

**AN INVESTIGATION OF THE MICROWAVE UPSET  
OF AVIONIC CIRCUITRY**

BY

**M. PYWELL  
B.Sc., C.Eng., M.I.E.E.**

Thesis submitted to the University of Central Lancashire  
in fulfilment of the requirements for the degree of

**MASTER OF PHILOSOPHY**

June 1996

The research was conducted in the  
School of Electrical and Electronic Engineering at  
the University of Central Lancashire in collaboration with  
British Aerospace Defence (Military Aircraft Division), Warton Unit.

## **COPYING RESTRICTIONS**

© British Aerospace Public Limited Company

*The copyright in this document, which contains information of a proprietary nature is vested in British Aerospace Public Limited Company, and its contents may not be reproduced, either wholly or in part, in any way whatsoever, nor may it be used by, or its contents divulged to, any other person whatsoever, without the written permission of British Aerospace Public Limited Company.*

## **DECLARATION**

The author was not registered as a candidate for another award of the University during the period whilst registered as a candidate for the degree for which submission is made. No material content in this report has been used in any other submission for an academic award.

## ABSTRACT

Circuit technology of the 1970-90 era appears fairly resilient to microwave radio frequency interference, with few reported occurrences of interference. However, a proposition has been developed which substantiates fears that new technologies, with their extremely high packing densities, small device p-n junctions and very high clock rates, will be very susceptible to interference throughout the microwave band. It has been postulated that the mechanism for this upset is demodulation and that it will come about by either the predicted changes in the microwave RF environment by the year 2000, or by a suitable choice of phasing and frequency at high power.

The postulation is studied by developing an overall ingress equation, relating incident power density at the aircraft to the load voltage at an avionic circuit component. The equation's terms are investigated to quantify their contribution to the likelihood of interference. The operational RF environment for aircraft is studied and predictions of the current and maximum future environments are made. A practical investigation of 2-18 GHz airframe shielding is described, with comparison of the results with those from a number of other aircraft and helicopter types. A study of ingress into avionic boxes is presented and is followed by the results of an investigation of energy coupling *via* the cables and connectors, including the development and practical examination of a coupling model based on transmission line theory. A study is then presented of circuit technology developments, electronic component interference and damage mechanisms, and evidence of upset of electronic equipment is given.

Investigations show that there is more 1-18 GHz upset of electronic equipment than originally thought and data suggest that thermal damage of active devices may dominate over-voltage stressing of p-n junctions. Aircraft investigations have shown that incident microwave radiation is attenuated approximately 20 dB by the airframe, in a complex fashion which does not lend itself to being modelled easily. Under some conditions this value of airframe attenuation is seen to approach zero, removing any shielding of avionics by the airframe for these cases. A predictor for airframe shielding independent of air vehicle type has been developed, based on cumulative density functions of all data from each of the aircraft types examined. The cable coupling model gives good agreement with measured data except for the dependency of load voltage on cable length and illuminating antenna position along the cable, for which an empirical equation has been developed. Computer power limitations and significant variations of most of the parameters in the overall ingress equation suggest that modelling of the complex innards of aircraft and avionics at these frequencies will remain impractical for the foreseeable future and that probabilistic models are the only achievable goal.

It is concluded that all avionic circuit technologies may well be upset as postulated above or by speculative High Power Microwave weapons, but that careful use of existing aircraft and equipment design methodologies can offer adequate protection. An improved protection regime is proposed for future aircraft and a number of future research areas are identified to enable better understanding of the microwave hazard to aircraft. The three areas which will add most to this understanding are modelling of the precise microwave environment to be encountered, further airframe shielding measurements and analyses, from all incidence angles and on different aircraft types, and the construction and cumulative probability function analyses of electronic component and equipment upset databases.

## CONTENTS

	<u>Page</u>
Title Page	i
Copying Restrictions	ii
Declaration	iii
Abstract	iv
Contents	v
List of Figures	viii
List of Tables	x
Acknowledgements	xi
List of Abbreviations	xii
List of Symbols	xiv
<b><u>Chapter 1: INTRODUCTION</u></b>	
1.1 Introduction to the Research	1-2
1.2 Objectives of the Research	1-3
1.3 Thesis Organisation	1-3
<b><u>Chapter 2: THE MICROWAVE ELECTROMAGNETIC ENVIRONMENT</u></b>	
2.1 Introduction	2-2
2.2 Current Environment	2-3
2.3 Predicted Future Environment	2-6
2.3.1 Worst Case Environment	2-6
2.3.2 Realistic Environment and Probability of Exposure	2-10
2.3.2.1 EUROCAE and HIRTA prediction methods and limitations	2-13
2.3.2.2 EW environment simulator as an accurate prediction tool	2-22
2.4 Concluding remarks	2-23
<b><u>Chapter 3: MICROWAVE ENERGY INGRESS INTO AIRFRAMES</u></b>	
3.1 Introduction	3-2
3.2 Prediction Methods	3-2
3.3 Practical Measurements	3-7
3.3.1 EMC Demonstrator Aircraft	3-7
3.3.2 Modern Aircraft	3-26
3.3.2.1 Military Aircraft	3-26
3.3.2.2 Airframe Attenuation on Modern Civil Aircraft	3-31
3.3.3 Discussion of Panel Tests in EMC Laboratory	3-32
3.4 Concluding Remarks	3-37

## **Chapter 4: MICROWAVE ENERGY INGRESS INTO AVIONIC EQUIPMENT**

4.1	Introduction	4-2
4.2	Overall Ingress Equation	4-2
4.3	Energy Penetration Through Case Material	4-6
4.4	Energy Penetration Through Apertures	4-9
4.4.1	The effects of apertures on attenuation of incident energy	4-9
4.4.2	The role of conductive gasketing at microwave frequencies	4-15
4.4.3	Optical apertures	4-17
4.4.4	Discussion of U.S. research on phenomenology of coupling	4-19
4.5	Ingress via Cables and Connector Combinations	4-21
4.6	Concluding Remarks	4-22

## **Chapter 5: INGRESS via CABLES/CONNECTORS**

5.1	Introduction	5-2
5.2	Transmission Lines and the 'Telegraphist's Equations'	5-3
5.3	Cable/Connector Ingress Model Development	5-5
5.3.1	Initial Model Development	5-5
5.3.2	Comparison of Model Results with Initial Empirical Data	5-14
5.3.3	Load Voltage Variation with Cable Length	5-19
5.4	Concluding Remarks	5-21

## **Chapter 6: EXPERIMENTAL INVESTIGATIONS**

6.1	Introduction	6-2
6.2	Validity of Model at Microwave Frequencies	6-2
6.2.1	Laboratory Investigation and Initial Comparison with Model	6-2
6.2.2	Load Impedance Effects	6-16
6.2.3	Cable Material and Construction	6-19
6.2.4	Comparison with 10 MHz Sampled Measurements	6-21
6.3	Energy Coupling vs. Cable Length	6-26
6.3.1	Examination of Cable Data Sets	6-26
6.3.2	Re-Radiation Postulation and Empirical Equation	6-29
6.4	Concluding Remarks	6-33

## **Chapter 7: MICROWAVE EFFECTS ON ELECTRONIC CIRCUITRY**

7.1	Introduction	7-2
7.2	Reported Upset	7-2
7.2.1	Circuit Technologies	7-2
7.2.2	Evidence of Upset of Electronics	7-3
7.3	Identification of Upset Mechanisms	7-10
7.4	Circuit Models as an Aid to Upset Prediction	7-14
7.5	Prediction of Circuit Upset at Microwave Frequencies	7-15

7.5.1	Completion of Ingress Equation	7-15
7.5.2	Upset Prediction Models	7-18
7.5.3	Protection Strategies Against Microwave Upset of Avionics	7-20
7.6	Concluding Remarks	7-22

## **Chapter 8: CONCLUSIONS AND SUGGESTIONS FOR FURTHER WORK**

8.1	Introduction	8-2
8.2	RF Environment Prediction	8-2
8.2.1	Conclusions	8-2
8.2.2	Suggested Further Research Areas	8-2
8.3	Airframe Energy Ingress	8-3
8.3.1	Conclusions	8-3
8.3.2	Suggested Further Research Areas	8-3
8.4	Equipment Energy Ingress	8-4
8.4.1	Conclusions	8-4
8.5	Ingress <i>via</i> Cable and Connector Combinations	8-5
8.5.1	Conclusions	8-5
8.5.2	Suggested Further Research Areas	8-5
8.6	Effects on Electronics	8-6
8.6.1	Conclusions	8-6
8.6.2	Suggested Further Research Areas	8-7

## **REFERENCES**

### **APPENDICES**

- A. Paper: 'The Control of RF Hazards in an Industrial and Airfield Environment' (1994).
- B. EMC Qualification of Avionics and Aircraft at Microwave Frequencies.
- C. Paper: 'Environment Models and Threat Simulators - High Quality and Lower Cost Validation of EW Systems' (1995).
- D. Prediction of cut-off frequency for peripheral slots and bay doors, and bay panel ingress characteristics
- E. Paper: 'Airframe Attenuation Measurements at Microwave Frequencies' (1990).
- F. Calculation of frequency spacing of cavity resonances for Port Gun Bay and bays behind Panels 55 and 56
- G. Listing of Cable Coupling Model
- H. I.E.E. Electronics Letters: 'Improved Prediction of Airframe Attenuation at Microwave Frequencies.' (1996)

## LIST OF FIGURES

2.1	Usage of 0.8-40 GHz band	2-3
2.2	Current Microwave Environment	2-6
2.3	High Power Microwave Sources	2-7
2.4	Predicted Power Density Profile	2-7
2.5	Projected Limits of Ultra-High Power Microwave Sources	2-9
2.6	Predicted Microwave Environment	2-10
2.7	Aircraft Transit Time over a Ground Radar	2-12
2.8	Radar Pulses Incident on Aircraft	2-20
2.9	Atmospheric attenuation of RF Signals	2-21
3.1	Inside of Front Avionics Bay with Test Measurement Antenna	3-6
3.2	Multipath: Transmit Antenna Depression Angle Dependency	3-8
3.3	Multipath: Transmit and Receive Antenna Separation	3-9
3.4	Location of Bays Investigated	3-10
3.5	2-12 GHz Airframe Attenuation Factors - Port Gun Bay	3-10
3.6	Test Equipment Arrangement For Aircraft Investigation	3-11
3.7	Attenuation Factors: Front Avionics Bay (Slide Test)	3-13
3.8	Attenuation Factors: Panel 55 Bay (Arc Test)	3-14
3.9	Different Bay Types Investigated	3-14
3.10	Frequency Dependence of Panels 55/56 Attenuation Factors	3-16
3.11	Comparison of Airframe Attenuation Statistics	3-18
3.12	Test Frequency Resolution	3-20
3.13	Total Number of Modes as a Function of Frequency	3-21
3.14	Composite Quality Factor For Bays Investigated	3-22
3.15	Panel 55 Bay Cavity Resonances	3-24
3.16	Resonance Damping: Best Fit Lines for Bays Investigated	3-24
3.17	12-17 GHz Attenuation Factors	3-25
3.18	Modern Airframe Materials	3-26
3.19	Typical CFC Panel Construction	3-27
3.20	Test Arrangement: 'Hole in the Wall' Shielding Measurements	3-33
3.21	Shielding Effectiveness of Full- vs. Half-Bolted Panels	3-35
3.22	Shielding Effectiveness With High/Low Conductivity Gaskets	3-36
4.1	Original Ingress Equation	4-3
4.2	Transmission Through a Conducting Sheet of Finite Thickness	4-6
4.3	Transmission Losses Through Aluminium	4-7
4.4	Magnetic Field Induced Coupling	4-11
4.5	Shielding Effectiveness vs. Aperture Major Dimension	4-12
4.6	Waveguide Shielding Characteristics	4-14
4.7	Typical Military Gasket Arrangement	4-16
4.8	Equivalent Circuit of Gasket	4-16
4.9	Shielded Window Mesh Termination	4-18

4.10	Transparency vs. Surface Resistivity	4-18
5.1	General Transmission Line	5-3
5.2	Loss-Less Transmission Line	5-4
5.3	Cable Coupling Model	5-5
5.4	Current Decay in a Plane Solid Conductor	5-9
5.5	Exact vs. Parallel Plane Comparison of Current Density	5-10
5.6	Internal Instrumentation of Dummy Avionics Box	5-15
5.7	General Layout of Initial BAe Cable Ingress Investigations	5-15
5.8	Cable Coupling: Un-screened Single Wire Pick-Up	5-18
5.9	Variation of Cable Pick-Up with Cable Metal	5-20
6.1	Cable Coupling Experimentation: Test Arrangement	6-3
6.2	Test Instrumentation	6-4
6.3	Comparison of 50 MHz and 10 MHz Measured Data	6-7
6.4	$V_L$ Envelope Magnitude vs. Test Frequency Resolution	6-8
6.5	Measured $V_L$ Statistics and Earlier BAe Spot Measurements	6-11
6.6	Comparison of Pywell and Anderson Cable Results	6-12
6.7	Maximum $V_L$ Amplitude Profile	6-13
6.8	Smith Figure 2-11 vs. Modelled Response	6-15
6.9	Smith Figure 2-17 vs. Modelled Response	6-15
6.10	Lumped Element Model of Connector and Load	6-17
6.11	$V_L$ Dependency on Series Inductance in Load	6-18
6.12	Modelled vs. Measured 50 MHz Data	6-18
6.13	Arrangement of Cores in Stranded Conductor	6-19
6.14	10 MHz Modelled vs. Measured Data	6-21
6.15	Effect of Cable Height on Frequency Spacing of Oscillations	6-22
6.16	Comparison Using Modified Height Input to Model	6-23
6.17	Effects of Cable Material on $V_L$ Profile	6-24
6.18	Final Comparison of 10 MHz Sampled vs. Modelled Data	6-25
6.19	Willis $V_L$ Data Dependency on Antenna Position	6-26
6.20	2m Cable $V_L$ Measurements vs. Antenna Position	6-27
6.21	Median $V_L$ Dependency on Cable Length and Antenna Position	6-28
6.22	Modelled vs. Measured Cable Length and Antenna Position Dependency	6-32
7.1	Circuit Technology Trends	7-3
7.2	Trends of RFI Occurrences and Minimum Power Density	7-6
7.3	IC Damage Threshold for 0.1 $\mu$ s RF Pulses	7-7
7.4	RFI Power Levels for Major IC Technologies	7-8
7.5	Typical Damage Threshold Levels for 1 $\mu$ s Pulses	7-8
7.6	Rectification Efficiencies of ICs	7-10
7.7	Variation of Rectification Efficiency with Device Size	7-11
7.8	Scanning Electron Micrograph of MESFET Damage	7-13

## **LIST OF TABLES**

2.1	Elements of Total Civil Aircraft RF Environment	2-15
2.2	Minimum Aircraft-to-Transmitter Distances	2-16
3.1	Key Aspects of Trials and Initial Statistics	3-17
3.2	Use of Composites in Military Aircraft	3-26
3.3	Airframe Attenuation Factors	3-29
3.4	Attenuation vs. Civil Avionics Location	3-31
3.5	Panel Type and Configurations Measured	3-33
4.1	Honeycomb Waveguide Cell Data	4-14
6.1	Key Features of Signal Generator, Amplifier and Analyser	6-5
6.2	Comparison of AEL H-1498 and EMCO 3105 Antennas	6-9
6.3	Attenuation Constant for Nickel vs. Steel	6-30
7.1	Upset Examples	7-4
7.2	Worst Case Assessment of Power in Circuit Device	7-16
7.3	Microwave Upset Protection Regime	7-21

## ACKNOWLEDGEMENTS

I wish to acknowledge the support given throughout this programme by my Supervisors, Professor Robert Simpson (of the University of Central Lancashire) and Mr. Ian MacDiarmid (Electromagnetic Hazards Consultant, of British Aerospace). This extends also to my former research colleagues Mike Price, who performed some of the practical investigations and co-authored one of the papers, Andy M. Wellington and Neil R.M. Ritchie, who conducted some of the more recent BAe microwave EMC investigations. I wish also to thank Dr. Tony Llewellyn (Systems Engineering EMC Controller) for comment on Chapter 3 and assistance with aircraft trials data kindly provided by Dr. Nigel Carter, Head of Electromagnetics at the Defence Research and Evaluation Agency, Farnborough.

Thanks also go to the Senior Management of Systems Development Department, Bill Green, Ken Martin and Keith Gardner, and Mike Everett, Mission Systems R&D Manager, for their continued support. Further, I am grateful to BAe Defence (Military Aircraft Division), for permission to publish the experimental data collected from work completed in respect of both this research and other related Company development activities.

The staff of the former Electromagnetics and Sensors & Electronic Warfare Development Groups deserve a mention, for they have all helped in one way or another and have been stimulating colleagues, friends and a challenge to manage - 'A-Teams' of the highest calibre. In particular, Dave A. Lee, the former Groups' Computing Expert, merits special mention for his support *inter alia* to my development of the cable coupling model; his help has been invaluable.

Last but not least I wish to thank my wife, Julie, to whom I am eternally grateful for her continual support, and for without whom this would never have come to pass. This work is dedicated to Julie and my daughter Samantha, who has only occasionally seen me during production of this thesis.

## LIST OF ABBREVIATIONS

A&AEE	MoD Armaments & Aircraft Evaluation Establishment, (now Defence Evaluation & Research Establishment)
AEL	American Electronic Laboratories (antenna manufacturer)
AM	Amplitude Modulation
ATC	Air Traffic Control
BAc	British Aerospace Defence (Military Aircraft Division)
BWO	Backward Wave Oscillator
CAD	Computer-Aided Design
CATIA	Computer-Aided Three-dimensional Interactive Application
CFC	Carbon Fibre Composite
CMOS	Complementary MOS
CpF	Cumulative Probability Function
CS	Conducted Susceptibility
CW	Continuous Wave
DEF. STAN.	Defence Standard
DRA(F)	Defence Research Agency (Farnborough)
EC	European Community of states
ECL	Emitter-Coupled Logic
EF2000	Eurofighter 2000 aircraft
EHF	Extra-High Frequency (3-30 GHz)
EM, EMC	Electromagnetic, EM Compatibility
EMCO	The Electro-Mechanics Company (antenna manufacturer)
EUROCAE	European Organisation for Civil Aircraft Electronics
ESPRIT	[EWES] Enhanced Scenario Preparation Interactive Tool
EW	Electronic Warfare
EWES	EW Evaluation System (software suite by Data Sciences U.K. Ltd.)
EWGA	[EWES] EW Graphical Analysis package
EWSG	[EWES] EW Scenario Generator
FBW	(Jaguar) Fly-By-Wire demonstrator aircraft
FDTD	Finite-Difference Time Domain
FEL	Free Electron Laser
FEP	Fluorinated Ethylene Propylene
FET	Field-Effect Transistor
FM	Frequency Modulation
GaAs	Gallium Arsenide
GHz	giga-Hertz ( $10^9$ Hz)
giga-FLOPS	$10^9$ Floating Point Operations per Second
GPS	Global Positioning System
GW	giga-Watt ( $10^9$ W)
HF	High Frequency (3-30 MHz)
HFET	Heterostructure FET
HIRF	High Intensity Radio Frequency
HIRTA	High Intensity Radio Transmission Area
HPGM	High Power Gyromagnetron
HPM	High Power Microwave
HSPICE	Version of SPICE by Meta-Software
IC	Integrated Circuit
ICAO	International Civil Aviation Organisation
IEE	Institution of Electrical Engineers
IEEE	U.S. Institute of Electrical and Electronics Engineers
IEMCAP	Integrated EMC Analysis Program ( <i>sic</i> )
IFF/SIF	Identification Friend or Foe; S-mode IFF
ILS	Instrument Landing System
IsPICE	Version of SPICE by Intusoft
kPA	kilo-Pascals
LORAN	LOng RANGE Navigation beacon system
LSI	Large Scale Integration IC

## ABBREVIATIONS (Continued)

MIL. STD.	(U.S.) Military Standard
MESFET	Metal-Semiconductor FET
MoD	(U.K.) Ministry of Defence
MOM	Method Of Moments
MOS	Metal Oxide Semiconductor
MSERFE	Minimum Service RF Environment
MSI	Mixed-Semiconductor Integrated Circuit; Medium Scale IC
MWCG	Multi-Wave Cherenkov Generator
NATO	North Atlantic Treaty Organisation
NCAP	Non-Linear Circuit Analysis Program
NEC	Numerical EM Code
NES	Naval Environment Specification
NM, N.Mile	Nautical Mile (6076.6 feet)
NWS	Naval Weapons Specification
PAN	Panavia (tri-national, Tornado) aircraft company
PC, PC-DOS	Personal Computer, PC-Disc Operating System
PoE	Point of Entry [of RF energy]
PRC	Plastic Rubber Compound
PRF	Pulse Repetition Frequency
psi	Pounds per square inch
PSPICE	Version of SPICE by MicroSim Corp.
PTFE	Polytetrafluorethylene
PW	Pulse Width
RADHAZ	Radiation Hazards
RAF	UK Royal Air Force
RAM	Radar Absorbent Material
RBS	ATC Remote Beacon System
RE	Rectification Efficiency
RF	Radio/Radar Frequency
RFI	Radio/radar Frequency Interference
RS	Radiated Susceptibility [tests]
SE	Shielding Effectiveness
SHF	Super-High Frequency (30-300 GHz)
SM	Safety Margin
SMA	Sub-Miniature type A (U.S. connector standard)
SPF-DB	Super-Plastic-Formed Diffusion Bonded
SPICE	Simulation Package with Integrated Circuit Emphasis
SRAM	Static Random Access Memory
SSI	Small Scale Integration IC ( <i>e.g.</i> TTL)
STANAG	(NATO) Standardisation Agreement
STP	Standard Temperature and Pressure
TACAN	Tactical Air Navigation
TEM	Transverse EM wave, mode of propagation
TLM	Transmission Line Modelling
TTL	Transistor-Transistor Logic
TWT	Travelling Wave Tube
UHF	Ultra-High Frequency (300-3000 MHz)
UK	United Kingdom
US	United States of America
USS	U.S. Ship
USSR	United Soviet of Socialist Republics (now Confederation of Independent States)
UUT	Unit Under Test
VHF	Very High Frequency (30-300 MHz)
VHSIC	Very High Scale IC
VIRCATOR	Virtual Cathode Oscillator
VLSI	Very Large Scale Integration

## LIST OF SYMBOLS

<b>a</b>	Diameter of cable, m
<b>A</b>	Irradiating antenna distance along wire from avionic box
<b>A<sub>e</sub></b>	Effective area of antenna, m <sup>2</sup>
<b>A<sub>E</sub></b>	Emitter Area, cm <sup>2</sup> or m <sup>2</sup> as stated
<b>A<sub>J</sub></b>	Junction area, m <sup>2</sup>
<b>b</b>	Distance between cable and image under the ground plane, m
<b>B</b>	Magnetic flux density, Tesla
<b>A<sub>AIRFRAME</sub>(f), A<sub>A</sub></b>	Airframe microwave attenuation factor, dB
<b>A<sub>BOX</sub>(f)</b>	Overall avionic box microwave attenuation factor, dB
<b>c</b>	Velocity of light, 2.997925 x 10 <sup>8</sup> ms <sup>-1</sup>
<b>C</b>	Capacitance per unit length of transmission line, Fm <sup>-1</sup>
<b>C<sub>s</sub></b>	Source parallel capacitance, F
<b>C<sub>b</sub></b>	Load parallel capacitance, F
<b>C<sub>π</sub></b>	Emitter-base capacitance, F
<b>d</b>	Major dimension of aperture, m
<b>D</b>	Electric flux density (or displacement vector), Cm <sup>-2</sup>
<b>e</b>	2.71828
<b>E</b>	Electric field, Vm <sup>-1</sup>
<b>E<sub>A</sub></b>	Absorbed pulse energy, Joules
<b>E<sub>z</sub><sup>i</sup></b>	Incident electric field parallel to ground plane and cable
<b>E<sub>ir</sub> to E<sub>3r</sub></b>	Electric field, reflected wave
<b>E<sub>it</sub> to E<sub>3t</sub></b>	Electric field, forward wave
<b>f or f</b>	Frequency (Hz, MHz or GHz as stated)
<b>FSL(f)</b>	Free Space Loss as a function of frequency, dB
<b>G</b>	Conductance per unit length of transmission line, Sm <sup>-1</sup>
<b>G<sub>CCT</sub>(f)</b>	Effective antenna gain of energy into circuit device, dB
<b>G<sub>T</sub></b>	Antenna gain with respect to isotropic, dBi
<b>h</b>	Height of cable above ground plane, m
<b>H</b>	Magnetic field, Am <sup>-1</sup>
<b>I, I<sub>L</sub></b>	Current; Load current
<b>J</b>	Current density, Am <sup>-1</sup>
<b>J<sub>o</sub></b>	Surface current density, Am <sup>-1</sup>
<b>J<sub>z</sub></b>	Current density at a depth z into a material, Am <sup>-1</sup>
<b>K, K', K''</b>	Proportionality constants (semiconductor device-specific)
<b>K(ω)</b>	Total electric field at height h
<b>L</b>	Series inductance per unit length of transmission line, Hm <sup>-1</sup>
<b>L<sub>b</sub></b>	Series inductance of connector lumped circuit model, H
<b>L<sub>i</sub></b>	Internal inductance of a wire, Hm <sup>-1</sup>
<b>L<sub>R</sub></b>	Receiver cable loss, dB
<b>L<sub>T</sub></b>	Transmission loss inside electronic box (expressed as a ratio)
<b>P<sub>C</sub></b>	Power density incident on cable, Wm <sup>-2</sup>
<b>P<sub>CCT</sub>(f)</b>	Microwave power delivered to circuit device, dBm or W
<b>P<sub>d</sub> or P<sub>D</sub></b>	Power density, (Wm <sup>-2</sup> , kWm <sup>-2</sup> , MWm <sup>-2</sup> as stated)
<b>P<sub>DAMAGE</sub></b>	Damage threshold power, W
<b>P<sub>E</sub></b>	Emitter perimeter, cm or m as stated.

SYMBOLS (Continued)

$P_{ERP}(f)$	Effective radiated power of transmitter, dBm or W
$P_f$	Component RFI power density
$P_L$	Power in the load, W
$R_r$	Proposed re-radiation resistance term, $\Omega m^{-1}$
$P_R$	Received power, dBm
$P_T$	Transmitter or amplifier power, dBm or W as stated.
$R$	Series resistance per unit length of transmission line, $\Omega m^{-1}$
$R_a$	Source parallel resistance, $\Omega$
$R_b$	Load parallel resistance, $\Omega$
$R_{CAP}$	Load capacitance's series resistance, $\Omega$
$R_i$	Internal resistance of a wire, $\Omega$
$R_s$	Surface resistance (or sheet resistivity), $\Omega/\text{square}$
$s$	Cable length, m
$S_f$	System RFI power density
$t$	Thickness of avionic box case material, m
$V_L$	Load voltage (dB $\mu$ V or V as stated)
$V_{L(ZERO)}$	$V_L$ measured at nearest point to avionic box
$V/S$	Aircraft Volume-to-Surface area ratio
$V_T$	Rectified offset voltage, V
$w$	Width of hole in box, m
$Z_A$	Source impedance of wire above a ground plane, $\Omega$
$Z_B$	Load impedance of wire above a ground plane, $\Omega$
$Z_i$	Internal impedance of wire, $\Omega$
$Z_o$	Characteristic impedance of transmission line, $\Omega$
$Z_1$	Twin line source impedance, $\Omega$
$Z_2$	Twin line load Impedance, $\Omega$
$\alpha$	Attenuation constant, nepers or dB per metre
$\beta$	Phase change constant, radians $m^{-1}$
$\gamma$	Propagation constant
$\delta$	Skin depth of RF energy inside conductor or dielectric, m
$\epsilon_o$	Absolute permittivity, $8.854 \times 10^{-12} \text{ Fm}^{-1}$
$\epsilon_r$	Relative permittivity
$\lambda$	Wavelength, m
$\mu_o$	Permeability of free space, $4\pi \times 10^{-7} \text{ Hm}^{-1}$
$\mu_r$	Relative permeability of material
$\rho$	Resistivity, $\Omega m^{-1}$
$\rho_r$	Resistivity relative to Copper
$\sigma$	Conductivity [reciprocal of resistivity], Siemens per m
$\tau$	Pulse width, seconds
$\omega$	Angular frequency, $\text{Rad.s}^{-1}$

# *Chapter 1*

---

## **INTRODUCTION**

## 1.1 INTRODUCTION TO THE RESEARCH

Radio frequency electromagnetic (EM) radiation has the capability to interfere with the normal operation of any technological or biological system. The four main classes of susceptible systems are humans, electrically initiated explosive devices on aircraft and in weapons, flammable atmospheres and ground-based or flying (avionic) electronic equipment. For this interference (RFI) to occur the system must be susceptible at the exposure frequency or frequencies and the radiation intensity must be sufficiently high. The effects of RFI of electronic equipment can range from inconsequential to catastrophic and lethal, with a number of civil and military aircraft crashes caused by sub-GHz frequency energy as evidence of the latter.

In the case of military aircraft illuminated by ground and airborne RF and radar transmitters, potential RFI of flying and weapon control systems is a real threat to mission success and aircrew survivability. Much world-wide effort has been expended in attempting to understand these electromagnetic threats and how to include protection measures in the design and construction of aircraft. As more and more civil aircraft are following the military aircraft route with full authority digital fly-by-wire control systems, the hazard posed applies equally to military and civil aircraft, both fixed wing and helicopters.

At the outset of this research Programme it was postulated that there may be avionic circuit upset problems caused by RFI in the supra-1 GHz part of the microwave (0.3-30 GHz) EM band, where little RFI had previously been reported. The combination of ever smaller and higher density circuit technologies used in avionics equipment, clock rates now in excess of 100 MHz, and an increasing microwave RF environment (including speculative High Power Microwave weapons) all appeared to point towards upset problems at some point in the future. An initial proposition was developed which voiced the fear that new circuit technologies such as VHSIC, with their extremely high packing densities and small (1-10 micron) device p-n junctions, would be very susceptible to interference throughout the microwave band.

## **1.2 OBJECTIVES OF THE RESEARCH**

The research described in this thesis is concerned with the quantification of the RFI risk to electronic equipment in the part of the microwave frequency band of most interest to BAe, *i.e.* 1-18 GHz, where most RF and radar transmitters to be encountered operate. The specific objectives of the research are outlined in brief below:

- a) To determine whether in fact avionics RFI can occur at these frequencies. If so, to determine whether it is an operational risk now or at what point in the future it will become evident. Further, to establish what circuit technologies are, or are likely to be adversely affected by microwave RFI.
- b) If microwave RFI is a realistic threat to electronics, to establish the signal parameters which cause the upset (*e.g.* frequency, power density, phase, modulation type and depth).
- c) To gain an understanding of the underlying mechanisms of the problem, in order to produce models and therefore aid the development of suitable protection strategies.
- d) To obtain research evidence to support the microwave EMC clearance of military aircraft with a minimum of tests on aircraft and a minimum of free space irradiation (atmospheric RF pollution), through appropriate and validated software models.

## **1.3 THESIS ORGANISATION**

The previous sections of this chapter give a brief outline of the potential hazards to military and civil aircraft operations posed by microwave EM radiation and the research objectives necessary to quantify the hazard and suggest appropriate protection measures.

Chapter 2 is devoted to an examination of the microwave environment in which aircraft have to operate. It covers not only the definition of the current civil and military environment, but also arrives at a prediction of that for the year 2000. Finally it addresses the key shortfalls of current RF environment modelling tools and techniques.

Chapter 3 presents an investigation of microwave energy ingress into airframes. It discusses prediction methods, reports on a major experimental study of airframe attenuation and considers others by the Defence Research Agency (Farnborough), concluding with a discussion of shielding measurements on metal and composite material panels in the BAe EMC Laboratory.

Chapter 4 considers energy ingress into avionic equipment boxes once it has penetrated the aircraft skin. An overall energy ingress equation is developed and the terms involving box material penetration and aperture ingress are examined and quantified. U.S. work on the energy coupling phenomenon is reviewed and the chapter concludes with a brief introduction to the subject of ingress *via* cable and connector combinations.

Chapter 5 describes energy ingress *via* cable and connector combinations and an initial model is developed, based on transmission line equations, describing the transfer function between energy incident on a wire entering an avionic box and the resultant voltage developed across a load within the box. Initial EMC Laboratory measurements of such coupling to a dummy avionic box are compared with the initial model output and with data by the small number of U.K. and U.S. researchers who have published data.

Chapter 6 gives the experimental results of a detailed laboratory investigation. Pseudo-swept (rather than spot) frequency test and measurement techniques enable a more comprehensive picture of cable ingress into boxes at these frequencies than previously published. Examination of the results and comparison with the initial model leads to a refined model and the determination of an empirical equation for load voltage as a function of cable length and illuminating antenna position along the cable.

Chapter 7 addresses the impact of microwave energy on avionic circuitry. Circuit technology advancements are discussed, and evidence of reported upset of electronics is presented. Electronic component upset mechanisms are considered, as is the use of circuit models as an aid to their prediction at these frequencies. The final term in the overall ingress equation commenced in Chapter 4 is determined and the topic of equipment and system upset prediction is covered. The chapter concludes with a consideration of protection strategies and a revised microwave upset protection regime is proposed.

The final chapter briefly summarises the research and includes suggestions for further research.

# *Chapter 2*

---

## **THE MICROWAVE ELECTROMAGNETIC ENVIRONMENT**

## 2.1 INTRODUCTION

To predict whether avionic circuitry of any technology will be upset by microwave energy, it is first necessary to quantify the power density levels the aircraft will be expected to operate in. The profile of power density vs. frequency is known as the Radio and Radar (RF) environment. Once quantified, it is then necessary to develop an ingress equation that relates incident Electromagnetic (EM) field on an airframe to voltage at the avionic circuit component. Such an equation (from Birken *et al.* [2-1]) has been developed further, identifying the constituent elements requiring modelling and those which are only ever likely to be derived from statistical treatment of empirical results. This is discussed in Chapter 4. It is shown that, from an assessment of the equation, there are three dominant factors. These are the external environment, shielding afforded to the avionics by the airframe and equipment box, and the susceptibility of the avionic circuitry in its box.

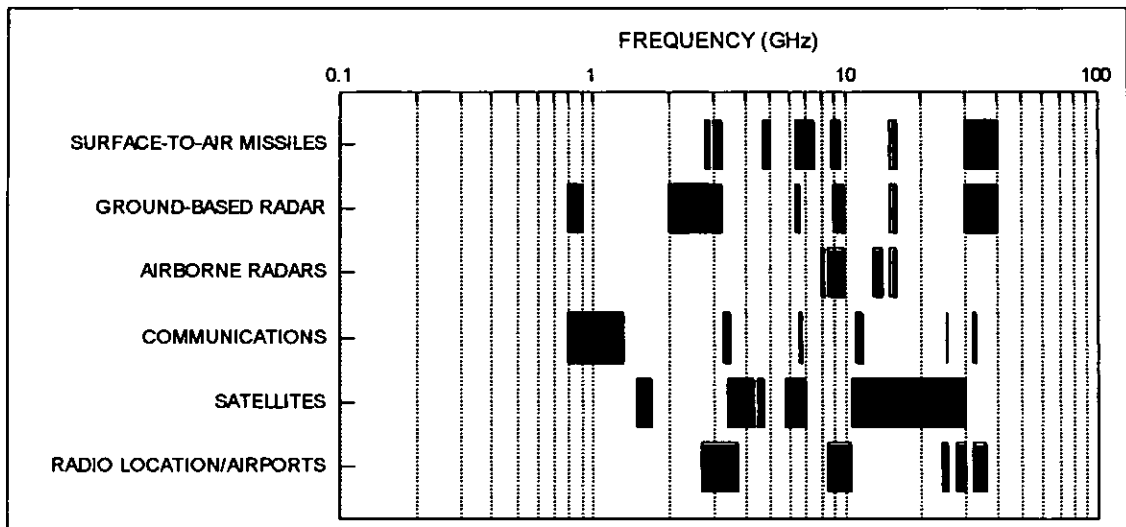
Military aircraft and (increasingly) civil aircraft with high electronic content, *e.g.* A300 series, have defined safe distances and heights from 10 kHz - 40 GHz high power transmitters. These distances equate to field strength levels at which an adequate safety margin exists to prevent upset of electrical and electronic systems. Intentional or inadvertent approach closer than these distances hazards aircraft and/or weapons. Severe effects have been demonstrated as more than one aircraft has crashed directly as a result of flying too close to a high power transmitter.

This chapter discusses the definition of the current microwave environment, supporting techniques and data, and develops a predicted worst case future environment. Environment prediction methods are then examined and the role, potential improvements and benefits of modern RF environment modelling tools are investigated.

## 2.2 CURRENT ENVIRONMENT

Many RF transmitters use the microwave band which, by international convention, covers 0.3-30 GHz. However, current radars more commonly have operating frequencies in the range 0.5-40 GHz. This research concentrates on the radar sub-band of most interest to BAe, 1-18 GHz, as military aircraft are most likely to encounter radar transmitters in this band during operational use. Fig. 2.1 shows 0.8-40 GHz military and civil usage.

Figure 2.1: Usage Of 0.8-40 GHz Band



Allen and Harlen of the National Radiological Protection Board provided a source list of RF and Microwave sources in the UK [2-2]. Unfortunately, it omitted military and civil aircraft, missile control radars, Government installations and ships in port. On assessing the document, predicting the increase since its publication in 1983 and estimating these omitted sources, the research work has shown that there are now between 44,500 and 45,000 individual microwave transmitters in the U.K. alone. It should however be noted that not all of these transmitters would be operating at any given time. The figures exclude cellular telephones and microwave ovens, estimated to currently number over one million units in the UK, which are *sources* in the strictest sense, but contribute little to the overall RF environment. Of the 45,000 transmitters 537 (March 1995) are high power systems covered by the Ministry of Defence-operated High Intensity Radio Transmission Area (HIRTA) scheme [2-3]. The number of transmitters, including transmitter 'retirements', is increasing at a rate of approximately 30 per annum at this time, a rate which is anticipated to continue over the next five years. HIRTA transmitters necessitate special horizontal and vertical avoidance distances to be observed when planning flight routes for fixed and rotary

wing military aircraft in UK airspace. The increase reflects the migration of communications systems from the lower (e.g. HF) to microwave frequencies, where the same data rate can be transmitted for a lower percentage of the available bandwidth.

However, the computer prediction HIRTA scheme covers primarily fixed ground high power transmitters, and these are mainly below 5 GHz. Before September 1992, mobile transmitters (ground, sea or air) were not covered and accordingly the scheme was of very limited use when trying to get an accurate picture of the then current microwave environment. The scheme was updated in late 1992 [2-4], introducing data on UK ground-mobile transmitters, and shipborne and airborne transmitters [2-5], although only for RAF and Royal Navy and former Soviet Union transmitters in these latter two categories. Despite this major upgrade, the HIRTA scheme, although fulfilling its intended purpose of overcoming the problem of RADHAZ (RF Radiation Hazards) to aircraft, does not enable accurate definition of the RF environment. It is a model scheme for the rest of the world, where such schemes do not yet exist. This situation causes particular problems when attempting to quantify safety margins for BAe aircraft operations in foreign countries, where details of transmitter types, powers and locations are often unknown.

There is no method at this time to allow determination of the actual microwave environment at a given point in UK airspace, since not all transmitters are included in the HIRTA scheme, and currently no environment measurements support the transmitter database. It has thus been concluded that measurements over a period of time, a difficult measurement task in itself, may be the only way to truly determine the *exact* microwave environment at a given location. Taylor and Hill [2-6] provided some of the first of the 'real microwave environment' measurements in 1977. The measurements, taken from an aircraft at 10-33 thousand feet over the California, Oregon and Nevada areas of the US, covered the range 1-3 GHz in 50 MHz bands. The power levels were measured in flight for the morning, afternoon and night cases, and the results showed that the 50 MHz occupancy to be lowest (as predicted) at night. Although recent advances have been made in Electronic Intelligence gathering equipment to allow easier data gathering and subsequent analysis, this early paper gives an idea of the variability of the microwave environment and the probable impossibility of its total and accurate prediction.

Ref. [2-7] covers the assessment of the RF environment at an operational, pseudo-military airfield in the UK. In the paper it was emphasised that the modelling and prediction

methods available at that time (1988) were inadequate for adequately defining the microwave RF environment, and that measurement with statistical treatment was the only sure way ahead. This situation was seen to have changed little by 1994 when the issue of accurate quantification and definition of the environment was discussed in Section 3 of the paper on RF Hazards Control [2-8], which forms Appendix A. In the paper the prime limitation of the HIRTA scheme was identified, that it (in common with other current assessment techniques) does not take into account the probability and time of irradiation of the aircraft by the transmitter(s) forming the environment. This aspect of time and probability of exposure is important in the determination of the potential for avionics upset and is discussed further in 2.3.2.

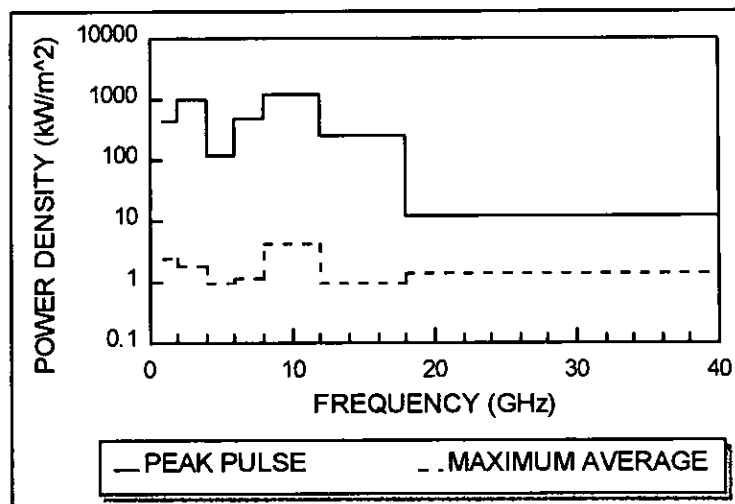
Literature searching and discussions with BAe's EM Hazards Specialist yielded some documents which purport to define the current military and civil microwave environments. They are briefly discussed below and a summary definition of the current environment is obtained by taking the worst case of all of them and presenting this on Fig. 2.2 (both for Continuous Wave and Pulsed emissions). This is thought to be a good baseline definition in the absence of an accurate picture.

Two NATO Standardisation Agreements (STANAGs), numbers 4234 [2-9] and 1307 [2-10] cover the NATO definition of the environment. The former covers that for the design of materials for use in weapons systems, whilst the latter covers the maximum Naval EM environment. This second document essentially covered the NWS (Naval Weapons Specification) 6 environment [2-11] which has now been superseded by NES (Naval Environment Specification) 1006 [2-12], which is the prime UK high RF power EMC Qualification specification.

The UK Minimum Service RF Environment (MSERFE) [2-13] largely reflects the two STANAGs above. A useful adjunct to the STANAGs is a paper by Larsen [2-14], where he presents peak and average for the total worst case environments for US, UK and French airports, and STANAG 3614AE [2-15]. This data is of particular interest since the French airport data is actually measured data, whereas the US and UK data is predicted. It should be noted that the worst case civil aircraft environment, initially indicated by MacDiarmid [2-16] and were later included in the European Civil Aircraft Equipment (EUROCAE) document [2-17], largely follows the military environment and is also included in Fig. 2.2.

A number of microwave transmitters exist on board the aircraft whose susceptibility to the external environment is under consideration, and the radar and Electronic Warfare jammer are the most powerful. These tend to pose little risk to on-board avionics as, to achieve high effective radiated powers, they use horn or phased array antennas, both of which yield beams with main lobes pointing away from the aircraft. These and the other (lower power) on-board microwave transmitters are therefore excluded from Fig. 2.2. As discussed later in Section 2.3.2, it will be seen that whilst the on-board environment may be inconsequential for the host aircraft, its transmitters form part of the external environment for any aircraft flying in formation with, or in close vicinity to it. Some extremely high power microwave sources are also discussed in Granatstein and Alexoff [2-18] which are not included in the current environment definition since most are currently only available under laboratory conditions. These are discussed further in Section 2.3.1.

Figure 2.2: Current Microwave Environment



## 2.3 PREDICTED FUTURE ENVIRONMENT

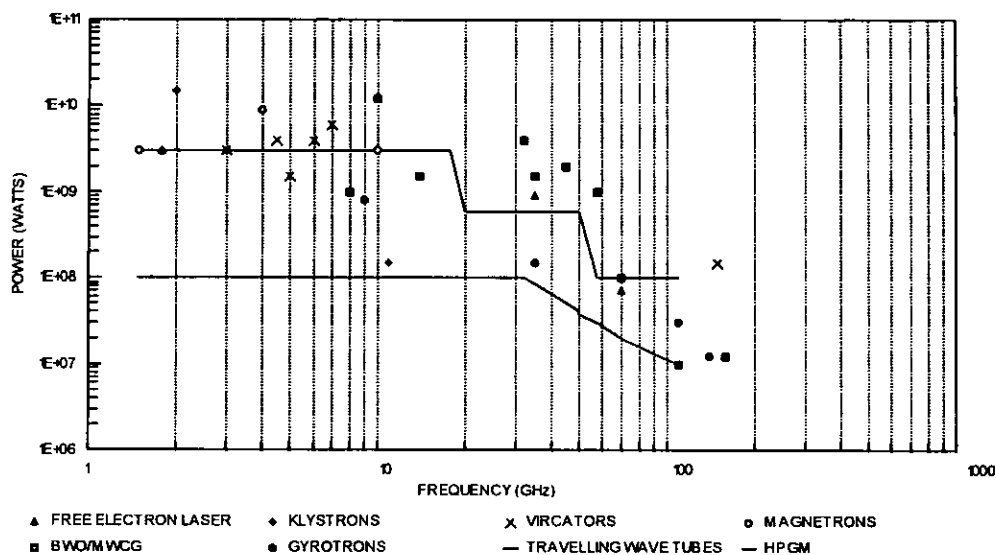
### 2.3.1 Worst Case Environment

To establish a worst case predicted future environment, unclassified baseline data was required on both high power sources and possible resultant power densities, which could then be used to develop a prediction. Literature searching yielded two papers which in part provided this baseline data. Denny [2-19],[2-20] summarised the predicted microwave hazard to future circuit technologies in his papers entitled "The Projected Susceptibilities of VHSIC/VLSI Devices to the Year 2000 EM Environment" (1986) and "Projected Trends in IC/EM Environment Interaction" (1987). The data from the papers forming part of the

baseline are given as Figures here: 2.3 'High Power Microwave Source Profile of the (1987) present' showing 5 GW peak in the 1-10 GHz region and 2.4 '1 km predicted Peak Power Density Profile' showing approximately 3.5 to 20 MWm<sup>-2</sup> in the 1-10 GHz region.

Figure 2.3: High Power Microwave Sources

Extracted from Denny [2-19], with Benford and Swegle data [2-22]



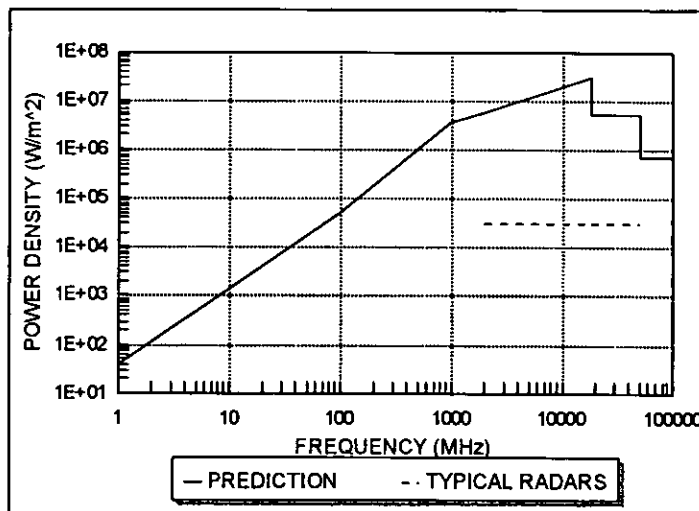
Lines = Denny data (1987); Symbols = Benford and Swegle data (1990).

BWO/MWCG: Backward Wave Oscillator/Multi-Wave Cherenkov Generator

HPGM: High Power Gyromagnetron

Figure 2.4: 1 km Predicted Power Density Profile

Extracted from Denny [2-19]

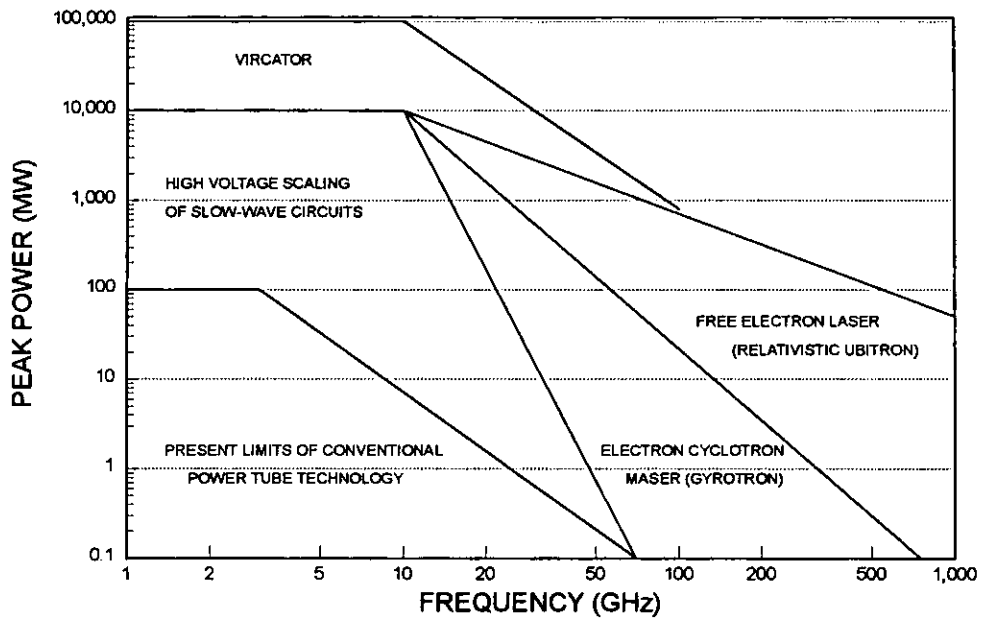


Granatstein and Alexoff [2-18] is a prime modern reference work on High Power Microwave Sources. It was published in 1987 and is the primary source of predictions of the microwave threat for the future. The so-called "Granatstein limit" is a theoretical high pulse power limit which has a maximum value of 105 MW at 1-10 GHz. R. Parker authored Table 13.1 of [2-18], which is reproduced as Fig. 2.5 and shows the projected limits of ultra-high power microwave source (<100 ns technology). Reference [2-18] covers most of the current devices, e.g. Vircators (Virtual Cathode Oscillators), Magnetrons and Free Electron Lasers (FELs).

Castro [21] noted in 1990 that the US were developing a new device called the multi-wave Cherenkov generator (MWCG), a similar type of which the Soviets were reported to have generated the then largest peak power, 15 GW, ever produced by a single assembly. Benford and Swegle, in their 1992 reference work *High Power Microwaves* [2-22], included the MWCG in data reflecting the 1990 status of peak powers of pulsed sources, and this data is included in Fig. 2.3 to demonstrate the progress made between 1987 and 1990. They noted in 1992 that the present state of the art was >10 GW achieved by MWCG and Relativistic Klystron. This steady rate of progress was underlined in 1992 when Green [2-23] reported an as yet un-ratified 20 GW from a single source, resulting from research under the Strategic Defense (*sic*) Initiative Organisation. Benford and Swegle also gave an opinion of the predicted future of 100 GW for peak pulse power, in agreement with [2-18], and average powers of 100 kW increasing to 1 MW.

It should be noted that the peak levels on these predictions are 100 GW in the range 1-20 GHz and, as such, are 20 times higher than those used by Denny in his predictions of IC upset levels for the year 2000 RF environment. Indications from Soviet and US work in this field, reinforced at a 1988 seminar on the latest advances in High Power Microwaves are that the 100 GW level may be reached by the year 2000, even if only by the use of paralleled Gyrotrons or Vircators with phased array horn antennas under laboratory conditions. The reported US near term experimental objective of 500 GWm<sup>-2</sup> for pulsed FELs is discounted at this time.

Figure 2.5: Projected Limits Of Ultra-High Power Microwave Sources

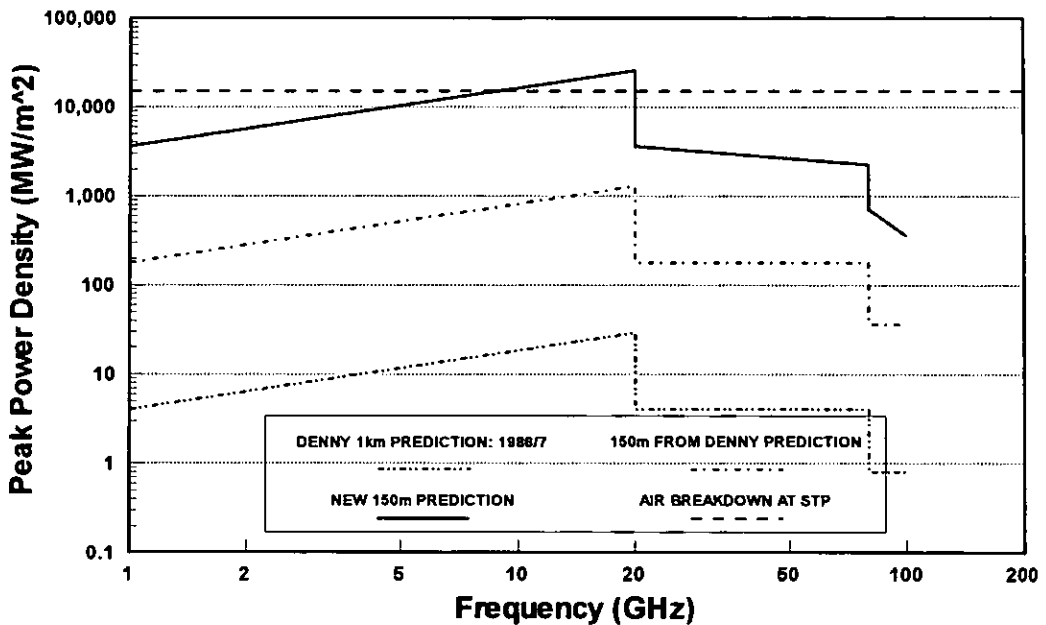


As mentioned in Section 2.2, the present peak microwave environment is thought to be dominated by the external, rather than by on-board microwave sources. For the future, with moves to make military aircraft more 'stealthy' and have tighter emissions control, on-board transmitter powers are likely to stabilise and certainly be reduced in some areas. Evidence is already seen with the inception of low probability of intercept and spread spectrum radars, as well as terrain matching systems, which delete much of the requirement for forward transmitting terrain following radars. In addition there have been a number of mentions of the development of High Power Microwave "Beam Weapons" since 1987, [2-21] and [2-24] to [2-26]. In 1987 Audone [2-24] reported that it had just recently been proposed to develop weapons capable of radiating the aircraft with extremely high levels of energy. These weapons, he reported, would use generators based upon new pulsed plasma magneto-hydro-dynamic technology, which convert the chemical energy of an explosive cartridge directly into pulsed electrical energy. Whilst it is known from [2-21], [2-23], [2-25], [2-26] and other sources that since then work has been carried out in the US and USSR, it is believed that, at the present rate of progress, it is unlikely that peak power density levels in the microwave band will exceed those predicted in Fig. 2.6.

From consideration of the preceding items in this section and taking into account that the ground-based transmitter 'threat' may be as close as 150 m to the aircraft, the current prediction of the future microwave environment is given as that of Denny multiplied by 20 and then scaled for 150 m and is presented in Fig. 2.6. It includes the dry air breakdown

power density at one atmosphere,  $15.3 \text{ GWm}^{-2}$  ( $2.4 \text{ MVm}^{-1}$ ), as an indicator of the eventual limiter to the microwave threat to aircraft. With present progress on high power pulse microwave sources, including that on multi-antenna arrays where the overall effect of air breakdown on the total effective radiated power is less, it is suspected that levels on this Fig. 2.6 may be reached within the next five years, even if only under laboratory conditions.

Figure 2.6: Predicted Microwave Environment



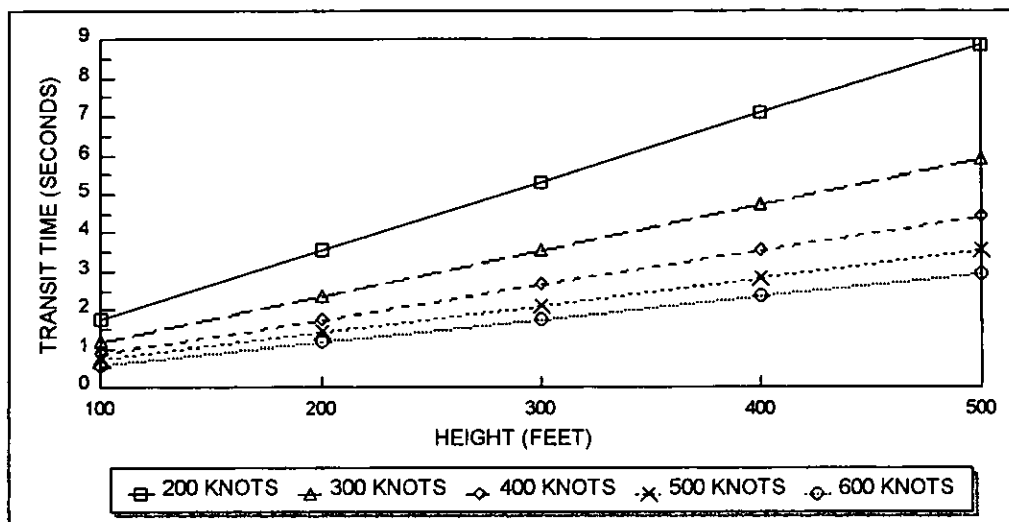
### 2.3.2 Realistic Environment and Probability of Exposure

Specification of the minimum necessary RF environment(s) in which aircraft have to operate is a key issue in the cost and development timescales of new and/or modified aircraft and their avionics [2-8]. Modern EMC specifications, which are usually based on a worst case 'static radar with generic RF parametrics permanently pointing directly at the aircraft' consideration with additional safety margins, simulate conditions which rarely, if ever, occur in real life. A number contain single value field strength levels across significant parts of the RF and radar bands, even though in some sub-bands transmitters do not exist. Thus, most avionics being designed and qualified today may be over-specified and there appears the possibility for cost and timescale reductions, which could be applicable across all military and civil platforms, if a better RF environment prediction were to exist or be developed. This issue is equally applicable to the design and specification of Electronic Warfare (EW) receivers, such as those in Radar Warners, Electronic Support Measures equipment and RF jammer systems. In this case a precise, time line definition of the RF environment is

required, in terms of power density, number of pulses per second and frequency sub-banding of energy reaching the aircraft. Currently, no BAe aircraft to date has had this definition established prior to contract award. Consequently, it is thought that such EW systems specified by BAe may, as for the EMC case, be over-specified.

The time line power density vs. frequency profile the aircraft is subjected to during its various mission types and phases, for peace-time and under active operational conditions, also affects RADHAZ. This is required to be known to ensure that aircrew are not hazarded and that there is no unacceptable hazard posed to on-board fuel systems and weapon systems containing electro-explosive devices. For each of the above cases: EMC, EW and RADHAZ, the item requiring determination is the profile of power density vs. frequency vs. exposure time, *i.e.* the *probability of exposure*, and, in the case of this research programme, the consequent *probability of upset* of avionic circuitry should the aircraft *actually* be irradiated with such an exposure profile. It is this exposure time aspect of the environment which, in conjunction with the aspect angle of aircraft irradiation (discussed in Section 2.3.2.2), is believed to be a substantial factor in determining the probability of upset of avionic circuitry, rather than merely the peak or mean power density to which the aircraft and its avionics are exposed. For example, if an aircraft in motion at 300 feet altitude and 300 knots is perfectly tracked as it approaches and overflies a ground-based radar, then the aircraft will only be illuminated at any appreciable level of power density (*i.e.*  $>0.1$  of the maximum, which occurs when the aircraft is directly overhead the radar) for 2.8 seconds. This example is expanded in Fig. 2.7, which shows this transit time for the normal military aircraft low level operations regime of 100 to 500 feet and through the speed envelope 200 to 600 Knots. In all cases this 'worst case' irradiation time is less than 10 seconds during which time the power density is above 0.5 of its maximum for only 56.3% of the transit time, further demonstrating the pessimism of the case of continuous irradiation at a fixed maximum power density.

Figure 2.7: Aircraft Transit Time Over A Ground Radar



In the case of non-tracking rotating, scanning or nodding (height-finder) radars the probability of the aircraft encountering the radar peak power density, *i.e.* on the antenna boresight rather than elsewhere in its main beam or its side lobes *and* being exposed to power densities above 0.1 x the maximum from a given transmitter for more than 2 seconds, is much less than unity; absolute quantification is discussed in Section 2.3.2.2. Far more likely, in typical aircraft vs. ground radar situations, is an exposure time of a few micro-seconds in any one radar's sweep. This aspect is complex and totally scenario dependent (*i.e.* quantity of radars, radar scan and RF parameters, their dispositions relative to the aircraft and aircraft flight path) and is discussed further in that Section.

There is likely therefore to be considerable difference between an exposure consideration where the transmitter is pointing continuously at the aircraft and both are stationary, and one where relative angles and range are changing with time and the transmitter is also scanning. This may explain, as discussed in Chapter 7, why there are many less occurrences of microwave upset than would be expected from consideration of:

- the current microwave environment (see Section 2.2),
- the low field strength levels to which earlier generation aircraft and avionics, many of which will remain in service for ten or more years, have been certified to (see Appendix B), and
- the airframe attenuation which can be guaranteed on both metal- and composite-skinned aircraft (see Chapter 3).

A precise and accurate definition of the RF environment at a given point in space therefore necessitates full knowledge of all transmitters, including their RF parametrics and azimuth and elevation beam patterns. In the common case of scanning, rotating and nodding antenna systems, the scan parametrics, *e.g.* rates, turn-around times (during which no transmissions take place) and start position, are also required to be known. This requires a large database of transmitter information for all but the simplest environment predictions. Computer models are then required to calculate, in the simplest case, free space loss between transmitter and aircraft to arrive at power density at the aircraft. This has to be calculated for all transmitters in the scenario and at high rates to ensure all received pulses (many of which are of the order of  $1\mu\text{s}$  duration) are included in the summation of power densities at the aircraft.

In the next section the capabilities and shortfalls of existing RF environment prediction techniques used for EMC purposes are examined. The abilities and limitations of an existing BAe software tool, the EW Evaluation System (EWES) [2-28] with its Scenario Generator, are also explored with a view to providing the basis of an accurate and high quality RF environment prediction tool covering EMC, EW and RADHAZ requirements.

### **2.3.2.1 EUROCAE and HIRTA prediction methods and limitations**

The U.K. Ministry of Defence operates a HIRTA scheme [2-4] for fixed and rotary wing *military* aircraft operating in the U.K., see Section 2.2. The need for such controls has been driven by the increasing avionics and electronic-controlled weapon systems content of military aircraft since the early 1960's. The weapons systems safety aspects have been covered *via* U.K. Ordnance Board documents, *e.g.* [2-13], which have existed in some form from those times. As the avionic content of military aircraft increased, *e.g.* the introduction of the Tornado and Harrier aircraft in the 1970's, the increased risk of upset was controlled by the introduction of the HIRTA scheme in 1984, which covers weapon, avionic and other electrical systems.

No similar need existed for *civil* aircraft as they neither carried weapon systems nor, until the late 1980's, did they contain fully computerised flight safety critical systems. With the advent of electronics into critical areas of civil aircraft, such as on the European Airbus A300 series of aircraft with their full authority digital fly-by-wire flight control systems, there emerged the need for an equal level of control of both civil and military aircraft avionics to ensure safe and correct operation in the proximity of high power radio and radar

transmitters. To control the risk to civil aircraft the U.K., in collaboration with other E.C. countries, their Airworthiness Authorities and the International Civil Aviation Organisation (ICAO) formed a body to address these issues, called the EUROpean Organisation for Civil Aircraft Electronics (EUROCAE). EUROCAE Working Group 33, Sub-Groups 2 and 3 in conjunction with the U.S. Society of Automotive Engineers (SAE) AE4R Committee have produced, between 1990 and 1994, four draft versions of an advisory document entitled 'Guidance to the Certification of Aircraft Electrical and Electronic Systems for Operation in the High Intensity Radiated Field (HIRF) Environment'; [2-17] is the 1993 draft, from which the 1994 draft varies little in the area of RF environment prediction techniques and levels. This document defines, amongst other EMC design and test procedures and processes, the external (to aircraft) RF environment, from which, in turn, a design and test environment for civil aircraft is developed. It should however be noted that [2-17] does NOT cover RF hazards to Electro-Explosive Devices (which is covered by the HIRTA scheme for military aircraft), humans or flammable atmospheres. Reference [2-17] actually contains six rather than one single definition of the civil aircraft environment, three for the *European* scenario and a matching set for the higher levels to be encountered in the *International* scenario. Their derivation, the underlying assumptions and calculation of field strength levels are now discussed.

The flight envelope of aircraft defined by the ICAO standard allows unrestricted flight, during normal operations, within 500 feet of the ground with the exception of certain 'restricted' [very high power transmitter] areas. The hypothesis that increasing field strength (due to diminishing aircraft-to-ground transmitter distance) equates directly to an increased likelihood of adverse effects in avionics is used to support the plausible argument that an aircraft emergency may result in deviation from normal flight path and may thus lead to exposure to a higher RF environment and an attendant increased risk. Consequently, although the derivation of environment is more involved (including assessment of approach and landing trajectories), the basic rationale used is one where a number of different classes of transmitters are categorised by the minimum distance an aircraft may approach them. The seven contributing environments to the total civil aircraft RF environment are given in Table 2.1.

Table 2.1: Elements of Total Civil Aircraft RF Environment

1)	<u><i>Airport - Fixed Ground Emitters:</i></u> Marker beacons, ILS (Localiser & Glide Slope), Weather Radar, TACAN, VHF and UHF communications and telemetry, Distance Measuring Equipment, Airport surface detection system, Airport and Air-route surveillance radars, Ground controlled approach radar, Non-directional beacon, Microwave landing system, Weather radar, ATC-RBS interrogator.
2)	<u><i>Airport - Mobile Ground Emitter:</i></u> Weather radar.
3)	<u><i>Airport - Other Mobile Ground Emitters:</i></u> HF, VHF and UHF communications, Doppler navigation radar, TACAN, Radio Altimeter, ATC-RBS beacon.
4)	<u><i>Aircraft-to-Aircraft (Interceptor):</i></u> On-board radars; HF/VHF/UHF comms.
5)	<u><i>Aircraft-to-Aircraft (Non-Interceptor):</i></u> Weather radar, HF communications.
6)	<u><i>Ground Environment:</i></u> Commercial HF, VHF FM and AM, and TV broadcast transmitters, Troposcatter communications, Radars, LORAN C installations.
7)	<u><i>Shipborne Environment:</i></u> HF and UHF communications, Various radars, IFF/SIF.

The minimum distances between the aircraft under consideration and each of these transmitters in these environments was then defined, as reproduced in Table 2.2. The worst case environment, which includes the extreme situations of least probability, is entitled 'Severe'. The 'Normal' environment is based on the representative maximum EM environment profile found in the vicinity of a number of European airports, *i.e.* it covers the more realistic possible interference situations of higher probability and thus contains somewhat lower field strength levels than in the 'Severe' case. The environment to be used in the design and test process for flight safety critical systems is entitled 'Certification' and lies broadly between the 'Severe' and 'Normal' environments.

Table 2.2: Minimum Aircraft-to-Transmitter Distances

TRANSMITTER	MINIMUM DISTANCE (Feet)*		
	SEVERE	CERTIFICATION	NORMAL
<u>Fixed airport transmitters:</u>			
- Airport radar	500 S	500 S	500 S
- Non-radar transmitters	250 S	250 S	250 S
<u>Mobile airport transmitters:</u>			
- Aircraft's weather radar	150 D	150 D	250 D
- All other	50 D	50 D	50 D
<u>General ground transmitters:</u>			
- 0-3 NM wedge from end of runway	500 S	500 S	500 S
- 3-5 NM wedge from end of runway	500 S	1000 S	1000 S
- 5-10 NM wedge from end of runway	500 S	1000 S	1500 S
- 10-25 NM radii of aircraft	500 S	1000 S	2500 S
<u>Air-to-Air:</u>			
- Interceptor aircraft	100 D	100 D	None
- Non-interceptor aircraft	500 D	500 D	None
<u>Ship-to-Air:</u>	300 S	750 S	None

\* S = Slant range; D = direct range.

The minimum distances for the matching set of environments for the International scenario are not given in [2-17] but are believed to be similar, with the differences in peak and average field strengths vs. frequency sub-banding being the result of higher power radar transmitters which may be encountered outside Europe (*i.e.* primarily in North America). The absolute values of field strength in the European and International environments in [2-17] are not discussed here as they have already been included in the considerations in Section 2.2 leading to the prediction of the worst case current microwave environment. Although a number of international agencies have been involved in the calculation of the field strengths at a civil aircraft from the transmitters described earlier in this section, it is relevant to discuss the methods used in support of defining the civil environment in the U.K. This is appropriate as the method used by EUROCAE is to use the HIRTA emitter database

and calculations (operated by BAeSEMA under contract to the U.K. MoD), as used in the definition of the military aircraft U.K. RF environment, described in Section 2.2.

For each transmitter in turn, a worst case is statically modelled where it is assumed to be permanently pointing its boresight directly at the aircraft under consideration. RF emitter parametric data used in the calculation is either supplied by the transmitter's manufacturer or estimated by the HIRTA database operator. The equations used are based on optical point source theory to give far field power density ( $P_d$ ) at the aircraft under consideration:

$$P_d = \frac{G_T * P_T}{4\pi r^2} \quad (\text{Wm}^{-2}) \quad \dots(2.1)$$

where:  $G_T$  = Antenna peak gain (as a ratio above isotropic)  
 $P_T$  = Transmitter power, less antenna feeder losses (W)  
 $r$  = Distance between transmitter and aircraft (m)

Appropriate near field adaptations, particularly relevant for sub-GHz emitters, and antenna radiation patterns only for sub-0.6 GHz emitters, where significant off-boresight elevation and azimuth sidelobes can be encountered, are given in Section 5 of [2-4]. For microwave antennas the transmitter-to-aircraft slant distance is compared to the near/intermediate field and intermediate/far field distances to establish whether the aircraft is in the Fresnel (near and intermediate) or Fraunhofer (far) field of the antenna. The boundaries, N-I and I-F, are given by:

$$\text{N-I} = \frac{D^2}{2\lambda} \quad (\text{m}) \quad \dots(2.2)$$

$$\text{I-F} = \frac{2D^2}{\lambda} \quad (\text{m}) \quad \dots(2.3)$$

where:  $D$  = largest antenna dimension (m)  
 $\lambda$  = wavelength of lowest antenna operating frequency (m)

If the aircraft is calculated to be in the near field, which extends to  $\frac{A}{2\lambda}$  (m) from the antenna where  $A$  is the area of the antenna ( $\text{m}^2$ ), then in practice the following equation is used for maximum near field power density:

$$P_d = \frac{3P_T G_T}{A} \quad (\text{Wm}^{-2}) \quad \dots(2.4)$$

This power density is assumed constant over the above distance, which is not the case in reality where substantial variation of electric and magnetic field strengths (and hence power density) occurs in this region.

The HIRTA scheme has limited treatment of co-located transmitters as it assumes that an aircraft will only be illuminated by the most powerful heightfinding (nodding) and tracking radars (if such exists at the site), and periodically by the most powerful rotating search radar. The combined mean effective radiated power of these emitters is used as though it emanated in all directions from a single, more powerful radar. With the possible exception of hovering or slow moving helicopters at very low levels, the above represents an extreme worst case assessment as military aircraft moving at over 300 knots above a few hundred feet altitude are unlikely to be irradiated at any appreciable level by ground emitters for more than a few seconds in reality as discussed in Section 2.3.2. A number of assumptions are applicable to the definition of the RF environments and the field strengths calculated for each transmitter in the scenario contributing to the definition of each of those environments. Some are contained in [2-17] and [2-4] and others appear in Jaeger [2-27] (one of the contributors to [2-17]). These, with commentary, and other identified limitations and shortfalls are given in the following list. Together these represent significant over-estimation of the RF environment as a threat to military and civil aircraft. Thus the HIRTA scheme and the various additional assumptions applied in the EUROCAE environment definition, although adequate for their intended purpose, *i.e.* ensuring military and civil aircraft safety when in proximity to high power RF transmitters, are considered to be very conservative. The items are grouped together in perceived order of importance to the generation of high fidelity definition of the RF environment.

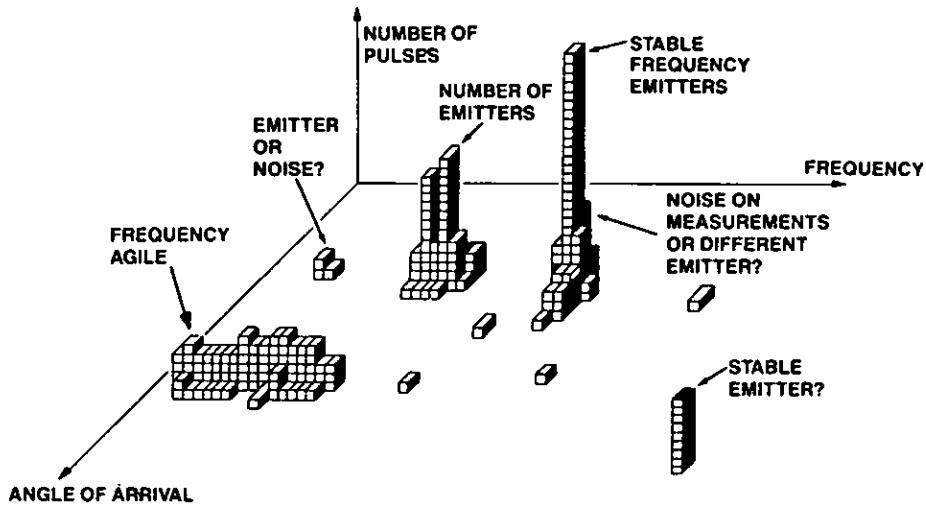
**High Importance:**

- 1) **Continuous illumination** of the aircraft by the transmitter is assumed, *i.e.* no modelling of emitter-aircraft relative motion and no consideration of sector scan, nodding, or antenna rotation.
- 2) **Transmit antenna modelling:** Maximum main-beam gain of the emitter antenna is used; *i.e.* no beam shape (main-beam width, side- and back lobes) are used. Beam squint is not taken into account. Antenna heights above ground due to antenna towers that were not 'part of the basic package' are not considered. If maximum antenna elevation angle is not available, 90° is assumed. Shipborne emitter antenna height is assumed to be 150 feet. Transmit antenna polarisation is not considered, which could have significant impact on coupling of energy through the airframe and into the avionics equipment; this aspect is examined in Chapter 3.

- 3) **Non-cumulative field strength** is calculated; *i.e.* the effects of illumination by more than one transmitter is not considered. Jaeger [2-27] claimed that 'Investigations have shown that the probability of addition is extremely low, as in the case of short wave transmitters, where some emitters are located at the same place.' This comment is probably only aimed at sub-GHz emitters and is unlikely to be true for an aircraft illuminated by a number of identical hostile fire control radars.
- 4) **Transmitted signal modulation** is not considered apart from the simple duty cycle defined for EMC qualification of avionic equipment and aircraft (see Appendix B). Only using worst case RF parametrics rather than a realistic set *vs.* time is pessimistic (*i.e.* *constant* illumination by a CW source is unusual, whereas radar mode changes between search, track, lock-on and back to search are more realistic).
- 5) **Civil Aircraft height**: Minimum heights of aircraft above ground transmitters are assumed to be as shown in Table 2.2. These result in much higher field strengths than would appear from a realistic assessment of the probability of an aircraft actually approaching this close, even during an emergency. As the field strength falls off as the inverse square of the inter-distance, any increase in the figures of Table 2.2 will appreciably reduce the field strength the aircraft would be expected to encounter.
- 6) **Average field strength** is a function of the duty cycle of the transmitted waveform, usually expressed as Pulse Width (PW) in seconds multiplied by Pulse Repetition Frequency (PRF) in Hertz. Emitters often have a range of operating PWs and PRFs and often emitter documentation does not enable determination of the precise operational maximum duty cycle; in this case the maximum values of PW and PRF from the documentation are used for a conservative estimate.
- 7) **Frequency Sub-Banding**: The highest individual field strength within the following frequency sub-bands is taken as the environment for the whole sub-band: 1-2, 2-4, 4-6, 6-8, 8-12, 12-20 and 20-40 GHz. Thus, for example in the latter two radar bands, an environment may be specified where none or only low power emitters exist in large parts of the band.
- 8) **Transmitter RF characteristics**: Transmitters are fixed frequency, PW and PRF; *i.e.* frequency agility and inter-pulse variations of PW and PRF, which are usual in military radar systems, are not considered. This aspect can be visualised in Fig. 2.8, from

[2-29], where various types of radar pulse waveforms incident on an aircraft are depicted as a number of pulses vs. frequency and vs. angle of arrival at the aircraft.

Figure 2.8: Radar Pulses Incident On Aircraft



### Medium Importance

- 1) **Multipath:** Although constructive ground reflections of HF band emissions are catered for (direct and reflected components assumed to be in phase), no consideration of multipath at microwave frequencies is made. At microwave frequencies a number of aspects require modelling: a) Multipath from other airborne transmitters (including forward ground bounce and from other aircraft in close proximity), b) Own transmitter returns (vertical ground bounce and from formation flyers). Specular and diffuse reflections equate to signal phase difference and thus changed amplitude at aircraft. When considering reflections from formation flyers (which includes the interceptor vs. civil aircraft case) there is also a need for some level of Radar Cross Section modelling of the other aircraft involved. Such modelling, especially in real or near-real time, is computationally intensive.
- 2) **Terrain modelling:** Flat earth is assumed, *i.e.* terrain is not included. Terrain modelling, including terrain screening, various terrain types and surface cultures within a scenario are required; including reflectivity aspects and sea states.
- 3) **Near field effects:** These are dependent on frequency, transmit and receive antenna size and are generally more relevant to large aircraft or low flyers. Although the HIRTA scheme caters for sub-0.6 GHz antenna arrays (especially those at HF), it assumes a worst case maximum near-field power density at all points within an antenna's near field.

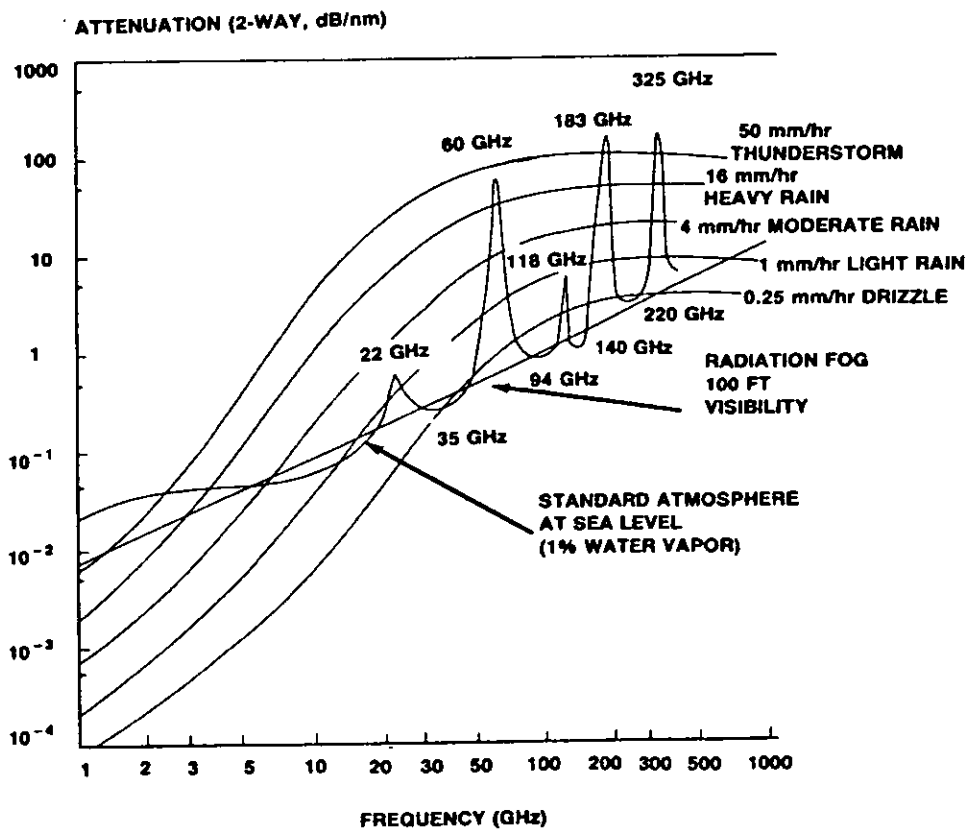
4) **Repeatability:** When modelling an environment with a moving aircraft and radars with appropriate scan motions it is important to be able to control antenna initial pointing angles, as these may be the dominant factors in whether and by how much the aircraft is illuminated by any given emitter in the scenario. The ability is thus required to specify emitter boresight start values (e.g. all radars point North, centre of scan on velocity vector of aircraft, or random). With this capability the range of field strengths an aircraft will encounter can be determined as a function of aircraft approach time and radars' initial pointing angles.

5) **Modulation on Pulse:** Improved fidelity is needed to better represent real radars.

**Lesser Importance**

1) **Atmospheric effects:** HIRTA and EUROCAE assume free space, *i.e.* no losses. Attenuation should be modelled varying representatively with frequency (including 'ducting' effects) and rainfall rates. Fig. 2.9 shows RF signal attenuation *vs.* frequency for various rainfall rates.

Figure 2.9: Atmospheric Attenuation of RF Signals



- 2) **Emitters on platforms, particularly aircraft:** Current systems largely employ 'point' platforms, *e.g.* each aircraft's emitters and sensors exist at one point in space. Need for wire grid 'model' of (at least) transmitting platform where emitter antennas may be placed.
- 3) **Transmitter Power:** The HIRTA emitter database only contains emitters with an effective radiated power greater than 500 Watts (25 dBW). All microwave transmitters, irrespective of power, should be included in a high fidelity environment definition.

#### **2.3.2.2 EW Environment Simulator as an Accurate Prediction Tool**

BAe, in its role as a major aircraft manufacturer and systems integrator, has a suite of appropriate models and simulators to support the conceptualisation, design and development of whole aircraft and their systems. One of these tools, the Electronic Warfare Evaluation System (EWES) by Data Sciences (U.K.) Ltd., is of major relevance to the prediction of the RF environment for EMC purposes. EWES is a suite of computer programmes for the development of EW equipment such as radar warning receivers and radar jammers (active electronic countermeasures). The positions of ground emitters and trajectories of mobile ground and airborne emitters are entered into the ESPRIT (Enhanced Scenario Preparation Interactive Tool) front end programme to enable computation of the received RF environment, at any specified location or aircraft, by the EW Scenario Generator (EWSG). This generates a time-ordered history file of all RF parameters of pulsed and CW waveforms at the specified aircraft. Post-scenario run analysis of the RF profile encountered by the aircraft can be conducted by the EW Graphical Analysis (EWGA) package or data can be exported for analysis on a variety of other analysis tools. Although primarily an EW design tool, EWES generates much of the RF information required for EMC environment definition. The method of use, appreciable computing resources, typical EWSG data listings and commonly used EWGA outputs are given in Figures 2, 3, 6 and 7 of [2-30] which is reproduced as Appendix C. Reference [2-30], the 1995 paper on environment definition published by this researcher with discussion support from his colleague, BAe's EWES specialist, includes the findings of Section 2.3.2.

The EWES suite adequately addresses many of the limitations and removes a number of the assumptions of HIRTA and EUROCAE environment definition for military and civil aircraft, as listed in Section 2.3.2.1. Some areas, *e.g.* terrain modelling and screening and 'repeatability', which are currently not in the EWES suite, are being implemented in a 1995

major upgrade to its capability. This upgrade is driven, *inter alia*, by the need to have common capabilities with BAe RF threat simulators (complex RF signal source generators with internal RF environment models, which have had such items specified by this researcher). Other shortfalls of, and potential improvements to the EWES suite are under investigation by this researcher as part of a BAe research programme. The potential use of EWES as an EMC environment prediction tool warrants further investigation.

## 2.4 CONCLUDING REMARKS

The precise definition of the external microwave environment levels is a key factor in determining whether or not microwave upset of any circuitry will occur. To date no definition of that level of quality is available. Although better predictions of the current environment have now been produced by the EUROCAE and HIRTA groups based on consideration of likely RF emitters to be encountered by civil aircraft operations at 500 feet height, on approach and take-off and landing, these predictions are overly pessimistic and are of little use to the definition of the military aircraft environment.

Since it has been identified that the EWES environment modelling capability addresses most of the shortfalls of the other tools and techniques, it is believed that there is significant scope for its use to develop *realistic* environment predictions upon which an estimation of probability of upset of avionics can be superimposed to yield higher quality EMC specifications. This topic is currently under investigation by BAe's research groups.

It is likely that the definitions of worst case current and future microwave environments arrived at in this research will continue to change in the near future, though probably at a lesser rate than in recent years. It is not considered that the peak values predicted in Fig. 2.6 will be exceeded, with the exception of speculative High Power Microwave weapons (which are outside the scope of this research), however it is quite likely that the frequency profile may change.

# *Chapter 3*

---

## **MICROWAVE ENERGY INGRESS INTO AIRFRAMES**

### 3.1 INTRODUCTION

In the early part of the research programme it was established that there were no suitable analysis tools in existence for the comprehensive modelling of energy ingress into airframes at microwave frequencies. However, more recently, software has become available with a limited applicability to this problem within affordable computing resources. Consequently attention was turned to a practical examination of the subject on a real aircraft. This examination allowed identification of average airframe attenuation factors at these frequencies, whilst highlighting actual ingress points on the airframe. Additionally this work supplied evidence on the dependency of energy ingress on the angle of arrival of the impinging EM wavefront. Microwave energy ingress into airframes is examined in some detail in this chapter, with commentary on prediction and modelling problems anticipated.

### 3.2 PREDICTION METHODS

The three-dimensional models used to date attempt to analyse a small portion of the airframe using one of three techniques: direct analytical, boundary element or finite difference. The Transmission Line Modelling (TLM) code is a time domain numerical technique [3-1] and is used for predicting fields, surface currents and wire currents on and in a body. Propagation is modelled by filling space and the body therein with a network of transmission lines. Through equivalence to Maxwell's equations the solution of the network, resulting in fields and currents, can be solved exactly. The frequency range over which the technique can be used depends on node spacing within the network; at least 6 nodes per wavelength ( $\lambda$ ) are needed [2-17].

The Numerical EM Code (NEC) is a frequency domain, boundary integral code for calculating the scattered field and surface current on conducting bodies [3-2]. The body's surface is discretised into either flat panels or wires. Self and mutual impedance of each wire and panel are inserted into a matrix which, when inverted and multiplied by the driving function (incident field), gives a matrix of currents on the panels or wires. These produce the surface current on the body. Frequency range of operation is computing resource-limited as panels and wires must be smaller than  $\frac{\lambda}{8}$  [2-17], although  $\frac{\lambda}{10}$  is often seen in the literature and smaller segment lengths can be required depending on local geometric constraints. Solution computing time is proportional to the square of the number of panels or wires for matrix filling, and to its cube for matrix inversion. NEC is but one code in this

class of thin-wire integral equation based moment methods, with MOM-3D as another, BAe-generated code [3-3]; see [3-4] for a comprehensive review of this class of methods.

Finite-Difference Time-Domain (FDTD) codes can model the complex environment inside a box, but computer memory and processing restrictions limit the volume of surrounding space to significantly less than is required for the practical modelling of whole aircraft above 0.5 GHz. The technique, based on basic discretisation algorithms by Yee [3-5], is an implementation of a time domain solution of Maxwell's equations. The body is modelled as a series of rectangles or parallelepipeds and the response at each time step is calculated using the results of the previous step. This solution can be transposed to the frequency domain with high accuracy, using a Fourier transform, and the frequency range of FDTD is dependent on the grid cell size. Ref. [2-17] indicates that five cells are required to resolve the shortest wavelength. Whilst methods of moment codes can also be used to model large objects, they require prohibitively greater memory requirements than FDTD methods [3-6].

All the above codes pose significant computing problems when the modelling of whole aircraft in the microwave region is considered. For accurate results when attempting modelling, NEC, using the  $\frac{\lambda}{10}$  criterion for example means segment lengths of at most 1.7 to 30 mm for the range 1 to 18 GHz. Thus, as SAAB (Sweden) experience has shown [3-7] using the FDTD technique, it is only possible to model airframe panel *joints* at 40 GHz (where  $\frac{\lambda}{10} = 0.75$  mm), the highest frequency of current interest in the EMC arena [3-8], [3-9] and [2-17], even with powerful CRAY computers. Clearly to model microwave ingress for a *whole* aircraft using such techniques would be a monumental task, even for the powerful computers available today. This is recognised within BAe; in a 1995 internal BAe presentation by the Industrial Supervisor, BAe's EM Hazards Specialist, it was stated that with current and extensive Divisional computing capabilities of 2.5 giga-FLOPS (peak) using a 32 process Parsytec Explorer it still takes 20 days to model the 15 million cells needed to represent a full fighter airframe at only 100 MHz. Even using the BAe corporate facilities at the Super-Computing Centre at Farnborough, the CRAY T3D and YMP computers, this figure only reduces to 3 days, still far too high and costly to be of use in practical EMC design applications. To perform similar modelling at 10 GHz would multiply this figure by  $10^4$ . It is thus predicted that using conventional techniques, e.g. NEC, and even assuming that the linear (on a log scale) rise in giga-FLOPS of affordable computing power continues, that *microwave* modelling of full fighter airframes using direct solutions will remain unattainable in the foreseeable future.

However, it is believed within BAe that a combination of asymptotic methods or the 'ray tracing' technique for far field analysis and use of direct solution methods for analysis of selected areas of field and structure interaction may offer a whole aircraft modelling solution at frequencies up to 18 GHz within the next five years. This combination, whilst in its infancy, offers much promise for the affordable and timely future analysis of complex structures of fighter aircraft size. In the intervening period the use of very high power computers now available renders such computational problems possible for relatively small, part-aircraft structures, even though, for example, to model the fields in a simple 1 m cubic, empty avionic bay would require 37 million cubic cells to analyse in three dimensions at 10 GHz, using  $\frac{\lambda}{10}$  as the cell size. However, if it were possible to use  $\lambda$  as the cell size then in such cases the figure would be substantially reduced.

Computer-Aided Design (CAD) models are used as the highest quality source of data on a given aircraft's exterior shape for direct, computer-to-computer importation into EM modelling codes. For example, CATIA (Computer-Aided Three-dimensional Interactive Application) [3-10], BAe's main aircraft CAD tool, currently provides data with a resolution of 5 mm for use in EM ingress modelling at up to 100 MHz. 5 mm equates, using the  $\frac{\lambda}{10}$  criterion, to an upper modelling limit of 6 GHz, and the resolution would need reducing to 0.75 mm to meet that criterion, or to 0.935 mm for the [NEC]  $\frac{\lambda}{8}$  one. CATIA already has sufficient resolution and accuracy to provide skin data to support EM modelling up to 40 GHz, with data already generated for detail manufacturing of EF2000 at a minimum resolution 0.025 mm and accuracy better than this, but the data sets for a whole aircraft at even 1 mm resolution preclude their current use in this respect. Thus, despite the advances predicted in the preceding paragraphs, at present realistic whole aircraft modelling at frequencies up to 40 GHz is thought to be impractical due to the processing load entailed. A further complication of modelling whole aircraft at 40 GHz is the need to model not only the aircraft skin, but also the complex internal support structure of the airframe and the equipments interspersed in that structure. Modelling of both the skin and the internal contents would need to be to the same resolution, equating to considerable computing capability increase above that available now, unless substantial simplification concerning internal equipments can be made and justified. Variations in internal construction between individual aircraft of a given type also makes direct modelling inappropriate. Derivation of values of airframe attenuation based upon practical measurements is thus likely to offer the best and most cost-effective solution to this problem at present.

An overall energy ingress equation has been developed, see Section 4.2, in which the first line of defence against avionic upset by the environment predicted in Chapter 2 is the shielding afforded to the circuitry by the airframe. However, practical considerations limit the magnitude of shielding achievable and only an arbitrary, frequency independent attenuation of 6-20 dB is used by military aircraft designers as an estimate for airframe attenuation. It was thus decided that the early phase of this research programme should concentrate on attempting to quantify the values of airframe attenuation to be found on most, metal-skinned fighter aircraft. Even though modern fighter aircraft are increasingly being manufactured using non-metallic materials, for the foreseeable future it is envisaged most fighter aircraft in the world will remain primarily metal in construction. The implications of using other airframe materials, *e.g.* Carbon Fibre Composites (CFC), is discussed in Sections 3.3.2 and 3.3.3 in comparison to those of 'standard' metal-skinned aircraft. As discussed earlier in this section, modelling at these microwave frequencies is not currently practicable and hence a practical programme of investigations on an aircraft followed. The objectives of this programme were constrained to measuring the absolute attenuation afforded by the airframe, examining any wavefront polarisation or angle of arrival dependency, and establishing whether energy ingress was *via* avionic bay peripheral slots or by some other, internal, energy transportation route.

Prior to conducting the investigations on the aircraft, cut-off frequencies for bay door peripheral slots and panel ingress characteristics were predicted. A model was developed which uses a flat plate concept of the aircraft panel and its peripheral slots. The periphery of each bay door and panel was considered to be a series of isolated individual slots, formed either by the spacing between fasteners or bolts, or by the corners of the panel or door involved. From aircraft drawings and physical measurements the bolt spacings were established for all the bays to be investigated. For each slot so formed its orientation to the local horizontal was noted and its cut-off frequency  $f_c$  calculated using:

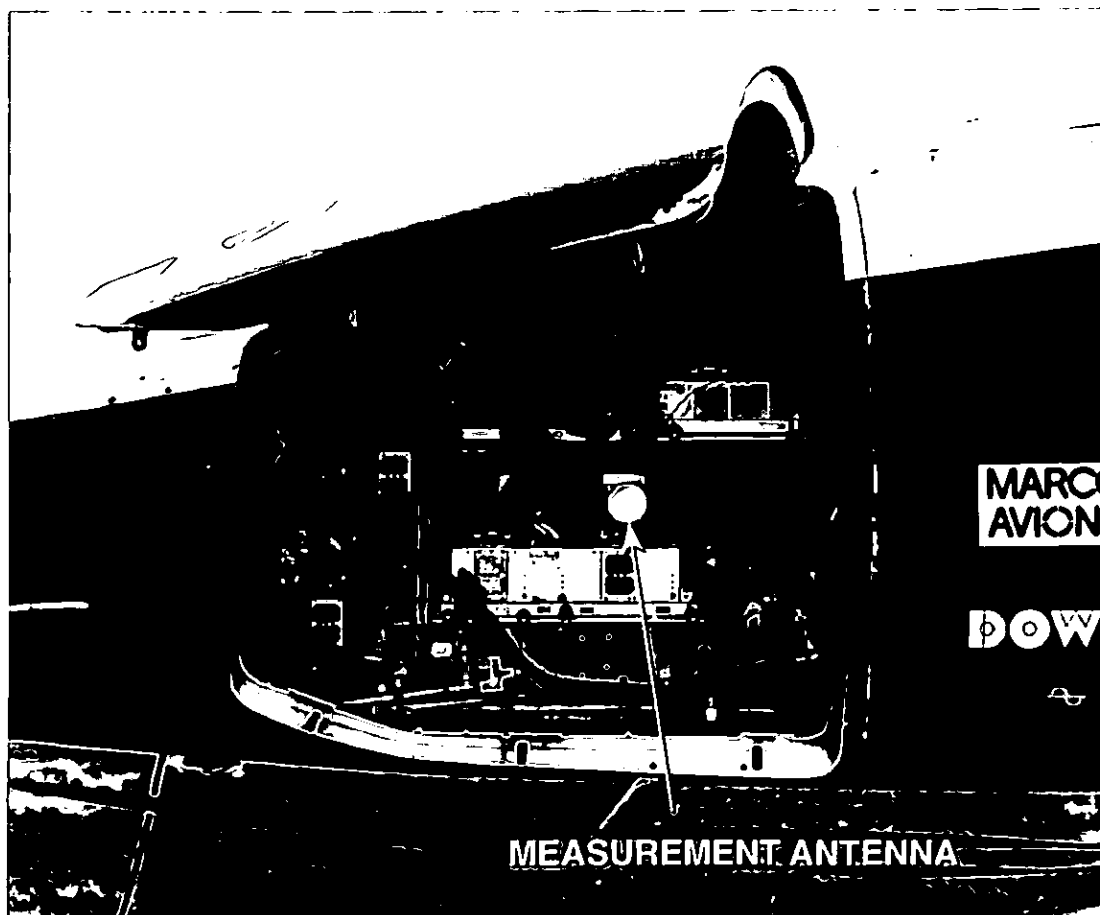
$$f_c = \left( \frac{c}{2d} \right) \quad \dots(3.1)$$

where  $d$  = major dimension of slot and  $c$  = velocity of light,  $3 \times 10^8 \text{ ms}^{-1}$ . The attenuation  $R$  offered to incident radiation was then calculated using:

$$R = 20 \times \log_{10} \left( \frac{d\lambda}{2} \right) \quad \dots(3.2)$$

where  $\lambda$  = wavelength of incident radiation. These predictions form Appendix A of [3-11] and are reproduced as Appendix D herein. Section D.4 of the Appendix gives the limitations of the predictions, explaining why it is thought that such a complex situation will be difficult to model by other than probabilistic methods. One aspect of this, cavity bay resonances, is exemplified by Fig. 3.1 which shows the complexity of the inside of the Front Avionics Bay of the aircraft investigated, noting that six avionics boxes are not fitted in this photograph. Although the model used represents a simple consideration of the problem, it was thought at the time to be adequate to achieve the primary goals of that phase of investigations, *i.e.* quantification of absolute values of airframe attenuation factor and an understanding of its dependency on angle of arrival and transmit antenna polarisation (which was limited to either horizontal or vertical only).

Figure 3.1: Inside Of Front Avionics Bay With Test Measurement Antenna



### **3.3 PRACTICAL MEASUREMENTS**

#### **3.3.1 EMC Demonstrator Aircraft**

The research reported here was conducted at BAe Warton on the metal-bodied Jaguar Fly-By-Wire demonstrator aircraft in 1987/8 [3-12] to [3-14] and 1988/9 [3-15] to [3-18] and [3-11] and has provided a considerable measurement data set to support the study of microwave EM energy ingress and propagation in airframes. Before measuring fields in the aircraft, much effort was expended characterising the open field test site and establishing the 2-18 GHz test technique. Measurements were taken 1.5-2.5 m above ground, where the aircraft fuselage would be during the tests. Investigations were conducted to determine the possibility of multipath affecting subsequent measurements. In multipath both the transmitter's direct wave and reflected wave arrive at the aircraft, resulting in a constructive and destructive interference field pattern along all axes of the aircraft. The effect of this at any given field measurement point is that the field measured may be higher or lower than that due to the direct wave alone. The reflected wave in this case was that due to the test site floor (no obstacles or buildings existed within 300 m of the site in the sector relevant to the investigations). Specular reflections only were considered since a directional transmit waveguide horn antenna was used, the test site floor was rough (asphalt) and, since continuous wave signals were to be used, only strong specular signals would adversely affect the airframe shielding measurements to any degree. Thus, for the conditions prevailing, diffuse multipath was not thought by this researcher and his co-worker Price [3-14] to have been important. This is supported by [3-19] where diffuse multipath effects are excluded as their contribution to the multipath effect seen at the receiving antenna due to these effects is insignificant compared to the effects due to specular scattering.

In accordance with specular reflection theory, the frequency, grazing angle and ground roughness data are used to determine the presence and magnitude of the multipath reflection, with the final attenuation value then determined by path length difference as a function of frequency. This value is then vectorially added to the received signal from the direct wave. Equations and methods of calculating multipath are given in [3-19]. During the investigation the following aspects were examined: alteration of transmit and receive antenna heights, alteration of the depression angle of the transmit antenna from the horizontal, and alteration of transmit-to-receive antenna distance. The first of these proved inconclusive due to instrumentation problems (difficulty of mounting and aligning antennas over a large height range). The depression angle test results, which were repeated over

grass where predominantly absorption and diffuse reflections would occur, showed no appreciable difference between the over-asphalt and over-grass cases, see Fig. 3.2. No peak occurs in the received signal, suggesting absence of strong specular reflections. To confirm these findings an investigation of variation in transmit-to-receive antenna was conducted to study the fluctuation of received signal with increasing distance. These tests were conducted over both a wet and dry test site to establish the effects of water.

The results, see Fig. 3.3, show no appreciable difference between a damp and dry test site and no nulls are seen in the received signal level. The received signal can be seen to be inversely proportional to the separation of the antennas, *i.e.*  $\propto r^{-1}$ , confirming that the losses are free space, *i.e.*  $20\log_{10}(r)$  where  $r$  is the inter-distance, with negligible contribution from ground reflections. Thus, although predictions showed multipath was possible for the configuration tested, the results showed no significant specular multipath effect to be present over the 11 m distance between the transmitter and position of the aircraft.

Figure 3.2: Received Signal vs. Transmit Antenna Depression Angle

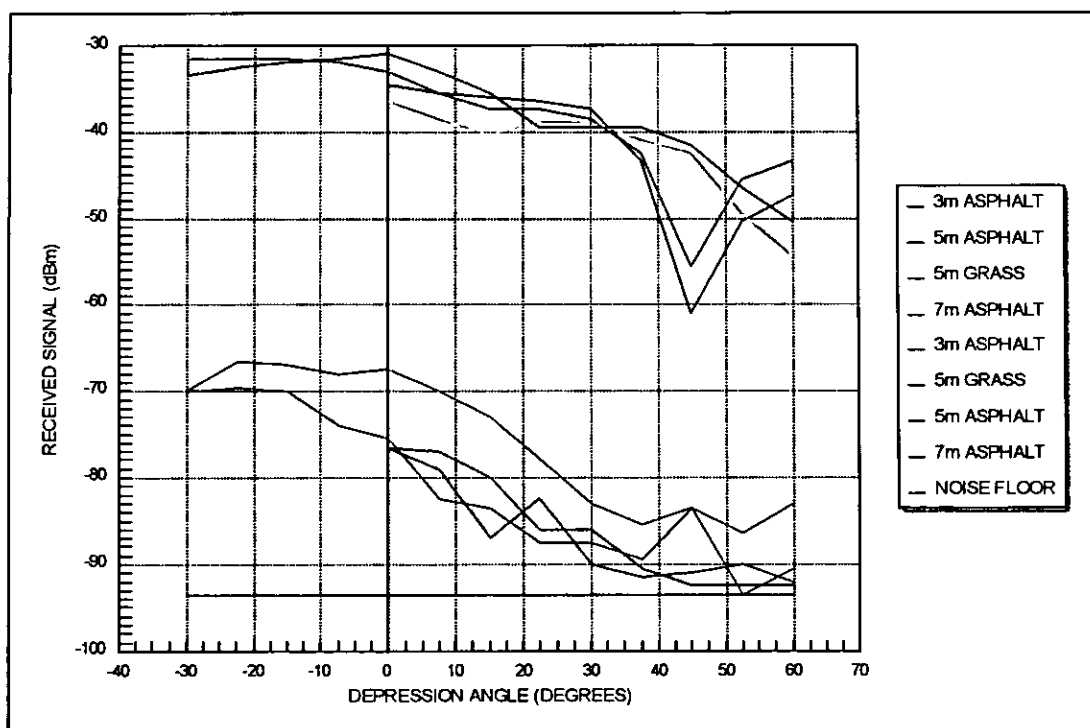
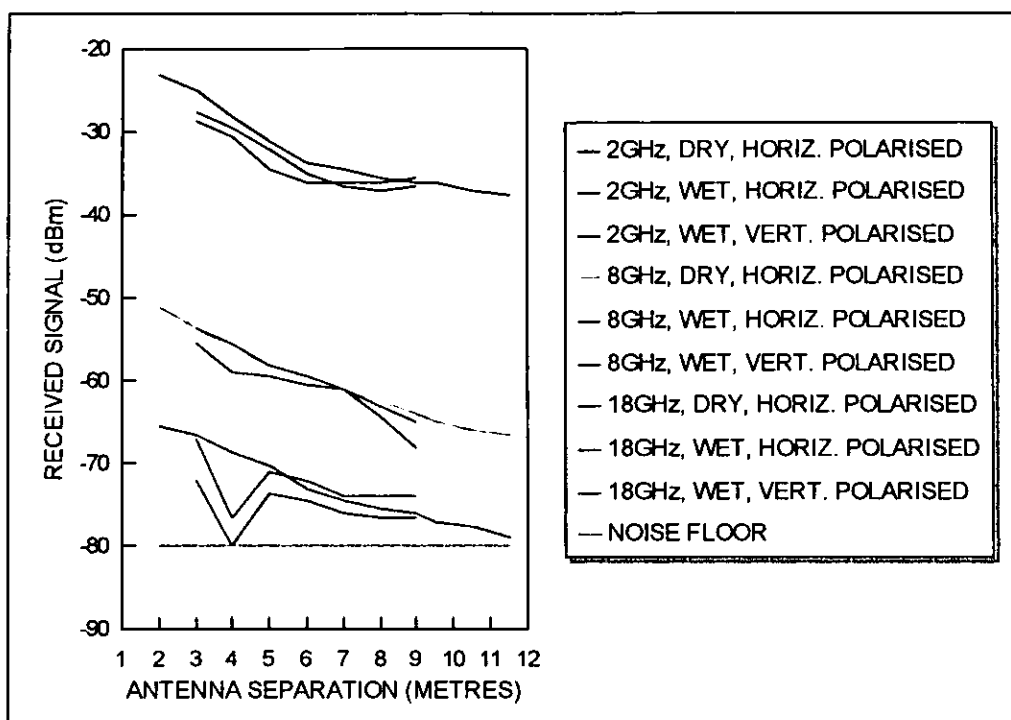


Figure 3.3: Received Signal vs. Antenna Separation



In the initial phase of investigations aircraft internal field measurements were taken at five 2-18 GHz spot frequencies for the Front Avionic Bay and the Port Gun Bay, see Fig. 3.4. Two transmitting configurations were tested, the 'Arc' and 'Slide'. The former attempted to assess the variation of airframe attenuation as a transmitter was moved in a 12 m arc centred on the centre of the aircraft, a similar situation to an aircraft flying past a rotating ground transmitter. The latter involved the irradiation of a relatively small 'footprint' on the aircraft to examine whether microwave energy enters a bay from slots and apertures in the near vicinity of the bay, or whether it is transported internally from elsewhere within the airframe. The existence of this small 'footprint' was confirmed during the site calibration phase of the investigations, see Fig. 11 of [3-17]. Results showed that a frequency dependent airframe attenuation factor existed of the order of 20 dB between 2 and 12 GHz, see Fig. 3.5. At 18 GHz insufficient transmitter power prevented any internal field measurements from being taken. The results as a whole showed that microwave energy penetrated the airframe across the band, with variations of attenuation factor with aspect angle apparently illustrating the effects of shielding and scattering caused by the aircraft wing and inboard pylon. However the exact method of energy ingress was still unclear since (metallic) taping over the joints around the Port Gun Bay door did not affect the original results.

Figure 3.4: Location Of Bays Investigated

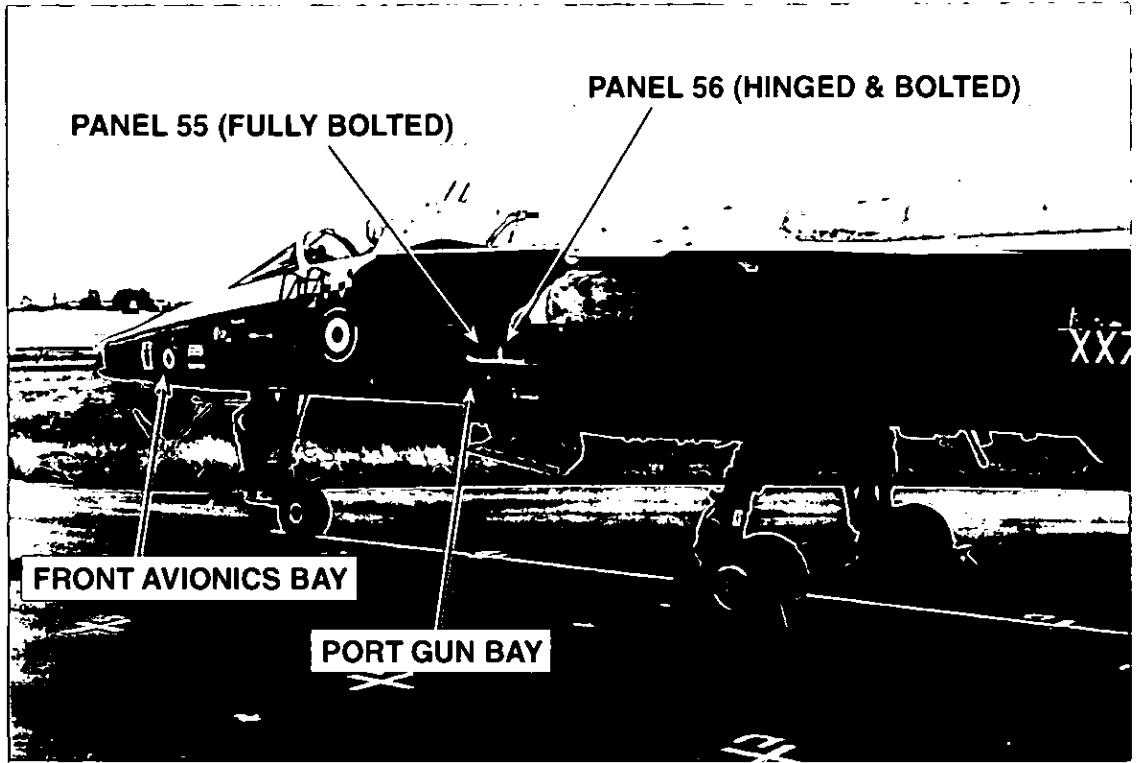
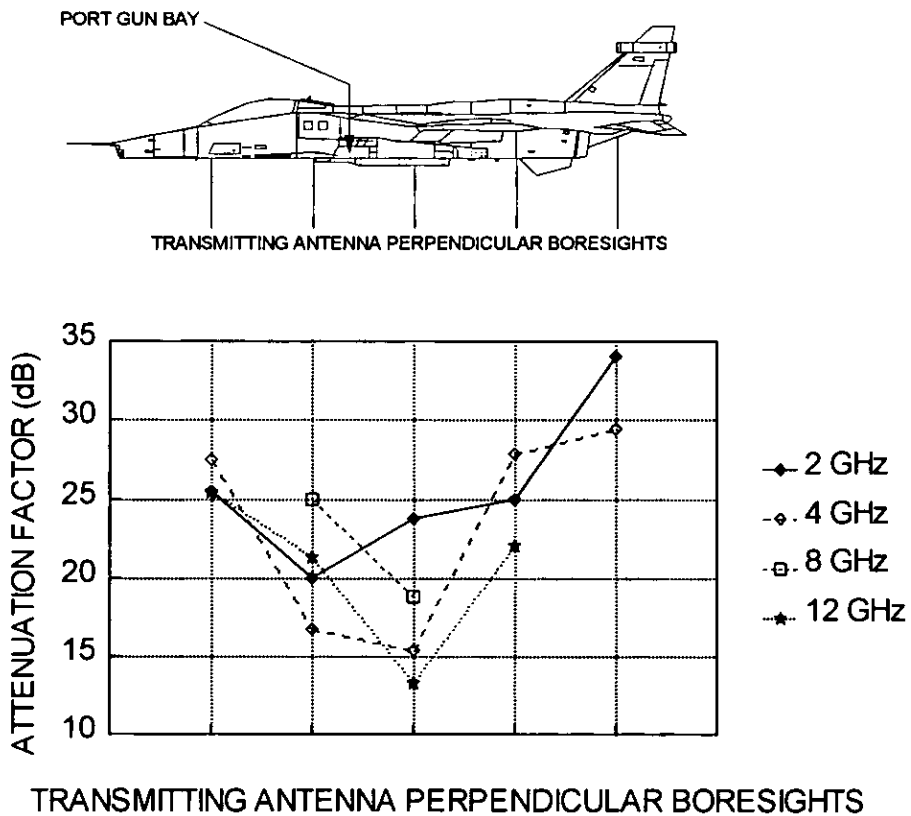


Figure 3.5: 2-12 GHz Airframe Attenuation Factors - Port Gun Bay



Following a proposal for further studies and improved measurement techniques [3-15], a test schedule covering the second phase of investigations was produced [3-16]. These investigations were different to the earlier work in three main areas:

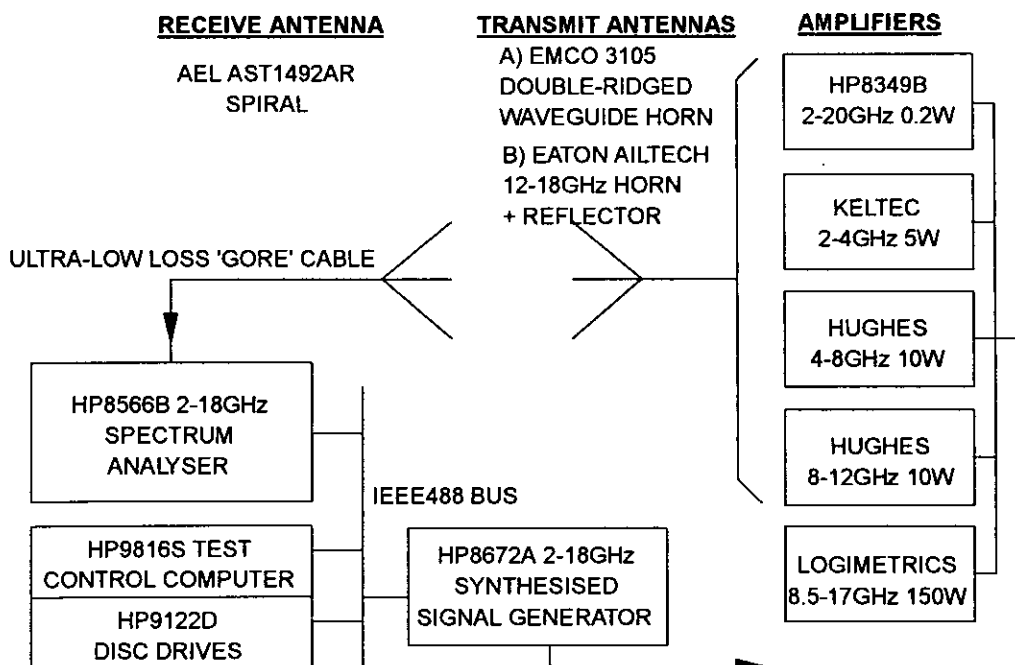
- i) Pseudo-swept frequency measurements in the range 2-18 GHz were to be used, rather than the five spot frequencies used in the earlier work. Pseudo-swept in this context means that a computer-controlled signal generation and measurement system, shown in Fig. 3.6, generated a series of RF emissions with frequency incrementing in 0.5 GHz steps or finer resolution as the research proceeded, with the measurements at each step taking 2-3 seconds (the variation due to test equipment response and settling times).
- ii) A higher power 12-18 GHz amplifier was to be used than the 0.2 W one used before.
- iii) Detailed examinations of energy ingress through bay door/access panel peripheral slots were to be carried out.

As for the earlier tests the value of airframe attenuation,  $A_A$  was calculated from the measured values as follows:

$$A_A \text{ (dB)} = P_{\text{EXTERNAL}} \text{ (dBm)} - P_{\text{INTERNAL}} \text{ (dBm)} \quad \dots(3.3)$$

where  $P_{\text{EXTERNAL}} =$  power measured at measurement location with no aircraft present, *i.e.* at site calibration, and  $P_{\text{INTERNAL}} =$  power inside bay with door or panel closed.

Figure 3.6: Test Equipment Arrangement For Aircraft Investigation



In each case the power measured was normalised to remove the variation in transmitter amplifier output with frequency and transmitter feeder and receiving antenna cable losses were accounted for, as were the gain vs. frequency characteristics of the transmit and receive antennas used. No noise breakthrough, *i.e.* test signal coupling to the instrumentation cabling and test equipment rather than to the receive antenna, was recorded during the investigations. Full sets of  $A_A$  statistical data and detailed discussions of all test results are given in [3-11],[3-17] for the Arc and Slide phases of the investigations for all four bays examined. Figs. 3.7 and 3.8 show the statistical data for the Slide tests on the Front Avionics Bay and Arc measurements on the Bay behind Panel 55, both for the horizontal transmit antenna polarisation case. The latter Figure also shows the associated 2-12 GHz  $A_A$  graph for each transmitter position, indicating the complexity of results interpretation.

For each transmitter position investigated, the 2-12 GHz measured  $A_A$  data sets were examined to establish the minimum, mean, maximum and standard deviation ( $1\sigma$ ). This enabled examination of angle of arrival dependency. The 12-18 GHz range was examined later in the programme when a higher power (200 W) RF amplifier became available, since the initial work showed that the 200 mW amplifier used at first gave signals which could not be measured above the noise floor with the bay door or panel closed. In those later tests, where only a limited data set was possible due to aircraft availability, a three-point data smoothing algorithm was used instead of the statistical treatment of the much larger data sets from the 2-12 GHz research, since only confirmation or otherwise of the attenuation trend with that for 2-12 GHz was required. For the discussions which follow on  $A_A$  trends by bay type and transmit polarisation, and subsequent comparisons between them, it was necessary to arrive at some common attribute. Analysis of the complex profiles were attempted by the use of a 'Figure of Merit' (FoM) approach, described in Appendix E. This approach, in which the higher the FoM the higher the probability of encountering a higher value of  $A_A$ , is illustrated in Appendix E, Figs. 11 and 12. When compared to Figs. 3.7 and 3.8 (noting that they are for different bays) the general trend with angle of arrival of the EM wave can be seen: higher  $A_A$  when either the transmit antenna is pointing away from the bay in question, or when obscuration of the bay by other parts of the airframe occurs, *e.g.* for nose-on irradiation of the aircraft. However, as noted in Appendix E, these values of FoM are not quantitative and therefore cannot be used directly to quantify  $A_A$  or compare values of  $A_A$  between different bays and test configurations. It was thus decided that the attribute

referred to above would be the mathematical average of the mean values of all data sets for each bay at each specific frequency. For the remainder of Section 3.3.1 this EMC demonstrator attribute will be referred to as the 'average'  $A_A$  value.

The value of airframe attenuation factor (approximately 25 dB) found in the earlier tests was confirmed, but with appreciable variation which was seen to be chaotically dependent on frequency when fine resolution frequency steps were used. Less evidence of the shielding and scattering caused by changing the angle of arrival of the radiation was seen during the first block of tests. The second set of tests covered 2-12 GHz internal field measurements in the Port Gun Bay, the bay behind the fully bolted Panel 55, and in the bay behind bolted/hinged Panel 56, see Figs 3.4 and 3.9.

Figure 3.7: Attenuation Factors: Front Avionics Bay (Slide Test)

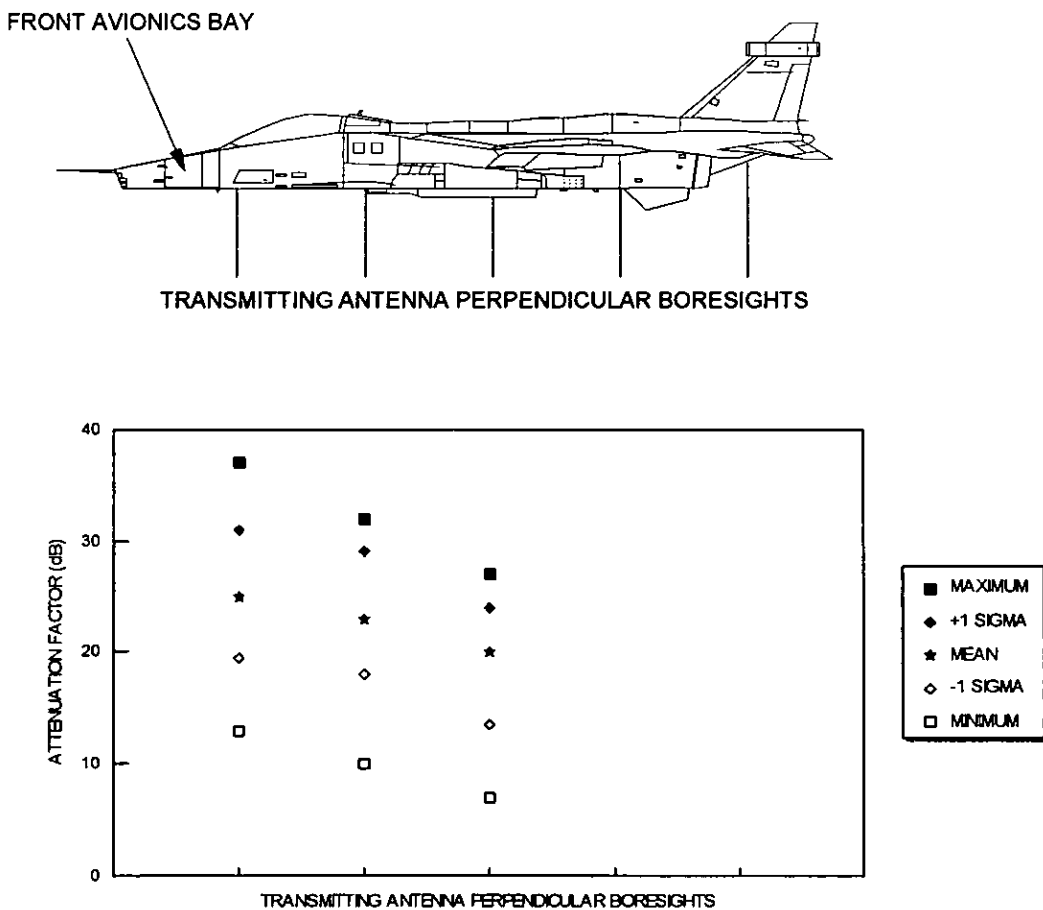


Figure 3.8: Attenuation Factors: Panel 55 Bay (Arc Test)

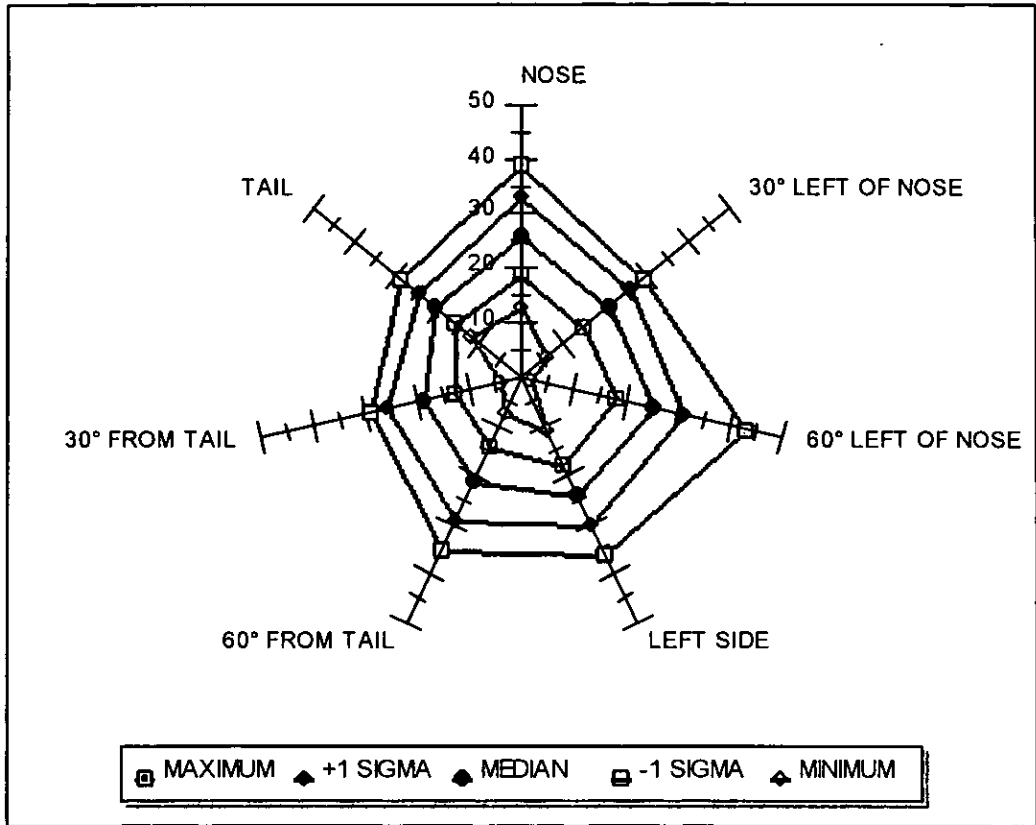
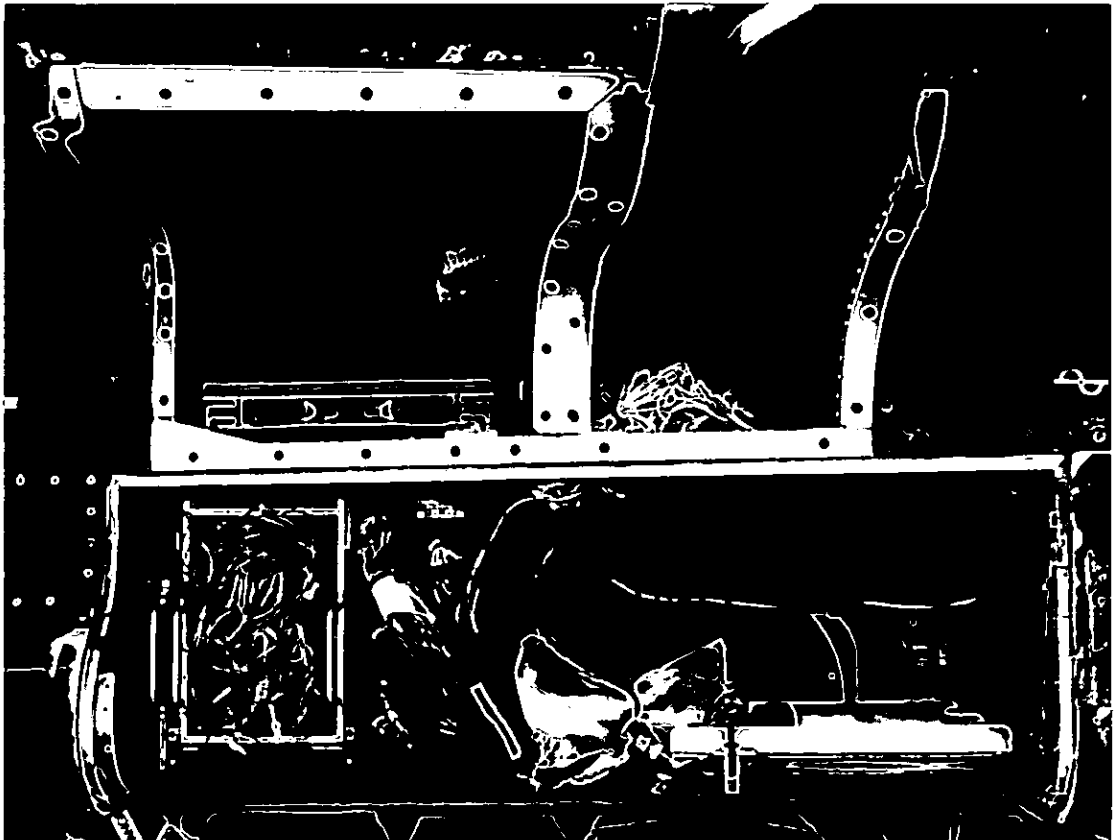


Figure 3.9: Different Bay Types Investigated

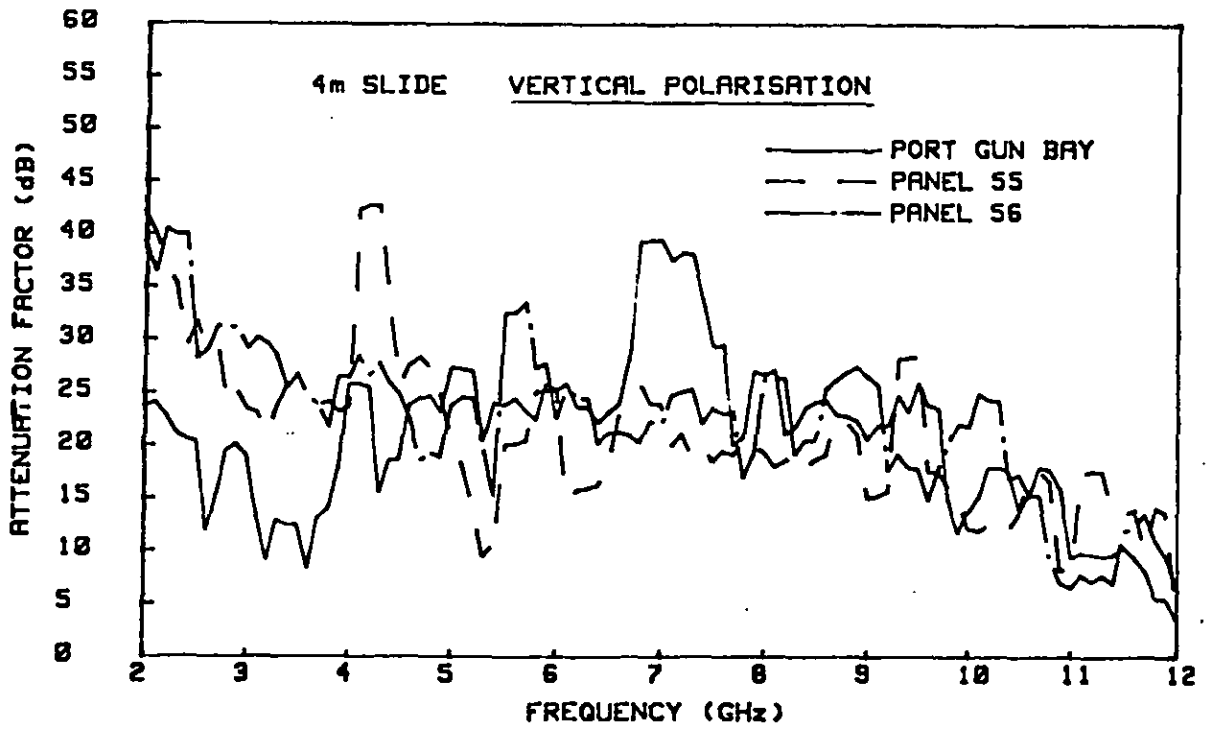
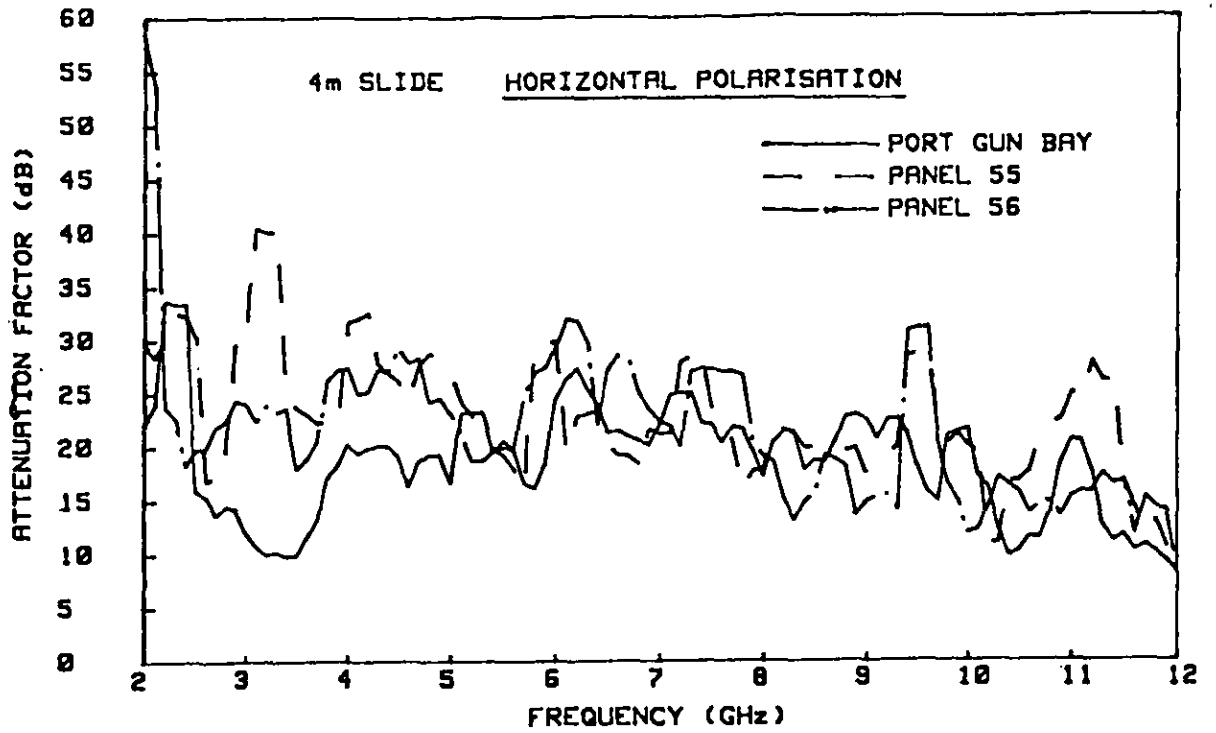


The 2-12 GHz results yielded average values of 22.4 and 13.0 dB respectively for the highly frequency dependent  $A_A$  for the shoot-bolt type bays (Front Avionic and Port Gun). For the bays behind bolted and bolted/hinged Panels 55 and 56 the average  $A_A$  were 19.8 and 19.2 dB respectively. The range of the 'average' attenuation factors for the bays lay between  $\pm 3.0$  and  $\pm 6.8$  dB. For the latter two bays and for both transmitting antenna polarisations, the results also showed (see Fig. 3.10) that the attenuation decreased at 17 dB per decade of increasing frequency which compares favourably with the 20 dB per decade predicted. However the cut-off frequencies predicted for the bolted bays were not seen in the measured data, with extrapolations of the latter giving approximately 18 GHz rather than the 6 GHz predicted. This phenomenon appears to result from limitations of the prediction model. The results suggest that airframe attenuation may have to be derived by a probabilistic assessment based on panel/door type, size of peripheral slot, airframe material and finish, and aperture sizes. No dependence of attenuation factor was seen with angle of arrival of the impinging wavefront for any of the four bays investigated, despite the initial indications from the first phase of the investigations.

The results of the 'Slide' measurements, with their small irradiation 'footprint' on the aircraft, strongly suggests that most 2-12 GHz ingress occurred via the panel's peripheral slot. However two sets of measurements, one with the transmitter head-on, the other with it tail-on to the aircraft, both gave only approximately 20 dB attenuation, rather than the much higher figure ( $>60$  dB) expected as the bay concerned was shielded from the transmitter. This remains to be explained, but suggests internal transportation of energy.

The average attenuation factors were approximately 20 dB for the bays investigated, but there were a number of frequencies and aspect angles where values of 0-10 dB were measured, with some seen at a maximum of 59 dB. This agrees to an extent with initial measurements by Willis on a prototype helicopter and two (unspecified, but certainly military) aircraft in 1986 [3-20], Carter, Stevens and Watkins on a Puma helicopter in 1991 [3-21], and measurements at BAe on a modern military aircraft in 1992. The prototype helicopter, illuminated from nose and tail gave attenuation of 21-36 dB for 2-18 GHz; whilst port and starboard gave much lower values at 5-20 dB and 5-10 dB respectively for 2-18 GHz. The two aircraft were only illuminated from the port side and values of approximately 35 dB (Avionics bay) and 25 dB (just above cockpit floor) were obtained. The modern aircraft measurements are covered in more detail in Section 3.3.2.1.

Figure 3.10: Frequency Dependence Of Panels 55/56 Bays' Factors



To see whether any trends in  $A_A$  exist, either between the fixed wing aircraft investigated or between the fixed and rotary wing aircraft, the data sets from these trials were examined. Table 3.1 gives the key aspects of each of the trials and results of initial statistical treatment of each trial's data sets.

Table 3.1: Key Aspects of Trials and Initial Statistics

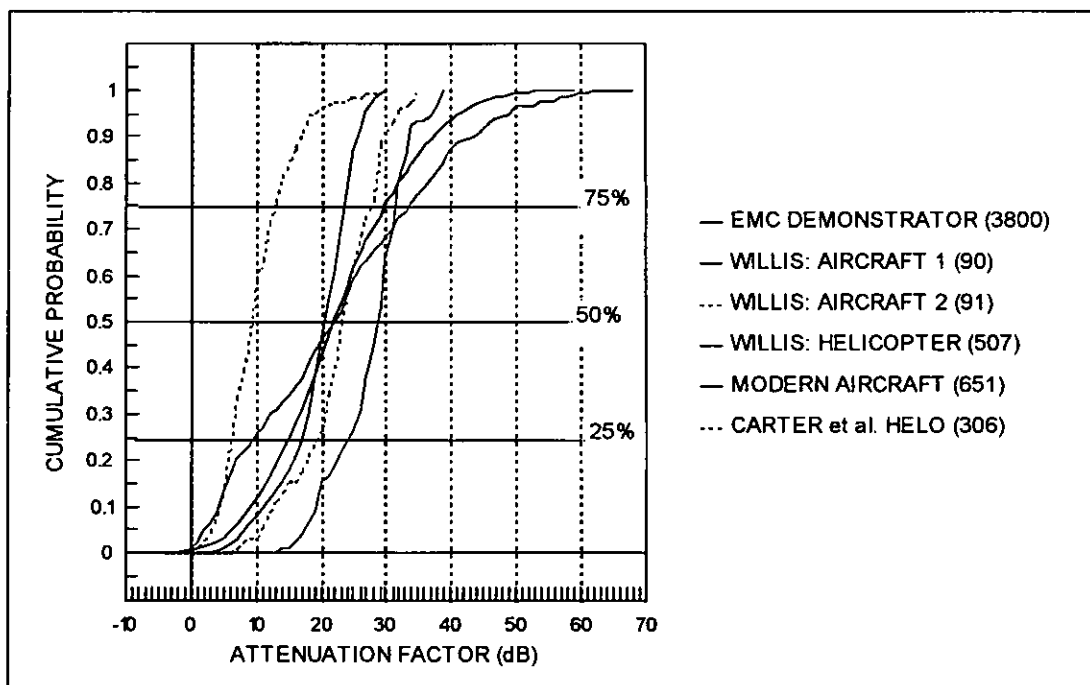
AIRCRAFT TYPE	RESOLN. (MHz)*	BAY TYPE	AVG (dB)	MAX (dB)	MIN (dB)
DEVPT. HELICOPTER	500	PILOT SEAT	26	31	18.5
	500	CENTRE CONSOLE	20	54	0
	500	CENTRE CABIN	13.8	39	0
	500	AFT CABIN	19.8	31	0
	500	RADIO	34.7	50	10
AIRCRAFT TYPE A	500	FRONT COCKPIT 0.3m OFF FLOOR	25	31	14
	500	PORT ELECTRICAL	32	39	28
AIRCRAFT TYPE B	500	FRONT COCKPIT 0.5m OFF FLOOR	21	27	7
	500	PORT AVIONICS	28.1	35	12
FLY-BY-WIRE JAGUAR	500	FRONT AVIONICS	22.4	43	2.5
	100	PORT GUN	13	44	-0.8
	100	PANEL 55	19.8	59	-3.2
	100	PANEL 56	19.2	59	-2.3
PUMA HELICOPTER**	50	INSIDE MAIN CABIN DOOR - DIRECTIONAL SENSOR	10.3	26.9	-1.6
	50	-ditto- ISOTROPIC SENSOR	---	24.6	-2.3
MODERN FIGHTER	50	STBD. AVIONIC BAY 1	24	36.9	12.8
	50	STBD. BAY 2: FRONT	22	36.9	15.7
	50	STBD. BAY 2: REAR	21	35.8	14.3
	50	PORT AVIONIC BAY 1: 3 m OFF GROUND	18	37.2	7.6
	50	PORT AVIONIC BAY 2: 1m OFF GROUND	25	43.4	17.6

\*The table gives the principal test resolution. For entries >50 MHz it is acknowledged that some individual tests were done with higher resolution.

\*\*Data sets unavailable, so directional sensor measurements, taken with horizontally polarised transmit and receive antennas and without mode stirring, were digitised from Figs.9-11 of [3-21] for use in Table 3.1 and Fig.3.11. Maximum and minimum isotropic sensor values for this table were scaled from all appropriate figures in [3-21].

The table shows a wide range of  $A_A$  values for the different fixed wing aircraft types and helicopters: maxima (34.4 dB), minima (31.2 dB) and average (24.4 dB). From the data examined there appeared little correlation between the data sets but it was observed that the bulk of many of the data sets lay within  $\pm 3$  dB of the set's median, particularly where measurements were taken with  $<100$  MHz resolution. A further observation was that the median of the average values of  $A_A$  was 21.0 dB with a  $1\sigma$  of 5.9 dB. Together these observations suggested the possibility of a *generic* trend of airframe attenuation and to examine this possibility the data sets were subjected to further statistical treatment. The technique used was to determine the cumulative distribution of each data set, *i.e.* the percentage of each data set *vs.* increasing  $A_A$ . Fig. 3.11 shows the resultant distributions by aircraft type examined, with the number of data samples given in parentheses.

Figure 3.11: Comparison Of Airframe Attenuation Statistics



These distributions are more useful than the rapidly changing  $A_A$  values with frequency in determining the contribution of  $A_A$  to the overall ingress equation and the potential for avionic circuit upset. Slight variations in frequency, aspect angle, transmit polarisation and internal measurement location can each change the attenuations measured, whereas this statistical representation tends to remain unchanged. The comparison of the EMC demonstrator and other data sets, each with a significantly lower number of data samples, suggests that the distributions would be closer to that of the EMC demonstrator if a

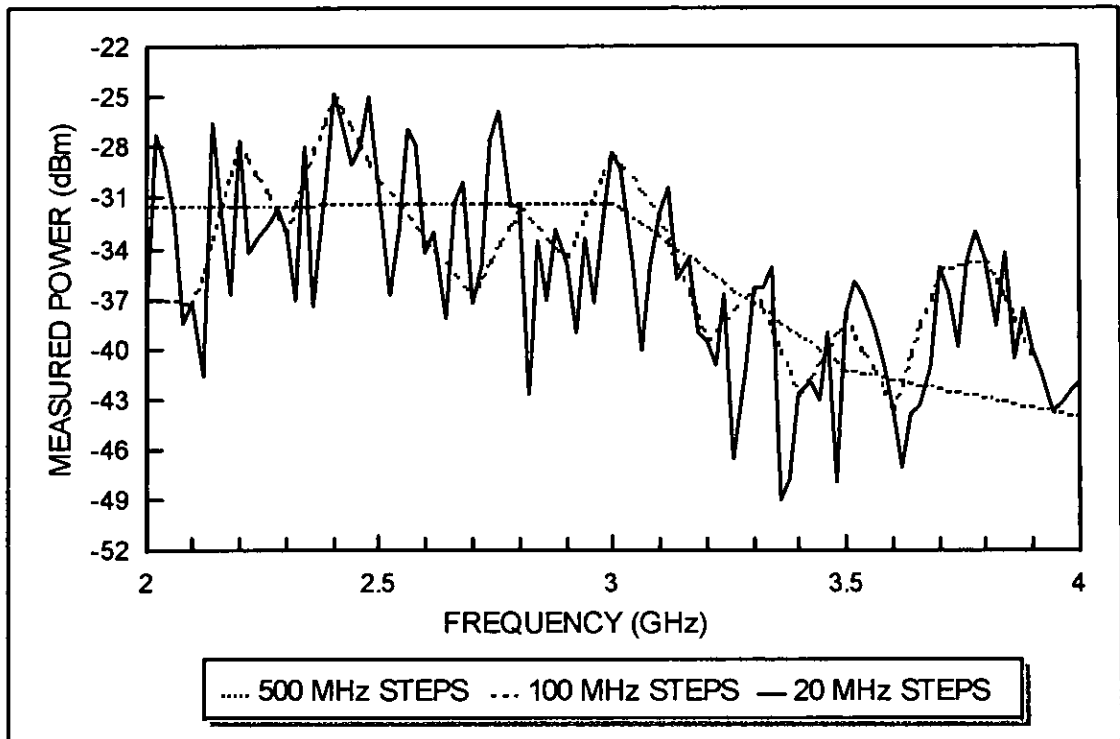
matching number of samples were available from the other trials. With the exception of the Carter *et al.* helicopter line, where only one data set has been analysed (see Table 3.1) and thus is thought to be of lower importance, Fig. 3.11 suggests that a prediction of  $A_A$  of  $21 \pm 9$  dB can be made which may also be independent of air vehicle type. These are important findings as, if true, it offers the potential for supporting the microwave EMC design and clearance of military and civil aircraft without tests on aircraft. Appropriate confidence in safe and correct system operation could then be gained through equipment EMC qualification laboratory tests and consideration of the contents of a database of equipment EMC results for a given aircraft. This is discussed in more detail in Chapter 7.

Further research is required to explore this potential, which offers substantial time and cost savings to both the civil and military sectors of the aircraft industry. Initially all available measured data, including that from other sources (*e.g.* SAAB are known to have taken measurements on the Gripen fighter), should be analysed by frequency sub-band to examine the validity of the  $A_A$  prediction, both by aircraft type and between individual aircraft of a given type. If the prediction is still deemed valid, further confidence should be attained by augmenting the existing data by selected measurements on BAe military aircraft types on which data does not yet exist.

The key findings of these airframe attenuation investigations have been published in the I.E.E. *Electronics Letters*, Vol.32, No.18 (29 August 1996), see Appendix H.

The attenuation factor on the EMC demonstrator was seen to have a behaviour similar to a low Q resonant cavity, which was more pronounced when tests were repeated with finer frequency steps. The original investigations were performed in 0.5 GHz steps, and a short investigation of the necessary resolution for adequate characterisation of the aircraft was carried out at 0.1 and 0.02 GHz steps in the range 2-4 GHz, where the results were still found to exhibit this behaviour, see Fig. 3.12. The remaining tests, which as with all the aircraft tests involved free space transmissions, were carried out at 0.1 GHz steps to minimise potential interference to other users of the band. Since there is believed to be significant analogy between the airframe, its avionic bays and the avionics boxes therein, this characteristic is expected to be apparent for each case. When the above work is taken into account, the average value of 2-12 GHz attenuation on this aircraft remains 18.6 dB, independent of angle of arrival and transmitting antenna polarisation.

Figure 3.12: Test Frequency Resolution



During the second phase of investigations an examination of cavity resonances in aircraft bays was carried out. Comparison of the Bay 55 and Bay 56 results against the predictions of Appendix F, which are based on cavity theory applicable at microwave frequencies [3-22] to [3-24], strongly suggests that at least two-, if not three-axis cavity excitation is present in both since the minimum frequency spacing of the resonances measured for each bay are less than 100 MHz (the measurement resolution). This is well below the 320.5 MHz (Bay 55) and 250 MHz (Bay 56) minimum values in Appendix F for single-axis excitation. The limited work done with 10 MHz measurement steps on the Front Avionics Bay showed resonances as close as 20 MHz with major excursions at approximately 200 MHz intervals. These results suggest that three-axis mode excitation is also present for this type of large (six times the volume of Bay 55) and cluttered bay. Such multi-axis excitation probably results from the distributed source formed by the multiple slots formed around the periphery of the bay door by bolt pairs. These peripheral slots are complex in shape, often having horizontal and vertical components, e.g. the Port Gun Bay. In conjunction with the large number of bay types on a given aircraft type, production build tolerances between the same bay on identical aircraft, variability of air gaps and materials between the bay door and its landing, intra-slot resonances, and different bay contents, these factors combine to make the accurate modelling of such peripheral slots and the

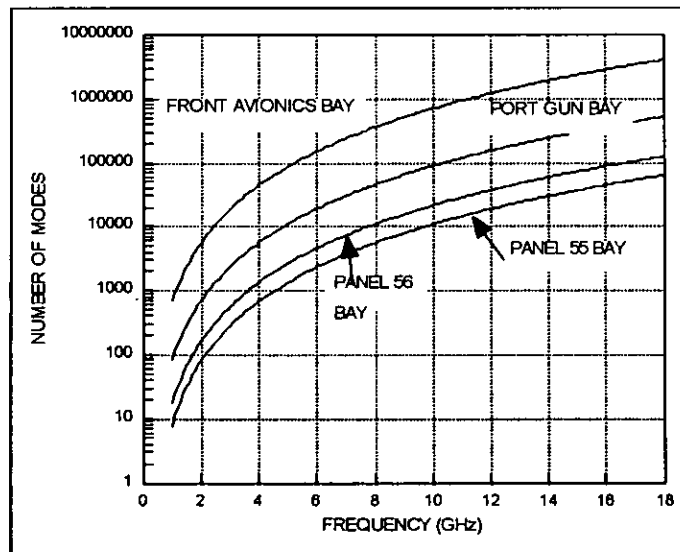
cavity resonances in the bay impractical. It is feasible that the ingress prediction of Appendix D could be improved by treating each door or panel as a multiple source emitter, where each individual slot's effects are superimposed. This would enable a better comparison with measured resonance spacing data and warrants further study.

The equations of Appendix F assume a totally closed, un-loaded and air-filled rectangular box with perfectly conducting inner surface, which behaves as a resonator with an infinite number of modes. At microwave frequencies the size of bays investigated (the smallest was 0.468 m x 0.426 m x 0.175 m and the largest was 1.61 m x 1.39 m x 1.0 m) can be considered to be well 'over-moded'. The total possible number of modes  $N_s(f)$  in such a cavity can be shown, see Crawford and Koepke [3-25], to be

$$N_s(f) = \frac{8\pi}{3}abd \left\{ \frac{f}{c} \right\}^3 - (a+b+d) \frac{f}{c} + 0.5 \quad \dots(3.4)$$

where  $abd$  is the cavity volume,  $f$  is frequency and  $c$  the velocity of light. Fig. 3.13, using Eqn. 3.4, shows the number of modes vs. frequency for each of the four aircraft bays (Aluminium construction assumed).

Figure 3.13: Total Number of Modes as a Function of Frequency



The avionics bays considered do not have perfectly conducting inner surfaces, have many items of differing permeability and permittivity in their volumes, and have apertures linking them to other bays within the airframe, each of which affect the resonant frequencies present. For example if the bay were totally filled with a material of relative permittivity

$\epsilon_r$  and relative permeability  $\mu_r$  then the resonant frequencies equation in Appendix F would be modified to:

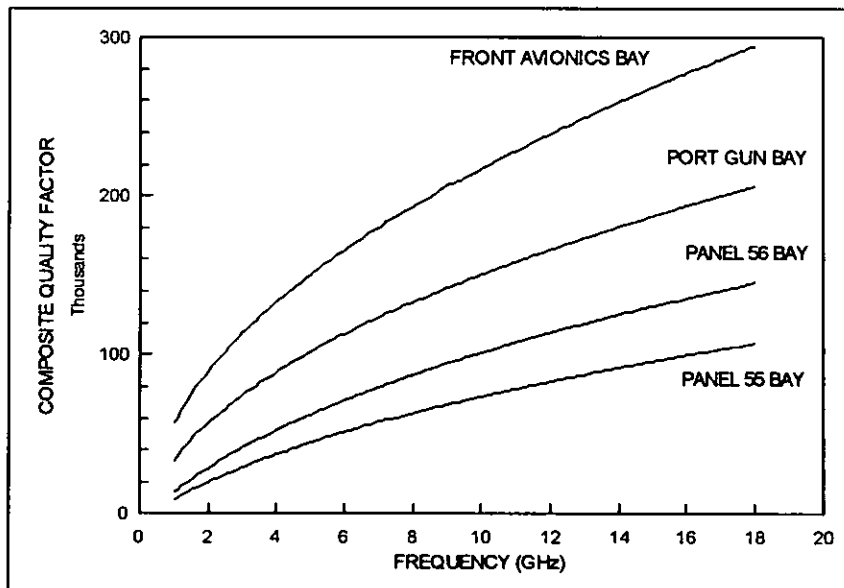
$$f = \frac{1}{2} \sqrt{\frac{\left(\frac{l}{x}\right)^2 + \left(\frac{m}{y}\right)^2 + \left(\frac{n}{z}\right)^2}{\mu_0 \mu_r \epsilon_0 \epsilon_r}} \quad \dots(3.5)$$

where  $x$ ,  $y$ , and  $z$  are the dimensions of the cavity;  $l$ ,  $m$  and  $n$  are the integers providing the mode numbers for the field pattern inside the cavity, e.g.  $TE_{lmn}$ ,  $\mu$  is the permeability and  $\epsilon$  the permittivity of free space (subscript  $o$ ) and that of the medium relative to free space (subscript  $r$ ). The amplitude of the resonances inside the cavity, of importance to the potential for avionic upset, is determined by the  $Q$  of the cavity, which in turn is optimised for an un-loaded, perfectly conducting, aperture-less cavity. Since, see Fig. 3.13, so many modes can exist in the un-loaded bays, each with its own  $Q$  value, it is not trivial to define a  $Q$  for each bay as a whole [3-25]. A composite  $Q$  can be obtained, see [3-25], from the following equation

$$Q = \frac{3}{2} \frac{V}{S \delta_s} \frac{1}{1 + \frac{3\lambda}{16} \left(\frac{1}{a} + \frac{1}{b} + \frac{1}{d}\right)} \quad \dots(3.6)$$

where  $V$  is the bay's volume,  $S$  its internal surface area,  $a, b, d$  its internal dimensions and  $\delta_s$  the skin depth of the bay wall at the frequencies concerned. Fig. 3.14 plots Eqn. 3.6 and shows the high values of  $Q$  attainable for the (unrealistic) completely closed bays.

Figure 3.14: Composite Quality Factor For Bays Investigated



In practice microwave resonators can have a  $Q$  between 1000 and 30000, but this is severely degraded by either losses in the cavity wall, noting that the surface roughness is

often comparable with the skin depth at microwave frequencies ( $2 \mu\text{m}$  at 1 GHz for copper); for a copper, air-filled cubic cavity resonant at 10 GHz, the Q is about 10,730 [3-24]. Avionic bays and boxes, being usually made of aluminium (of lower resistivity than copper), would be unable to attain such values of Q due to losses in the walls, even if un-loaded. Lossy material loading and the inclusion of apertures (which enable energy loss from the cavity), both of which exist for all practical bays and boxes, further degrades attainable Q. In practice the contents of avionics bays are complex, see Figs. 3.1 and 3.4, and have some components (e.g. cable looms) which can move a number of microwave wavelengths in all three axes with time and aircraft manoeuvres, and thus do not lend themselves to being analysed by mathematical modelling.

By carefully lining the sides and rear of three of the bays with Radar Absorbent Material (RAM) it was shown that the substantial cavity resonances, present within them, could be considerably reduced in amplitude and modified in frequency content (as covered earlier in this section). This effect is demonstrated for the Panel 55 bay in Fig. 3.15, where measurements were taken with the receiving antenna deep in the bay, first without RAM and then with the RAM lining. Although both measured profiles have the wide amplitude variation with frequency previously seen during these investigations, the difference between them is 20 dB for much of the range 2-12 GHz. Similar profiles were seen for the Front Avionics Bay and the Panel 56 Bay and 2-12 GHz damping of 12 and 17 dB respectively was measured. Fig. 3.16 shows best fit line for the Panel 55 bay and those for the other two bays are similar, see [3-11], Figs 19 and 20. As for many of these aircraft investigations, little difference is seen between the transmit polarisations, and the Figure demonstrates the appreciable amount of damping achievable with a simple installation of RAM. It is probable that these figures could have been higher but for the fact that, due to the many pipes, equipment trays and wiring looms within the bays, it was impossible to completely line the sides and rear of each bay. It was also impossible to completely cover the large aperture in the wall between the Panel 55 and Panel 56 bays. Failure to completely line all but the door of the bay prevents a categorical statement that bay resonances are *only* excited by the energy entering *via* the door/panel peripheral slots, although for the bays investigated the results show this to be the most probable conclusion. Further work is warranted as these results suggest that selective RAM placement within bays can considerably reduce the bay internal field amplitude, thus offering a potentially low cost safety margin against the risk of avionic upset.

Figure 3.15: Panel 55 Bay Cavity Resonances

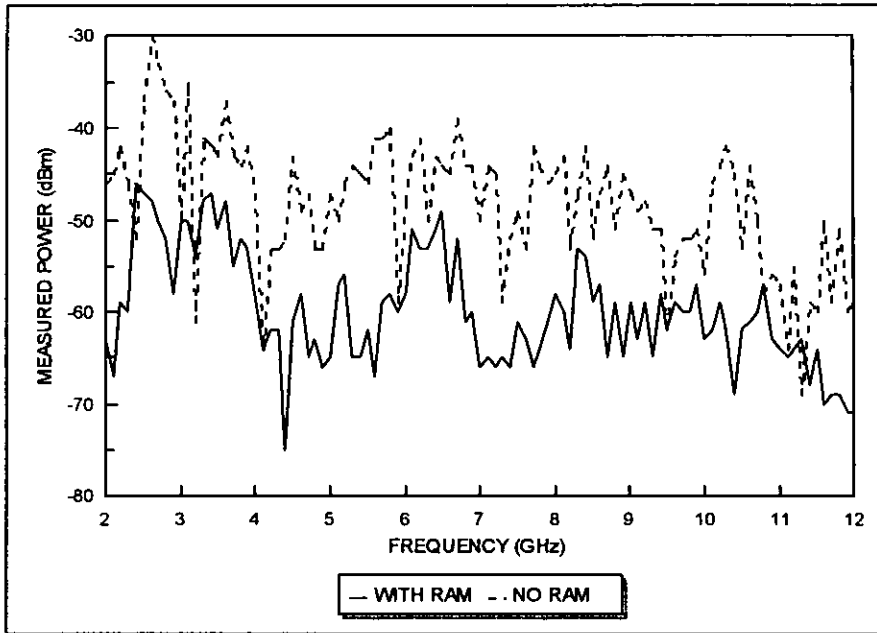
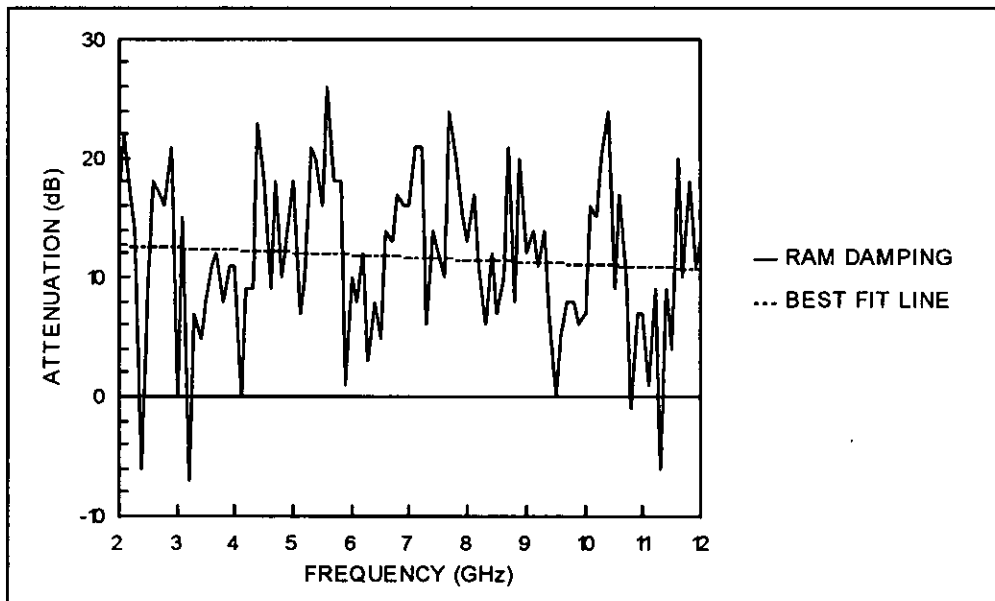


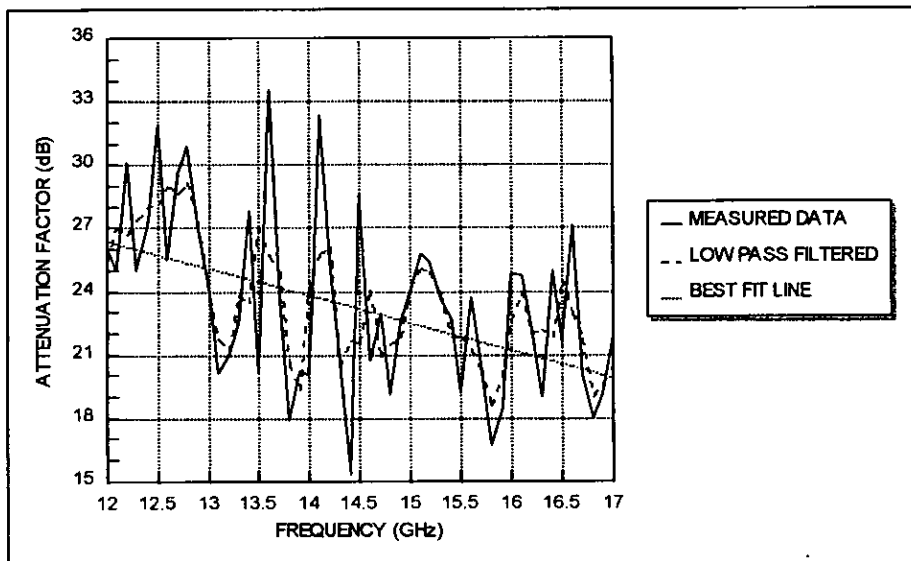
Figure 3.16: Resonance Damping: Best Fit Line for Bays Investigated



The final investigations conducted on the demonstrator aircraft covered airframe attenuation measurements in the 12-17 GHz region [3-12] which had previously not been successful due to inadequate RF transmitter power. These were not full characterisation tests, but briefly examined whether the zero attenuation factor effect at 18 GHz, indicated by the earlier 2-12 GHz bolted bay results (see Fig. 3.10), in fact existed. The investigation, conducted with a test resolution of 0.1 GHz, did not confirm this effect but,

in common with many of the 2-12 GHz measurements, yielded an average  $A_A$  of 23.5 dB. Fig. 3.17 shows a decreasing profile with increasing frequency at approximately 13 dB per decade. No conclusion could be made with the small amount of data and the end of aircraft availability prevented further examination of the 2-12 and 12-17 GHz boundary between the two phases of tests. A possible reason for the effect not occurring is that, with increasing frequency, the impedance of the peripheral slots on the fully bolted panel investigated increases, thus reducing the joint leakage. This topic is covered in Chapter 4.

Figure 3.17: 12-17 GHz Attenuation Factors



In conclusion, the BAe aircraft investigations provide a body of evidence to support the postulation that 2-17 GHz energy ingress is predominantly via apertures in the immediate vicinity of the bay of interest and is more usually *via* the peripheral slot of the door or panel fronting that bay. Due to the complexity of the airframe microwave energy ingress situation uncovered by the aircraft tests, it was recommended [3-4] that no further work be done on-aircraft until research work on simple models of bays and their front panels/peripheral slots and gasketing was carried out in a controlled RF environment. These recommendations were subsequently expanded into a proposed set of bolted panel shielding investigations in [3-26] which were conducted later, see Section 3.3.3. The results of the airframe attenuation research [3-27] were presented at the I.E.E. 7th International Conference on EMC, see Appendix E. Of additional note is that, in the post-presentation discussion, one U.S. delegate at the conference noted that these findings were in line with U.S. and Israeli work.

### 3.3.2 Modern Aircraft

#### 3.3.2.1 Military Aircraft

Most modern military aircraft just reaching in-service use or currently under development have substantially increased amounts of composite materials, *e.g.* CFC, used in the construction of the airframe skin compared to earlier generation metal-skinned aircraft. Table 3.2 shows this trend, in terms of percentage by skin area (rather than overall weight), whilst Fig. 3.18 depicts the distribution of materials in a modern aircraft and Fig. 3.19 shows the typical construction of a CFC aircraft panel.

Table 3.2: Use Of Composites In Military Aircraft

AIRCRAFT	FIRST FLIGHT	COMPOSITES (%)
McDonnell Douglas F/A 18	1974	10
BAe Harrier II	1978	24
Dassault Rafale	1986	50
SAAB Gripen	1987	30
Lockheed YF-22	1990	28
BAe Eurofighter 2000	1994	90

Figure 3.18: Modern Airframe Materials

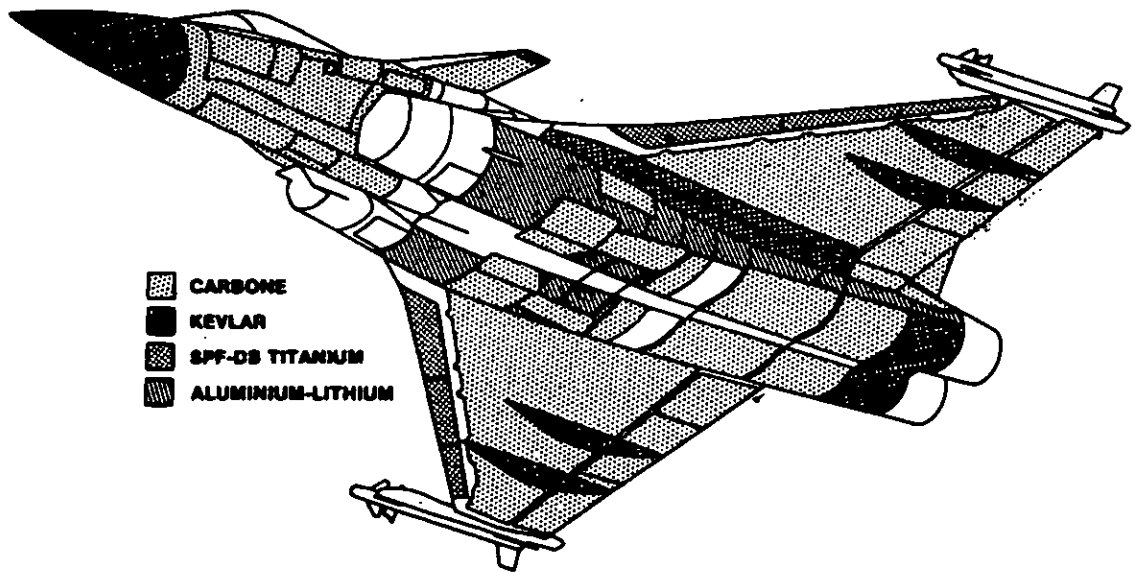
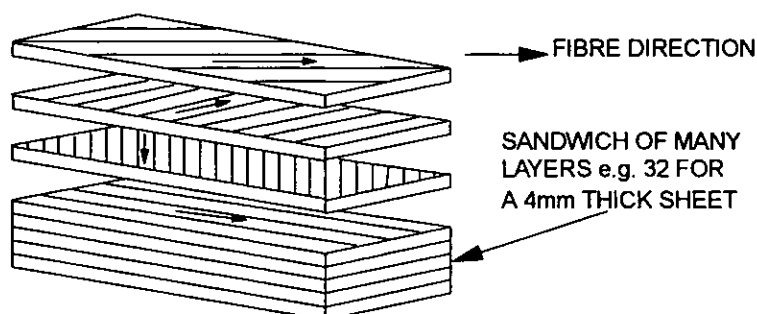


Figure 3.19: Typical CFC Panel Construction



The use of such materials, whether in sandwich or honeycomb construction aircraft skins, raised the possibility of additional RF energy ingress as their shielding performance is worse than the aluminium and other metals traditionally used in airframe manufacture. This is to be expected as  $\sigma$  for CFC is 0-20  $\text{kSm}^{-1}$ , some 1000 times lower than for aluminium (35-40  $\text{MSm}^{-1}$ ). Although this topic had been well researched in the HF band by the commencement of this research programme, the shielding performance of these materials at microwave frequencies had not been quantified. Following on from the aircraft research reported in Section 3.2 recommendations were made to investigate this topic in the BAe EMC Laboratory at Warton and the results are discussed in Section 3.3.3.

Subsequent to the aircraft research conducted by the this researcher, microwave airframe attenuation measurements have been carried out on a modern BAe aircraft constructed with significant amounts of CFC. The basic test process utilised was as for the EMC demonstrator work, with measurements conducted on two avionics bays high up on the right hand side of the airframe and two on the left hand side, one at the same height as those on the right (2.59m above ground) and one close to the bottom of the fuselage (1m above ground). The positions of the left hand side bays with respect to aircraft nose and wing root were similar to the Front Avionics Bay and Port Gun Bay tested earlier, see Fig. 3.4. The range 1-18 GHz was tested and, as for the earlier tests, both transmit antenna polarisations were examined. Two aspects were different to the metal-skinned aircraft tests: Firstly, illumination aspect angle was not investigated, rather for each bay the transmitting antenna was moved in a  $90^\circ$  arc off the nose of the aircraft with the spectrum analyser in 'peak hold' mode to determine the angle for the highest signal (*i.e.* minimum airframe attenuation) at the measurement antenna in the bay. Secondly, a relatively new technique for ensuring the maximum field in the bay's volume is measured wherever the measurement antenna is located. This technique, called 'Mode Stirring', is essentially the same as used in domestic microwave ovens. It has been steadily gaining acceptance over the last three years, can be

used for equipment EMC qualification in screened rooms and is now included in [2-17]. Crawford and Koepke [3-25] describe the technique, its application and limitations.

A mechanical paddle is located within the cavity (bay) and rotated by a motor at a rate dependent on the response time of the avionics within the bay; a typical rate is 1 revolution per second. This produces a field distribution which varies with time at each point in the bay for each position of the paddle. The 'stirred' field has a higher average value at any point than that which would exist without the paddle because the paddle changes the cavity boundary conditions, so a slightly different resonant frequency spectrum is excited at each paddle position, see Davenport *et al.* [3-28] and its references. Hence a large number of modes contribute to the field at each point within the cavity's volume, producing a fairly uniform time-averaged field there. At frequencies much greater than fundamental cavity resonance, where many modes can be excited, equipment in the bay is subjected to uniformly distributed plane waves incident from all directions. For the bays investigated such a high number of modes is possible, see Fig. 3.13, and a fairly uniform modal density (another criterion suggested in [3-25] for technique validity) is assured. As described in [3-25] the technique is only valid for a minimum stirring effectiveness of 20 dB (*i.e.* the ratio of measured power without the stirrer moving to that with it in motion), for paddle minimum dimension of  $\frac{\lambda}{2}$  at the lowest frequency (150 mm at 1 GHz in this research), and a minimum of 30 modes [2-17]. To achieve these in cluttered, small bays is impossible. The substantial, though unpredictable reduction of the high Q possible (see Fig. 3.14) in these bays when loaded with avionics, in conjunction with the reality that bays are leaky cavities, make the use of this technique on an aircraft less than perfect, compared to its use in screened rooms which is fully justified in [3-25].

The results of the tests are given in Table 3.3 and subsequently discussed with respect to this researcher's investigations on the EMC demonstrator aircraft, see Section 3.3.1. The table contains geometric mean  $A_A$  values for the tests, which were conducted with 50 MHz test resolution.

Table 3.3: Airframe Attenuation Factors

BAY No. + SIDE	TRANSMIT ANTENNA POLARISATION			
	VERTICAL		HORIZONTAL	
	FREQ. (GHz)	AVERAGE ATTEN. (dB)	FREQ. (GHz)	AVERAGE ATTEN. (dB)
1, RIGHT HAND	1-1.3	15	1-3	20
	1.3-8	22	3-14	27
	8-18	25	13-18	25
2, RIGHT HAND-FRONT	1-8	20	1-5	23
	8-18	25	5-13	26
			13-18	23
2, RIGHT HAND-REAR	1-8	20	1-8	20
	8-13	22	8-12	23
	13-18	20	12-18	20
1, LEFT HAND	1-2.6	10	1-2.6	16
	2.6-8	15	2.6-18	>20
	8-18	20		
2, LEFT HAND	1-8	20	1-4.2	20
	8-18	>25	4.2-18	>30

On examination of the ten 1-18 GHz spectrum analyser plots supporting the data in Table 3.2 it is observed that:

- 1) Worst case  $A_A$  of 10 dB for 1-8 GHz and 20 dB for 8-18 GHz were established and the cumulative probability function of these measurements compare favourably with that for the EMC demonstrator measurements, see Section 3.3.1 and Fig. 3.11 therein. Initially this appears surprising as the modern aircraft has a CFC skin with metal mesh inner surface and all of the panels tested are also fitted with conductive Plastic Rubber Compound (PRC) which, as will be seen in Chapter 4, can lead to a better EM shield for the inside of the bays than the un-gasketed shoot-bolt and bolted panels on the EMC demonstrator aircraft. However, the PRC used is bonded only to the panel landing on the airframe, thus enabling ease of panel removal and re-fitment. Unfortunately this means the gasketing-to- panel interface is not necessarily low impedance at microwave frequencies and this is believed to be the reason that higher  $A_A$  values were not seen. The comparison of EMC demonstrator and modern aircraft data in Section 3.3.1 suggests that this is the case. The frequency dependence of the data sets is difficult to establish for the limited data available.

The decreasing  $A_A$  with increasing frequency, seen in this researcher's investigations but not apparent in these data sets, is believed to result from the test technique used: that of spectrum analyser 'peak search/hold' whilst moving the transmitting antenna in an arc about the bay under test.

- 2) Most of the data samples in the ten attenuation graphs lies between 20-35 dB, which agrees with the earlier work. The maximum, seen only for one bay at approximately 10.2 GHz, is 43.6 dB and the minimum, again seen on only one (but a different) bay at approximately 1.7 GHz, is 7.9 dB [the case is Bay 1, Left Hand Side, Vertical Polarisation]. The  $A_A$  trend is similar to the EMC demonstrator investigations, see Fig. 3.11, with the bulk of the measurements showing appreciable attenuation in line with the estimate of 6-20 dB used by military aircraft designers since the early 1970's, with only a few values seen below 10 dB and a few above 40 dB.
- 3) The maximum peak-to-peak excursion of any of the profiles is only 16.4 dB and most of the profiles lie within  $\pm 5$  dB of the average, compared with up to 55 dB between adjacent samples and profiles of  $\pm 10$  to  $\pm 15$  dB seen during the EMC demonstrator investigations. The reason for this is that the mode stirring technique, due to its averaging ability [3-25], removes most of the peaks in the received power profile seen in the un-stirred case, in effect yielding the worst case (*i.e.* minimum)  $A_A$  profile for the bay in question. This effect was investigated by Carter *et al.* and is shown in Figs. 9 and 10 of [3-21]. These figures also demonstrate that imperfect mode stirring is present (in the helicopter tests reported) as proposed earlier in this section, in that not all of the frequency dependent peaks and troughs are removed as suggested in [3-25] might be the case for perfect mode stirring.

From examination of the results of these more recent tests in conjunction with those of the earlier investigations, it would appear that the concept of probabilistic modelling of airframe attenuation, based on tests on multiple aircraft/bay types and numbers, has merit and is likely to offer the best and most cost-effective solution until maturation of the rigorous computational EM modelling tools and techniques discussed in Section 3.2.

### 3.3.2.2 Airframe Attenuation on Modern Civil Aircraft

The EUROCAE User's Guide [2-17] addresses airframe attenuation in two ways. Firstly as a set of values which attempt to establish a relatively conservative upper bound on the transfer function of aircraft EM energy penetration (in terms of internal field strengths), and secondly by use of the all-encompassing statement: 'If the precise attenuation in any specific circumstances is doubtful then the attenuation must be measured.' More realistically the draft also allows for modelling and/or measurements to support estimates for a specific aircraft, noting (as discussed in Section 3.2) that modelling techniques are currently 'limited in effectiveness by the ability to model significant details of aircraft structure, pertinent points of entry, and internal zone cabling and configuration.' The User's Guide concludes, in accord with this research, that 'The most accurate approach to determine internal environments is to apply a blend of test and analysis using the results from the testing to "calibrate" the model.' The generic values contained in the User's Guide for 0.1-18 GHz are dependent on avionic equipment location and are given in Table 3.4:

Table 3.4: Attenuation vs. Civil Avionics Location

<u>LOCATION CATEGORY</u>	<u>EM ENVIRONMENT AT AVIONICS LOCATION IN AIRFRAME</u>	<u>ATTN. (dB)</u>
T	Well protected, <i>e.g.</i> enclosed bay in all-metallic aircraft.	32
U	Partially protected, <i>e.g.</i> avionics bay in an all metallic aircraft.	20
V	Moderate, <i>e.g.</i> that found in the more EM open areas of an aircraft composed principally of metal.	12
W	Severe, <i>e.g.</i> that may be found in non-metallic aircraft or exposed areas in metallic aircraft.	6
Y	---ditto---	0

Such guidance, as will soon be applicable to civil aircraft when the User's Guide is formally agreed amongst the participating nations, is believed to be a sensible improvement to be adopted for the EMC design of military aircraft, although the exact values to be used and their frequency dependence requires further study. This study, as for the RF environment case discussed in Chapter 2, is likely to show that frequency independent values in the microwave band are unnecessarily severe for both military and civil aircraft.

### 3.3.3 Discussion Of Panel Tests In EMC Laboratory

In Section 3.3.1, it was noted that an investigation of bolted panel microwave shielding in the controlled EM environment of the BAe EMC Laboratory at Warton was proposed. This aimed to increase the then limited knowledge of the microwave attenuation properties of aircraft panel materials and the joints associated with them. The investigations covered:

- attenuation of panel materials used in modern aircraft, including CFC 'honeycomb', where two outer skins of CFC are spaced by a lightweight honeycomb CFC structure. Literature and other searching had also identified the need to examine the potential for microwave energy 'leakage' through composite material panels on three counts. Firstly un-ratified information suggested that researchers in the U.S. had measured microwave leakage through CFC material. Secondly such leakage (in the form of surface transfer impedance values at 2 GHz similar to those at 1 MHz) had been reported by Walker and Heintz [3-29]. Thirdly CFC, unlike metal, is not homogeneous and, because of manufacturing techniques, can have small regions of non-conducting material through which microwave energy ingress could occur. Two samples were examined, one with fine copper mesh, used for lightning strike protection, bonded to one face.
- potential benefits on shielding effectiveness of using high and low conductivity conductive gaskets in, or conductive tape across joints, including an initial examination of the effects of paint in the joint.
- the effects of bolt spacing *via* comparison of two panels, one with twice the number of bolts of the other, to also explore the reason why some of the EMC demonstrator aircraft measurements did not agree with predictions of cut-off frequency.

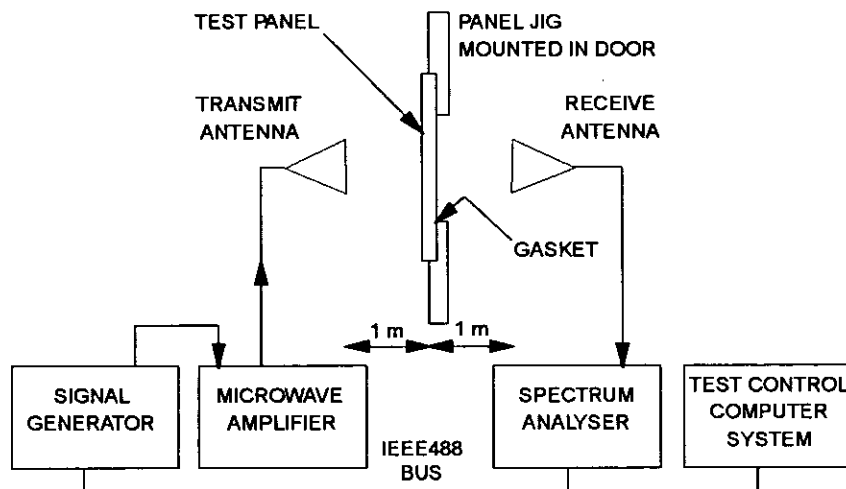
The test methodology used and results obtained are fully reported in [3-30] by the researcher, Wellington. Shielding Effectiveness (SE) in dB was ascertained using the standard 'hole in the wall' technique, detailed in MIL-STD-285 [3-31] and shown schematically in Fig. 3.20, where

$$SE = 10\log_{10}\left(\frac{P_h}{P_p}\right) \quad \dots(3.7)$$

and  $P_h$  = received power with no panel fitted

$P_p$  = received power with panel/gasket fitted.

Figure 3.20: Test Arrangement For 'Hole In Wall' Shielding Measurements



All panels were approximately 491 mm x 217 mm to match the aperture in the door between rooms of the EMC Laboratory and Table 3.5 gives the panel configurations tested. Measurements were taken for 1-4 and 8-18 GHz (4-8 GHz was not tested due to amplifier unavailability). Unless stated 50 MHz measurement resolution was used, as suggested in Section 3.3.1 to be an appropriate balance of adequate characterisation vs. test time. A summary of the findings of these investigations is presented below:

Table 3.5: Panel Type And Configurations Measured

<b>MATERIAL</b>	<b>DEPTH</b>	<b>OTHER DATA</b>
ALUMINIUM	3 mm	
CFC	3 mm	SIMILAR TO ABOVE
CFC	28 mm	HONEYCOMB WITH 1mm SKINS
CFC	28 mm	AS PREVIOUS + COPPER MESH ON ONE SKIN
ALUMINIUM	3 mm	FULL SET OF 48 BOLTS TO MATCH THE 'HOLE IN WALL' LANDING
ALUMINIUM	3 mm	24 EQUI-SPACED BOLTS
ALUMINIUM	3 mm	PREVIOUS PANEL: TWO SAMPLES OF CONDUCTIVE GASKETTING AND CONDUCTIVE ADHESIVE TAPE
ALUMINIUM	3 mm	PREVIOUS PANEL: GASKETS AND TAPE ISOLATED FROM PANEL

**Aluminium to CFC Comparison for 3 mm thick panels:** The range of levels of SE seen was 28-90 dB. Results for 1-1.4 GHz for aluminium show a 15-20 dB improvement in SE over the CFC panel. SE >2 GHz for both panels follow similar trends and levels. However, >8 GHz CFC gave higher SE than aluminium by up to 20 dB over certain frequency sub-bands and this was found to be the case for both transmit antenna polarisations. The researcher noted that all values of SE measured for both panels were much lower than predicted and

attributed this difference to the effects of joint leakage around the periphery of the panel, a conclusion supported in Chapter 4. It is thought that the case where CFC apparently offers better shielding performance than aluminium is erroneous, with the different materials at the peripheral slot interface resulting in different frequency-dependent performance of the joints which dominates the SE values measured.

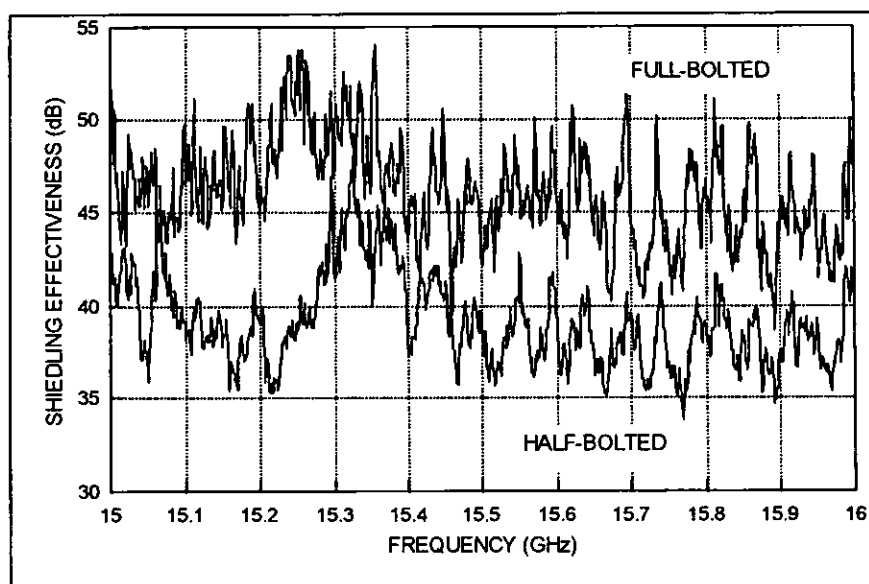
CFC Honeycomb Panels With/Without Copper Mesh: Values of SE seen were 25-70 dB and both panels showed similar transmit antenna polarisation trends. Conducted with 20 MHz test resolution, both panels showed very similar levels of SE (within 5 dB) with isolated peaks seen in both panels' results up to 4 GHz. Above 8 GHz the protected panel has higher SE by up to 10 dB with more isolated peaks than the plain panel. However, over certain frequency ranges, the plain panel SE is up to 8 dB higher than the protected one. The extra SE predicted by the researcher for the copper mesh was not seen and this was attributed to the mesh behaving as poorly connected individual strands, rather than a homogenous sheet of copper at these frequencies, where the mesh size is  $\ll$  wavelength.

For the test configuration used, with the mesh isolated from the jig landing, any additional shielding would result from increased reflection and increased attenuation loss in the mesh. It is thought that, as for the previous tests, peripheral slot leakage is dominating the SE values measured and that for the extra shielding to have been seen, the mesh would have had to be well bonded to the jig landing. Some additional confidence in the results of the BAe tests arises from the similar SE levels resulting from tests performed on various composite panels by Chromerics Inc. [3-32],[3-33].

Fully (48) and Half (24)-Bolted 3mm Aluminium Panels: As the prime aim of this test was to investigate the frequency dependence of the bolt spacings difference between the two panels, 1 MHz test resolution was used. Predictions of cut-off frequency of 3.13 and 7.89 GHz were made for the 24 and 48 bolt panels respectively. For 1-3 GHz the resulting profiles were almost indistinguishable as predicted and were, at maximum, within 3 dB of each other. The range of SE values seen was 32-91 dB, with the maximum values for both panels seen at 1.1 GHz, for vertical polarisation only. Although the raw data presented in [3-30] is difficult to analyse due to the substantial variation between samples, *e.g.* up to 20 dB between 1 MHz samples, some general trends can be observed. The range of SE values seen was 24-90 dB. For 8-10 GHz the fully bolted panel is 10-15 dB higher, for 10-12 GHz up to 10 dB higher, and for 12-18 GHz is 5-15 dB higher than the half-bolted panel. These

results, of which Fig. 3.21 is an example, agree with predictions, which give a 10 dB difference between the panels for frequencies higher than 7.89 GHz. So, even though the SE benefit of closer bolt spacing can be seen in the results, further analysis of the data (presented in graphical form in [3-30]), including low pass filtering, is required if more information is to be gleaned.

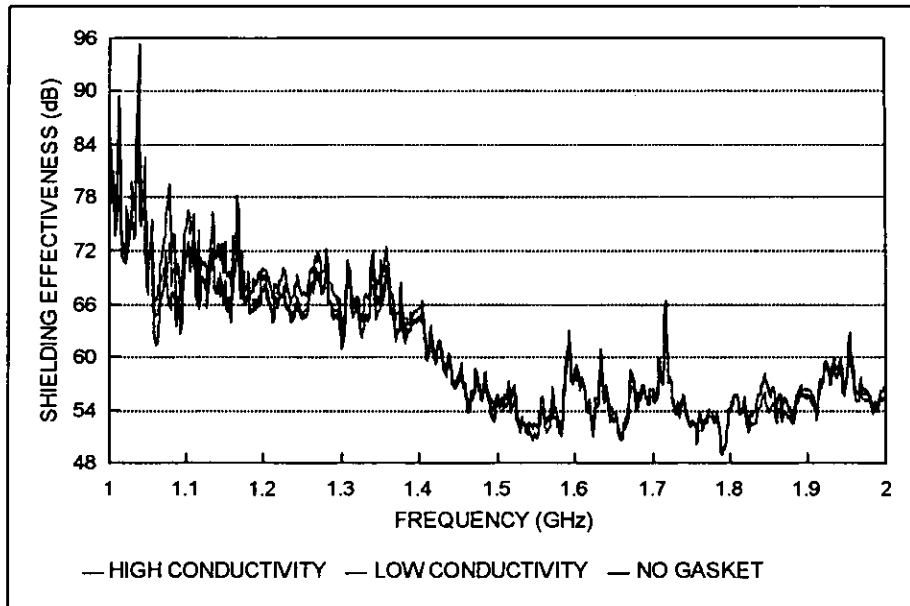
Figure 3.21: Shielding Effectiveness of Full- vs. Half-Bolted Panels



Effects of Low and High Conductivity Gasketing and Conductive Tape: A test resolution of 20 MHz was used for these tests, which were conducted with the 24 bolt aluminium panel only and compared gasketed and taped panel performance with that of a bare panel. From 1-1.3 GHz, for horizontal polarisation only, the low conductivity gasket gave an improvement of 10 dB, whilst the high conductivity one gave at most 5 dB improvement. As before, the substantial inter-sample SE variation prevents definitive analysis of the results, see Fig. 3.22 which shows the vertical polarisation data and is typical of the results of this phase of the investigations. For 1.3-4 GHz no improvement was seen with either gasket for either transmit antenna polarisation, within the 3 dB measurement error budget. There was also no significant difference in the performance of the two gaskets for 8-18 GHz, where a polarisation independent general improvement of 10 dB was measured, with a maximum of 20 dB at some frequencies. Although the range of SE seen was 28-100 dB, the bulk of the SE values did not achieve the 80 dB claimed by the gasket samples' manufacturer. This was thought by Wellington to be due to differences in test methods employed, a point with which this researcher agrees, but was not possible to prove due to

lack of data from the manufacturer. Use of conductive tape (with its conductive adhesive) gave a general improvement of 20 dB for 2-4 and 8-18 GHz.

Figure 3.22: Shielding Effectiveness with High/Low Conductivity Gaskets



With the aluminium panel electrically isolated from the door aperture using Sellotape as a simulation of paint (as would be the case in reality on an aircraft), the improvements seen with the gaskets in place were greater than those above, with both gasket types yielding improvements of up to 20 dB for 1-2 GHz and by 10 dB for most of 2-4 and 8-18 GHz. This increase at lower microwave frequencies probably results from further capacitive loading of the peripheral slot which then becomes lower impedance at these frequencies. The observed range of SE was 30-70 dB.

The overall conclusions to be made from this research phase in terms of its impact on the ingress of microwave energy into airframes are that:

- 1) CFC panels, particularly those with lightning strike protection in the form of copper mesh on the inside skin of a honeycomb construction, provide essentially the same SE levels >1 GHz as their traditionally used 3 mm aluminium counterparts.
- 2) Commercially available conductivity gasketing of panels can offer microwave SE improvements of typically 10 dB and up to 20 dB. It is thought that higher SE could be achieved for an aircraft panel or bay door, where optimised installation of the gasketing would be possible, compared with the Laboratory situation.

### **3.4 CONCLUDING REMARKS**

Two of the major findings of the aircraft investigations have particular relevance to this research programme. Firstly there are very few occasions where the attenuation values measured on in-service aircraft arrangements approach the minimum required attenuation values to prevent 1970's and 1980's avionics from being subjected to levels of power density approaching their qualified level. Secondly, the DEF. STAN. 59-41 military microwave EMC qualification levels are at least 52 dB lower than predictions of the current mean RF environment and this is exacerbated by the necessary addition of safety margins. Despite the apparent bleakness of the above, a problem is not thought to exist at this time because:

- a) very few avionics problems have actually been seen world-wide in the microwave band on either military or civil aircraft, see Chapter 7. Flying restrictions applied to U.K. fixed and rotary wing military aircraft also ensures that they are not subjected to these very high power densities,
- b) for the future, the latest military EMC Specification has levels which are considerably higher than earlier microwave test specifications, thus ensuring that equipment is cleared to the external environment.
- c) the EUROCAE User's Guide encompasses the best practices concerning civil aircraft equipment design and qualification, appropriate RF environments and aircraft certification techniques and levels.

However it should be noted that future avionic circuit technologies are likely to be more susceptible to the RF environment than those of the 1970's, which are currently in use in present day in-service aircraft. This topic is covered in Chapter 7.

Another conclusion is that the frequency-independent values of airframe attenuation assumed in the aircraft and avionic equipment design process are unnecessarily severe >1 GHz. The research has shown that a significant spread of 1-18 GHz attenuation factors (-3.2 to 59 dB) can occur, although a possible vehicle-independent correlation has been demonstrated between the cumulative probability functions for the aircraft types examined. This represents a step improvement in the ability to estimate microwave airframe attenuation for a given aircraft type and offers the potential for supporting EMC design and qualification without the need for aircraft tests. Further study is recommended, commencing with a wider statistical survey of such data from other aircraft types.

# *Chapter 4*

---

## **MICROWAVE ENERGY INGRESS INTO AVIONICS EQUIPMENT**

## 4.1 INTRODUCTION

Microwave energy entry into an avionics equipment box may occur through three routes: cables (including connectors), apertures (comprising holes, slots and joints), and through the box material itself. In assessing the potential upset of circuitry within the avionics box three questions need to be answered:

- a) What is the maximum relative energy ingress by each route?
- b) At what frequency or over what frequency range does the dominant mechanism of ingress change from cables/connectors to apertures?
- c) Is the assumption that there is minimal ingress through avionic box material true for typical avionics boxes?

This chapter attempts to answer these questions through the development of an overall energy ingress equation and investigation of the attributes of the three potential energy ingress routes before proceeding, in Chapters 5 and 6, to a detailed investigation of the ingress route comprising cables and connectors.

## 4.2 OVERALL ENERGY INGRESS EQUATION

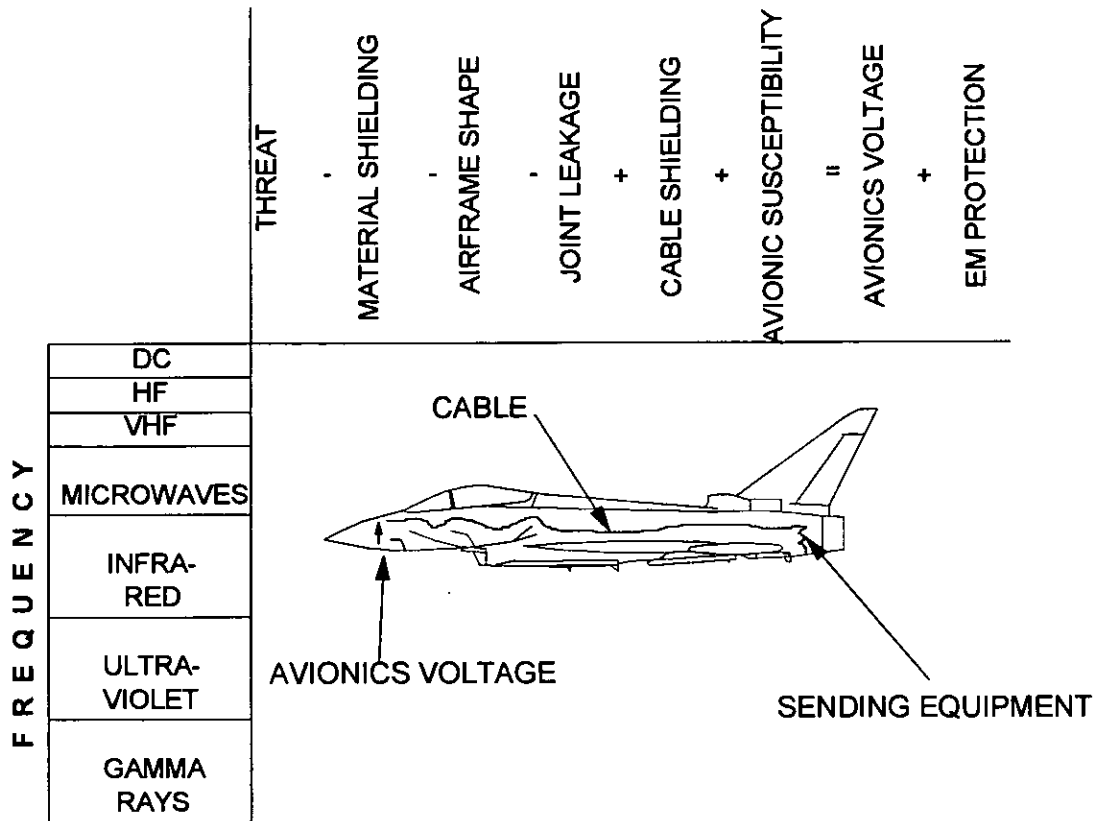
In conducting this assessment of the microwave threat to avionic circuitry, an equation for upset must be developed. A top level equation, describing the voltage presented to a circuit element in an avionic box as a result of EM irradiation of an aircraft, is in Birken *et al.* [4-1]. Eqn. 4.1 gives a modified form of this, which is applicable across the EM spectrum. It is also given pictorially in Fig. 4.1:

$$\begin{array}{r}
 \text{EM} \quad - \quad \text{MATERIAL} \quad - \quad \text{AIRFRAME} \quad - \quad \text{JOINT} \quad + \quad \text{CABLE} \quad + \quad \text{AVIONIC EM} \\
 \text{THREAT} \quad \text{SHIELDING} \quad \text{SHAPE} \quad \text{LEAKAGE} \quad \text{SHIELDING} \quad \text{SUSCEPTIBILITY} \\
 \\
 = \text{AVIONICS} \quad + \quad \text{EM} \\
 \text{VOLTAGE} \quad \text{PROTECTION}
 \end{array} \quad \dots(4.1)$$

Eqn. 4.1 can be represented more analytically as Eqn. 4.2, with each term having frequency dependency, denoted by (f):

$$P_{\text{CCT}}(f) = (P_{\text{ERP}}(f) - \text{FSL}(f)) - A_{\text{AIRFRAME}}(f) - A_{\text{BOX}}(f) + G_{\text{CCT}}(f) \quad \dots(4.2)$$

Figure 4.1: Original Ingress Equation



In this equation the first two terms have units of power in dBm and the others are gains or losses with units of dB. The definition of each term, with comments, is given below.  $P_{CCT}(f)$  is the power delivered to the circuit or component whose susceptibility is in question. Modelling is thought by this researcher to be possible and is certain to be dependent on circuit technology. This is discussed in Chapter 7. Whether  $P_{CCT}(f)$  has sufficient magnitude to cause upset is dependent upon the susceptibility of the avionics. Minimum susceptibility levels are given by the relevant EMC Qualification specification. Appendix B provides details of the EMC qualification specifications and test methods used on avionic equipment and aircraft to ensure safe and correct operation when they are exposed to power densities below the specified levels.  $P_{ERF}(f)$  is the Effective Radiated Power of the source of the microwave radiation, usually expressed as the product of the transmitter power and the antenna gain, either in dBm or Watts. This can be calculated and a prediction vs. frequency is given in Chapter 2.  $FSL(f)$  is the Free Space Loss of the radiation with distance from the antenna, see discussion in Chapter 2. It should be noted that for the purposes of this research the air is assumed to be dry, at standard atmospheric pressure and conditions, *i.e.* the worst case is assumed.

( $P_{ERP}(f) - FSL(f)$ ) is the power density incident at the airframe, see Section 2.3.  $A_{AIRFRAME}(f)$ , hereafter referred to as  $A_A$ , is the airframe microwave attenuation factor and replaces Material Shielding and Joint Leakage (for the airframe) in Eqn. 4.1. It is the transfer function between external irradiation incident on the aircraft's outer skin,  $P_{EXTERNAL}$ , and power density measured in an equipment bay within the airframe,  $P_{INTERNAL}$ , see Section 3.2 and is the ratio of two power densities:

$$A_A = 20 \log_{10} \left( \frac{P_{EXTERNAL}}{P_{INTERNAL}} \right) \quad \dots(4.3)$$

If resonances within an aircraft bay are present, the magnitude of  $P_{INTERNAL}$  can lead to a negative  $A_A$ , i.e. a 'gain' factor, see Section 3.3.1. In the aircraft investigations there were four cases of apparent negative  $A_A$ , but these were initially believed to have been a measurement problem. Subsequent to examination of both King *et al.* on cavity-backed slot irradiation [4-2], [4-3] and Carter *et al.* [3-21], the four data samples were re-examined and found to be valid negative values, the minima of which appear in Table 3.1. The largest value of this 'gain' from this researcher's work and in [3-21] is 3.2 dB and thus it is reasonable to estimate that this may be between 0-4 dB for a metal-skinned fighter aircraft. The contribution of bay resonances to  $A_A$  is unlikely ever to be fully analysed since there is substantial variation in the size, shape and internal content of equipment bays, including coupling effects to adjacent bays. It was suggested in Section 3.3.1, that  $A_A$  may have to be derived by a probabilistic determination and that such a determination would need to be based on panel or door type, size of peripheral slot, airframe material, aperture sizes, *etc.* Some modelling aspects of these resonances may be identical to those in avionic boxes, see below, since there is considerable analogy between a lossy Faraday (shielded) cage and both airframe and avionics box.

The Airframe Shape factor in Eqn. 4.1 represents a relationship between the vehicle's volume to surface area ratio (V/S) and its shielding effectiveness. The factor determines surface currents on the airframe and whether any enhancements occur, *e.g.* due to the resonant effects of a long thin cylinder *vs.* the lesser value for a sphere. Electric and magnetic shielding values at microwave frequencies are very high for typical aircraft construction: 5029-21241 dB has been calculated for 1-18 GHz using Eqns. 4.36 and 4.37 of Carter [3-23]\*. Examination of Birken's Shape factor graphs, Figs. 4 and 5 of [4-1], shows that the difference between spherical and cylindrical shape is only 2 dB, and that

---

\*During this work an incorrect calculation was discovered resulting in the whole of Table 4.1 of [3-23] being in error. This has been pointed out to the author.

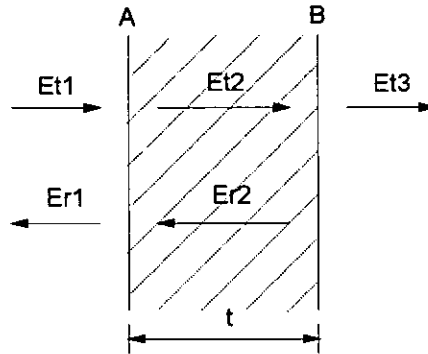
magnetic shielding effectiveness varies by 8 dB for V/S of 0.5-1.0, the range of all BAe fighter-sized aircraft. Both of these values are negligible when compared to the >5029 dB values above and thus the Airframe Shape factor is considered insignificant at microwave frequencies and can be discounted.  $A_{\text{BOX}}(f)$  is the avionic box microwave attenuation factor, as for  $A_A$  above. This is a function of energy coupling through cables and connector combinations, apertures (including joints and slots, e.g. for cooling) and case material. These are discussed in subsequent sections of this Chapter. The potential for 'gain' caused by resonances within the box is postulated by analogy to avionic bay resonances. No figure is available but an initial estimate of the maximum gain is 4 dB *via* this analogy.  $A_{\text{BOX}}(f)$  will be dependent on shape, size, and the avionic circuitry contained therein and is discussed in Section 4.4 and circuitry aspects considered in Chapter 7.  $G_{\text{CCT}}(f)$  is the gain of the effective antenna coupling the microwave energy within the avionic box to the circuit device in question. At the frequencies under consideration it is likely that this will be a combination of radiation impinging directly on the circuit device, and energy pick-up on both circuit board tracks close to the device and the device's own pins and leads. The value of this factor is believed to be heavily dependent on the circuit technology used and this topic is covered in Chapter 7.

Having established the above equation it is necessary to consider further the subject of microwave energy ingress into avionics equipment. Any avionics box may be considered as a imperfect RF shield to incident microwave and other frequency energy. The overall shielding effectiveness of such a box is made up of five components. These may be best considered in three groups: a) case material, b) apertures (holes, slots and joints) and c) the combination of connector and cables. The following sections consider each of these potential sources of ingress, thereby deriving an equation for  $A_{\text{BOX}}$ , and identifying the dominant factor in microwave energy entry into an avionic equipment box.

### 4.3 ENERGY PENETRATION THROUGH CASE MATERIAL

Transmission of EM energy through a thin sheet of conducting, though not lossless material can be appreciable dependent on the sheet's thickness,  $t$ , its material, and the frequency of the RF energy. 'Thin' in this context is when  $t$  is comparable to  $\delta$ , the skin depth of the energy in the material.  $\delta$  is that depth into the sheet where the current density has decayed to  $1/e$  of the value at the surface of the material. The derivation of  $\delta$  is covered in Chapter 5. Fig. 4.2 shows the general case in consideration:

Figure 4.2: Transmission Through A Conducting Sheet Of Finite Thickness



In Fig. 4.2,  $Z_1$  is the impedance of free space,  $377 \Omega$ , approximating to the air on either side of the avionic box wall A-B, and  $Z_2$  is the impedance of the case material.  $E_{t1}$  is the incident wave,  $E_{t2}$  the forward wave transmitted through the material, and  $E_{t3}$  represents the wave transmitted into the air beyond the case material.  $E_{r1}$  is the backward wave reflected from the air-wall boundary at A and  $E_{r2}$  is the backward wave reflected from the internal boundary at B. For the case where  $t$  is larger than  $\delta$ , and overall transmission loss is  $\gg 15$  dB, an approximation can be made that multiple reflections within the sheet can be neglected. From [3-23] the total loss through such a sheet can be then shown to be:

$$LOSS_{TOTAL} = LOSS_A + LOSS_{AB} + LOSS_B \quad \dots(4.3)$$

$$\text{where } LOSS_A = -10 \log_{10} \left( \frac{4R_s}{Z_1} \right) \quad \text{dB} \quad \dots(4.4)$$

$$LOSS_{AB} = -10 \log_{10} \left[ \exp - \left( \frac{2t}{\delta} \right) \right] \quad \text{dB} \quad \dots(4.5)$$

$$LOSS_B = -10 \log_{10} \left( \frac{8R_s}{Z_1} \right) \quad \text{dB} \quad \dots(4.6)$$

and where  $R_s$ , the surface resistance (sheet resistivity) of the case material, is given by:

$$R_s = \frac{1}{\sigma \delta} \Omega/\text{square} \quad \dots(4.7)$$

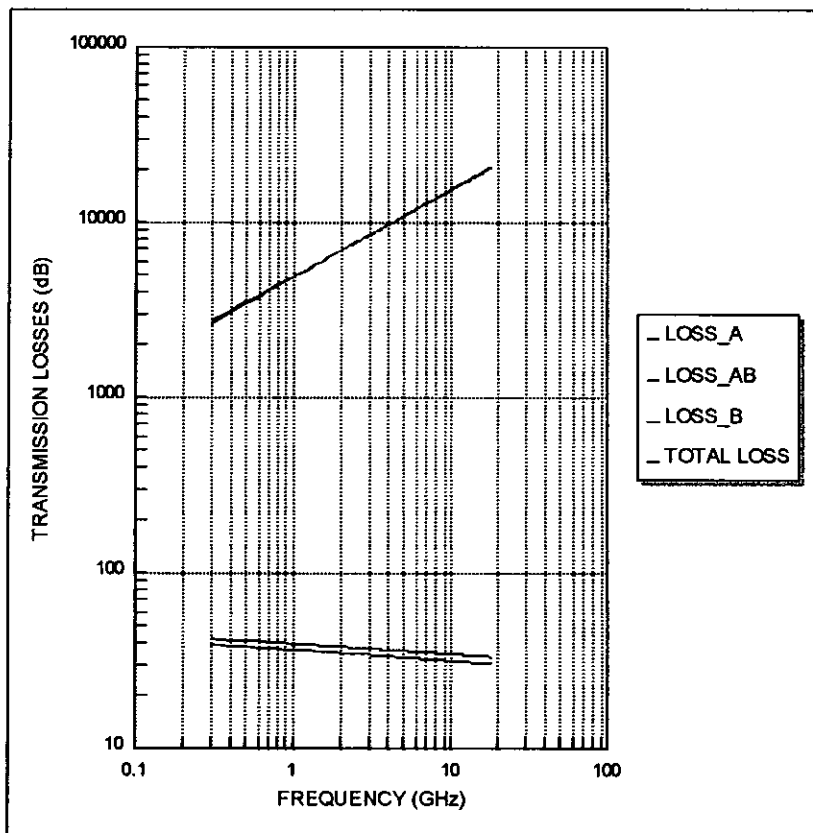
where  $\sigma$  is the material's conductivity, in Siemens per metre, and

$$\delta = \sqrt{\frac{1}{\pi f \sigma \mu}} \text{ metres} \quad \dots(4.8)$$

see Chapter 5, and  $\mu = \mu_0 \mu_r$  with the former being the permeability of free space,  $4\pi \times 10^{-7} \text{ Hm}^{-1}$ , and the latter being the relative permeability of the material.

A typical avionic box is made of primed and painted aluminium or aluminium alloys. Often it has been cast (to minimise joints, for EMC and other mechanical reasons) and has typical side or panel thickness which is a minimum of 1.5 mm. For aluminium, the values  $\sigma = 35 \text{ to } 40 \times 10^6 \text{ Sm}^{-1}$  and  $\mu_r = 1$  can be used to evaluate the minimum attenuation for 1-18 GHz. If the lower value of  $\sigma$  is used for conservatism, a skin depth for 1-18 GHz can be calculated using Eqn. 4.8 to be  $2.69 \text{ } \mu\text{m}$  at 1 GHz, reducing to  $0.634 \text{ } \mu\text{m}$  at 18 GHz. Thus, for the minimum  $t$  value of 1.5 mm, the case material is between 556 and 2366 times  $\delta$  in thickness, justifying the earlier approximation that no multiple reflections occur within such thicknesses of aluminium sheet at these frequencies. Substituting these values of  $\sigma$  and  $\delta$  into Eqn. 4.7 and then for  $R_s$  into Eqns. 4.4 to 4.6 enables the transmission losses in Fig. 4.3 to be calculated.

Figure 4.3: Transmission Losses Through Aluminium



This total transmission loss, 4919-20614 dB for 1-18 GHz, is so high that this ingress route is negligible >1 GHz and a term is not required for this aspect of the  $A_{\text{BOX}}(f)$  element of the

ingress equation. This is supported by Weekley [4-4], where a 1.016 mm aluminium barrier shielding value of >100 dB was calculated across the range 10 kHz to 18 GHz. This barrier, in conjunction with special aperture treatments, enabled total box shielding values of 47-76 dB. This resulted in the reduction of 1-18 GHz external fields from 4-17  $\text{kVm}^{-1}$  (*i.e.* similar to the 'Current Microwave Environment' in Fig. 2.2) to calculated internal fields between 0.7-27  $\text{Vm}^{-1}$ . These equate to a minimum 37-5 dB safety margin above the measured susceptibility of the circuitry in that particular box. The findings of this section also suggest that screening avionic circuitry should not be a problem even with the thinnest case material typically used. In fact, this is not so as two key assumptions have been implicitly made in the above calculations: that the box is:

- 1) a perfect enclosure with no apertures, a completely unreal situation. In Section 4.4 it will be shown that dramatic reductions in shielding effectiveness can occur with the smallest of apertures for 1-18 GHz.
- 2) not resonant at any frequency in the range 1-18 GHz, a real possibility based upon the analogy argument with aircraft avionic bays, postulated in the discussion of the bay resonance 'gain' factor in Section 4.2. Taking a typically large avionic box as 0.3m x 0.3m x 0.2m then, using the equation in Appendix E for the resonant frequency of an empty rectangular cavity, the resonant frequency is calculated at 1.03 GHz. Other resonances will occur above this frequency and, for boxes with smaller volumes, cavity resonances in the 1-18 GHz band are suggested by cavity theory (see Appendix E). This aspect is discussed in Section 4.4.

This also shows that, when considered with the results in Section 3.3.3, the Material Shielding part of the  $A_A$  factor can also be considered to be so high as to be negligible for metallic airframes (where aluminium skin thickness of 1.6 mm is common), or have a minimum value of only 30 dB lower than aluminium, *i.e.* still negligible, if it is made of modern composites. The resulting conclusion of this section is that the material shielding components of the both avionic box and airframe attenuation factors,  $A_{\text{BOX}}(f)$  and  $A_A$ , are negligible. Thus these factors equate to the Joint Leakage term of Eqn. 4.1, or more generally to terms covering the degradation of each shield by apertures, of which joints are but one type. This aspect is covered in the next Section.

## 4.4 ENERGY PENETRATION THROUGH APERTURES

There is considerable analogy between airframes and avionic boxes. Both offer protection to the avionic circuitry, in the form of shielding, and may be viewed as lossy Faraday cages, with energy ingress resulting from various shield wall imperfections. Evidence presented in Chapters 3 and 4 strongly suggests that for 1-18 GHz these imperfections, in the form of slots, holes and joints, represent the dominant energy ingress route for both airframe and avionic boxes. Other imperfections include lamps, potentiometers and Visual Display Unit screens. However the shield degradation of a number of these is difficult to quantify by prediction or measurement and this is discussed further in this Section.

### 4.4.1 The Effects Of Apertures On Attenuation Of Incident Energy

Avionic boxes fall into two main categories with regard to apertures:

- those which are installed within avionics bays, *e.g.* computers and navigation sensors. These are typified by construction of screwed and/or bolted panel, or cast variety; front and/or rear connectors fixed to the case; ventilation holes (most often) in bottom and front panels; and sides and top panel usually without holes; removable for maintenance.
- those which are cockpit-mounted. There are two types, visual display units (*e.g.* head-up display and radar displays) and control panels. In the former the primary difference to the bay-mounted box is optical apertures, which are discussed in Section 4.4.3. The latter differs in that rarely do they have need for ventilation holes and thus the box construction is usually cast, with the front panel bolted to the box. In addition, connectors are only rear-mounted and multiple knobs, switches and indicators (bulbs and displays) penetrate the front panel.

Formulas for field penetration through circular and elliptical holes in the idealised case of a wall with *zero* thickness were developed by Bethe [4-5], [4-6] and have become accepted. Predictive work in the area of apertures in walls with *finite* thickness has been conducted over the last twenty years [4-7] and Butler *et al.* produced a bibliography of apertures in a thick screen [4-8] in 1978 covering much of this earlier work. Many researchers, including Vance [4-9], Harrison [4-10] and Schelkunkoff [4-11] have also analysed the mechanisms by which EM fields at the surface of conducting shield can penetrate and appear on the other side. More recently (1990), and building on this earlier

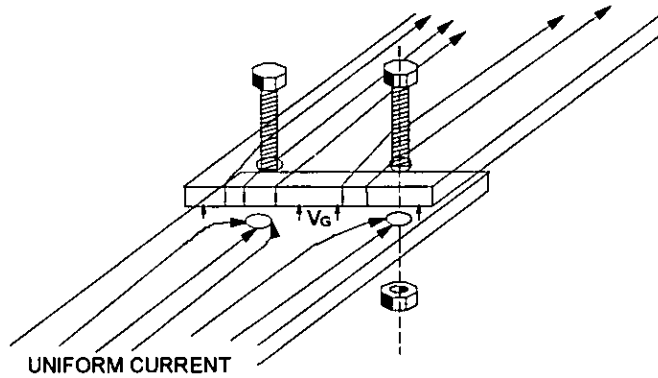
work, Gluckstern and Diamond [4-7] derived integral equations for the potential and field distribution within a circular hole in a plane conducting wall of finite thickness induced by uniform far fields. These were then used to obtain the electric and magnetic dipole moments induced on the opposite side of the wall from the incident field. Although the topic has been well researched, the detailed application of these equations to practical avionics boxes is not well understood [2-17]. The key difficulties are that:

- avionics boxes are not identical in size, shape and case construction.
- apertures vary substantially in number, shape and size between boxes.
- non-linear contact resistances and geometrical complications are common, *e.g.* gap shapes, bolt spacings and gasket compression.

Thus, each box represents a computationally intensive task at these frequencies and, as for the airframe case, modelling does not currently provide a practical solution to the problem of aperture ingress. However, through a combination of less complex analysis of aperture ingress and many years of practical experience by avionics manufacturers, various design rules have now evolved. Whilst the consideration of the detailed equations in [4-5] to [4-11] are outside the scope of this thesis, it is necessary to understand the mechanisms involved to determine appropriate values for shielding effectiveness degradation caused by apertures. An examination of current avionic box screening techniques was thus conducted and a number of equations, especially those by Grant [4-12], were identified as relevant to the design of avionic box apertures at microwave frequencies.

Field penetration occurs through three mechanisms: diffusion through the case material (see Section 4.3) and EM coupling through apertures and mechanical joints. In the magnetic coupling case, a magnetic field causes a current to flow on the surface of a conductor. This current develops a voltage drop across the contact resistance of a joint or gasket which exists on the outer and inner sides of the joint as indicated in Fig. 4.4. If this current flows through an inductance which is common to both inner and outer surface of the shield then the voltage drop will exist on both sides also. Slots, holes, spaces between bolts or other fasteners, gaps between braided wires are all associated with common or mutual inductances in this context. Likewise, shunt capacitance is associated with joints, gaskets and slots and typically a joint may be represented by this capacitance in parallel with a series combination of resistance and inductance.

Figure 4.4: Magnetic Field Induced Coupling



Note: The gap voltage  $V_G$  close to a bolt is due to the inductance of the bolt and contact resistance of plates.  $V_G$  between bolts is affected by inductance of adjacent bolts and capacitance of gap between plates.

Madle [4-13] states that the transfer impedance of any aperture or joint can be reduced to the general form of:

$$Z_{TR} = [R(f) + j\omega L + j\omega M_{12}] \text{ in parallel with } \left[ \frac{1}{j\omega C} \right] \text{ ohm} \quad \dots(4.9)$$

- where  $R(f)$  = frequency dependent resistance ( $\Omega$ )
- $L$  = Inductance common to both plates of shield (H)
- $M_{12}$  = Mutual inductance between the two plates (H)
- $C$  = Shunt capacitance (F)
- $\omega$  =  $2\pi * \text{frequency (Rad.s}^{-1}\text{)}$

Coupling of an electric field, which is normal to the shield, through apertures and/or joints can induce a current in a wire within, in effect making part of the wire behind the aperture behave like a plate of a capacitor, with the other plate outside the shield. In this case the Transfer impedance can be expressed as

$$Z_{TR} = \left[ \frac{1}{j\omega C_{12}} \right] \quad \dots(4.10)$$

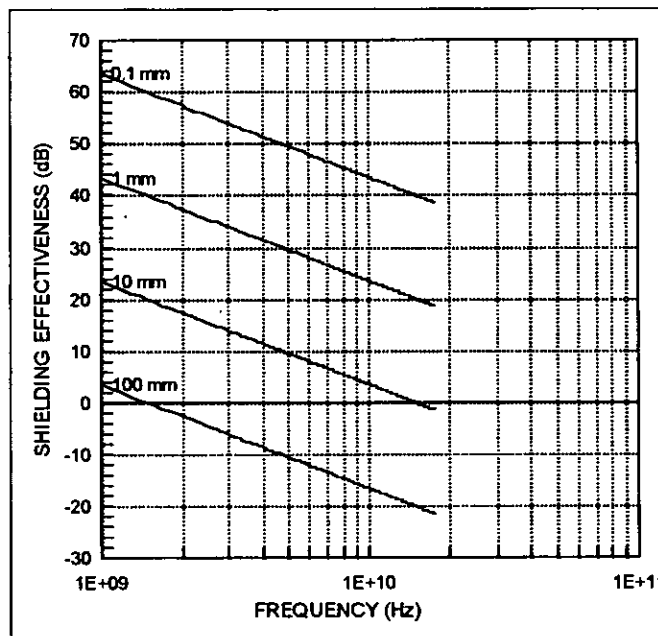
where  $C_{12}$  = mutual capacitance between wire and exterior of shield (F).

With reference to [4-12], EM leakage through an aperture depends upon the longest dimension of the aperture,  $d$ , and the wavelength,  $\lambda$ , of the radiation field. When  $\lambda < 2d$ , the EM energy passes freely through the aperture. When  $\lambda = 2d$ , the shielding effectiveness is zero and this occurs at the cut-off frequency,  $f_c$  where  $f_c = c/2d$  and  $c =$  propagation velocity of the wave (the speed of light for air-spaced apertures). When  $\lambda > 2d$ , the signal is attenuated by an amount  $R$ , where

$$R = 20 \log \left( \frac{\lambda}{2d} \right) = 20 \log \left( \frac{c}{2df} \right) \text{ dB} \quad \dots(4.11)$$

for  $\lambda/2 > d > t$  and where  $t$  is the thickness of the case material.  $R$  for a number of aperture major dimensions is shown in Fig. 4.5

Figure 4.5: Shielding Effectiveness vs. Aperture Major Dimension



This figure demonstrates the importance of minimising apertures of any type at microwave frequencies. The reduction of shielding of 20 dB per decade of increasing frequency agrees with [2-17] and was also discussed in Section 3.3.1. Indeed, in the frequency range of interest, 1-18 GHz, the hole's major dimension at which shield attenuation is 55 dB can be calculated from re-arranging Eqn. 4.11 as 0.26 mm decreasing to 14.8  $\mu\text{m}$  with increasing frequency. Ref. [2-17] states 55 dB as the box attenuation typically required in the region 0.4-2 GHz for civil aircraft to protect avionics 'if highly susceptible components' are used in and is in line with [4-4] which achieved attenuation of between 76 dB (1 GHz) reducing to 47 dB (18 GHz). Ref. [2-17] suggests that 55 dB is applicable up to 8 GHz but, interestingly, also suggests that the attenuation requirement can be reduced

by some 40 dB between 1-10 GHz as a result of the combination of reducing wire coupling, which is stated as being 20 dB per increasing decade frequency, and decreasing component susceptibility which in [2-17] is stated as 'typically improves by 20 dB per decade, expressed in power terms...' Above 8 GHz no avionic testing and analysis is required by [2-17] unless a specific component or circuit susceptibility exists. These aspects of [2-17] are discussed in Chapters 6 and 7. The figures calculated above lead to the conclusion that with any box holes, joints or other discontinuities it is very difficult to provide any significant level of shielding, particularly in the upper part of the 1-18 GHz range. This has been seen during BAe EMC Laboratory tests on two avionics boxes from the 1980's, one with a cast case but many apertures and one which, to microwave radiation, was essentially a collection of eight flat panels loosely bolted together with no gasketing. Neither was particularly resilient to microwave energy ingress but the latter was shown to provide very little shield attenuation between 1-18 GHz.

These actions can be taken to maximise protection offered to the circuitry:

- Cast avionic box construction has an inherent reduced number of joints.
- Ventilation apertures of significant overall area are often required. Attenuation levels may be appreciably enhanced compared to a single large hole by sub-dividing the hole into groups of smaller holes, *i.e.* with higher  $f_c$ . The spacing of these holes must be at least the largest dimension of the hole to prevent adjacent holes appearing as one larger hole, with a halving of  $f_c$  and accompanying 6 dB reduction in shielding. Eqn. (11) of [4-12] describes the attenuation for multiple holes in a shield where the spacing factor is not taken into account. Wire mesh with appropriate aperture size and depth can also be used in this respect.
- Small spacings between bolts or screws around the whole periphery of any panels, ensuring that each corner is bolted, maximises  $A_{\text{BOX}}$ . Many bolts with short spacings give much higher attenuation than few bolts with large spacings as the slots formed in the former case have much higher  $f_c$  than the latter.
- Where regular panel access is required, precision machined matching faces with stepped, corrugated or flat profiles should be considered. An alternative is the screened room door peripheral 'finger stock' method.

- When a hole in the shield has a cross Section less than or equal to the thickness of the shield it acts as a waveguide below  $f_c$ . By taking advantage of the waveguide absorption characteristic, the use of holes in thicker material than the rest of the box can be used to achieve significant attenuation compared with a similar hole in the usual 1.5 mm aluminium case material. The amount of attenuation is a function of material thickness (t) to the width of the hole (w) and, for ratios of about 4:1, is above 100 dB [4-12]. Multiple waveguides, commonly arranged as a 'honeycomb', suffer a slight reduction in shielding as for plain holes but can still achieve >55 dB attenuation. Fig. 4.6 shows the significant increase in shielding with increasing t/w ratio for an individual waveguide below  $f_c$ , demonstrating the appreciable attenuation improvement over standard holes, whilst Table 4.1 shows typically available honeycomb waveguide cell data.

Figure 4.6: Waveguide Shielding Characteristics  
(From [4-12])

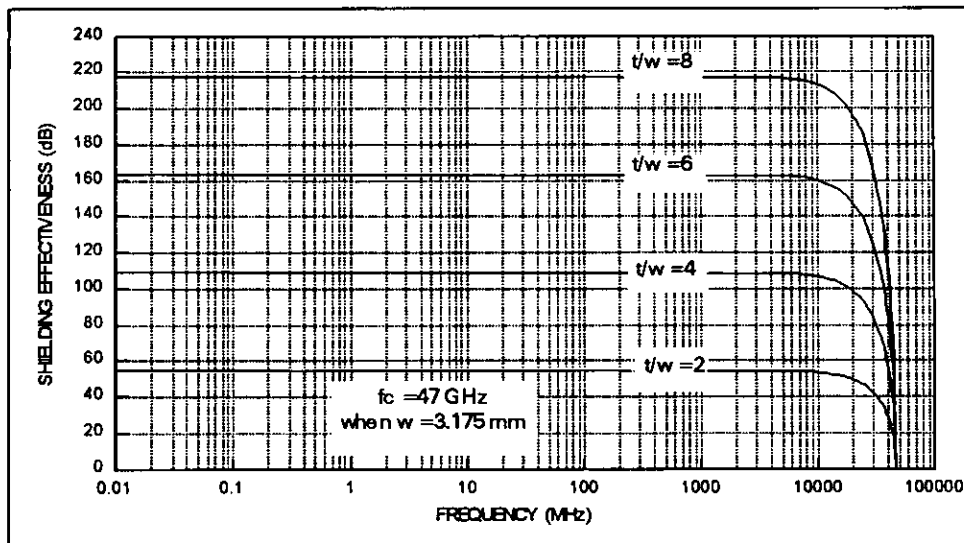


Table 4.1: Honeycomb Waveguide Cell Data  
(Extracted from [4-12])

CELL SIZE (w) in mm	CELL DEPTH (t) in mm	RATIO (t/w)	$f_c$ (GHz)	ABSORPTION (dB)
3.2	6.4	4	47	109
4.8	19.1	6	47	164
6.4	25.4	4	31	109
	25.4	5+	31	146
		4	24	109

- Gasketing should be used on panels as covered in Section 4.4.2. Ensure any joints, which form a capacitor whose magnitude is a function of joint area, are welded or sealed with high conductivity sealant or, as a last resort at these frequencies, a high overlap area can be used.

#### 4.4.2 The Role Of Conductive Gasketing At Microwave Frequencies

As discussed in Section 4.4.1, any slot or joint in the shield forming the avionic box results in substantial energy ingress compared to diffusion through the case material itself. In order to obviate or reduce this ingress path to acceptable levels a number of techniques can be utilised, falling into two major categories: panel and landing profile machining (*e.g.* stepped, lipped or corrugated) and conductive gasketing. A number of gasket types now exist, *e.g.* wire mesh, spiralled tinned beryllium-copper [4-4], vinyl or silicone polymers with silver, silver and nickel, or carbon fillers [4-13], [4-14], and conductive Plastic Rubber Compound (PRC). PRC is particularly useful in joints and for panels (both avionic box and airframe), though due to its glue-like consistency, is unsuitable for panels where regular removal is required. Gasketing is required where enclosures require apertures with major dimension  $> \frac{\lambda}{2}$ , where the EM threat is above 0.1 GHz and the total shielding required is  $> 30$  dB [4-12]. It is also required where dissimilar mating materials are used at the joint or lid edge, and where environmental seals are needed. Gaskets are thus invariably required for the range 1-18 GHz to enable overall screening above 30 dB to be achieved for avionic boxes. More usually a combination of lipping and gasketing is required to achieve the highest levels of protection, *i.e.* above 80 dB, generally needed to protect avionics against the current microwave environment, [4-4], [4-14] and see Chapter 2.

A typical military avionic gasket arrangement is shown in Fig. 4.7, demonstrating the combination of machining, and gasket. In this way continuous electrical contact around and between fasteners can be ensured. The gasket can be represented as a lumped parameter circuit comprising a parallel RLC network as in Fig. 4.8. Usually the values of resistance and inductance are small but, as in the case of corrosion, the value of inductance can become appreciable and contribute to degradation of shielding. To enable maximum contact area and minimum resistance between the gasket and the mating surfaces, the gasket is compressed using the closing action of the panel's fasteners and conductive paint may be used on the mating surfaces. Typical pressures required are 345-690 kPa (50-100

psi) for solid silicone and 172-345 kPA (25-50 psi) for the soft sponge silicone material with internal wires [4-13].

Figure 4.7: Typical Military Gasket Arrangement

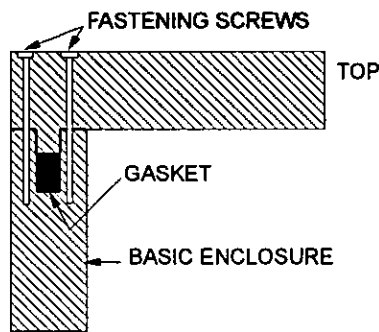
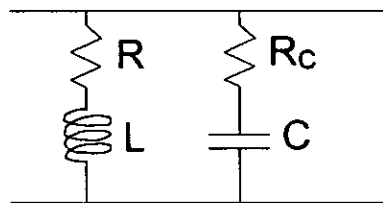


Figure 4.8: Equivalent Circuit Of Gasket



In order to obviate ingress via the panel periphery or joint path the conductivity of the gasket material must approach that of the case material to enable shielding attenuation values of the same order as an aperture-less box of that material. Whilst this is impractical in the range 1-18 GHz, high values of attenuation can be achieved, with modern conductive silicone-based gasket materials capable of a minimum of 100 dB over the range 29 MHz to 10 GHz [4-13]. Bates *et al.* [4-15] gave test data on a then new expanded PTFE polymer gasket loaded with carbon which showed better shielding effectiveness ( $110 \pm 10$  dB for 1-18 GHz) than a 'Corrosion resistant' silver-plated aluminium filled silicone ( $90 \pm 25$  dB for 1-18 GHz).

When gasketing is applied to all joints, panels and connector entry points, and appropriate ventilation aperture screening measures (see Section 4.4.1) are incorporated, 90-110 dB of gasket screening effectiveness is seen to be capable of enabling adequate protection against the current environment [4-4] and [4-14]. Thus the contribution of gasketing to the  $A_{\text{BOX}}$  term in the overall ingress equation is highly box construction dependent but can, where good protection measures as outlined above are adopted, be high enough for this ingress route to be discounted in determining the potential for avionics upset.

### 4.4.3 Optical Apertures

The two main optical apertures on modern military aircraft are the canopy, often a perspex or glass and plastic combination, and Visual Display Units (VDU), *e.g.* head-up display and cockpit-mounted navigation and weapon aiming displays. The canopy often offers zero shielding, see [2-17], other than in the case where windscreen heater elements form a simple filter. The combination of unscreened canopy and low shielding of VDUs has, in the past, led to upset of cockpit displays by radars, a topic which is covered in Chapter 7. Unlike other apertures allowing microwave energy ingress into the interior of an avionic box, optical apertures ('windows') must have acceptable optical transmission characteristics at all times. Two methods of shielding are currently used for this application, fine mesh metal and thin film coatings on the VDU. Mesh screens are commonly used for screening at frequencies below 1 GHz and comprise a knitted wire mesh made from Monel, tin-plated copper-clad iron, tungsten, copper or copper alloys. They are typically 1-5 mm thick and have optical transmission of > 60 % over the visible light spectrum. For the very fine mesh density (100 per inch) required for shielding 1-18 GHz effectiveness of >50 dB, very small (0.001 inch [25  $\mu\text{m}$ ]) wire diameter must be used and silver-plated stainless steel is required to survive the weaving process, but this mesh type is more expensive than the others by a factor of approximately five. Methods of calculating the attenuation of mesh shields and the trade-off of *vs.* optical transmission efficiency is given in [4-16] and [4-12]. There are three current techniques for the peripheral termination of such screens at the edges of the window aperture and these are shown in Fig. 4.9.

The other class of window shielding is thin film coatings. These can be used to coat VDUs, luminescent crystal displays, light emitting diodes or other types of display surfaces. The more common application is to VDU surfaces where thin films of silver or gold are vacuum spluttered onto the glass or polycarbonate window surface. To maintain adequate optical transparency a trade-off *vs.* surface resistivity has to be made, the result of which is an optimum of 72% optical transmission where surface resistivity is 10-14  $\Omega$  /square [4-12], equating to a frequency dependent shielding value of 38 dB at 1 GHz, reducing to 18 dB at 18 GHz. Fig. 4.10, from [4-12], shows this trade-off of transparency *vs.* resistivity.

Figure 4.9: Shielded Window Mesh Termination

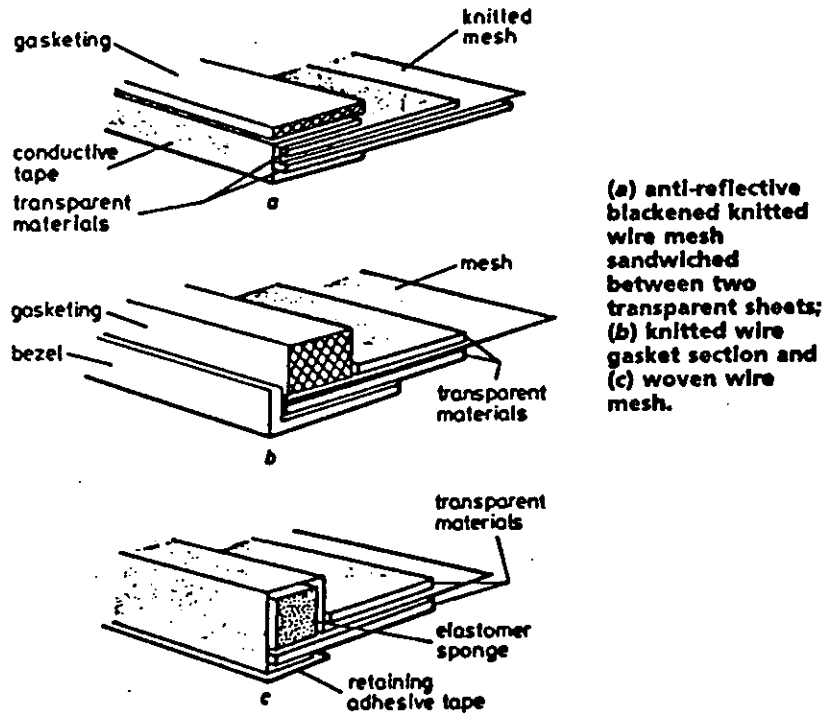
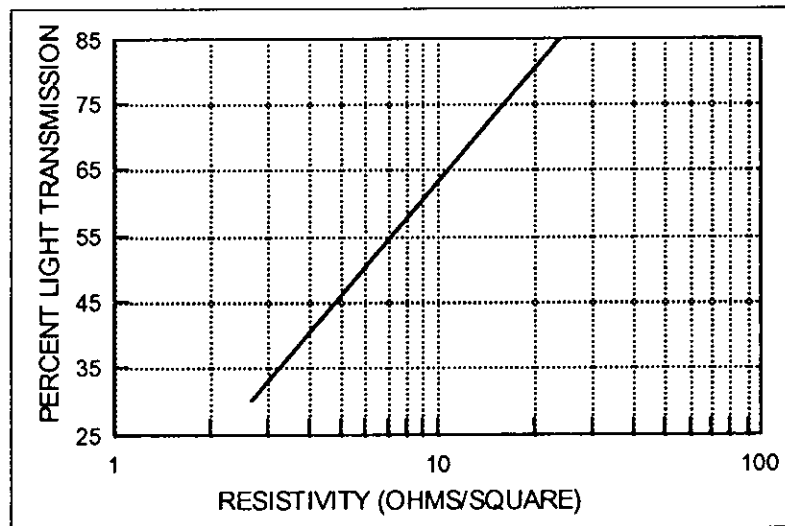


Figure 4.10: Transparency vs. Surface Resistivity



Films are currently available in the range 76  $\mu\text{m}$  -1 mm in thickness, with surface resistivities in the range 5-20  $\Omega/\text{square}$  and with optical transmission of 70-80% [4-17]-[4-19]. This shows that, although 50 dB of shielding can be achieved through the use of silver-plated stainless steel mesh screens, such apertures form the highest microwave ingress routes in avionic boxes whose other apertures are suitably screened as described in Sections 4.4.1 and 4.4.2. To achieve the 80 dB levels required to protect internal circuitry, further internal shielding of the optical element of the avionics is required.

#### 4.4.4 Discussion Of U.S. Research On Phenomenology Of Coupling

King *et al.* in the U.S. have researched the phenomenology of 0.1-18 GHz EM coupling [4-2] and have conducted a number of experiments of microwave EM energy coupling through slots over the same frequency range [4-3]. A number of their findings, most of which are in agreement with work by Cabayan [2-25], are relevant to this research programme in the areas of determining airframe and avionic box attenuation and cavity resonance gains. These findings are discussed below:

- The average field coupled to a probe behind a cavity-backed slot is up to 20.8 dB greater when the cavity is present, although the energy coupled is the same with or without the cavity. These findings are in line with the negative  $A_A$  values discovered in the avionic bay cavity investigations discussed in Section 4.2. Those values, 0-4 dB, are smaller than those seen by King and are consistent with the damping of bay cavity resonances by increasing insertion of materials within the cavity, a conclusion which is also supported by the lack of negative  $A_A$  values seen in the data sets from the modern aircraft measurements (see Table 3.1). For the King work only a single wire and miniature probe existed in the cavity tested, for the EMC demonstrator research the bay had approximately 40% loading by volume with box mounting and cooling trays, connectors and cabling, and air and fuel pipes, but with some six avionics boxes missing, see Fig. 3.1. The bays in the modern aircraft were likewise unpopulated with avionics boxes, but with a loading by volume of approximately 50%. It is thought that a similar damping of cavity resonances will apply to the avionic box case, *i.e.* the maximum 'gain' can be initially assumed to have a value of 3 dB, since avionics boxes tend to have loading by volume  $\approx 90\%$ .
- King reported coupling to a field probe inside a cavity-backed slot as insensitive to the position of the probe with respect to the slot. This would suggest that mode stirring during aircraft bay shielding measurements is not actually required. This does not agree with other work on mode stirring. King also noted that inside the cavity there appeared to be no radiation zone, and the whole volume is in the near field, but that with the slot only, *i.e.* without the cavity, the pick-up decreased characteristically with the reciprocal of distance from the slot. This latter aspect is to be expected as the arrangement is behaving like a slot antenna.

- Placing a large cavity behind an ingress path, such as a slot, creates multitudes of sharply peaked cavity resonances resembling spectral noise. King also noted that when the aspect ratio of aperture (height/width)  $> 10:1$ , pronounced peaking (Q) occurs at resonance. This is seen to an extent in the aircraft bay investigations of Chapter 3, where the peripheral slots on every bay tested had ratios well above 10:1.
- A wire in a cavity behaves like a long-wire antenna, with energy coupling response (antenna gain) decreasing as the reciprocal of frequency above first wire resonance, with cavity resonances adding a highly resonant structure to the measured load voltage. This will be seen in Chapter 5 to be consistent with the observations of this researcher and his former colleague, Price, on energy coupling to a wire entering a dummy avionics box. The exact frequency dependence is the subject of the modelling and empirical work of Chapters 5 and 6.
- 15% lossy fill in a cavity backing a slot leads to a reduction of coupling, though not dramatic, *i.e.*  $5\pm 3$  dB above 1 GHz. and  $8\pm 3$  dB above 8 GHz. This is consistent with the RAM lining of bays investigation of Chapter 3, although in that research all internal walls but the face of the bay were lined, whereas for King's work only one piece of RAM was inserted, at the top of the cavity. Worthy of note also from King's work is that addition of a small piece of ferrite absorber on the wire in the cavity (with no RAM inserted) caused some change in the attenuation response shape, but little change to its overall amplitude: minimal  $< 9$  GHz and  $< 5$  dB for 9-18 GHz. Only by fully covering the wire with a ferrite sleeve could this be improved and then only increasing (with frequency) to 8 dB maximum at 18 GHz. This suggests that protection of circuitry within a box needs to be achieved by minimising the fields and currents reaching the inside of that box, rather than attempting to filter wires inside.
- Aperture shape and size determine shielding effectiveness, This is seen in the Chapter 3 experimental work and is suggested by Grant's equations, see Sections 4.4.1 and 4.4.2.

In supporting the comments in Section 4.2 on bay and box resonance 'gains', these results suggest that not only are these factors positive and potentially large (5-20 dB), but also that circuit elements within an avionics box may be subject to an average field independent of component location. This consequently suggests that the margin of safety for avionic upset at microwave frequencies may be lower than previously thought.

## 4.5 INGRESS VIA CABLES/CONNECTOR COMBINATIONS

All conductors in an airframe act as receiving antennas, although due to position, orientation, length, and source and load impedances their efficiency can vary substantially with frequency and polarisation of incident fields. Most conductors concerned with avionics have extremely low efficiencies [2-17] and thus are unimportant as ingress paths. Those which have high efficiencies and/or resonate with the incident field can pose a significant upset risk to the avionic circuitry via wire-borne injection of microwave currents into circuitry and re-radiation of energy from the wires once inside avionic boxes. EM energy coupling from external fields to the airframe and cables within is at a maximum due to resonances for the cases where the lengths of either or both are multiples of  $\frac{\lambda}{2}$  or  $\frac{\lambda}{4}$  of the RF energy. The maximum of these resonances usually occurs when airframe and/or cable length equals  $\frac{\lambda}{2}$  or  $\frac{\lambda}{4}$ ; which equate to length ranges of 75-150 mm at 1 GHz and 4.2-8.3 mm at 18 GHz. At these higher frequencies transmission losses in cables become more important, a topic which is covered in detail in Chapters 5 and 6. Thus, as outlined in [2-17] (which represents current thinking in the U.K., U.S. and Europe), this means that significant coupling of energy occurs close to the box. For a given length of wire  $s$  when the frequency is increasing [2-17] states that the coupling is low when  $\lambda \gg 4s$ , maximum for  $\lambda = 4s$  and at higher frequencies decreasing proportionally with  $\lambda$  (*i.e.* with the reciprocal of frequency). This is reflected in the laboratory layout of box and transmitting antenna for the radiated susceptibility EMC qualification tests in the various specifications within Appendix B. U.S. and U.K. research [4-20], [4-21], [3-14], [3-20] and including that during this programme has, however, shown measurable pick-up at up to 3.05 m away from the load in a simulated avionics box. These data, which are more than the highest estimate of significant wire coupling of  $2\lambda$  [4-22] and equate *in extremis* to approximately  $20\lambda$ , questions the validity of using the 'rule of thumb' within the international EMC community that  $\frac{\lambda}{2}$  is the maximum distance that significant coupling of concern to the potential upset of circuitry can occur.

## 4.6 CONCLUDING REMARKS

From consideration of the elements of an overall equation developed to describe energy ingress to circuit device level, it is concluded that the aperture ingress route is dominant for both airframe and avionic boxes at microwave frequencies. It is also concluded that ingress through the case material of avionic boxes is negligible at these frequencies, but that cable pick-up may not be as relatively insignificant at microwave frequencies as previously thought by the international EMC community. Of the five factors in the equation developed there are two, airframe and box attenuation (which include the effective 'gains' caused by internal resonances excited by aperture ingress), which pose complex and time consuming modelling problems on even the most powerful computers available. These may thus lend themselves only to probabilistic determination.

Equations exist to adequately handle aperture ingress where the shape of the aperture is regular, *e.g.* circular or slot. These do not suffice for complex shapes such as the peripheral slots of panels of which an avionic box may be manufactured, although energy ingress may be minimised in this case *via* the use of adequate gasketing material. Where gasketing is used, in conjunction with a cast or welded joint box and appropriately screened ventilation apertures, the primary ingress path is *via* the cable and connector route.

It has been shown that the box material ingress route is minimal for avionic boxes that aperture ingress can be reasonably well predicted for most cases. Since no adequate models existed to describe energy coupling to cables at microwave frequencies, it was decided that this topic of cable and connector combination ingress should be critically examined to establish the true situation in this area. The outcome of this examination, covered in Chapters 5 and 6, enables quantification of its contribution to the  $A_{\text{BOX}}(f)$  term in the overall ingress equation described in Section 4.2. Examinations of possible ingress prevention techniques suggest that with adequate application of existing EMC shielding techniques, a significant amount of protection can be afforded to avionic circuitry at the avionic box, rather than airframe level. Techniques include the use of gasketing, including conductive plastic rubber compound and silicone-based conductive gaskets; depth, shape and size of waveguide ventilation slots; and finger seals or machined lipping or corrugations on box panel edges.

# *Chapter 5*

---

## **INGRESS VIA CABLES/CONNECTORS**

## 5.1 INTRODUCTION

To assess the potential upset of normal operation of electronic circuitry contained within a conducting equipment case, two mechanisms must be considered:

- a) The dominant ingress mechanism; diffusion through the case material, aperture leakage or conducting penetrations.
- b) The susceptibility of the internal circuitry to conducted and radiated interference energy.

To answer these questions it is necessary to quantify energy ingress by the three routes, examine their frequency dependency, and draw a comparison. It was decided that cables and connector combination ingress would be examined in some detail first, since it is generally thought by the international EMC community, *e.g.* [2-17] that, due to the wavelengths (0.01-1m) and transmission modes involved, little energy will enter an avionics box via its cables, other than that coupled to those cables within  $\frac{\lambda}{2}$  (0.5m maximum) of the box under consideration. As noted in Chapter 4 some U.S. and U.K. research [4-20], [4-21], [3-14], [3-20] and that during this programme has, however, shown measurable pick-up at up to 3.05m away from the load. To better understand the mechanism involved in this ingress theoretical models are needed. The first stage of this research was the development of a model for worst case coupling to an unshielded wire, based on equations derived by A.A. Smith Jr. [5-1] for coupling of EM energy to transmission lines below 1 GHz, and comparison with U.S., U.K. and BAe test results to examine the validity of its use above 1 GHz. The second stage, reported in Chapter 6, covers investigations arising from the results of the first stage, involving 2-18 GHz experimentation using aircraft cable entering an avionic box and refinement of the model in the light of the measured data.

## 5.2 TRANSMISSION LINES AND THE 'TELEGRAPHIST'S EQUATIONS'

With reference to transmission line theory, the following section covers the conversion of EM energy incident on a single wire above a ground plane into wire currents and thence into the terminal load voltage,  $V_L$ . Fig.5.1 shows the equivalent circuit of a short section, of length  $dz$ , of a general, infinitely long two-wire transmission line. The line has distributed series impedance  $Z \Omega$  and shunt admittance  $Y$  Siemens per unit length. For steady state conditions, using complex notation, the general differential equations for voltage and current against distance are (for sufficiently small  $dz$ ):

$$\frac{dV}{dz} = -ZI \quad \dots(5.1)$$

$$\frac{dI}{dz} = -YV \quad \dots(5.2)$$

For the lossless line case, as depicted with its equivalent circuit in Fig.5.2,  $Z$  and  $Y$  in Eqns.5.1 and 5.2 are replaced by  $L$  and  $C$ , the line distributed inductance and capacitance per unit length. Thus the differential length  $dz$  has an inductance  $Ldz$  and capacitance  $Cdz$ . By taking the partial derivatives of Eqns.5.1 and 5.2 with respect to the elemental length  $dz$  and then cancelling the term  $dz$ , the voltage and current change along the line at any instant is given by Eqns.5.3 and 5.4, which are known as the 'Telegraphist's Equations'.

$$\frac{\partial V}{\partial z} = -L \frac{\partial I}{\partial t} \quad \dots(5.3)$$

$$\frac{\partial I}{\partial z} = -C \frac{\partial V}{\partial t} \quad \dots(5.4)$$

By differentiating Eqn. 5.1 and substituting in Eqn. 5.2 gives:

$$\frac{d^2V}{dz^2} = \gamma^2 V \quad \dots(5.5)$$

where  $\gamma = \sqrt{ZY}$  ... (5.6)

Figure 5.1: General Transmission Line

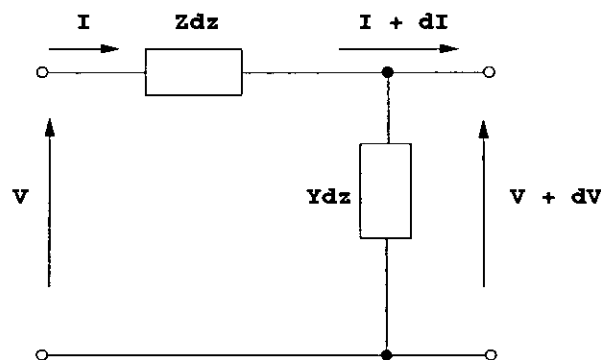
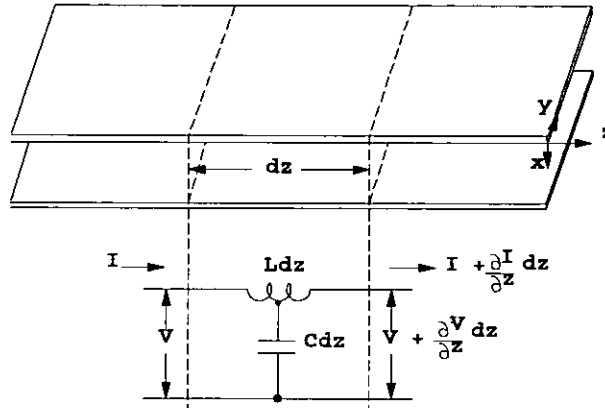


Figure 5.2: Loss-Less Transmission Line



The solution to Eqn. 5.5, which is a second order differential equation, is of the form

$$V = V_+ e^{-\gamma z} + V_- e^{+\gamma z} \quad \dots(5.7)$$

Then, from Eqn. 5.1, the corresponding solution for current is

$$I = \frac{1}{Z_o} [V_+ e^{-\gamma z} - V_- e^{+\gamma z}] \quad \dots(5.8)$$

where

$$Z_o = \frac{Z}{\gamma} = \sqrt{\frac{Z}{Y}} = \sqrt{\frac{(R+j\omega L)}{(G+j\omega C)}} \quad \dots(5.9)$$

The characteristic impedance,  $Z_o$ , is in general complex, indicating that the voltage and current for a single travelling wave are not in phase.  $\gamma$  is known as the propagation constant and is also generally complex:

$$\gamma = \alpha + j\beta = \sqrt{ZY} = \sqrt{(R+j\omega L)(G+j\omega C)} \quad \dots(5.10)$$

so that if Eqn. 5.7 is re-written using  $\alpha$  and  $\beta$  we have:

$$V = V_+ e^{-\alpha z} e^{-j\beta z} + V_- e^{\alpha z} e^{j\beta z} \quad \dots(5.11)$$

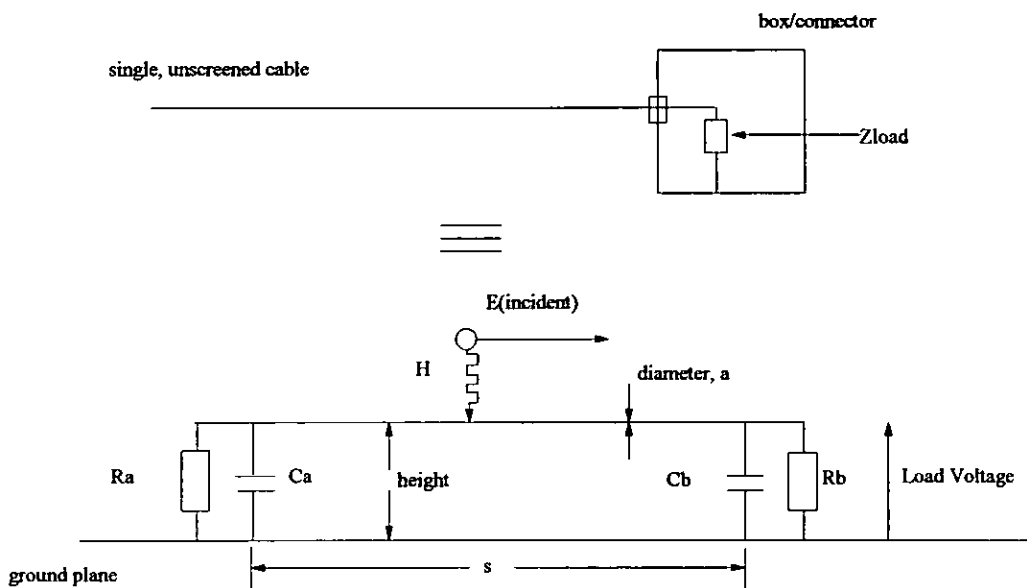
In this last equation  $\alpha$  is the exponential attenuation (in nepers per metre) of the wave and is called the attenuation constant. The constant  $\beta$  is the amount of phase shift per unit length (in radians per metre) of the wave and is called the phase change constant.

### 5.3 CABLE/CONNECTOR INGRESS MODEL DEVELOPMENT

#### 5.3.1 Initial Model Development

The bulk of practical data on avionic and electronic equipment upset between 1 MHz and some tens of GHz supports the premise that the higher the RF energy coupled to an electronic system, the more likely it is to be upset. Indeed, from other BAe work by this researcher, there appear few cases where this premise has been incorrect. Thus it is the maximum (*i.e.* worst case) voltage generated in the load inside the avionic box which is of most interest and which is to be modelled. To quantify this maximum  $V_L$  the specific case considered is where a plane wave is incident, perpendicular to the ground plane, with the electric field  $E_z^i$  parallel to the wire, thus providing maximum energy coupling to it from an incident plane EM wave. The circuit assessed is given in Fig. 5.3, where a wire of diameter 'a' and length 's', is suspended at a height 'h' above the ground plane. The left hand termination impedance  $Z_A$  is represented by a resistance,  $R_A$ , in parallel with a capacitance,  $C_A$ . Likewise the right hand termination impedance  $Z_B$ , across which the RF-induced voltage  $V_L$  appears, is represented by a resistance,  $R_B$ , in parallel with a capacitance  $C_B$ . This initial model does not consider the specific effects of parasitic capacitance of the connector interface, but takes them into account as part of the load impedance. The axes definition for this assessment is: x - perpendicular to the ground plane, y - perpendicular to wire, in the plane of the ground plane, and z - along the wire. From this definition and the statement above concerning the incidence of the wave front on the wire, it can be seen that the electric field is independent of y and z.

Figure 5.3: Cable Coupling Model



The source and load impedances respectively are given by

$$Z_A = \frac{R_A}{1+j\omega R_A C_A} \quad \text{and} \quad Z_B = \frac{R_B}{1+j\omega R_B C_B} \quad \dots(5.12)$$

where  $\omega = 2\pi f$  and  $f$  = frequency in Hertz.

This configuration can be analysed, as detailed in Section 1.4 of [5-1], by considering the ground plane replaced by an image of the cable, its terminating impedances and the incident field, thus making it equivalent to an isolated, air-spaced twin wire line. For equivalence the isolated line spacing  $b = 2h$  and its terminations  $Z_1$  and  $Z_2$  are equal to twice  $Z_A$  and  $Z_B$  respectively. The characteristic impedance of the wire above the ground plane (*i.e.* the wire and its image) is equivalent to the two wire, air spaced case as in Eqn. 5.9:

$$Z_o = \sqrt{\frac{(R+j\omega L)}{(G+j\omega C)}} = \sqrt{\frac{L(1-\frac{R}{\omega L})}{C(1-\frac{G}{\omega C})}} \quad \dots(5.13)$$

where  $R$ ,  $G$ ,  $L$  and  $C$  are the resistance, conductance, inductance and capacitance per unit length of the line respectively. So, for the loss-less, air-spaced line Eqn. 5.13 reduces to

$$Z_o = \sqrt{\frac{L}{C}} \quad \dots(5.14)$$

which, for the two wire, air spaced wire above a ground plane, results in

$$Z_o = 120 \ln\left(\frac{2b}{a}\right) = 276 \log\left(\frac{h}{a}\right) \quad \dots(5.15)$$

where  $a$  = wire radius (m) and  $h$  = height above ground plane (m).

The propagation constant,  $\gamma$ , of a uniform transmission line is given in Eqn. 5.10, which can be expanded to:

$$\gamma = \sqrt{(j\omega)^2 LC} \sqrt{\left(1 + \frac{R}{j\omega L}\right) \left(1 + \frac{G}{j\omega C}\right)} \quad \dots(5.16)$$

For higher frequencies, where  $\omega L \gg R$  and  $\omega C \gg G$ ,  $\gamma$  can be evaluated by using the first two terms only of the binomial expansion  $(1+X)^n = 1+nX+\dots$

$$\begin{aligned} \gamma &\approx j\omega \sqrt{LC} \left[ \left(1 + \frac{R}{2j\omega L}\right) \left(1 + \frac{G}{2j\omega C}\right) \right] \\ &\approx j\omega \sqrt{LC} \left[ 1 + \frac{1}{2} \left( \frac{R}{j\omega L} + \frac{G}{j\omega C} \right) \right] \\ &= \frac{1}{2} \left( R \sqrt{\frac{C}{L}} + G \sqrt{\frac{L}{C}} \right) + j\omega \sqrt{LC} \quad \dots(5.17) \end{aligned}$$

So, equating real and imaginary parts,  $\alpha$  and  $\beta$  are given by

$$\alpha = \frac{1}{2} \left( R \sqrt{\frac{C}{L}} + G \sqrt{\frac{L}{C}} \right) = \frac{R}{2Z_0} + \frac{GZ_0}{2} \quad \text{nepers/metre} \quad \dots(5.18)$$

$$\beta = \omega \sqrt{LC} = \frac{2\pi}{\lambda} \quad \text{radians/metre} \quad \dots(5.19)$$

where  $\lambda = \frac{c}{f}$  and  $c = 2.997925 \times 10^8 \text{ ms}^{-1}$ . On most lines, especially air-spaced ones, losses in the line due to the shunt conductance  $G$  are negligible compared with the conductor skin losses. Hence  $\alpha$  can be simplified to

$$\alpha = \frac{R}{2Z_0} \quad \text{nepers/metre} \quad \dots(5.20)$$

To evaluate  $\alpha$ , which is considered to be an important factor in the microwave band assessment, it is necessary to find the resistance per unit length of the line. This is found by examining the internal impedance of a plane conductor then applying this to the special case of a round conductor. This impedance value, for a single wire conductor, comprises a resistive term and an internal inductance. The wire materials under consideration are all conductors which satisfy Ohm's Law,

$$\mathbf{J} = \sigma \mathbf{E} \quad \dots(5.21)$$

where  $\mathbf{J}$  = current density,  $\text{Am}^{-1}$

$\sigma$  = conductivity,  $\text{Sm}^{-1}$

$\mathbf{E}$  = applied electric field,  $\text{Vm}^{-1}$

Substituting Eqn. 5.21 into the complex form of Maxwell's equation

$$\nabla \times \mathbf{H} = \mathbf{J} + j\omega \mathbf{D}$$

gives, since the electric flux density  $\mathbf{D} = \epsilon \mathbf{E}$ :

$$\nabla \times \mathbf{H} = (\sigma + j\omega\epsilon) \mathbf{E} \quad \dots(5.22)$$

Since the divergence of the curl of any vector is zero,

$$\nabla \cdot \nabla \times \mathbf{H} = (\sigma + j\omega\epsilon) \nabla \cdot \mathbf{E} = 0$$

Thus

$$\nabla \cdot \mathbf{D} = \rho = 0 \quad \dots(5.23)$$

To derive the differential equation which determines field penetration into the wire, we take the curl of the Maxwell curl equation for electric field:

$$\nabla \times \mathbf{E} = -j\omega \mathbf{B}$$

and using the definition of permeability

$$\mathbf{B} = \mu \mathbf{H} = \mu_0 \mu_r \mathbf{H}$$

where  $\mathbf{B}$  = magnetic flux density, Tesla

$\mathbf{H}$  = magnetic field,  $\text{Am}^{-1}$

$\mu_0$  = vacuum permeability,  $4\pi \times 10^{-7} \text{ Hm}^{-1}$

$\mu_r$  = relative permeability

we have, using Vector Identity 7 of Lorraine and Corson [5-2],

$$\nabla \times \nabla \times \mathbf{E} = \nabla(\nabla \cdot \mathbf{E}) - \nabla^2 \mathbf{E} = j\omega\mu \nabla \times \mathbf{H} \quad \dots(5.24)$$

Then by using Eqn. 5.23 and substituting Eqn. 5.22 in Eqn. 5.24 and neglecting displacement current, we have

$$\nabla^2 \mathbf{E} = j\omega\mu\sigma \mathbf{E} \quad \dots(5.25)$$

and likewise for current density

$$\nabla^2 \mathbf{J} = j\omega\mu\sigma \mathbf{J} \quad \dots(5.26)$$

We now consider an infinitely deep conductor with a uniform field parallel to the conductor's surface. With the electric field vector in the z direction and assuming no variations with y or z, then Eqn. 5.25 becomes,

$$\frac{d^2 \mathbf{E}_z}{dx^2} = j\omega\mu\sigma \mathbf{E}_z = \tau^2 \mathbf{E}_z \quad \dots(5.27)$$

where  $\tau^2 = j\omega\mu\sigma$

Since  $\sqrt{j} = \frac{(1+j)}{\sqrt{2}}$  (taking the root with the positive sign), then

$$\tau = (1+j) \sqrt{\pi f \mu \sigma} = \frac{1+j}{\delta} \quad \dots(5.28)$$

where  $\delta = \frac{1}{\sqrt{\pi f \mu \sigma}}$  ... (5.29)

and  $\delta$  = the Skin Depth, the depth at which the current has decreased exponentially to 1/e (36.8%) of its value at the conductor's surface. A complete solution of Eqn. 5.27 in terms of  $\delta$  is

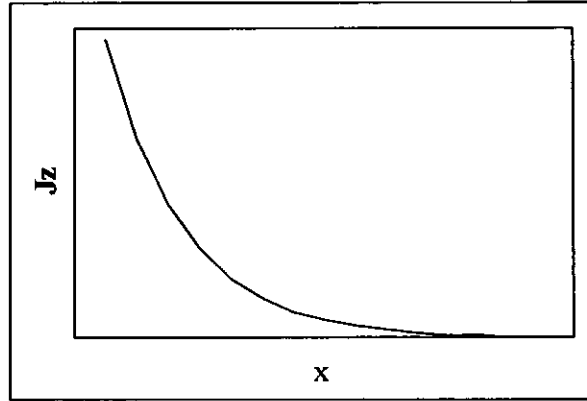
$$\mathbf{E}_z = \mathbf{E}_0 e^{-\frac{x}{\delta}} e^{\frac{-jx}{\delta}} \quad \dots(5.30)$$

where  $\mathbf{E}_0$  is the electric field at the conductor's surface and  $x$  is the distance into the material. Likewise the current density at a depth  $x$  in the material is given by

$$\mathbf{J}_z = \mathbf{J}_0 e^{-\frac{x}{\delta}} e^{\frac{-jx}{\delta}} \quad \dots(5.31)$$

where  $\mathbf{J}_0$  is the surface current density. This decay of current density with increasing depth into a conductor is depicted in Fig. 5.4.

Figure 5.4: Current Decay in a Plane Solid Conductor



The total current flowing in the plane conductor is found by integrating the current density, as in Eqn. 5.31, from the surface to an infinite depth. For a unit width

$$\mathbf{J}_z = \int_0^{\infty} \mathbf{J}_z dx = \int_0^{\infty} \mathbf{J}_0 e^{-(1+j)\left(\frac{x}{\delta}\right)} dx = \frac{\mathbf{J}_0 \delta}{(1+j)} \quad \dots(5.32)$$

The surface electric field is given by surface current density as

$$\mathbf{E}_{z0} = \frac{\mathbf{J}_0}{\sigma} \quad \dots(5.33)$$

Now, internal impedance for unit length and width is defined as

$$Z_s = \frac{\mathbf{E}_{z0}}{\mathbf{J}_z} = \frac{1+j}{\sigma \delta} \quad \dots(5.34)$$

By defining

$$Z_s = R_s + j\omega L_i \quad \text{then equating real and imaginary parts:}$$

$$R_s = \frac{1}{\sigma \delta} = \sqrt{\frac{\pi f \mu}{\sigma}} \quad \dots(5.35)$$

and

$$\omega L_i = \frac{1}{\sigma \delta} \quad \dots(5.36)$$

Having examined the plane conductor case we now proceed to consider the round wire case, a conductor of circular cross section. Eqn. 5.26, the differential equation for current density, can be expressed in cylindrical co-ordinates as:

$$\frac{d^2 \mathbf{J}_z}{dr^2} + \frac{1}{r} \frac{d\mathbf{J}_z}{dr} + \tau^2 \mathbf{J}_z = 0 \quad \dots(5.37)$$

where  $\tau^2 = -j\omega\mu\sigma$  or  $\tau = j^{-\frac{1}{2}} \sqrt{\omega\mu\sigma} = j^{-\frac{1}{2}} \frac{\sqrt{2}}{\delta} \quad \dots(5.38)$

The differential Eqn. 5.37 is in the form of a Bessel equation and it can be shown, see p.179 of [3-24], that

$$\mathbf{J}_z = \sigma \mathbf{E}_o \frac{\text{Ber}(\sqrt{2} r/\delta) + j \text{Bei}(\sqrt{2} r/\delta)}{\text{Ber}(\sqrt{2} r_o/\delta) + j \text{Bei}(\sqrt{2} r_o/\delta)} \quad \dots(5.39)$$

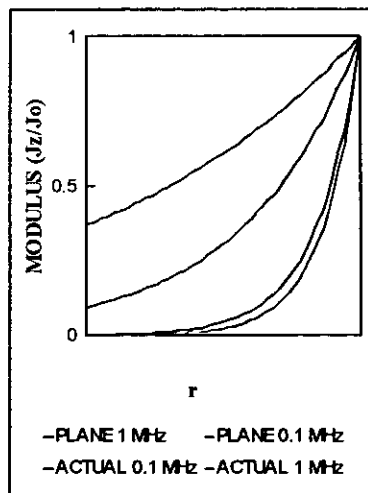
where  $r_o$  = radius of wire and  $r$  = radius at which  $\mathbf{J}_z$  is calculated and

$$\text{Ber}(\sqrt{2} r/\delta) \equiv \text{real part of } \mathbf{J}_o(j^{-1/2}[\sqrt{2} r/\delta])$$

$$\text{Bei}(\sqrt{2} r/\delta) \equiv \text{imaginary part of } \mathbf{J}_o(j^{-1/2}[\sqrt{2} r/\delta])$$

These real and imaginary parts of the complex Bessel function are tabulated in many references, e.g. [3-24]. A comparison of  $\mathbf{J}_z$  within the wire by the exact Eqn. 5.39 and that for a planar conductor, Eqn. 5.31, shows that, for high ratios of wire radius to  $\delta$ , there is little error in analysing a wire using the latter equation. The actual and infinite parallel plane values of  $\mathbf{J}_z$  against wire radius are shown in Fig. 5.5, which shows that for high values of  $\frac{r_o}{\delta}$  (wire radius/skin depth) the difference between the Bessel function solution and that using the infinite plane one is minimal for values of  $\frac{r_o}{\delta} > 7.55$  (i.e.  $> 1$  MHz for 1mm copper wire). Ramo *et al.* note 'Thus, if ratio of wire radius to delta is large, it seems that there should be little error in analyzing the wire from the results developed for plane solids.' Calculations of  $\frac{r_o}{\delta}$  for 1 mm diameter copper wire 2 and 18 GHz yield 460.8 and 1382.3 respectively, which are  $\gg 7.55$  and adequately justify the use of the infinite plane equation for  $\delta$  in the model.

Figure 5.5: Exact vs. Parallel Plane Comparison of Current Density



The impedance of a round wire is found from the total current in the wire and the electric field at the surface. Now the current  $I$  is given by the line integral of magnetic field around the wire periphery:

$$\oint \mathbf{H} \cdot d\mathbf{l} = I \quad \text{or} \quad 2\pi r_o \mathbf{H}_\phi |_{r=r_o} = I \quad \dots(5.40)$$

Magnetic field is obtained from the surface electric field by Maxwell's equation:

$$\nabla \times \mathbf{E} = -j\omega \mu \mathbf{H} \quad \dots(5.41)$$

The fields  $\mathbf{E}_z$  and  $\mathbf{H}_\phi$  alone are present in a round conductor with no variations in  $z$  or  $\phi$ , and only  $r$  derivatives remain, so Eqn. 5.41 becomes

$$\mathbf{H}_\phi = \frac{1}{j\omega \mu} \frac{d\mathbf{E}_z}{dr} \quad \dots(5.42)$$

It can be shown from the solution of Eqn. 5.37 that  $\mathbf{J}_z$  in a circular conductor is

$$\mathbf{J}_z = \frac{\sigma \mathbf{E}_o}{\mathbf{J}_o(\tau_o)} \mathbf{J}_o(\tau)$$

Using  $\mathbf{E}_z = \frac{J_z}{\sigma}$  we then have  $\mathbf{E}_z = \mathbf{E}_o \frac{\mathbf{J}_o(\tau)}{\mathbf{J}_o(\tau_o)}$  ... (5.43)

By substituting in Eqn. 5.42 and remembering from Eqn. 5.38 that  $\tau^2 = -j\omega \mu \sigma$ ,

$$\mathbf{H}_\phi = \frac{\mathbf{E}_o \tau}{j\omega \mu} \frac{\mathbf{J}'_o(\tau)}{\mathbf{J}_o(\tau_o)} = -\frac{\sigma \mathbf{E}_o}{\tau} \frac{\mathbf{J}'_o(\tau)}{\mathbf{J}_o(\tau_o)} \quad \dots(5.44)$$

where  $\mathbf{J}'_o(\tau)$  represents  $\left[ \frac{d}{d(\tau)} \right] \mathbf{J}_o(\tau)$

From Eqn. 5.40  $\mathbf{I} = -\frac{2\pi r_o \sigma \mathbf{E}_o}{\tau} \frac{\mathbf{J}'_o(\tau_o)}{\mathbf{J}_o(\tau_o)}$  ... (5.45)

and thus the internal impedance per unit length is

$$Z_i = \frac{\mathbf{E}_z |_{r=r_o}}{\mathbf{I}} = \frac{\omega \mathbf{J}_o(\tau_o)}{2\pi r_o \sigma \mathbf{J}'_o(\tau_o)} \quad \dots(5.46)$$

### Solution for arbitrary frequency

To solve Eqn. 5.46 for arbitrary frequencies we have

$$Z_i = R + j\omega L_i = \frac{jR_s}{\sqrt{2} \pi r_o} \left[ \frac{Ber'q + jBei'q}{Ber'q + Bei'q} \right]$$

where  $Ber'$  and  $Bei'$  are derivatives of  $Ber$  and  $Bei$  and

$$R_s = \frac{1}{\sigma \delta} = \sqrt{\frac{\pi j \mu}{\sigma}} \quad \text{and} \quad q = \frac{\sqrt{2} r_o}{\delta}$$

or 
$$R = \frac{R_s}{\sqrt{2} \pi r_o} \left[ \frac{\text{Ber}q\text{Bei}'q - \text{Bei}q\text{Ber}'q}{(\text{Ber}'q)^2 + (\text{Bei}'q)^2} \right] \quad \Omega\text{m}^{-1} \quad \dots(5.47)$$

and 
$$\omega L_i = \frac{R_s}{\sqrt{2} \pi r_o} \left[ \frac{\text{Ber}q\text{Bei}'q + \text{Bei}q\text{Ber}'q}{(\text{Ber}'q)^2 + (\text{Bei}'q)^2} \right] \quad \Omega\text{m}^{-1} \quad \dots(5.48)$$

### High frequency solution

At high frequencies, the complex argument  $\tau r_o$  is large. It may be shown that  $\frac{J_o(\tau r_o)}{J_o'(\tau r_o)}$  approaches  $-j$  and the high frequency approximation to Eqn. 5.46 is

$$Z_i = \frac{j(\omega)^{-1/2}}{\sqrt{2} \pi r_o \sigma \delta} = \frac{(1+j)}{2 \pi r_o \sigma \delta} \quad \dots(5.49)$$

or 
$$R = \omega L_i = \frac{1}{2 \pi r_o \sigma \delta} \quad \Omega\text{m}^{-1} \quad \dots(5.50)$$

For the model under consideration  $r_o = \frac{a}{2}$  and  $\sigma = \frac{1}{\rho}$  so Eqn. 5.50 becomes:

$$R = \omega L_i = \frac{2\rho}{\pi a \delta} = \frac{\rho}{\pi a \delta} \quad \dots(5.51)$$

The resistance of a wire above a ground plane, being the equivalent of a twin wire line, is thus given by

$$R_{\text{twin}} = \frac{2\rho}{\pi a \delta} = \frac{2}{a} \sqrt{\frac{\rho f \mu}{\pi}} \quad \Omega\text{m}^{-1} \quad \dots(5.52)$$

since, as shown earlier in this section,

$$\delta = \frac{1}{\sqrt{\pi f \sigma \mu}} = \sqrt{\frac{\rho}{\pi f \mu}} \quad \text{metres.}$$

Thence  $R_{\text{twin}}$  can be expressed in terms of relative permeability and resistivity as

$$R_{\text{twin}} = 1.66 \times 10^{-7} \frac{\sqrt{\rho_r \mu_r f}}{a} \quad \Omega\text{m}^{-1} \quad \dots(5.53)$$

where

$$\rho = \rho_r \rho_c$$

$\rho_c$  = resistivity of Copper,  $\Omega$ -metre

$\rho_r$  = resistivity, relative to Copper

$$\mu = \mu_o \mu_r$$

$\mu_o$  = air permeability,  $4\pi \times 10^{-7} \text{ Hm}^{-1}$

By substituting Eqn. 5.53 into Eqn. 5.20, we have

$$\alpha = 8.3 \times 10^{-8} \frac{\sqrt{\rho_r \mu_r f}}{a Z_o} \quad \text{nepers/metre}$$

and by substituting for  $Z_o$ , this gives

$$\alpha = 3 \times 10^{-10} \frac{\sqrt{\rho_r \mu_r f}}{a \log_{10} h/a} \text{ nepers/metre} = 2.6 \times 10^{-9} \frac{\sqrt{\rho_r \mu_r f}}{a \log_{10} h/a} \text{ dBm}^{-1} \quad \dots(5.54)$$

Common and differential mode currents flow in a twin-wire and method of images consideration of a single wire over a ground plane, but only the differential mode current flows in the latter case. This is the only current which gives rise to a voltage in the load and is thus the only one considered here. The line can thus be considered to be excited by an infinite number of distributed small voltage generators along its length. If  $K(z)$  is the distribution then the elemental voltage across a given length of line,  $dz$ , is given by

$$dV(z) = K(z)dz \quad \dots(5.55)$$

By reference to transmission line theory as expounded in Appendix E, Sections 4 and 5 of [5-1], the summation of the contributions from all the  $dV(z)$  voltage generators (*i.e.* integrating over the line length  $s$ ) gives a current of

$$I(z) = \frac{Z_o \cosh \gamma(s-z) + Z_2 \sinh \gamma(s-z)}{Z_o D} \times \int_0^z K(z) [Z_o \cosh \gamma z + Z_1 \sinh \gamma z] dz$$

$$+ \frac{Z_o \cosh \gamma z + Z_1 \sinh \gamma z}{Z_o D} \times \int_0^s K(z) [Z_o \cosh \gamma(s-z) + Z_2 \sinh \gamma(s-z)] dz \quad \dots(5.56)$$

where  $D = (Z_o Z_1 + Z_o Z_2) \cosh \gamma s + (Z_o^2 + Z_1 Z_2) \sinh \gamma s \quad \dots(5.57)$

and, resulting from the method of images,  $Z_1 = 2Z_A$ ;  $Z_2 = 2Z_B$ . The load current as a function of  $\omega$  is then found by substituting  $z = s$  in Eqn. 5.56, giving

$$I(s, \omega) = \frac{2}{D} \int_0^s K(s, \omega) [Z_o \cosh \gamma s + Z_1 \sinh \gamma s] ds \quad \dots(5.58)$$

noting that, from the method of images, the differential current in a wire above a ground plane is twice that in an isolated, twin-wire case. This equation for the load current then becomes, by performing the integration:

$$I(s, \omega) = \frac{2}{\gamma D} [K(\omega) [Z_o \sinh \gamma s + Z_1 (\cosh \gamma s - 1)]] \quad \dots(5.59)$$

Now  $K(z, \omega)$ , which is the total electric field at a height  $h$  above the ground plane, is given by

$$K(z, \omega) = E_z^i(h, z, \omega) - E_z^i(0, z, \omega) \quad \dots(5.60)$$

where the first term is the incident field in the  $z$  direction at  $x = h$ , and the second term is that for  $x = 0$ .

Thus, at the ground plane ( $x = 0$ )  $E_x = 0$ , and  $K(z, \omega)$  becomes

$$K(\omega) = E_{\text{total}} = E_z^i e^{+\beta h} - E_z^i e^{-\beta h} = E_z^i (2j \sin \beta h) \quad \dots(5.61)$$

Finally, by substitution for  $K(\omega)$  and since  $V_L(\omega) = I(z, \omega)Z_B$  we have:

$$V_L(\omega) = \frac{2Z_B}{\gamma D} \left[ (2j \sin \beta h) E_z^i [Z_0 \sinh \gamma s + Z_1 (\cosh \gamma s - 1)] \right] \quad \dots(5.62)$$

This equation forms the basis of the model and a computer programme incorporating the equation was designed and coded to allow investigation of the physical phenomenon of coupling and enable subsequent model refinement.

### 5.3.2 Comparison Of Model Results With Initial Empirical Data

To gain confidence in the model as an initial representation of a real cable, loaded at both ends, entering an avionics box, a direct comparison of the model with available empirical data was conducted. Each of the data sources is discussed, followed by presentation and discussion of the comparison. Price [3-14] performed 2-18 GHz EMC Laboratory measurements aimed at quantifying the maximum pick-up inside an avionics box. A dummy avionics box with a single 0.5m, open circuit cable was investigated, by irradiating it at five spot frequencies. The internal instrumentation of the box is shown in Fig. 5.6 and the general test layout in Fig. 5.7, showing the position of the transmit horn antenna relative to the box and cable, all inside the three-sided RAM enclosure. Transfer functions of 5.0 (maximum) and 0.16 (minimum) mV/mWm<sup>-2</sup> with no obvious frequency dependency were derived from cable end voltage vs. estimated illuminating power density. Negligible difference in the voltages was seen between CW and pulsed radiation. Radiation pattern distortion when attempting to measure the external field necessitated this assumption that illuminating power density was equal to transmitter power minus feeder loss plus antenna gain. This distortion, resulting from using the relatively large antenna with the cable clearly in the near field (0.2m from the cable, necessary in order to achieve detectable voltages with the low power signal generator used) reduces the quality of the transfer function values.

Figure 5.6: Internal Instrumentation Of Dummy Avionics Box

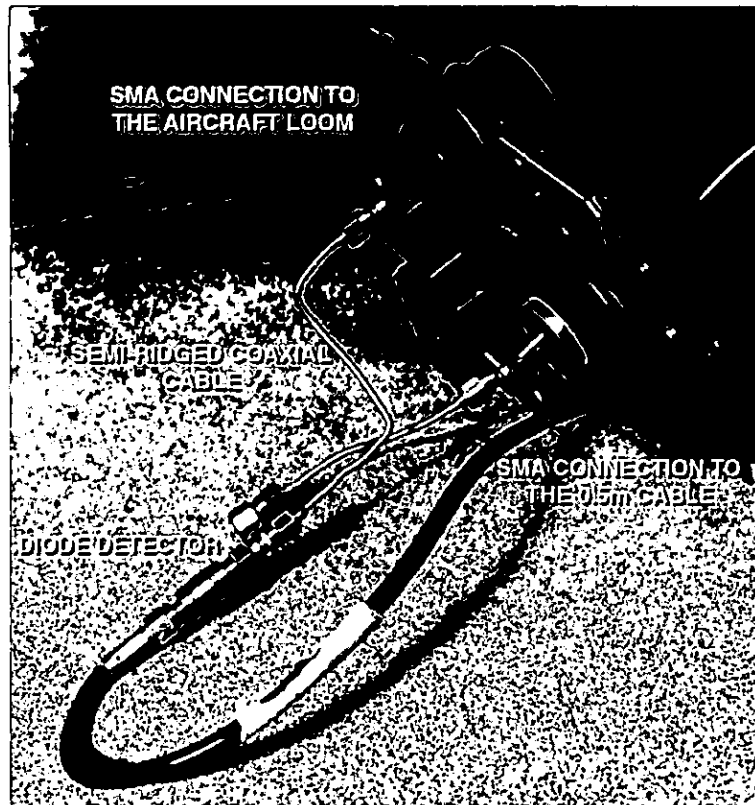
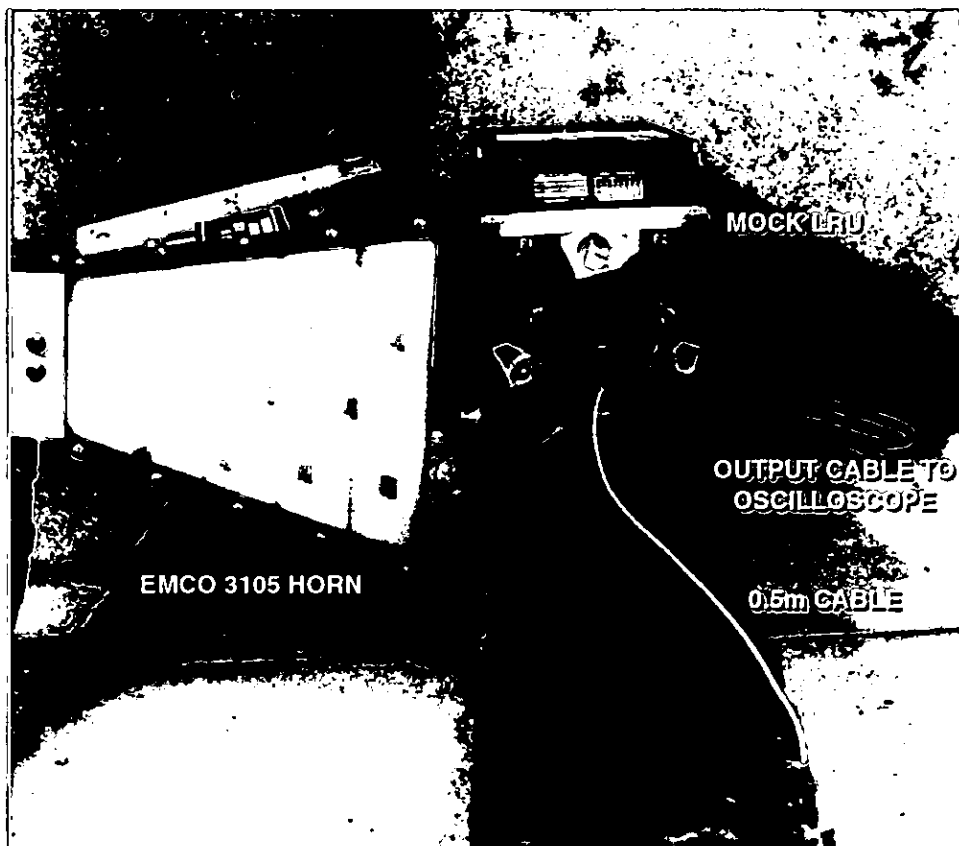


Figure 5.7: General Layout Of Initial BAe Cable Ingress Tests



Willis [3-20] irradiated a 2m single wire, loaded at each end by a 50 ohm load, at nineteen spot frequencies between 1 and 10.9 GHz using a wide angle double-ridged waveguide antenna. In these EMC laboratory tests he observed a decrease in load voltage with increasing frequency and noted that, >1 GHz, pick-up was more pronounced when the transmitting antenna was illuminating the 1m of wire at the measurement end of the cable rather than the far end 1m of cable. Ditton [4-21] examined the effects of variation of source and load impedance on the pick-up on a 0.6m cable at 3.0 and 9.1 GHz. He concluded that  $V_L$  did not appreciably change as a function of load, for the three load combinations tested. He also noted that an earlier U.S. cable coupling study [5-3] had shown that an unshielded cable had a maximum effective aperture close to that calculated for a  $\frac{\lambda}{2}$  dipole. In conducting further tests of a 0.19m cable at 3.0, 5.6 and 9.1 GHz, he observed no increase in maximum pick-up. Both cables tested were longer than  $\frac{\lambda}{2}$  for the frequencies tested. Roe [4-20] irradiated a 0.61m and a 3.05m cable at eight spot frequencies in the range 120 MHz to 2 GHz, concluding that his results appeared to show  $V_L$  to be independent of length, twist or routing. From this data Roe produced, by the method of least squares fit, an equation for load voltage:\*

$$V_L = P_R + 5.86 - 10 \log_{10}(f)^2 + 10 \log_{10}(P_D) \quad \text{dB}\mu\text{V} \quad \dots(5.63)$$

where  $P_R$  = Received Power (dBm) and  $P_D$  = Incident Power Density ( $\text{Wm}^{-2}$ ).

In arriving at values of source and load impedance for insertion into the model a typical circuit configuration was chosen, that of cascaded operational amplifiers. The 741 operational amplifier is still widely used in modern military avionics, as are transistors of the BC107 and BCY70 genre. Its input is based on the traditional long-tailed pair, using transistors with characteristics similar to the 2N930. The values used in the model,  $75\Omega$  in parallel with 30 pF for  $Z_A$  and  $9.8 \text{ M}\Omega$  in parallel with 3 pF for  $Z_B$ , are typical values taken from published work [5-4]. The cable material chosen was 0.001 m diameter copper, to match that used in aircraft and most of the referenced earlier research. The length chosen, 10 m, is typically the longest cable length in a fighter aircraft of length 15 m and wingspan 14 m. A height above ground plane of 0.05 m was chosen, the value used in avionics EMC qualification testing (see Appendix B) and the value used by at least Willis.

---

\* Roe's equation did not match the data presented in the paper, and two errors were discovered which were notified to Roe. The revised equation appears here.

Fig. 5.8 shows the comparison between the empirical data of Price (BAe), Willis (U.K.), Ditton (U.S.) and Roe (U.S.). The Roe data is the maximum pick-up, estimated by adding the one sigma value of 5-6 dB to the data sets presented in [4-20]. Eqn. 5.63 is also included, extrapolated above 2 GHz, to explore the possibility of its use in the 2-18 GHz band as an initial indicator of maximum pick-up. The model output shows an approximate 20 dB decrease per decade frequency similar to the other data sets, with a  $\frac{\sin x}{x}$  voltage spectrum envelope. The waveform, with its many deep troughs and marked amplitude variation over small frequency steps, is reminiscent of the Chapter 3 airframe attenuation profiles.

Definitive comparison between the unlike data sets is not possible as the experimental configuration is not described for the non-BAe data, but trends have been identified and qualitative observations made. The gradient of the Willis and Price data is similar to the Roe equation, at approximately 20 dB decrease in  $V_L$  per decade increasing frequency, *i.e.* a  $\frac{1}{f}$  dependency. There is marked amplitude difference between the data sets, with a maximum difference of 33 dB (= a voltage ratio of 1995). The absolute amplitude is significantly different between the Willis and Price data, and between the Willis and 1-2 GHz Roe data, and the Roe equation can be seen to lie half way between the Willis and Price data. Based on the findings of the aircraft investigations it is probable that an erroneous picture of amplitude is given by these data sets, all of which are from spot frequency tests. Those pseudo-swept frequency measurements (see Section 3.3.1) showed significant resonances, some only 20 MHz apart, with adjacent values as much as 50 dB different and, as shown in Fig. 3.12, the test frequency resolution can appreciably affect the profile. It is thus considered likely that all the data sets in Fig. 5.8 are broadly similar and clustered more closely about the Roe empirical equation.

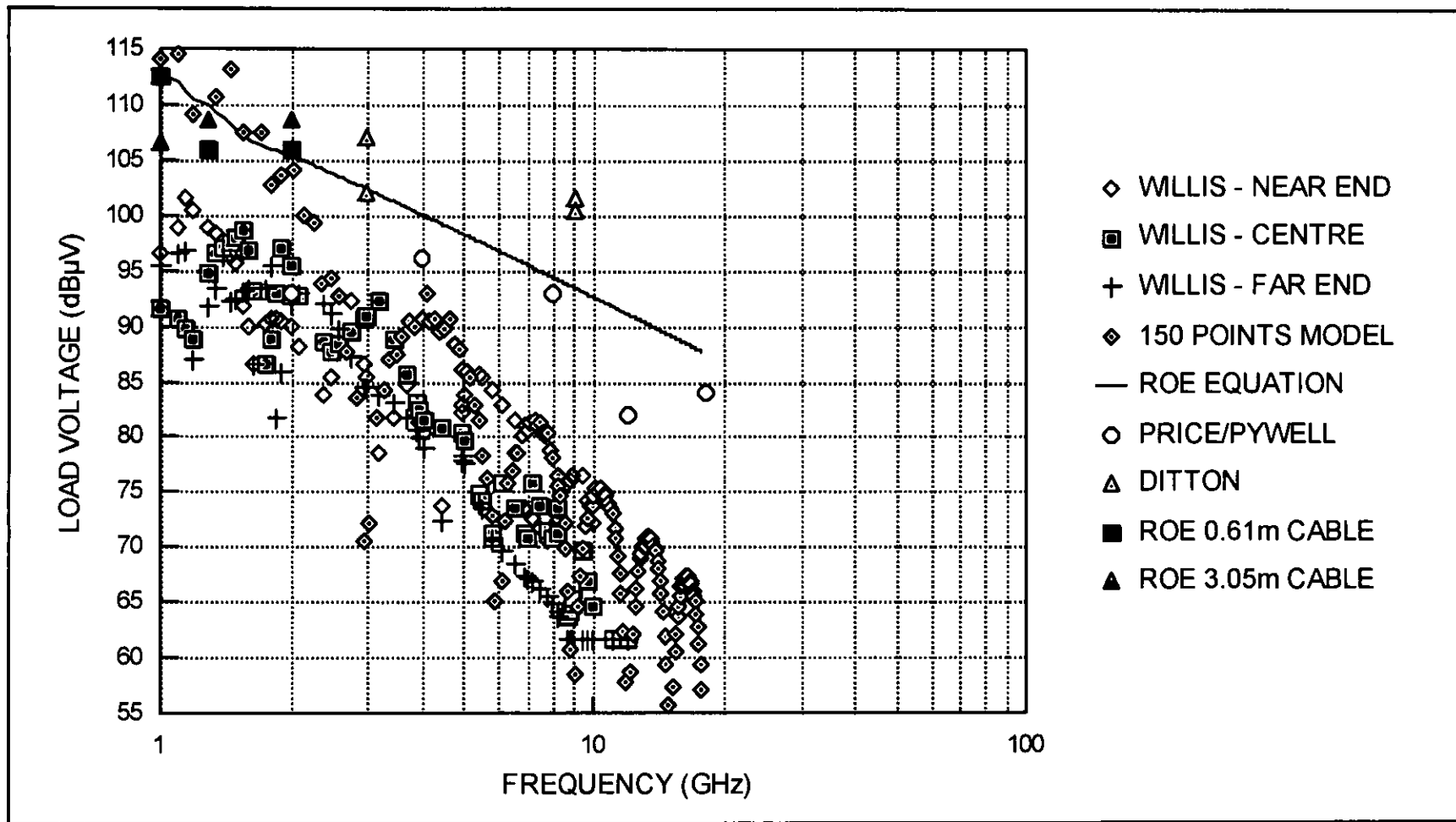


Figure 5.8: Cable Coupling: Unscreened Single Wire Pick-Up

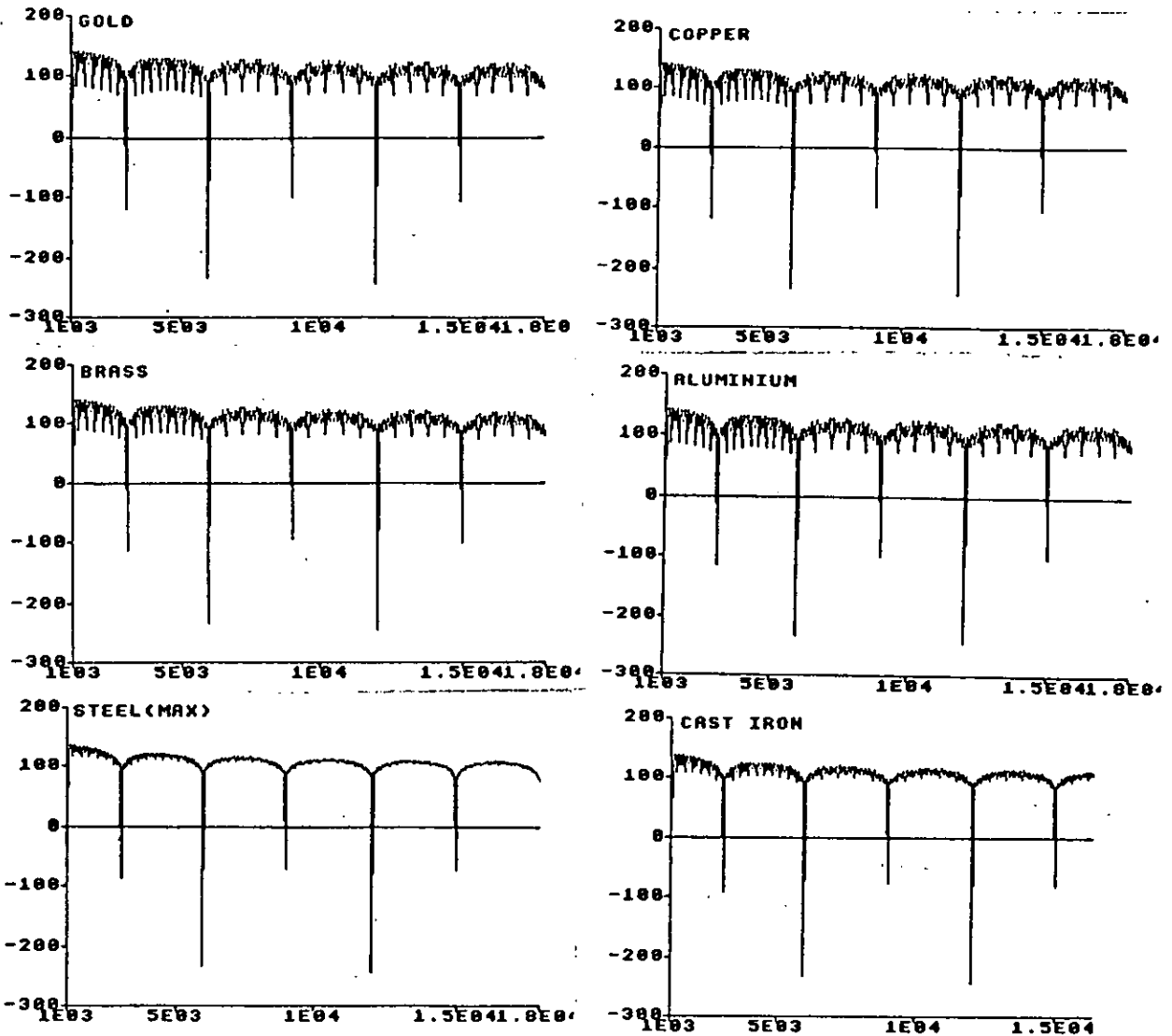
A further aspect which may well affect the comparison of the different measurement data sets with each other and with the model is the question of what source and load impedances, cable length, height above ground plane, cable material and incident power density were used by the non-BAe researchers. Wherever possible data has been normalised to  $1 \text{ Wm}^{-2}$  but many of the other parameters used by those researchers are unknown, thus preventing a true comparison and highlighting the need for further experimentation where modelled and controlled test data can be compared.

### 5.3.3 Load Voltage Variation With Cable Length

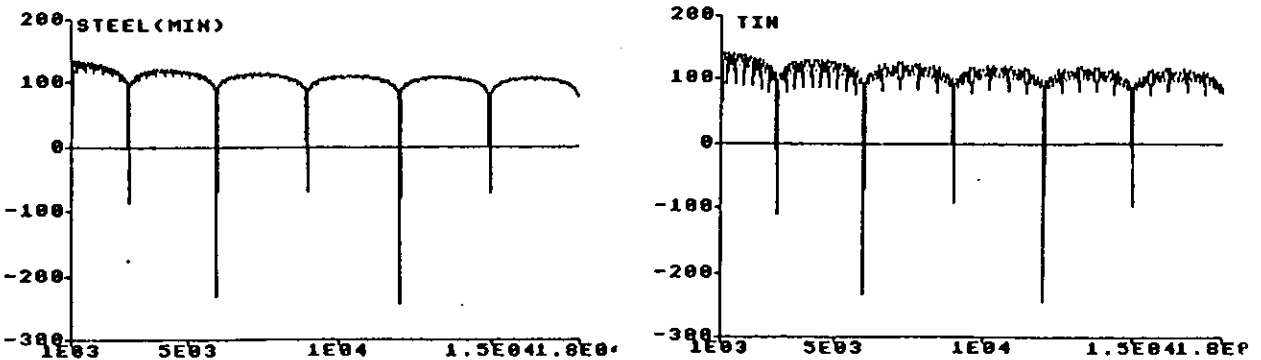
The main item of interest with respect to the coupling of microwave energy to cables is why pick-up is considered to be negligible at distances further than  $\frac{\lambda}{2}$  from the load, irrespective of frequency [2-17]. The inadequate resolution of the existing data sets for adequate coupling characterisation led to the deferment of detailed investigation of the  $V_L$  dependency on cable length  $s$  until appropriate measured data was available; Chapter 6 covers these subsequent investigations.

The observation that detectable  $V_L$  had been seen for cables of length up to 3.05 m can only be reconciled with the 'negligible' opinion above, voiced in many papers (of which [2-17] is one of the more recent and authoritative applicable to the E.C.), if levels of  $V_L$  potentially capable of causing avionic upset reach a plateau at  $\frac{\lambda}{2}$  from the box and get no higher for longer cable lengths. For this to occur a mechanism would need to occur whereby energy coupled to the cable is absorbed and/or re-radiated. Absorption is a function of skin depth  $\delta$ , see Eqn. 5.29, and is covered in the lossy cable model. An extra term was thus proposed for the model, a 'Re-Radiation' term,  $R_r$  to explain the extra loss which would have to occur for  $s \geq \frac{\lambda}{2}$ . This term was postulated to arise from re-radiation of microwave energy from the cable as the microwave current flows down the cable. To provide an indicator for the development of  $R_r$ , wire material effects on  $V_L$  were investigated using the model.  $\delta$ , which was thought to be an element in the additional term, is directly affected by the relative resistivity of the cable material ( $\mu_r = 1$  at these frequencies for conductors). Fig. 5.9 shows the effects of using eight different cable materials for the case where  $Z_A = \text{open circuit}$ , *i.e.* comparable with the dummy avionic box tests reported earlier in this section, which were to be repeated with higher frequency resolution (see Chapter 6). Little change is seen in the overall envelope, but there is significant damping of the many resonances when using materials with high resistivity, *e.g.* steel.

Figure 5.9: Variation Of Cable Pick-Up With Cable Metal



ALL X-AXES ARE FREQUENCY (MHz)  
ALL Y-AXES ARE LOAD VOLTAGE (dB $\mu$ V)



## 5.4 CONCLUDING REMARKS

Many relevant parameters used by the researchers identified in Section 5.3.2 are unknown, thus preventing a true comparison between the available empirical data and with the model. Further experimentation was thus needed where modelled and controlled test data could be compared. From the data so far presented (including that in Chapter 3), a need was also identified for this experimentation to include a pseudo-swept frequency resolution investigation to:

- a) enable the adequate characterisation of coupling, where the measurement steps chosen are small enough to ensure all peaks and (of lesser importance) troughs are captured.
- b) obtain an upper bound on the  $V_L$  profile, normalised to unit incident power density.

Examination of the outputs of the model and earlier U.K. and U.S. empirical data suggests an additional loss term, the general form of which is thought to be a multiplier  $fn(\text{cable length})$ , which:

- a) has a maximum value of 1 for a cable of 3.05m (the maximum length discovered by the author, during literature and other searching, for measured pick-up in this band),
- b) increases as a function of increasing frequency above 1 GHz,
- c) contains a re-radiation term, potentially operating along the whole cable length. This could be modelled by considering the cable as a number of small dipole elements, of length say  $\frac{\lambda}{20}$ , and ignoring ground plane effects initially.
- d) has a component dependent on skin depth, which in turn depends on the relative resistivity of the cable material.

Chapter 6 addresses all the above through high resolution cable coupling measurements conducted for different cable lengths and the subsequent investigations using, and refinement of, the model.

# *Chapter 6*

---

## **EXPERIMENTAL INVESTIGATIONS**

## 6.1 INTRODUCTION

This chapter covers investigations arising from the results of Chapter 5, the development of an initial cable coupling model and the comparison of results with available test data. High resolution (10 and 50 MHz steps), pseudo-swept 2-18 GHz measurements were conducted for an aircraft cable of different lengths entering an avionic box. Investigations were then conducted using the model. Use was made of the measured data leading to refinement of the model. These investigations aimed to determine:

- a) the validity of the model for predicting microwave coupling and an upper bound on the load end voltage,  $V_L$ , profile, normalised to unit incident power density.
- b) the maximum frequency step size for adequate characterisation of energy coupling, where the steps chosen are small enough to capture all peaks and troughs.
- c) whether measurable coupling occurs for cable irradiation at distances  $> \frac{\lambda}{2}$  remote from the load and, if so, to describe the dependency of  $V_L$  on cable length.

## 6.2 VALIDITY OF MODEL AT MICROWAVE FREQUENCIES

To determine whether the coupling model is valid  $>1$  GHz ([5-1] covers  $\leq 1$  GHz) it was necessary to demonstrate correlation between measured and modelled data. The modelling approach taken was to examine load impedance and cable material effects on  $V_L$ , to arrive at an adequate set of input parameters to the model which gave minimum difference between modelled and measured data. This allowed exploration of the possibility that the model may be valid  $>1$  GHz in unaltered form. From this basis the subsequent modelling study of the cable length dependency and re-radiation postulation was conducted.

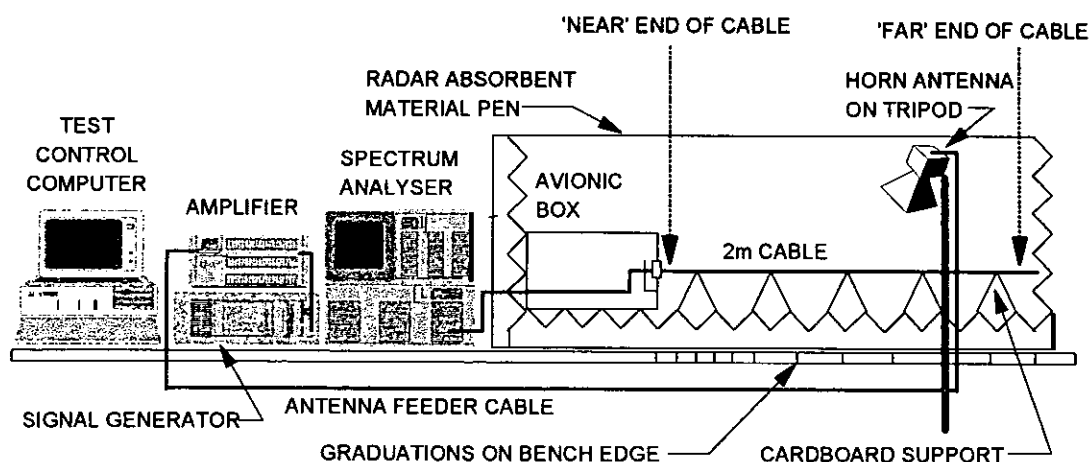
### 6.2.1 Laboratory Investigation and Initial Comparison with Model

To satisfy the requirements of the investigation the test item chosen was the same dummy avionic box used in the earlier BAe work [3-14], see Fig.5.7. A 2m length of single core aircraft cable to PANAVIA Standard 6411 [6-1] was threaded through one of the connector's socket holes and soldered to the internal SMA connection in the same way as for the earlier tests, see Figs. 5.6 and 5.7. This length was chosen for three reasons of which the most important was that, with the exception of Roe's 3.05m tests [4-20], it was the same [3-20] or exceeded the lengths used by other researchers, [4-21], [5-3] and Anderson [6-2]. It also represents the maximum cable length within a large (0.5 x 0.5 x

1.0m) avionics bay, which has cables which can be routed in any combination of directions (usually around edges). This length also enabled four sets of data for investigations of the dependency of  $V_L$  on length.

Each data set comprised 2-18 GHz pseudo-swept measurements for a number of illuminating antenna positions along the length of the cable, noting that the 3 dB beamwidth of the antenna used resulted in a 0.5m illumination 'footprint' on the cable. The cable was shortened by 0.5m after each set of measurements, *i.e.* data was acquired for cable lengths of 2.0, 1.5, 1.0 and 0.5m. Aircraft cable was chosen rather than the enamelled copper wire used by the other researchers (see previous paragraph) for realism and to enable direct comparison with the results of the earlier BAe research, which was conducted with a 0.5m length of the same type of aircraft cable [3-14]. All of the measurements were conducted using CW microwave signals, with signal detection by a spectrum analyser. The test arrangement is shown in Fig.6.1. The box and cable were arranged within a corner RAM pen in the screened EMC Laboratory with the cable positioned perpendicular to the box face and suspended above the pen floor with cardboard at intervals over the cable's full length. Positioning marks were made on the supporting test bench at 0.25m intervals over the length of the cable, to ensure the boresight of the antenna was positioned at these distances from the box face. Marks were also made at 0.1m intervals from 0.1-0.5m for the last test, where the cable had been cut to 0.5m. Throughout this chapter the terms 'near end' and 'far end' illumination refer to the perpendicular position of the antenna to the cable as annotated in Fig. 6.1.

Figure 6.1: Cable Coupling Experimentation: Test Arrangement



The computer-controlled signal generation, irradiation system and measurement equipment is shown schematically in Fig.6.2. The synthesised signal generator used is an industry standard, with excellent frequency and amplitude stability, see Table 6.1, and very low residual FM characteristics. Likewise, the spectrum analyser had the best amplitude and frequency accuracy available, see also Table 6.1. The BAe test control software effected pseudo-swept frequency testing by instructing the signal generator to produce a signal of a specified power and frequency, then waiting for the spectrum analyser to perform a search for the peak, store the maximum and take a power measurement at that frequency prior to moving up to the next frequency. This 'settling' time per frequency step in the pseudo-sweep from 2-18 GHz is that needed to ensure high quality measurements with the equipment used and was calculated as 2.36 seconds per frequency step. This differs from EMC qualification test requirements, see Chapter 3 and Appendix B, for avionics and aircraft to have exposure periods representative of real world RF environments and which are linked to potential avionic susceptibilities. Ref. [2-17] suggests exposure times of up to 2 seconds could realistically be expected, but limits test times thus '*...exposure at any one test frequency should not exceed 5 seconds.*' This is discussed further in Chapter 7.

Figure 6.2: Test Instrumentation

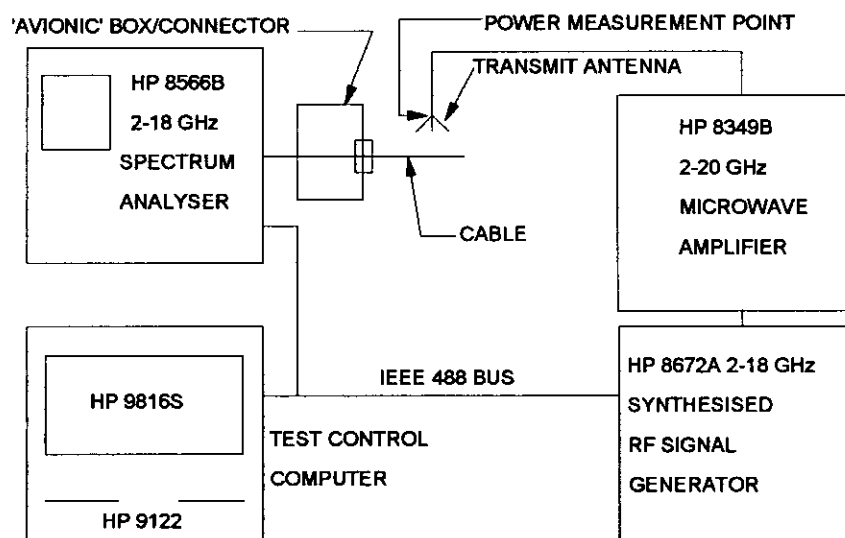


Table 6.1: Key Features of Signal Generator, Amplifier and Analyser

<b>HP 8672A: 2-18 GHz Synthesised Signal Generator</b>			
*	Worst case accuracy	Power	1-1.5 dB for 2-18 GHz
		Frequency	10 MHz ( <i>i.e.</i> <0.5%)
*	Other key features	Harmonics	< -25 dBc
		Spurious	< -70 dBc for 2.0-6.2 GHz < -64 dBc for 6.2-12.4 GHz < -60 dBc for 12.4-18.0 GHz
		Phase noise	-100 dBc at 100kHz from carrier
		Output switching	<20 ms (<10 ms typical)
		Stability	ageing rate: < $5 \times 10^{-10}$ /day temperature: < $1 \times 10^{-10}$ /°C line voltage: < $5 \times 10^{-10}$ /(+5% to -10%)
<b>HP 8349B: 2-20 GHz 100 mW (+20 dBm) Microwave Amplifier</b>			
*	Harmonics	(at full output)	< -20 dBc for 2-11 GHz < -30 dBc for 11-20 GHz
*	Spurious		-50 dBc
*	Noise Figure		< 13 dB, typical
<b>HP 8566B: 100 Hz - 22 GHz Spectrum Analyser</b>			
*	Worst case accuracy	Power	±3 dB
		Frequency	<10 MHz ( <i>i.e.</i> <<0.5%)
*	Other key features	Drift	<5 kHz/minute of sweep time
		Residual FM	< -110 dBm
		Image Responses	< -70 dBc
		Multiple Responses	<-60 dBc

### Experimental limitations

The mechanical set-up of the experiment, shown in Fig.6.1, was well controlled, with accurate and repeatable antenna positioning along the cable under test established by positioning the tripod mast against the calibrated marks on the edge of the RAM-covered test bench. The cable was parallel with the edge of the bench to within ±2.5 mm and, by careful positioning of the cardboard supports, was seen to have minimal droop (not measured but estimated to be less than 5 mm for all cases). Care was taken to ensure that the cable did not move during any of the measurements taken for each of the four lengths investigated. Measurement errors resulting from antenna angular re-positioning were minimised by conducting received signal peak search (whilst moving the antenna) at the commencement of measurements at each cable length. Instrumentation pick-up measurements, conducted twice during the investigations, showed none above the instrumentation system noise floor. With the exception of one data sample, which was at

the noise floor, all experimental results were >5 dB above the instrumentation noise floor and were thus considered valid. This validity was reinforced when the medians of all data sets were examined and each found to be at least 22.8 dB above the noise floor. Repeatability measurements, conducted for the calibration of the box-to-analyser cable and during the test cable pick-up experiment, established repeatability to within 3 dB. In all, including the above, 30 sets of data were collected. The test equipment in Table 6.1 dominated the overall experimental error budget and this leads to an estimated maximum experimental error budget of  $\pm 8$  dB. The measurements were conducted over RAM, simulating infinite height above ground plane, rather than at the 0.05m height of most EMC specifications for three reasons. First, the repeatability aspect of this research dictated the same configuration as the earlier BAe investigations, which were conducted over the same type of RAM. Secondly, the SHF/EHF field-to-wire coupling model enhancement to IEMCAP\* by Brock *et al.* [6-3] showed that the maximum coupled current reached a maximum plateau at heights above the ground plane of greater than  $\frac{\lambda}{2}$ . Finally, measurements in [6-2] supported this although, as noted by Taylor and Harrison [6-4] (who also agreed with the plateau conclusion) a discrepancy exists between [6-2] and [6-3] which they thought was due in part to difficulty in determining accurately the height variation in  $V_L$  at the low heights (3/8" and 2") reported in [6-2].

### **Discussion of Test Frequency Resolution**

The two key differences between these investigations and the earlier BAe research were the use of pseudo-swept rather than spot frequency measurements and the use of a different illuminating antenna and a discussion on these differences follows. An important factor in assessing whether the model is valid >1 GHz is the minimum frequency step size (referred to hereafter as 'resolution') necessary for adequate coupling characterisation. The choice of appropriate resolution is also important in practice as aircraft and avionics EMC qualification test time, and hence cost, is directly proportional to the resolution used. Carter *et al.*, who conducted the most recent airframe attenuation measurements, see Section 3.3.2.1, used 50 MHz steps as he did on an earlier helicopter investigation [3-21] where he noted *'The step size was a compromise between providing adequate frequency resolution and minimising test time.'* The aircraft research reported in Section 3.3.1 suggested that a frequency resolution of <20 MHz would be required and for the first measurements taken, those of far end illumination of the 2m cable, a test resolution of 10

---

\* IEMCAP = Intrasystem EMC Analysis Program

MHz was utilised. The test duration was 63 minutes, excluding the 2-10 to 10-18 GHz changeover time (necessary because of data storage limitations of the test control software), which equates to an average 2.36 seconds each of the 1601 measurements. The second set were conducted with 50 MHz resolution to enable comparison with the 10 MHz set and with the similar data gathered with 20-500 MHz resolution during the Chapter 3 aircraft investigations, see Table 3.1. Fig.6.3 shows the comparison between the 10 MHz and 50 MHz resolution data, with the two data sets offset by 10 dB for visualisation. Fig.6.3 also shows the same behaviour, similar to a low Q resonant cavity, as seen during the aircraft research (Section 3.3.1), with many closely spaced peaks and troughs. Fig.3.12 showed that the received signal envelope increased as the resolution used decreased from 500 MHz to 100 MHz and thence to 20 MHz. This effect can be used to determine the minimum resolution necessary for adequate characterisation, *i.e.* the resolution where the increase in the envelope  $< 1.5$  dB (the analyser accuracy). The delta increase in envelope between the higher and lower of pairs of adjacent test resolutions is shown in Fig.6.4. This shows that the increase in envelope reduces with decreasing resolution and graphical examination of the aircraft data trend shows that for 10 MHz resolution, which was not used in the aircraft investigations, the further increase in envelope size can be estimated at 1.6-2.6 dB. This agrees with the cable data which shows a 2.9 dB increase in envelope when using 10 MHz compared to 50 MHz resolution.

Figure 6.3: Comparison of 50 MHz and 10 MHz Measured Data

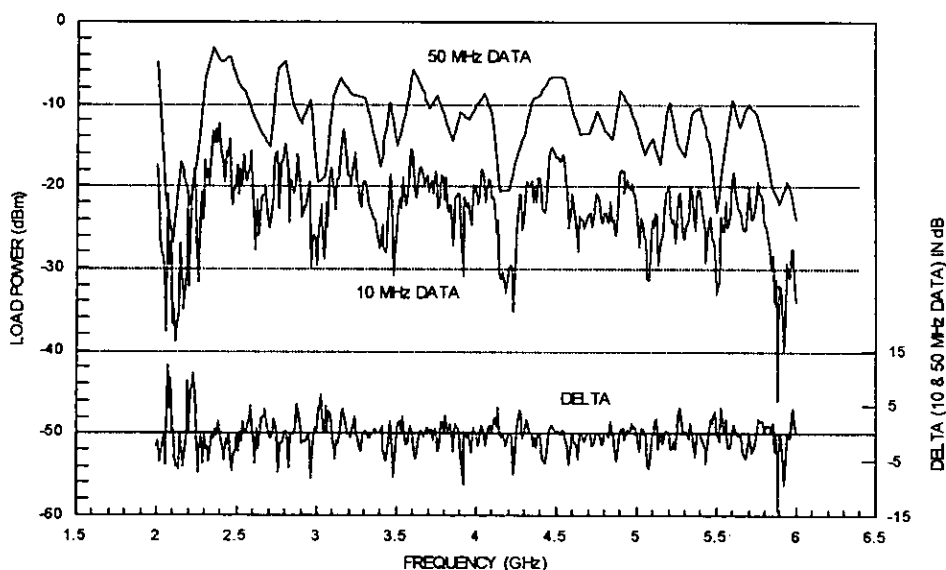
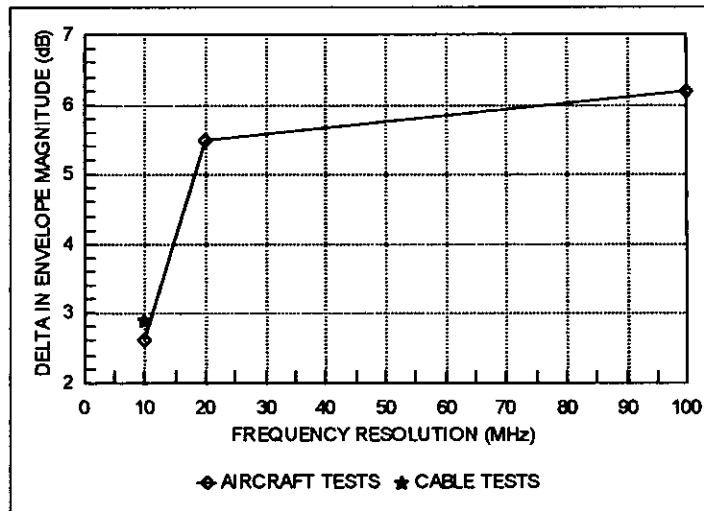


Figure 6.4:  $V_L$  Envelope Magnitude vs. Test Frequency Resolution



An interesting aspect noted during this examination of the aircraft data supporting Fig.3.12 and Table 3.1, and the cable data of Fig.6.4 was that the median and  $1\sigma$  values for the data sets being compared were within 0.3 dB of each other, with the maxima and minima increasing by almost equal amounts. Following consideration of the trade-off of possible error in the profile with resolution vs. constraining the experiment's duration within practical limits, the remainder of measurements were conducted with 50 MHz resolution. The above suggests that the optimum resolution for characterisation of microwave coupling, *i.e.* where the error in  $V_L$  envelope is  $<1$  dB, lies no more than an order or two below 10 MHz. This knowledge was passed [6-5] to Barber and Rayment, the only other two U.K. researchers known to be examining potential microwave upset of circuitry, who were using coarse (250 and 100 MHz) resolution in their work [6-6], [6-7]. The use of  $<10$  MHz resolution is explored using the cable coupling model later in this chapter. The potential effect of mode stirring, see Section 3.3.2.1, on the conclusion to use 50 MHz resolution was examined. Figs. 9-11 of [3-21] shows that many of the maxima of the 2-18 GHz airframe attenuation ( $A_{A(max)}$ ) measured are removed (without stirring  $A_{A(max)} = 30$  dB; with stirring  $A_{A(max)} = 20.8$  dB), giving a pessimistic view of the attenuation available. A similar effect, if present for the coupling of energy to a cable entering an avionics box, could lead to the artificial depression of  $V_L$  maxima, apparently increasing the safety margin of correct circuit operation in a given power density. This aspect warrants further study.

## Illuminating Antenna

Section 5.1 of [3-14] notes that the power density measured at 0.2m from the EMCO 3105 antenna, *i.e.* the antenna-to-cable spacing, was quite different to that theoretically predicted and that the reason was distortion of the antenna's radiation pattern [as the cable was well within the 7.14m far field boundary of the antenna]. The close proximity of the antenna (the only one available at the time) to the cable, accentuated in Fig.5.7, was necessary to enable measurable  $V_L$ . For this chapter's investigation a different antenna was needed, one which would enable measurable  $V_L$  with the amplifier power available with the cable in the antenna's far field, and with a <0.5m illumination 'footprint' on the cable. The antenna chosen was the smaller AEL H-1498, a double-ridged waveguide 2-18 GHz horn antenna. Table 6.2 compares the features relevant to the investigation:

Table 6.2: Comparison of AEL H-1498 and EMCO 3105 Antennas

3 dB Beamwidth	Gain	Size (cm)			Far Field		Footprint*
		Aperture		D	at 2GHz	at 18GHz	
(degrees)	(dBi)	H	W			(m)	(m)
AEL: 45	6.1-12.5	7.3	12.5	9.8	0.21	1.88	0.51
EMCO: 53	7.5-21.5	15.8	24.4	27.9	0.79	7.14	0.2

\* Footprint on cable at distance used in investigations.

The tripod-mounted transmitting antenna was arranged so that the boresight was approximately 45° down from the horizontal but perpendicular to the cable, with horizontal polarisation to maximise energy pick-up on the cable and minimise extraneous reflections from areas of the EMC Laboratory without RAM screening. The initial visual boresighting of the antenna with the cable at 1m from the avionic box, was followed by spectrum analyser peak searching to enable maximum attainable illumination power density and hence  $V_L$ . The antenna face to cable distance was measured at 0.615m, *i.e.* in the antenna far field.

## Measurements

Starting with the antenna illuminating the far end of the 2m cable, 2-18 GHz measurements were made. The antenna was then moved 0.25m closer to the box face and the measurements made again. This was repeated in 0.25m steps to 0.25m from the box. 0.5m of cable was cut off and the measurement cycle repeated, this time from 1.5 to 0.25m. This was repeated for a cable length of 1.0m. Finally, for a 0.5m cable length, measurements

were taken in 0.1m steps from 0.5 to 0.1m. Noise floor measurements were taken to ensure that the cable test data was sufficiently above the noise floor (>6 dB) to be considered valid measurements. Instrumentation pick-up checks were conducted at the start and finish of the investigations using a 50Ω load connected to the spectrum analyser feeder cable inside the box instead of the cable under test and repeatability measurements were also made.

### Data Processing

Power  $P_R$ , in dBm, was measured using the spectrum analyser. This data needed treatment to convert it into  $V_L$  in dBμV at the 'load' in the box (*i.e.* at the bulkhead 50Ω connector between the aircraft cable and the spectrum analyser cable), normalised to an incident power density of 1 Wm<sup>-2</sup>. This treatment comprised compensation for amplifier power output variations and transmit antenna gain vs. frequency characteristics, and for losses in the box-to-analyser received signal cable. The treatment, detailed below, was conducted partly on the Hewlett-Packard test control computer and completed, after data translation to PC-DOS format, on a DX2-50 PC, where the data analysis and modelling investigations were conducted. The transmitter power vs. frequency,  $P_T$ , as measured at the antenna feeder output, see Fig. 6.2 (*i.e.* output of the signal generator, power amplifier, three cables and an in-line connector) was measured using the spectrum analyser with a 30 dB attenuator on its input. The antenna gain vs. frequency,  $G_T$ , was taken as the measured data provided by its manufacturer. The loss vs. frequency profile of the received signal cable,  $L_R$ , was measured using the signal generator and spectrum analyser. The incident power on the cable,  $P_c$ , is given by

$$P_c = \frac{\text{ERP (in dBm)}}{4\pi r^2} = \frac{(P_T + 30)G_T}{4\pi(0.615)^2} = \frac{(P_T + 30)G_T}{4.7529} \text{ (dBm/m}^2\text{)} \quad \dots(6.1)$$

The power in the 50Ω load in the avionics box,  $P_L$ , is that measured by the spectrum analyser ( $P_R$ ) minus  $L_R$ . Its normalisation to 1 Wm<sup>-2</sup> (+30 dBm/m<sup>2</sup>) and conversion to  $V_L$  into 50Ω is given by Eqns.6.2 and 6.3:

$$P_L = (P_R - L_R) + (10 \log(4.7529) + 30 - (P_T + 30)G_T) \text{ dBm} \quad \dots(6.2)$$

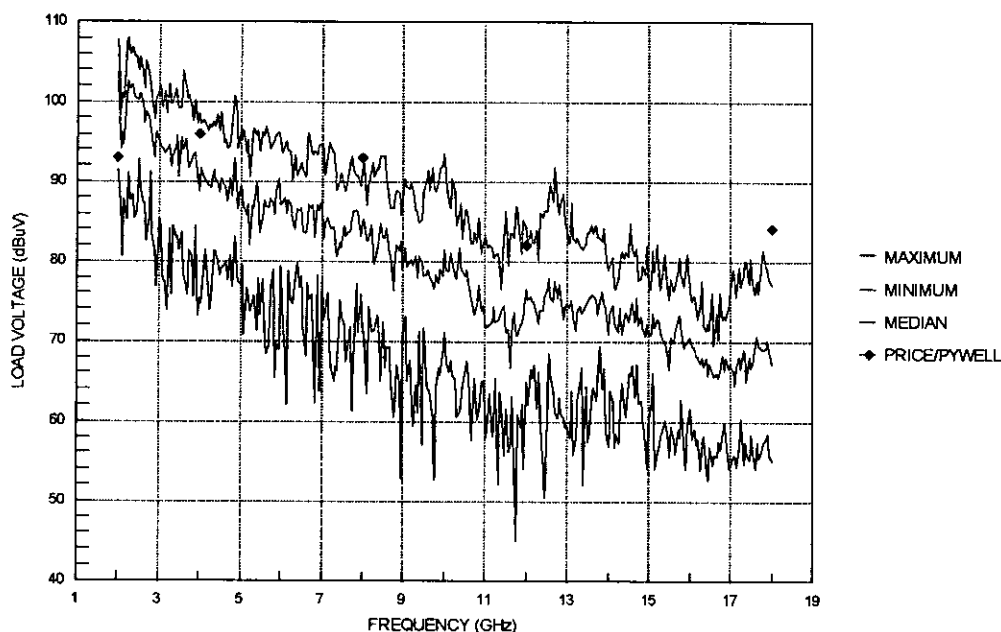
$$V_L = 20 \log \left[ 10^6 \sqrt{10^{\left(\frac{P_L}{10}\right)} \times 10^{-3} \times 50} \right] \text{ dB}\mu\text{V} \quad \dots(6.3)$$

The 2-10 and 10-18 GHz data sets were then concatenated.

## Repeatability and Comparison with Other Researchers' Data

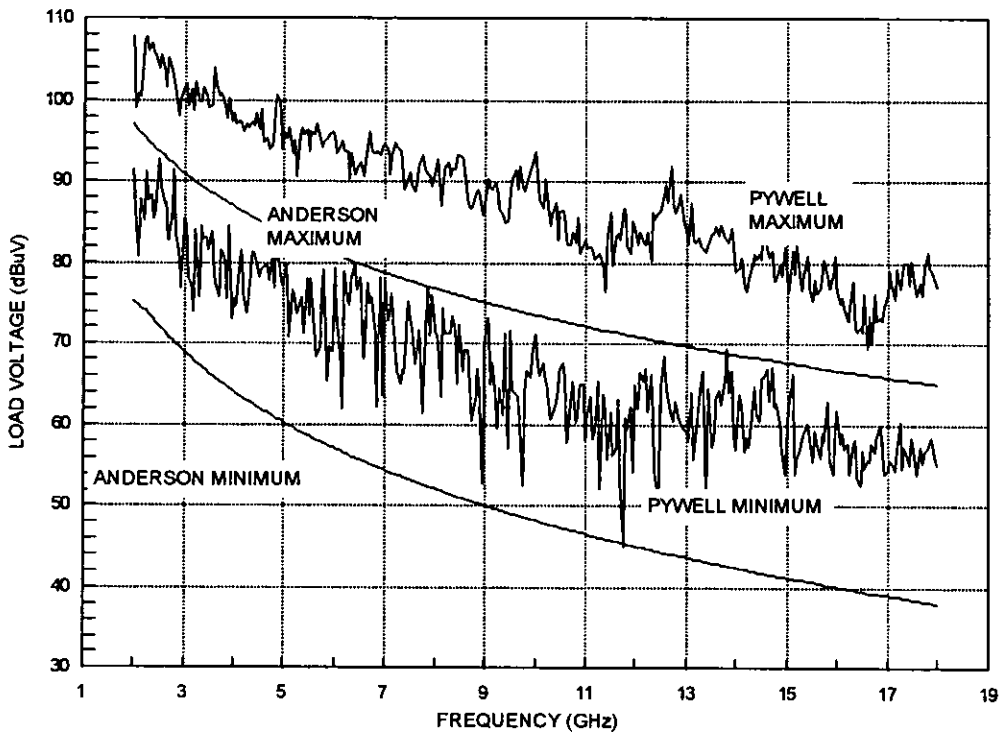
To enable comparison with the BAe spot frequency measurements of Section 5.3.2 and with data by other researchers, the maximum, minimum and median profiles vs. frequency were statistically generated from the measured  $V_L$  data sets. Fig.6.5 contains a comparison of the measured data with that from Section 5.3.2 and clearly shows the good repeatability achieved. Only the 18 GHz spot value (whose error budget was  $\pm 10$  dB) lies outside the swept frequency profiles, by 3.5 dB, and this is within the  $\pm 8$  dB error budget applicable to those profiles.

Figure 6.5: Measured  $V_L$  Statistics and Earlier BAe Spot Measurements



The measured data was compared to that by Anderson [6-2], who conducted a similar experiment, but where source and load impedance were  $50\Omega$ . He also notes the highly resonant load voltage profile reported here, but presented the upper and lower bounds (calculated in the same way as for Fig.6.5) to his measured data in [6-2] rather than any actual results. Fig.6.6 shows the comparison of this researcher's minimum and maximum  $V_L$  profiles with those of Anderson. The amplitude profiles are comparable, noting that the 10-20 dB differences in maxima are probably due to the differences in experimental configuration, in particular, cable length. This aspect is examined later in this chapter using the coupling model.

Figure 6.6: Comparison of Pywell and Anderson Cable Results



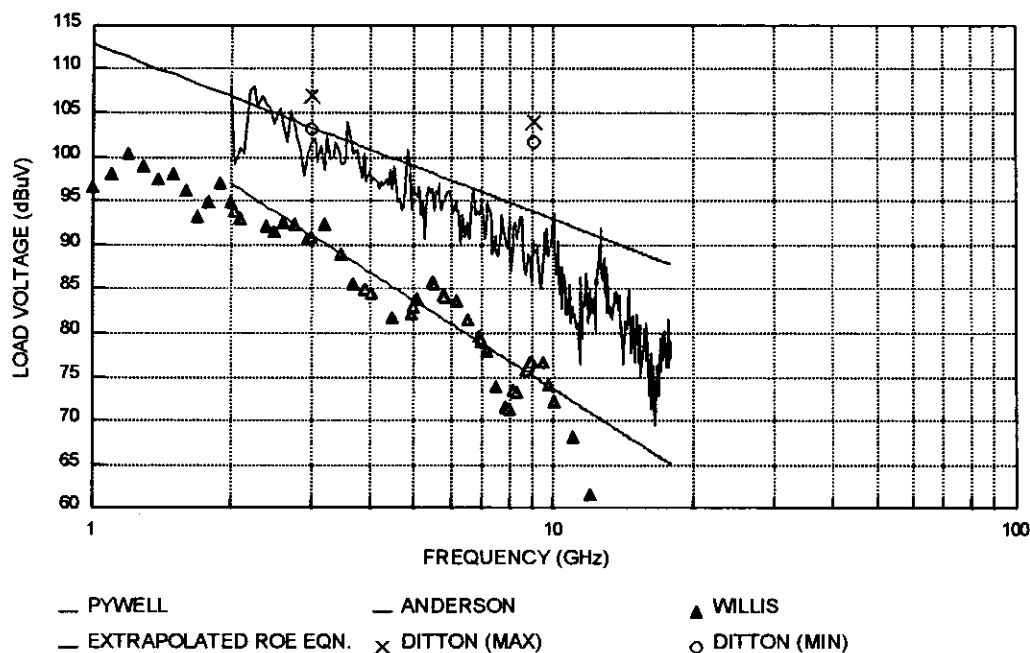
### Upper Bound on $V_L$ Profile

Fig.6.7 shows the maximum  $V_L$  profiles obtained by this researcher, Anderson, Willis [3.20] (spot frequencies) and Ditton [4-21], who conducted measurements at 3.0 and 9.1 GHz. Ditton investigated *inter alia* the effects of coupling to one of a twisted pair of un-shielded wires, of length 0.6m, with different source and load impedances and with the other wire grounded at each end. An important finding was that the maximum  $V_L$  measured did not vary appreciably, at most 3.7 dB, as a function of load impedance, and maximum and minimum values are thus shown in Fig.6.7 to show this effect. Fig.6.7 also contains an extrapolation of Eqn.5.63 to examine its applicability above 2 GHz.

The dependency of the data sets in Fig.6.7 per decade frequency are comparable, from 20.0 dB (Eqn.5.63), through 20.6 dB (2-8 GHz) to 29.7 dB (8-18 GHz) (this researcher), to 33.4 dB (Anderson). The Willis spot frequency data follows the Anderson line and is assumed to have approximately the same frequency dependence. The slope of the four profiles equates to a  $\frac{1}{f^2}$  to  $\frac{1}{f^{3.3}}$  dependence, which agrees with [6-2] where the observed bare wire slope of approximately 30 dB/decade was attributed to the effective aperture  $\left(\frac{1}{\lambda^2}\right)$  characteristic of electrically long wire antennas (20 dB/decade frequency) and end effects of

the connector and transition to the 50Ω load used. The measurements in [4-21] concur, indicating that the maximum effective aperture of such a wire is approximately the same as a half-wave dipole at microwave frequencies. However, [6-4] (reporting on [6-3]), notes that the predicted maximum coupling decreases with frequency as  $\frac{1}{f}$ , which is not supported by any of the measured data considered herein.

Figure 6.7: Maximum  $V_L$  Amplitude Profile



Analysis of this researcher's high resolution empirical data has shown (see also the earlier discussion on *Test Frequency Resolution*) that up to 14 dB of amplitude error could be applicable to the other three data sets on Fig.6.7, as a result of under-sampling (which is usually random in nature, rather than frequency dependent). Correction for the under-sampling could result in the slope of the Anderson and Willis data approximating to this researcher's profile, but the correction is not possible with the available data. It is concluded from this analysis that un-screened wire coupling has a frequency-banded dependency of 20 dB/decade up to 8 GHz and 30 dB/decade for 8-18 GHz. The measured data also supports the use of Eqn.5.63 as an initial coupling predictor of maximum coupling up to 8 GHz and, with modification to change the slope to 30 dB/decade frequency, from 8 to 18 GHz. The possibility exists that this modification could be valid above 18 GHz and further research would be required to confirm this.

## Model Validation

An essential part of the modelling of microwave energy coupling to a cable conducted has been the modification and validation of the model at each stage of its evolution as the research has proceeded. Rigorous manual calculations were conducted on each of the modules when first coded during the software design prior to validation tests. The final validation tests comprised direct comparison with Figs. 2-11 and 2-17 of [5-1]. To enable this the model was modified to reflect the twin transmission lines in these figures. The initial validation showed the model outputs to have maximum amplitudes 3 dB higher than the [5-1] figures. This was investigated and the reason found to be an error in Eqn.2-15 of [5-1]. The model follows [5-1] in this area, with  $Z_o$  being calculated thus:

$$Z_o = 276 * \log\left(\frac{2b}{a}\right) = 276 * \log\left(\frac{h}{a}\right) \quad \dots[5-1] \text{ Eqn.2-15}$$

where  $a$  = wire diameter,  $h$  = wire height above ground plane,  $h = b/2$  ...[5-1] Eqn.2-13

where  $b$  = conductor spacing of equivalent isolated twin wire transmission line. On further inspection and investigation of this aspect it can be seen that an error exists in [5-1], as Eqn.2-13 (p.31) states  $h=b/2$ , but Eqn.2-15 (p.31) states  $2b/a = h/a$ , or  $h=2b$ , a factor of 4 different, explaining why an input of four times the height above ground plane produced the correct value of  $Z_o$ . Eqn.2-15 of [5-1] should therefore be

$$Z_o = 276 * \log\left(\frac{2b}{a}\right) = 276 * \log\left(\frac{4h}{a}\right) \quad \dots(6.4)$$

The error is an isolated case, with all subsequent [5-1] equations and graphs inspected being correct.\* This error had affected all modelling carried out up to this point, *i.e.* including all connector impedance, cable material and some of the cable length dependency investigations, and led to (at most) an increase in  $V_L$  of 3 dB. With this modification incorporated and with input parameters set appropriately to match each of the lines on the two [5-1] Figures, a number of model runs were conducted. A revised number of points was used, 4000 per frequency sweep, equating to 25 kHz steps for Fig.2-17 and 250 kHz steps for Fig.2-11, higher resolutions than proposed in Section 6.3.2 for that necessary for adequate characterisation of microwave energy coupling to avionics bays, cables and circuitry. The model outputs were overlaid on the appropriate [5-1] Figure and these are presented as Figs. 6.8 and 6.9.

---

\* Smith, the author of [5-1], has been notified of this revision.

Figure 6.8: Smith Figure 2-11 vs. Modelled Response

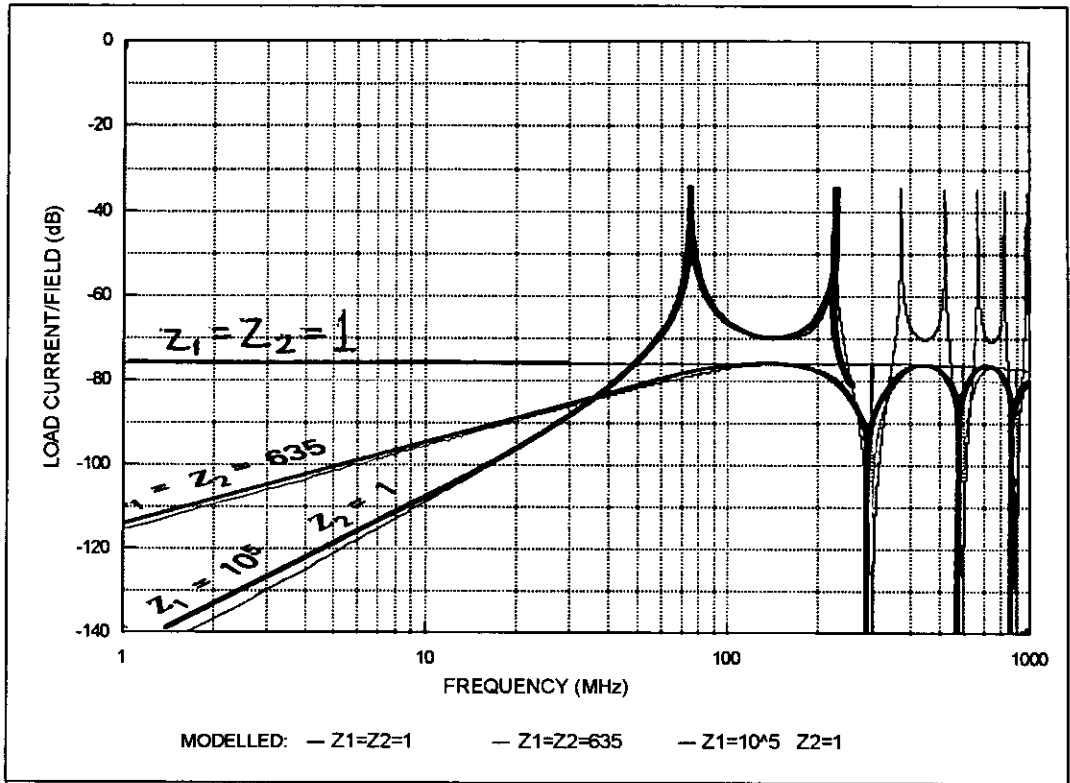
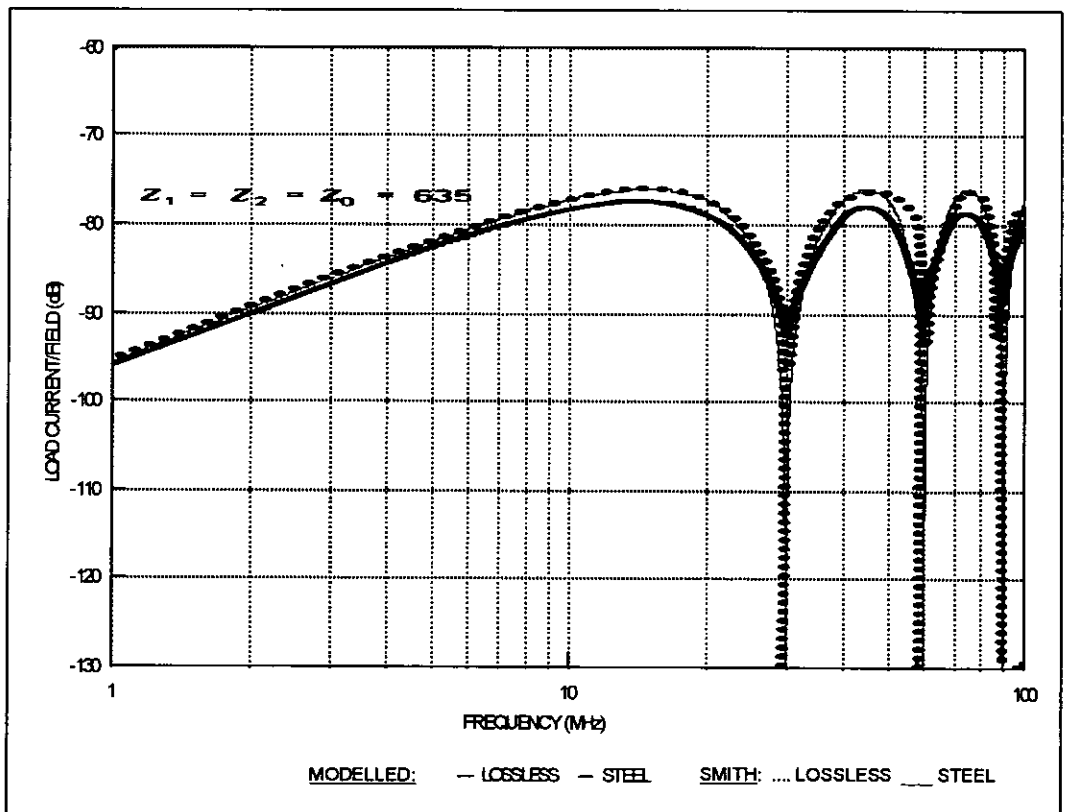


Figure 6.9: Smith Figure 2-17 vs. Modelled Response



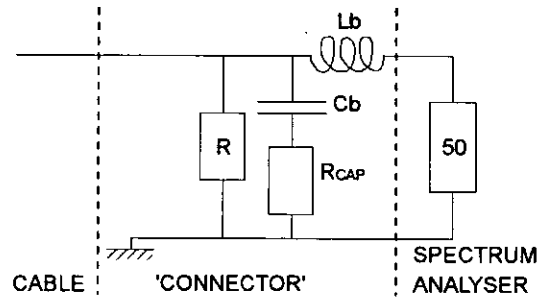
Good correlation can be seen between the three modelled data sets and the three lines on [5-1] Fig.2-11. It can be seen that the original Figure omitted (probably for clarity) the  $Z_1=Z_2=1\Omega$  line above 30 MHz and, of more relevance to this research, the  $Z_1=10^5\Omega$ ,  $Z_2=1\Omega$  line, where no data is presented above 250 MHz. The modelled data shows that the former line continues to 1 GHz, as expected from inspection of the equation. In addition, the one discontinuity on the latter line is seen to actually be a series of discontinuities of the same profile as those discussed in Section 6.2.2, thus confirming the suspicion that this aphysical response, which does not occur in any aircraft or laboratory microwave coupling measurements seen to date, is a feature of the basic transmission line equations used in [5-1]. Good correlation can also be seen between the modelled and [5-1] Fig.2-17 for the lossless and steel conductor cases. The differences between the lossless lines at 50-60 MHz is believed to be an error on the Smith figure in that this part of his curve is not symmetrical with the 30-40 MHz portion of the same line. A similar problem can be seen on the Smith steel conductor data line between 60-80 MHz. This is reinforced by examination of [5-1] Fig.2-18, where the peaks and nulls profile of lossless and steel cable is symmetrical for each line and both data sets are synchronised in profile. The small amplitude and profile difference in the nulls is attributed to differences in the relative permeability and resistivity of the steel used in the model. The values in [5-1] are not stated, whereas the model uses the maximum values for steel in [5-1] Table 1-1.

### 6.2.2 Load Impedance Effects

The load impedance  $Z_B$ , across which  $V_L$  is developed, was expected to be a major factor in matching modelled to measured data. Ref. [6-3] noted how impedance was one of the most sensitive parameters in transmission line-based models (*e.g.* IEMCAP and Eqn.(5.62)). For the configuration tested, with the  $50\Omega$  dominating  $Z_B$ , large changes in  $V_L$  were not expected for small variations in other components of  $Z_B$ . This was demonstrated in [4-21] where six load impedances were examined, from  $55+j75\Omega$ , through  $50\Omega$  to  $88-j55\Omega$ , and at most 3.7 dB difference was seen in  $V_L$ .  $Z_B$ , representing the connector, the box internals and parasitics in between the connector, case and wire, is shown in Fig.6.10. It comprises the spectrum analyser input (which has negligible C and L), the short semi-rigid cable to the box internal bulkhead connector, and the connector assembly through which the cable passes (see Fig.5.6). The connector assembly and semi-rigid cable can be considered to be equivalent to a lumped circuit model comprising series  $L_b$ , shunt R and shunt C with series  $R_{CAP}$ . Variations in each of these parameters were investigated in turn. It is assumed that

impedances match at each of the physical interfaces, *e.g.* at the wire to semi-rigid waveguide bulkhead. This is justified in this research as any mismatch reflections would most probably reduce  $V_L$  (*i.e.* lessening the risk of circuit upset), although there is an unlikely possibility that the resonances caused could enhance  $V_L$  at the expense of  $I_L$ .

Figure 6.10: Lumped Element Model of Connector and Load



For the initial modelling the circuit configuration was as in Fig.5.3, with the load impedance comprising  $50\Omega$  (spectrum analyser input) with zero  $C_b$  and the source impedance represented an open circuit cable by a very high  $R_a$  ( $10^{64}\Omega$ ) with a shunt  $C_a$ . Cable diameter was set at 1mm and height above ground plane at 0.51m ( $\approx 3\lambda$  at 2 GHz and  $\approx 30\lambda$  at 18 GHz; noting from Section 6.2 that maximum  $V_L$  saturates for  $h > \frac{\lambda}{2}$ ). For this arrangement the model outputs were compared with 50 MHz measured data for variation in  $C_a$  of 0-10 pF and 0.5 pF gave the closest match. The first element examined was the variation of  $C_b$ , with all other elements but the 50  $R_b$  set to zero.  $C_b$  was varied between 0-10 pF in 2 pF steps to identify any trends in modelled  $V_L$ . The 2 pF profile was shown to be nearest to the measured data and further modelling at either side of 2 pF showed the  $V_L$  profile to reduce in amplitude. This value was thus chosen for the remaining investigations. The shunt resistance  $R$  was then varied over the representative range 100 k $\Omega$  - 100 M $\Omega$ . Trivial calculations show that, due to  $R$  shunting the  $50\Omega$ ,  $V_L$  is insensitive to variations of  $R$  in this range. The model was modified to enable input of  $R_{CAP}$  in series with  $C_b$  and a series inductance  $L_b$ , see Fig.6.10. In practice  $0 < R_{CAP} < 0.1\Omega$  and, with  $L_b = 0$  nH and the other terms as previously stated,  $V_L$  dependency on  $R_{CAP}$  was examined for  $0 < R_{CAP} < 0.10\Omega$  in 0.02 $\Omega$  steps. The modelled  $V_L$  showed a decrease of (at most) 0.018 dB $\mu$ V, which is considered negligible, and  $R_{CAP}$  was set to zero for the remaining modelling. Finally, with  $R = R_{CAP} = 0\Omega$ ,  $L_b$  was varied between 0-5 nH, the range for a short piece of the semi-rigid coaxial cable. Fig.6.11 shows the difference between  $V_L$ (maximum), which occurs for  $L_b = 5$  nH, and the 0-4 nH data. It shows that in this case  $V_L$  is 5.5 dB $\mu$ V higher than for  $L_b = 0$  nH at 2 GHz, reducing to 1 dB $\mu$ V higher at 5 GHz. Above 5 GHz there is less than 1 dB difference for  $0 < L_b < 5$  nH. A comparison of the measured data with the model output, for  $C_b = 2$  pF,  $R = R_{CAP} = 0$  and  $L_b = 5$  nH, is given in Fig.6.12 which shows the modelled and

measured maximum  $V_L$  profiles to be within 10 dB, but that there is substantial difference in frequency and amplitude content.

Figure 6.11:  $V_L$  Dependency on Series Inductance in Load

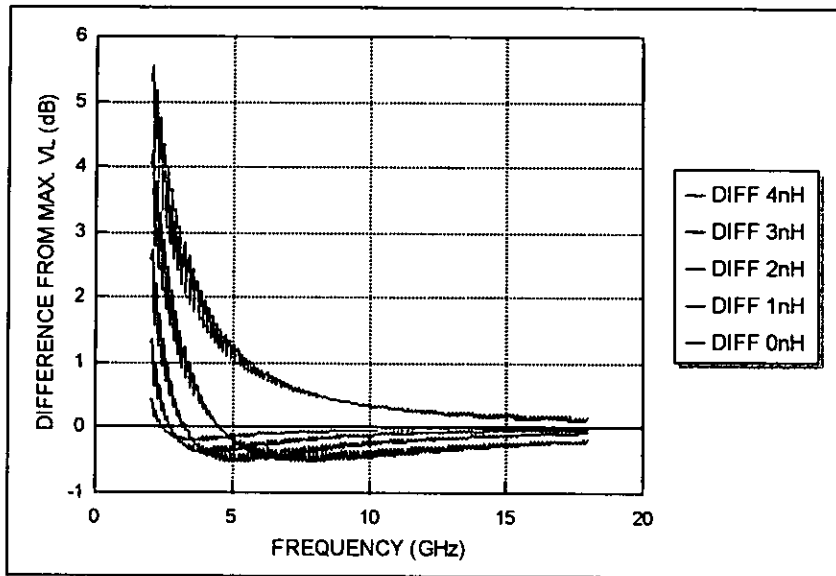
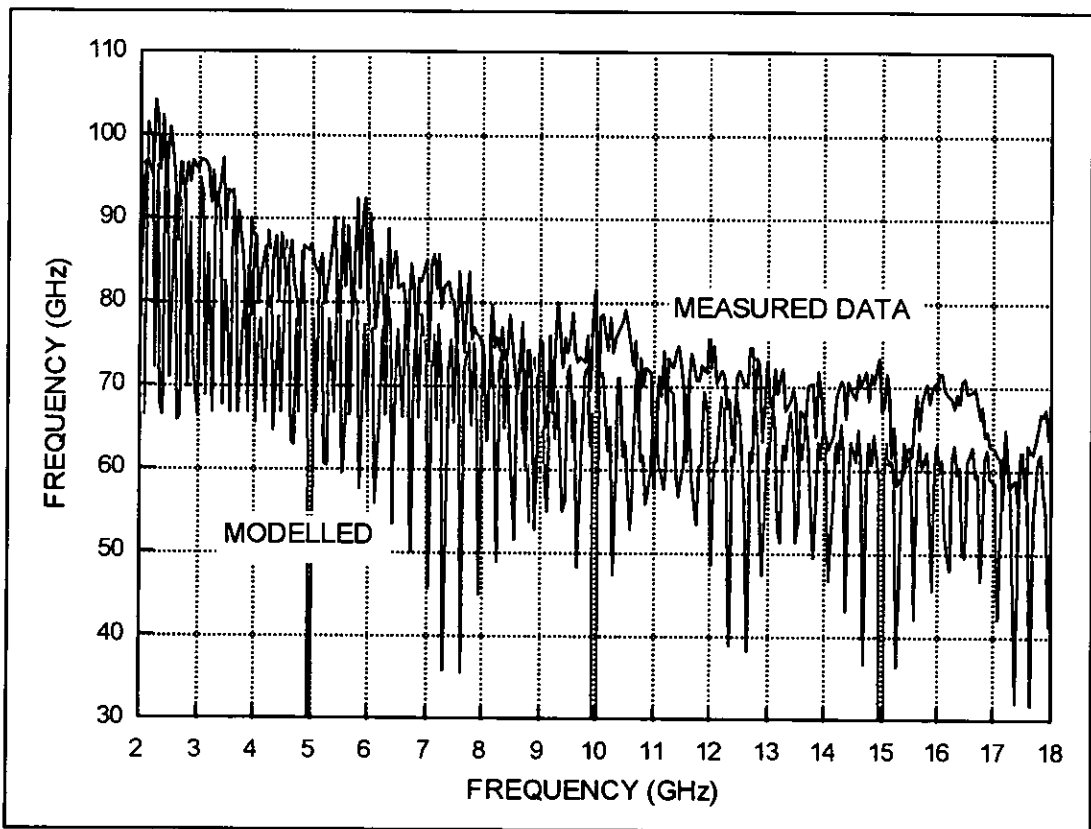


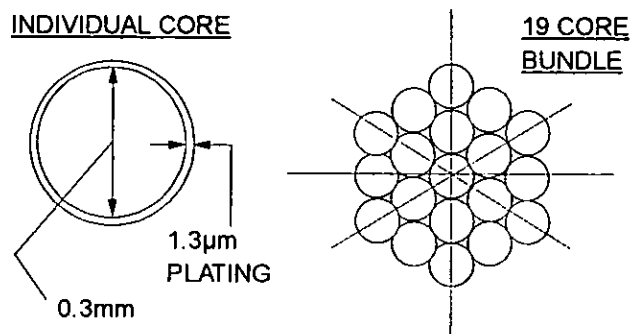
Figure 6.12: Modelled vs. Measured 50 MHz Data



### 6.2.3 Cable Material and Construction

To achieve a match between measured and modelled results, having determined  $Z_A$  and  $Z_B$  representative of the experimental configuration, it was necessary to examine the cable used during the experiment to ensure the correct inputs were used in the model. The cable used in the laboratory investigations was type DP012 to specification [6-1], manufactured by British Insulated Cable Company. This cable has a single insulated conductor and is often used on modern military aircraft. Aircraft cable, rather than enamelled copper wire as used by the other researchers referred to in this Chapter, was chosen for realism. For flexibility the conductor comprises 19 individual cores, each of 0.3mm diameter, which are helically stranded together to give a nominal full conductor diameter of 1.45mm. This overall conductor is then lap wound with insulation tape, with 67-69% overlap, of Du Pont 'KAPTAN' FEP, *i.e.* 0.001" polyamide with 0.0001" each side of Fluorinated Ethylene Propylene (FEP). This is then over-wrapped with white PTFE tape with a PTFE lacquer top coat, giving a total cable diameter of nominally 2.00mm (the sample used was 2.00mm as measured with a vernier calliper). For a perpendicular cut through the cable there are thus three layers of KAPTAN ( $\epsilon_r=3.1$ ) and a single PTFE over-wrap ( $\epsilon_r=2.0$ ), of total radial thickness 275 $\mu\text{m}$  and forming a dielectric sheath. The impact of this potentially lossy sheath was not considered since, as previously stated, this research concentrates on derivation of the *maximum*  $V_L$  to be encountered at a potentially susceptible component. There is a possibility that it contributes to the loss term covered in Section 6.3.2 and this forms a topic for further study. The conductor construction was considered to determine any changes necessary to the inputs to the model, as up to this point a non-stranded, 1mm diameter copper conductor had been assumed. The cross-section of stranded cables is described in Dummer and Blackband [6-8] and Fig.6.13 shows the arrangement for the 19 core conductor used.

Figure 6.13: Arrangement of Cores in Stranded Conductor



Each core in the cable used is nickel-plated copper, for environmental protection, with a minimum plating thickness of  $1.3\mu\text{m}$ . For the model the connector bundle in Fig.6.13 can be represented as a single copper core plated with nickel on the outside only. This is justified in [6-8] where it is noted that at frequencies where skin effect is prominent (as is the case for 2-18 GHz) the current in the cores may be considered as concentrated on the surface. Ref. [6-8] also notes that for all but the most accurate computations it is permissible to neglect the effects of helical lay on  $Z_o$  and C, L and per unit length. This is because the effects of the elliptical cross-sections (of the cores due to twisting) and internal inductance are small, of the same order and opposed in sign. By manipulation of the cross-sectional areas of the 19 cores and the plating area on each, an equivalent single core conductor diameter of  $1.3077\text{mm}$  and the nickel plating thickness of  $5.647\mu\text{m}$  are determined. This is interesting as the skin depth for nickel can be calculated using Eqn.5.29 to be  $3.316\mu\text{m}$  (2 GHz) to  $1.105\mu\text{m}$  (18 GHz). Since the minimum plating thickness is  $5.647\mu\text{m}$ , all the microwave current flows in the plating material, rather than some in the plating and the remainder in the copper core. Thus, for the model, the conductor can be assumed to be wholly nickel, whose  $\rho_r=5.05$ . A 10 MHz resolution model run\* was conducted for a 2m nickel cable of diameter ( $1.3077\text{mm} + 2*5.647\mu\text{m}=\text{ ) } 1.3191\text{mm}$  with the remaining inputs as derived in Section 6.2.2, see Fig. 6.14. The maximum of the measured data was 104.4 dB and that of the modelled data was 104.5 dB, representing the best correlation of measured and modelled data so far.

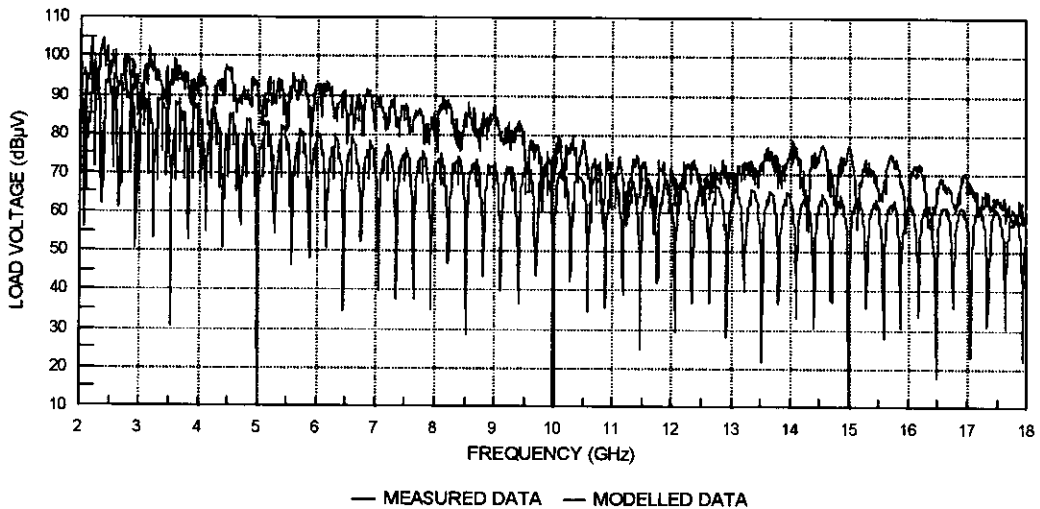
---

\* The error in [5-1] discussed in *Model Validation* was discovered late in this modelling phase, but all the figures presented in this chapter use the corrected model.

#### 6.2.4 Comparison With 10 MHz Sampled Measurements

The preceding Sections have described the validation of the model and the determination of representative termination impedances and cable parameters. Comparison of the model with the one set of 10 MHz resolution measured data, see Fig.6.14, reveals a level of detail not seen before in published literature.

Figure 6.14: 10 MHz Modelled vs. Measured Data



Prior to investigating the re-radiation postulation as the reason for the diminishing  $V_L$  seen with reducing cable length and increasing antenna distance from the box, three aspects arise from inspection of Fig.6.14. These are the three deepest nulls at 5, 10 and 15 GHz, the difference in oscillation frequency spacing between measured and modelled data, and the  $V_L$  envelope difference between them. The nulls, which are evident in all the modelled data but do not occur in practice, were investigated by model runs at resolutions decreasing in steps to 20 kHz. By using scatter rather than line graphs, it was observed that only one value at each frequency lay below 0 dB $\mu$ V (at -112, -119.4 and -122.6 dB $\mu$ V for 5, 10 and 15 GHz respectively). By conducting a further 1001 point (2mHz resolution) model run centred on 5 GHz, a number of data points were seen below 0 dB $\mu$ V, but only one point below -75 dB $\mu$ V, again highlighting interpolation by the analysis computer and plotter as a major contributor to this erroneous picture. Examination of Eqn.5.62 shows that  $V_L$  will oscillate according to the  $\sin(\beta h)$  term in the numerator, giving rise to deep nulls and peaks. Ref. [6-4] concurs with the observation that these nulls are an aphysical function of the model's base equations. To compensate for this, an estimate of the actual minima of the deep nulls

was made for the data set of Fig.6.14 as 38, 25 and 20 dB $\mu$ V for 5,10 and 15 GHz respectively. A lower limit to the  $\sin(\beta h)$  term was arrived at by sequential approximation to these  $V_L$  values, ensuring that the term did not change the other values in the data set by  $>0.05$  dB $\mu$ V. This term in Eqn.5.62 (reproduced here) was modified, see Eqn.6.5, and incorporated in the model.

$$V_L(\omega) = \frac{2Z_B}{\gamma D} \left[ (2j \sin \beta h) E_z^i [Z_0 \sinh \gamma s + Z_1 (\cosh \gamma s - 1)] \right] \quad \dots(5.62)$$

$$(\sin(\beta h) + \text{sgn}(\sin(\beta h)) \times 0.006) \quad \dots(6.5)$$

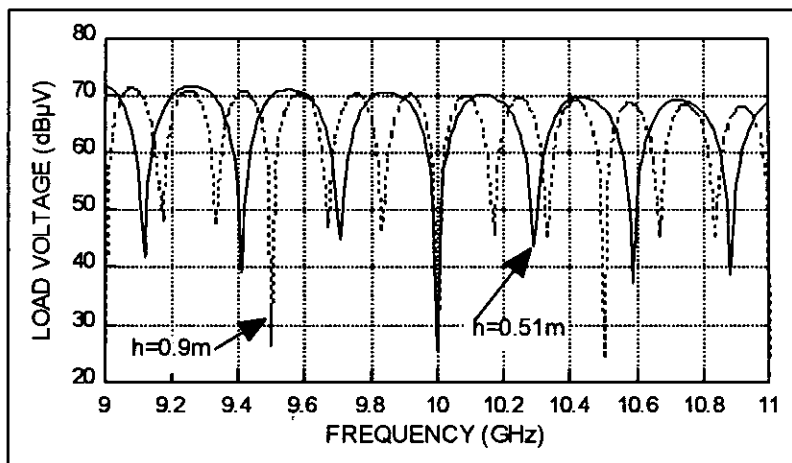
where 'sgn' denotes whether the function is positive or negative.

The modified model successfully removed the deep nulls, increasing the profile's similarity with the measured data. Verification of no adverse effects of this change was conducted by six model runs, at different heights in the range  $15\text{mm} < h < 0.9\text{m}$ , which also served to confirm the earlier researchers' findings that  $V_L$  does not increase for increasing cable heights above the ground plane of  $h > \frac{\lambda}{2}$ , see Section 6.2.1. This also enabled examination of the frequency spacing difference between modelled and measured data seen in Fig.6.14. The  $|\sin(\beta h)|$  term of Eqn.5.62 causes the oscillations and, whilst the  $V_L$  amplitude does not increase for  $h > \frac{\lambda}{2}$ , its frequency spacing, is given by:

$$\beta h = \pi, \text{ which is } f = \frac{c}{2 \cdot h} \quad \dots(6.6)$$

This can be seen in Fig.6.15, which shows the profiles for  $h=0.51\text{m}$  ( $3.4\lambda$  at 2 GHz,  $30.6\lambda$  at 18 GHz) and  $h=0.9\text{m}$  ( $6\lambda$  at 2 GHz,  $54\lambda$  at 18 GHz).

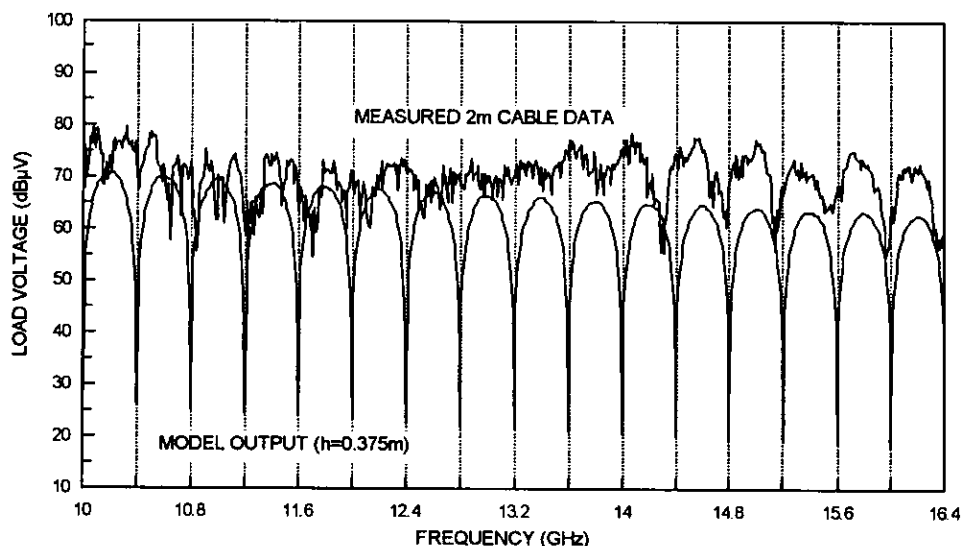
Figure 6.15: Effect of Cable Height on Frequency Spacing of Oscillations



Inspection of the measured cable data for Fig. 6.14 shows that the frequency spacing of nulls is 400 MHz, with  $\pm 10$  MHz variations between 2-18 GHz, and that the model's

spacing ( $h=0.51\text{m}$ ) is 294 MHz. The model input of  $h$  was changed to 0.375m, the value calculated using Eqn.6.6 for 400 MHz spacing. Fig.6.16 shows the resulting comparison between the 2m measured data and the model outputs, demonstrating good frequency correlation, but with a residual amount of null positioning error. Closer examination of the measured profile gives the spacing as 416 MHz, *i.e.*  $h=0.3605\text{m}$ , with  $1\sigma = 45.5$  MHz. Further study of this aspect, with laboratory tests at a number of heights over a ground plane, is required if this  $V_L$  dependency is to be fully understood.

Figure 6.16: Comparison Using Modified Height Input to Model



Comparison of Fig.6.16 (10 MHz resolution) also showed for the first time that the model's output oscillations could also be seen in the measured data. Fig.6.12, in common with all the data sets taken with 50 MHz resolution, does not show this detail. For 10-16.4 GHz in Fig.6.16, 16 cycles occurred in the modelled data and 13 clearly visible cycles in the measured data (none were discernible for 10-11 GHz). The peak-to-null median values were for modelled data: 44.5 dB $\mu$ V and for measured data: 16.5 dB $\mu$ V, a difference of 28 dB. The model's peak-to-null magnitude is determined by resistive cable losses, the result of  $\alpha$  (a function of  $\sqrt{\rho_r}$ ,  $\sqrt{\mu_r}$  and  $\sqrt{f}$ , see Eqn.5.54). Fig.6.9 (10m length) and [5-1] Fig.2-18 (100m length) show the difference between a matched steel line, where  $\alpha$  is 61.7 times that of copper, and the lossless case. A decrease in peak-to-null magnitude for the steel case is shown, with the magnitude also reducing with frequency, since  $\alpha$  increases with  $\sqrt{f}$ . This is pronounced for the 100m case, as  $\alpha$  is in dBm $^{-1}$ , with the oscillations totally suppressed at 100 MHz. The possibility that the difference was caused by an increased  $\alpha$  was explored *via* 2m cable model runs, with  $h=0.3605\text{m}$  (as calculated on the

previous page) and four cable material inputs: lossless, copper ( $\rho_r=1$ ,  $\mu_r=1$ ), nickel ( $\rho_r=5.05$ ,  $\mu_r=1$ ) and steel ( $\rho_r=12.7$ ,  $\mu_r=1$ ). Fig.6.17 highlights two aspects: the predicted reduction in peak-to-null magnitude can be seen, and the  $V_L$  profile loses its noisy appearance with increasing  $\alpha$ , making the steel profile closely resemble the measured data. The median peak-to-null magnitude of the steel data in Fig.6.17 is 16.0 dB $\mu$ V *i.e.* within 0.5 dB $\mu$ V of the measured data. Three possible causes for this  $\alpha$  multiplier of 27.5 exist, but, as only one 10 MHz data set was taken, no conclusion can be drawn. These causes are dielectric losses in the FEP/PTFE cable sheathing, mismatch losses (neglected in the model, see Section 6.2.2) and increased resistance caused by using a stranded rather than single conductor cable. Ref. [6-8] indicates the latter results from the increased conductor length due to helical lay within the stranded bundle and concentration of RF current at the peripheral surface of the conductors at the outside of the bundle. Ref. [6-8] lumps these effects together and allows for stranding by multiplying the RF resistance of a single conductor by a form factor of 1.25, which has been '*well confirmed experimentally*'. Further measurements on cables with different materials are required to understand this  $\alpha$  multiplier of 27.5.

Figure 6.17: Effects of Cable Material on  $V_L$  Profile

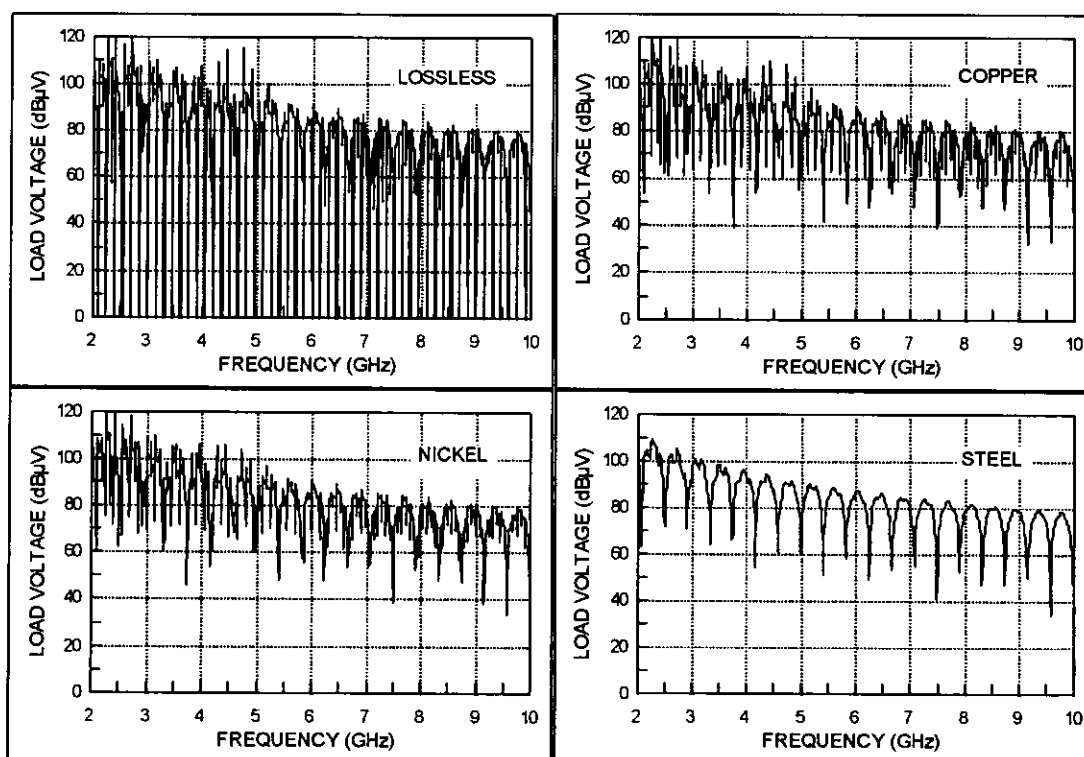
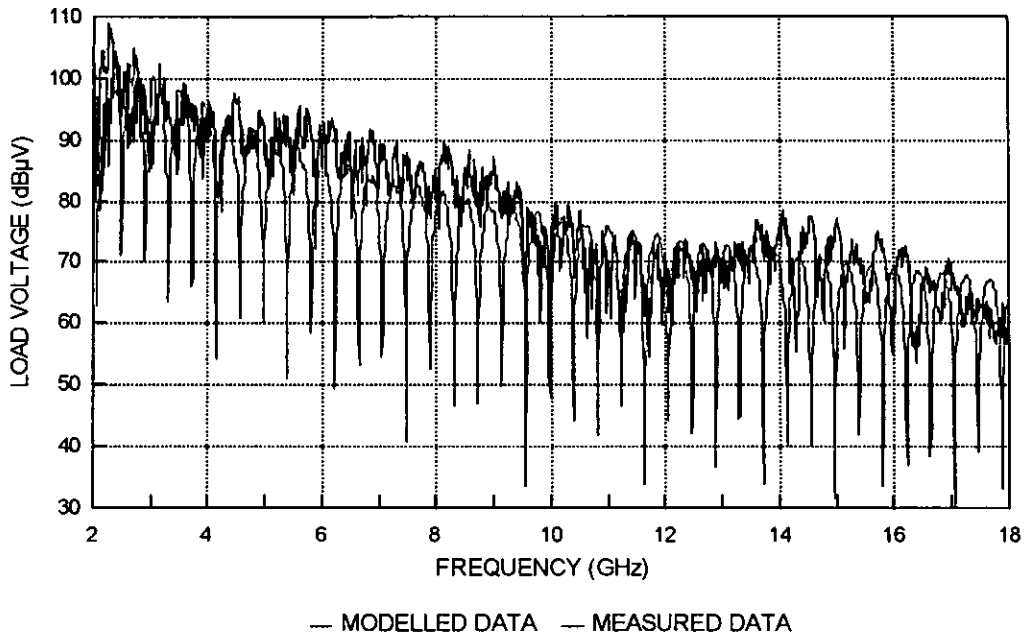


Figure 6.18 shows the final comparison of the 2m, 10 MHz measured data with the refined model, demonstrating that, assuming the multiplier is verified, correlation of modelled and measured maximum  $V_L$  can be achieved if a good definition of the test configuration is known.

Figure 6.18: Final Comparison of 10 MHz Sampled vs. Modelled Data

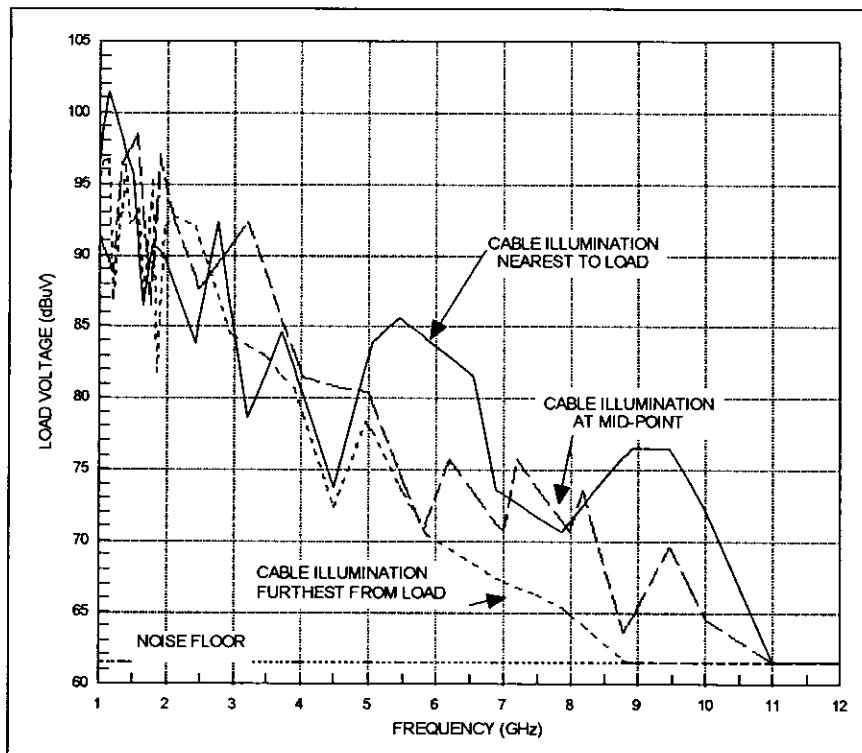


### 6.3 ENERGY COUPLING vs. CABLE LENGTH

#### 6.3.1 Examination of Cable Data Sets

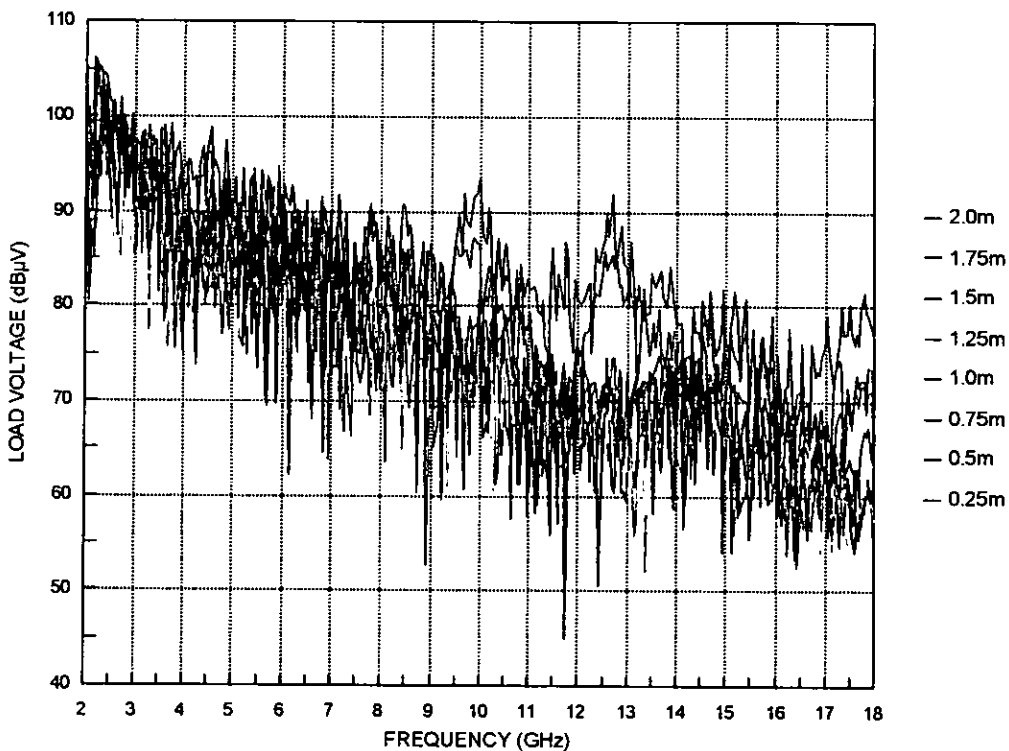
An important part of the laboratory research was the investigation of the Chapter 5 re-radiation postulation. Ref. [6-2] also supports the postulation, although little data is presented in the paper to substantiate the statement: *'However, the data does indicate that at line lengths of greater than  $\frac{\lambda}{2}$  there is an energy loss due to reradiation that needs to be included in the models based on the telegrapher's equations.'* Ref. [4-21] also noted that *'Both cable lengths [0.6m and 0.19m] were greater than  $\frac{\lambda}{2}$  yet no additional pickup occurred due to increased length.'* and that the maximum effective aperture of the shorter wire was close to that of the 0.6m wire and the half-wave dipole model. In his investigation of coupling to a 2m wire when far end or centre illuminated, Willis [3-20] noted that *'In the higher frequency range the pickup was more pronounced when the transmitting antenna was illuminating the area nearest the detector [near end of the 2m wire].'* This can be seen in Fig.6.19 where, despite the coarse frequency resolution, there is a clear trend >5 GHz of decreasing  $V_L$  with antenna distance from the load. This suggests that the re-radiation factor is a function of cable length or remoteness of the load from the illuminated portion, and frequency.

Figure 6.19: Willis  $V_L$  Data Dependency on Antenna Position



Initial analysis of this researcher's data showed no correlation with either cable length or antenna distance from the avionic box. Fig.6.20 shows the processed measurements for the 2m cable to demonstrate the large and frequency dependent amplitude variation typical of all cable lengths investigated. The initial inspection did show that most data sets have similar maximum  $V_L$  envelope profile with frequency, that the profiles are very similar for cable length  $>0.5\text{m}$  ( $3\lambda$  at 2 GHz) and that measurable  $V_L$  existed for the 2m cable when illuminated at its far end. This latter aspect concurs with U.S. work [4-20] where measurable signals existed for far end illumination of a 3.05m cable.  $V_L$  in Fig.6.20 is similar for all data sets up to 8 GHz and  $>8$  GHz the envelope of all  $V_L$  values (for all cable lengths and antenna positions investigated) is 15 dB maximum, with no distinct frequency trend.

Figure 6.20: 2m Cable  $V_L$  Measurements vs. Antenna Position



A more detailed analysis of the 24 data sets for the four cable lengths antenna position data sets was undertaken and a clear trend of median  $V_L$  dependency on cable length was established, see Fig.6.21, which agrees with Willis's observation (see Fig.6.19), although no trend was seen in the maxima or minima of the data sets.

Figure 6.21: Median  $V_L$  Dependency on Cable Length and Antenna Position

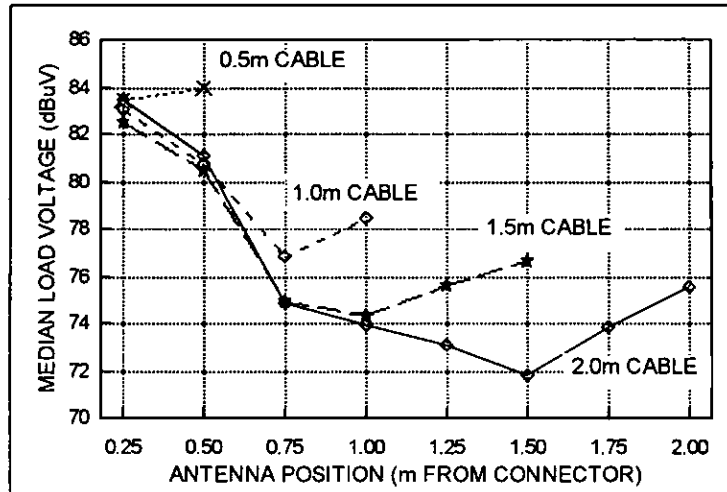


Fig.6.21 shows that there is a 6-8.5 dB reduction in  $V_L$  in the first 0.75m from the box. A similar trend is difficult to establish for the 0.5m cable, since only one antenna position is the same as the other cables (the 0.25m value on Fig.6.21 is interpolated but is within the range of values of the other cables, adding confidence to the observation). The  $V_L$  profile for the three longer cables, which is clearly a function of cable length and antenna position, comprises three main elements: a steep reduction, a lower gradient reduction and an upturn whose eventual destination is unknown. The breakpoints for the 2.0m cable occur at  $5\lambda$  and  $10\lambda$  at 2 GHz or  $33.3\lambda$  and  $66.7\lambda$  at 18 GHz, a relationship suggesting that a further profile element occurs at  $2.5\lambda$  (2 GHz) or 0.375m. This antenna position was not measured, but it can be argued that Fig.6.21 shows a fourth, lower gradient profile element between 0.25 and 0.5m. This indicates a dependency with antenna position of  $2.5A\lambda$ , where  $A$  = antenna position in metres from the box. A similar profile exists for the 1.5m and 1.0m cable lengths, but with the lower gradient slope and upturn elements occurring for antenna positions 0.5m (1.5m cable) and 1.0m (1.0m cable) nearer the box. This suggests a  $V_L$  cable length dependency of  $0.5s$  where  $s$  = cable length. It is considered that these findings confirm the postulation, and this dependency is discussed further in Section 6.3.2. Examination of the experimental arrangement shows that potential for cable illumination by side-lobes existed, which could have affected the measurements. For the antenna used, where the side-lobes are small (<10 dB below boresight gain), this is not thought to have adversely affected the experiment. For any future cable coupling research, the use of RAM collars should be considered to suppress the transmission of microwave currents along those parts of the cable which are not required to be illuminated, noting that their use may also artificially enhance the loss (and consequently depress  $V_L$ ).

### 6.3.2 Re-Radiation Postulation and Empirical Equation

The research reported in this Chapter suggests that transmission line-based models can be used in the 2-18 GHz range, conditional upon precise definition of test configuration, especially load impedance. It was established through model runs with cable lengths set to 2, 5, 10 and 50m, where identical  $V_L$  amplitude profiles were seen and granularity suppression with increasing length, that the model did not exhibit the significant amplitude reduction with cable length and antenna position away from the avionic box, as seen in the laboratory measurements. Consequently, investigations were conducted into how such an effect might be included in the model. These investigations, covered in this section, were based on representing the effect as a cable material loss and include the derivation of an empirical equation describing the effect. The cable material loss approach is appropriate as the measured data suggests transmission on the wire is probably no longer TEM, which is assumed in the model.

Table 1-1 of [5-1] gives  $\rho_r$  and  $\mu_r$  which, suitably updated, were used in the model. The investigation of cable material effects on  $V_L$  (Section 6.5.2 and the earlier part of this section) showed that transit from copper to steel *via* nickel removed much of the waveform granularity and reduced the  $V_L$  envelope magnitude, with the steel case bearing much similarity to the measured data. This suggested that an increased  $\alpha$  term with a resistive element (re-radiator) in the transmission line equations could be the explanation for both the difference between modelled and 2m cable measured data and  $V_L$ 's cable length dependency as seen in Fig.6.21. To explore this the cable resistance per unit length was increased from  $R \Omega m^{-1}$  to  $(R+R_{rad}) \Omega m^{-1}$  where  $R_{rad}$  is the proposed re-radiation resistance. To quantify  $R_{rad}$  the difference between  $\alpha$  for steel and nickel was calculated using the precursor to Eqn.5.54 and equated to the extra term thus:

$$\alpha = \frac{R+R_{rad}}{2Z_o} = 8.3 \times 10^{-8} \frac{\sqrt{\rho_r \mu_r} f}{aZ_o} + \frac{R_{rad}}{2Z_o} = \alpha_{original} + \frac{aR_{rad}/2}{aZ_o} \quad \dots(6.7)$$

$\alpha$  was calculated for nickel and steel at three points, see Table 6.3, and regression analysis conducted on the difference between them to arrive at a value:

$$R_{rad} = 39.728f + 317.0781 \Omega \quad \dots(6.8)$$

Table 6.3: Attenuation Constant for Nickel vs. Steel

Frequency	Alpha (x10 <sup>-3</sup> nepers/metre)		
	2 GHz	10 GHz	18 GHz
Nickel	9.1	20.4	27.3
Steel	197.3	441.2	591.9
Difference	188.2	420.8	564.6

Comparing this modified  $\alpha$  for nickel with that of steel gave agreement to within  $\pm 3.5\%$ . The model was modified to include  $R_r$  and a 2-18 GHz, 10 MHz resolution run conducted which showed that the resultant  $V_L$  profile using nickel matched that using steel as the cable material. This modification did not, however, provide any change in the length dependency of  $V_L$ . A different approach, that of describing the cable as a series of radiating Hertzian dipole elements was studied. From [3-24] the radiation resistance of such an element is given by:

$$R_{\text{rad}} = 80\pi^2 \left(\frac{dl}{\lambda}\right)^2 \quad \Omega \quad \dots(6.9)$$

where  $l$  = the dipole length. Connors [6-9] notes that the nearest practical approach to the Hertzian dipole is for  $dl \leq \frac{\lambda}{10}$ , for which the characteristic of uniform current along its length can still be assumed valid. If we consider the 2m cable and  $\frac{\lambda}{10} = 1.7\text{mm}$  at the highest frequency (18 GHz), a  $dl$  value of 0.17mm equates to  $\frac{\lambda}{100}$ , which easily satisfies the above criterion. In this case the cable is  $2/0.00017 = 11765$  dipoles in length and, assuming series addition of  $R_{\text{rad}}$ , would give  $0.07896\Omega$  per dipole, or  $928\Omega$  in total. This is counter-intuitive as the cable entering the avionic box is by analogy a monopole and  $R_{\text{rad}}$  for a monopole is shown [3-24] to be  $36.8\Omega$  at resonance, much lower than the above figure. This was examined further, for  $\frac{\lambda}{10} \leq dl \leq \frac{\lambda}{80}$ , but with the similar results. To ensure this equivalence to a monopole was achieved, an analysis was conducted of the change in  $dl$  with frequency which resulted in

$$dl = \frac{\lambda}{(140.3677f - 10.5276)} \quad \dots(6.10)$$

which, on calculation, gives  $R_{\text{rad}}$  of  $108.14\text{E-}4\Omega$  at 2 GHz,  $4.068\text{E-}4\Omega$  at 10 GHz and  $1.247\text{E-}4\Omega$  at 18 GHz. Eqn.6.10 was temporarily programmed into the model and a comparison made between  $R_r$  using this equation vs. using Eqn.6.8. The Hertzian dipole version gave a lower value than the nickel-to-steel factor across 2-18 GHz and thus contributes little to the explanation of the  $V_L$  dependency on cable length.

The possibility that higher order transmission modes, which radiate effectively, were being excited was considered. Much work has been conducted in this area, including [4-3],

Adams *et al.* [6-10] and [6-4] and their references. The consensus is that the higher order modes are undoubtedly excited to some degree, particularly in cases where, as in this research, line separations  $>5\lambda$  but that their effect on current distribution does not appear to be significant for the cases investigated. The currents were also concluded to be of a relatively simple form, explainable in terms of TEM modes. To conclude the investigation of cable length and antenna position dependency, an examination of Fig.6.21 was conducted to determine an empirical equation describing the dependency. This approach had also been taken by Brock *et al.* [6-3] who noted that the enhanced IEMCAP algorithm uses transmission line predictions  $<1$  GHz, a weighted average between the transmission line model and the new empirical model for  $1 < f < 3$  GHz, and the empirical model predictions  $>3$  GHz. The empirical models were derived from a series of experimental measurements performed in a mode-tuned chamber and from the bounding behaviour of bare wire coupling as characterised by method-of-moment calculations. The examination yielded Eqn.6.11, which was developed by curve-fitting using the  $(2.5*A)$  relationship identified in Section 6.3.1 as a basis. Eqn.6.11 is valid for the limited number of cable lengths and antenna positions investigated.

$$V_L = V_{L(ZERO)} + 7 * \left( 1 - 1.3 * A * \sin\left(\frac{2.5A}{s}\right)^2 \right) \text{ dB}\mu\text{V} \quad \dots(6.11)$$

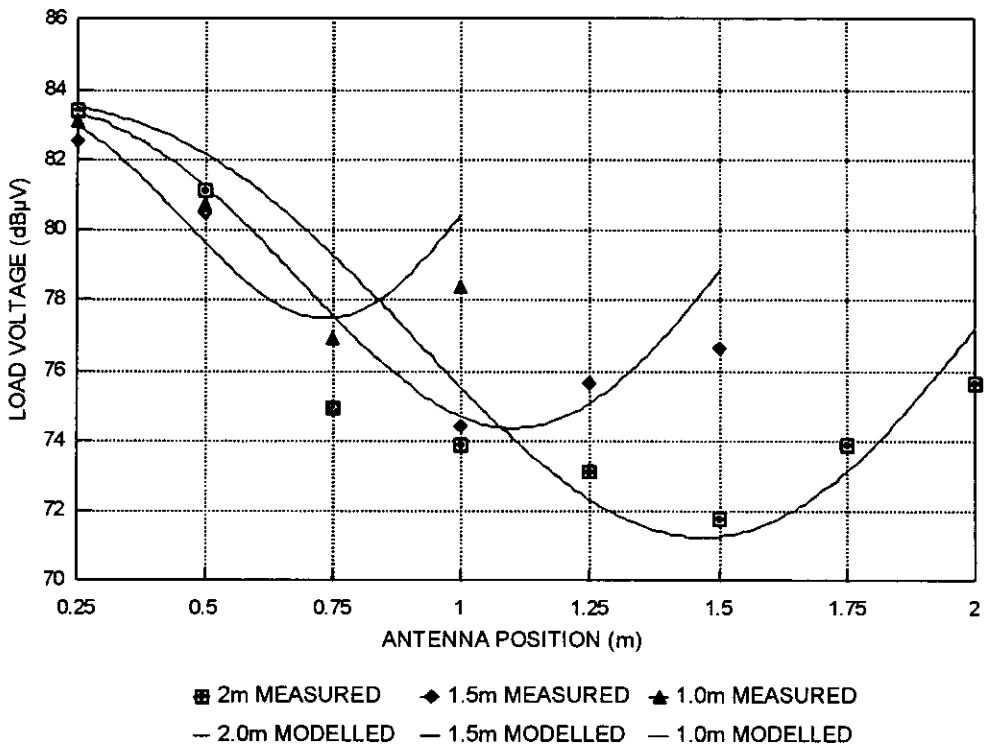
where A = antenna position in metres from the avionic box

s = cable length in metres

$V_{L(ZERO)}$  =  $V_L$  measured at nearest point to box (76.7 dB $\mu$ V in this case)

A comparison between Eqn.6.12 and the Fig.6.21 data is presented in Fig.6.22 and agreement in all cases to within +4.4 to -1.1 dB is achieved. Further test data is required to enable refinement of this equation and extend its validity to the general case.

Figure 6.22: Modelled vs. Measured Length and Antenna Position Dependency



Future work should include modelling partial illumination of a cable at various distances from the load and further laboratory investigations to examine this length dependency in more detail, using a greater number of cable lengths and antenna positions. The illuminating antenna for this work requires development, as a much smaller 'footprint' on the cable is required than was achieved in these investigations. Modification of the model could then follow, possibly based upon modelling footprint illumination by voltage source phase change over a given length of the cable. Appendix G is the model listing (less Eqn.6.11).

## 6.4 CONCLUDING REMARKS

The research covered in this chapter has shown that validated transmission line-based models can be used to predict maximum  $V_L$  per  $Wm^{-2}$  in the range 2-18 GHz. The key factors in achieving this are the precise knowledge of the line termination impedances (including connector impedance and parasitics) and construction characteristics of the cable under consideration, and use of modelling and measurement resolution of at worst 10 MHz. These models require an extra term to describe the reduction in  $V_L$  with cable length and illuminating antenna distance from the load. The postulation of re-radiation of energy from the wire as the cause was examined, but no satisfactory term was derived for the model. However, statistical analysis of the laboratory test data showed clear trends of  $V_L$  with length and antenna position, which enabled the development of an empirical equation describing the dependency.

There is a need for further research on a number of topics of which the more important are laboratory tests to further investigate the cable length and antenna position dependency and thus refine the model, and an examination of the smallest resolution required for complete characterisation of microwave field coupling to cables, to minimise the  $V_L$  error bound.

It is important to recognise that point-to-point agreement of modelled and measured data does not exist and will never be possible due to the nature of the problem and its dependency on small details, often uncontrollable, and thus coupling to a cable is best predicted on a statistical basis, with the  $V_L$  maximum profile being of most relevance to the potential for avionics upset.

# *Chapter 7*

---

## **MICROWAVE EFFECTS ON ELECTRONIC CIRCUITRY**

## 7.1 INTRODUCTION

This chapter examines reported microwave upset of electronics, civil or military, the identification of upset mechanisms, modelling of circuitry and its contribution to the prediction of upset. Eqn.4.2, the overall ingress equation in Section 4.2, is re-visited and the last term quantified, enabling a prediction of the power delivered to a circuit inside an avionics box. A determination of required protection levels then follows from examination of this received power profile vs. the results of the investigation of electronic component and system upset. Finally, an improved microwave EM hazard protection strategy is proposed.

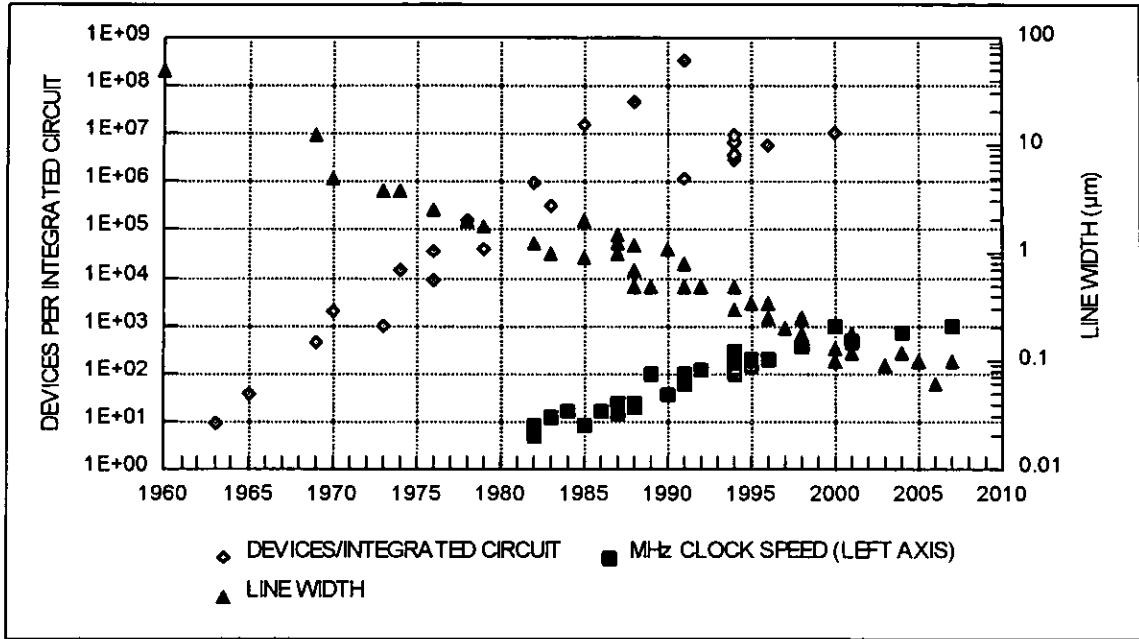
## 7.2 REPORTED UPSET OF ELECTRONICS

### 7.2.1 Circuit Technologies

The RF susceptibility of circuitry was thought, see Section 1.1, to be a function *inter alia* of the circuit technology used in the avionics of military or civil aircraft. Before proceeding to an examination of reported electronics upset an investigation of circuit technology developments and predictions was undertaken. Refs. [2-19] and [7-1] to [7-17] were extracted from literature search and their relevant aspects of transistors/integrated circuit, device minimum line width (*i.e.* device size) and processor clock rates were distilled into Fig.7.1. Examples of all transistor and IC technologies, including the latest VHSIC devices, are now in many processors, radars and EW systems on military aircraft and ships world-wide [7-3]. An example is the latest UK military fighter's computer processor IC, the Motorola 68020, which has a gate size of 1.0  $\mu\text{m}$ . Fig.7.1 includes predictions of future growth by the companies where data was published, *i.e.* NEC, Sony, Toshiba, the [US/EC] Advanced Lithography Group and the Semiconductor Industry Association, and shows a steady increase in device density per IC of 250 times/decade and a continuous increase in circuit speed of 20-30 times/decade, agreeing with [7-5]. As the device sizes reduce below 0.25 $\mu\text{m}$  they transit from being transistors to a new class of 'resonant tunnelling' devices. These devices are described under the heading 'Nano-electronics' [7-18] and [7-19], a field where the Japanese in particular are active, with 15 nm line widths thought an achievable goal by the year 2000. In parallel with this increase in IC performance, there have been similar advances in discrete devices, with many transistors designed to operate above 1 GHz (the highest speed at this time, by a Hetero-structure Field Effect Transistor [HFET], is 175 GHz). Increased operating

frequencies make more of the RFI 'in-band' and thus are capable of causing upset. Ref.[2-19] estimated that, in going from 0.35-5 GHz, devices are likely to experience a 10 dB susceptibility increase.

Figure 7.1: Circuit Technology Trends



### 7.2.2 Evidence Of Upset Of Electronics

The term 'Upset' is defined as RF *Interference* (RFI) or permanent *damage*. RFI is transitory in nature, *i.e.* with RF applied interference occurs, which in itself could cause a life-threatening situation, and with the RF off the electronics returns to normal operation. Component damage renders that function inoperative and irrecoverable and can, dependent upon the equipment affected, result in mission termination or aircraft loss. Digital circuit latch-up is a specific state which forms a sub-set of both the RFI and damage categories of upset. In the latch-up state, the circuit element ceases responding to inputs and remains so even after removal of the RF, until the circuit is powered down and re-initialised. In some cases, *e.g.* CMOS ICs, such latch-up can lead to IC damage as the device draws currents higher than its capability. Latch-up is caused by a parasitic transistor, formed during the IC fabrication process, which forms an unintentional Silicon-Controlled Rectifier-type switch. Transitory effects are particularly relevant to civil or military aircraft in flight, where, see Section 2.3.2, transmitter-to-aircraft sight line angle rates and ranges are continuously changing. This probability of illumination, in conjunction with the highly probabilistic microwave ingress path to the circuit, explains why microwave RFI problems

are rarely reported from flight, although they have been seen at various frequencies during aircraft ground EMC tests. RFI <0.4 GHz with all classes of electronics is a known phenomenon which can be alleviated, if not eradicated, by good EMC design practice and installation, *e.g.* in [2-17]. The situation >0.5 GHz is less understood and >1 GHz there is a dearth of understanding which this research aims to resolve. Table 7.1 gives a selection of reported upset effects.

Table 7.1: Upset Examples

AIRCRAFT	YEAR	SOURCE	EFFECT	REF
USS Forrestal: Aircraft Carrier	1967	Carrier radar	Poorly shielded plug: Missile fired into other aircraft: 134 dead \$72M damage	[7-20]
Black Hawk Helicopter	since-1982	Radar/radio masts	Several crashes attributed to RFI of flight control systems	[7-21]
Various civil	since-1986	Portable devices	24 pilot reports of RFI due to passenger-operated electronic devices	[2-26]
B747-100	1995	Camcorder	Slow left turn	[7-22]
B747-200	1995	2 Laptops	Compass moved 15°	[7-22]
Augusta 109 Helicopter	1995	U.K. HIRTA	Spurious engine readings, to normal after 7-10s	[7-23]
Various	1995	Radio Masts	Spurious readings on GPS	[7-23]

Until the commencement of this research there had been little openly published data on the microwave upset of components and systems, and it was generally thought that, due to the poor coupling mechanisms involved on aircraft >400 MHz, no real problem existed above this frequency. This research has uncovered a variety of component and equipment upset data, of *inter alia* (now) openly published U.S. research, from BAe EMC trials on a number of aircraft and BAe EMC Laboratory investigations on PCs and avionic equipment. The investigations have also revealed that open publication of equipment, system or product failures at any frequency is rare and is likely to remain so for commercial-legal (liability claims) and national security reasons. The following data on equipment upset has thus necessarily had its source disguised, by merging civil and military data and other means, to allow its use in this thesis. The subsequent data on component upset is fully referenced, openly published research.

### Equipment Upset

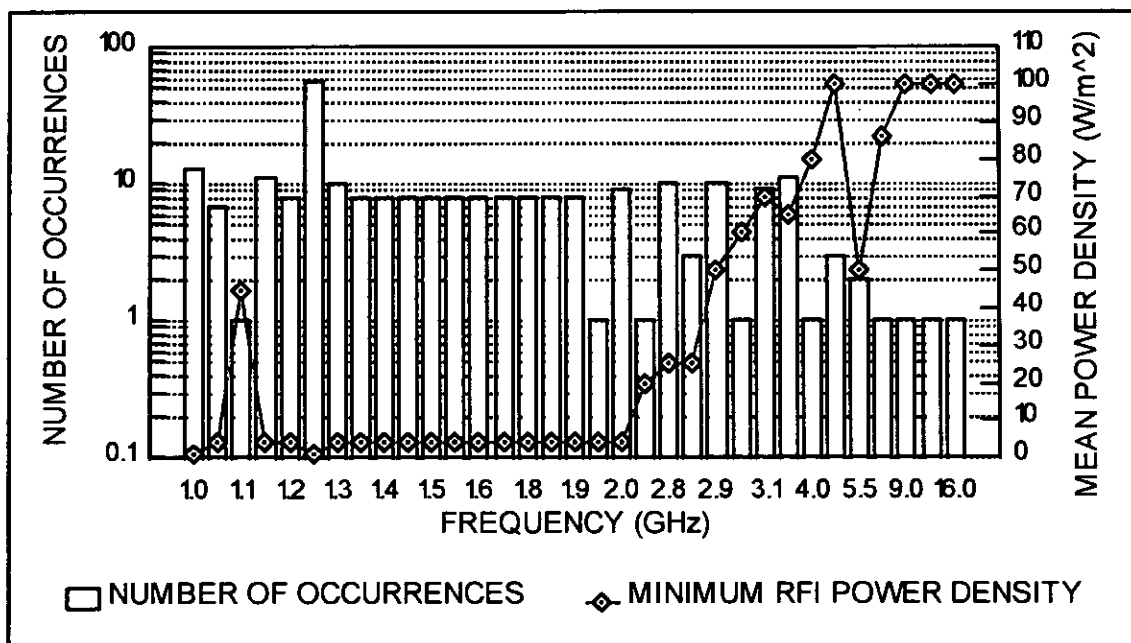
Few reported microwave effects exist, with most avionic systems functioning normally up to and above high peak power densities ( $>1 \text{ kWm}^{-2}$ ). Pre-1989 only two RFI incidents were reported, a Head-Up Display [7-24] (which was high up in the exposed cockpit, with radiation entering the un-screened optical aperture and affecting the timebase circuitry) and an unrepeatable avionic occurrence during an aircraft EMC trial [7-25]. BAe EMC qualification research demonstrated repeatable microwave RFI of two avionic equipment types [7-26], [7-27]. This included unintentional damage of 2 bipolar transistors, 2 FETs and a 741 operational amplifier in one equipment, which had been successfully EMC qualified, on exposure to very high power densities. This was investigated and explained by inadequate box shielding for circuit protection from radiation of this intensity, 80 dB above its design specification. One phase of this research involved high power irradiation of an avionic equipment in the EMC Laboratory where a 4 dB improvement in failure thresholds was achieved by wrapping Aluminium foil around the cable loom for the first  $1.5-4.8\lambda$  from the connector at the frequencies investigated. This supports the view referenced in Chapter 5 that cable-borne 1-18 GHz energy coupled at  $>\frac{\lambda}{2}$  can be enough to cause upset. Aluminium tape applied to all seams of the [7-27] unit's four loose-fitting side panels resulted in a RFI  $P_d$  improvement of 12 dB minimum (with the available RF power it could no longer be upset).

In a study of microwave upset of avionics [7-28] it was shown that various levels of microwave RFI had been encountered on thirteen avionic equipments, one of which was a similar unit to the unrepeatable item above. None of these cases could be considered serious, with ten being operationally insignificant and the others recommended for further study. As computers, which are usually un-screened, are the most sensitive ground-based civil electronics to RFI, investigations were conducted into their 1-18 GHz susceptibility [7-29] to [7-31], in addition to those on three early generation microprocessor boards [7-32]. The latter author observed that 1-10 GHz RFI was rare for  $P_d < 1 \text{ Wm}^{-2}$  but that failures were frequent  $< 1 \text{ GHz}$  at  $P_d$  up to  $1 \text{ Wm}^{-2}$ . A valid worry was the nature of the RFI effects: these included wild running displays, similar alpha-numeric in all display elements and display absence. Failures were also seen where incorrect data was displayed, which is of greater concern operationally as an operator may act inappropriately rather than, in the case of the clearly recognisable faults, not act at all based on the information.

Similar RFI effects have been seen during this researcher's related industrial experience and further study is warranted. Braun [7-33] conducted 0.3-2.0 GHz RS measurements of four hand-held Global Positioning System receivers showed a range of RFI effects *e.g.* auto-switch-off/on, display errors and one where, as cautioned above, the unit was capable of giving incorrect information to the user. The RFI thresholds observed were: for CW signals:  $5.2 \text{ mWm}^{-2}$ , for single pulse:  $586\text{-}7665 \text{ Wm}^{-2}$ , and for 1 kHz repetition rate:  $586\text{-}2394 \text{ Wm}^{-2}$ . It should be noted that 1-2 GHz RFI occurred for all the GPS units tested at levels below  $10.6 \text{ mWm}^{-2}$  ( $2 \text{ Vm}^{-1}$ ).

Fig.7.2 is a distillation of available civil and military microwave RFI data. It shows the number of occurrences independent of equipment type and minimum upset mean power density vs. frequency, noting that the latter also shows a trend of decreasing severity of RFI with increasing frequency. Of note is that no flight-reported occurrences of microwave upset have been found. Consideration of the susceptibilities of the 1970's and early 1980's technologies, installations and shielding practices involved suggest that the RFI is predictable and which now could be prevented through improved EMC design and shielding practice. It is concluded that some current and older standards of avionic equipment are upset at levels to be encountered in today's microwave RF environment.

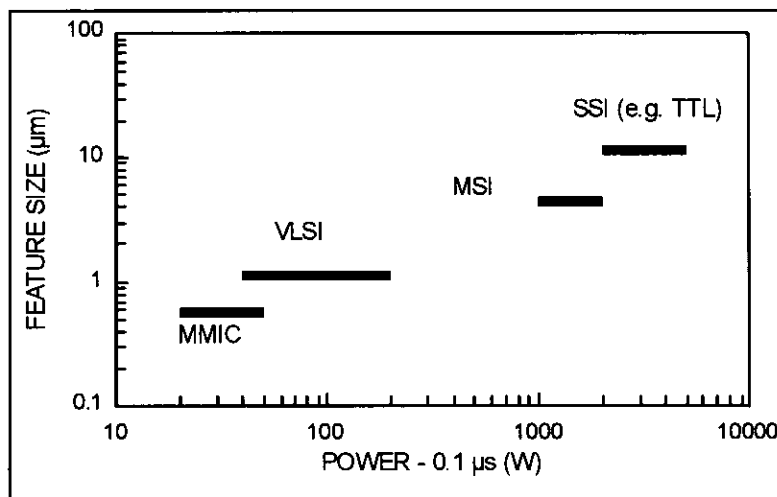
Figure 7.2: Trends of RFI Occurrences and Minimum Power Density



### Component Upset

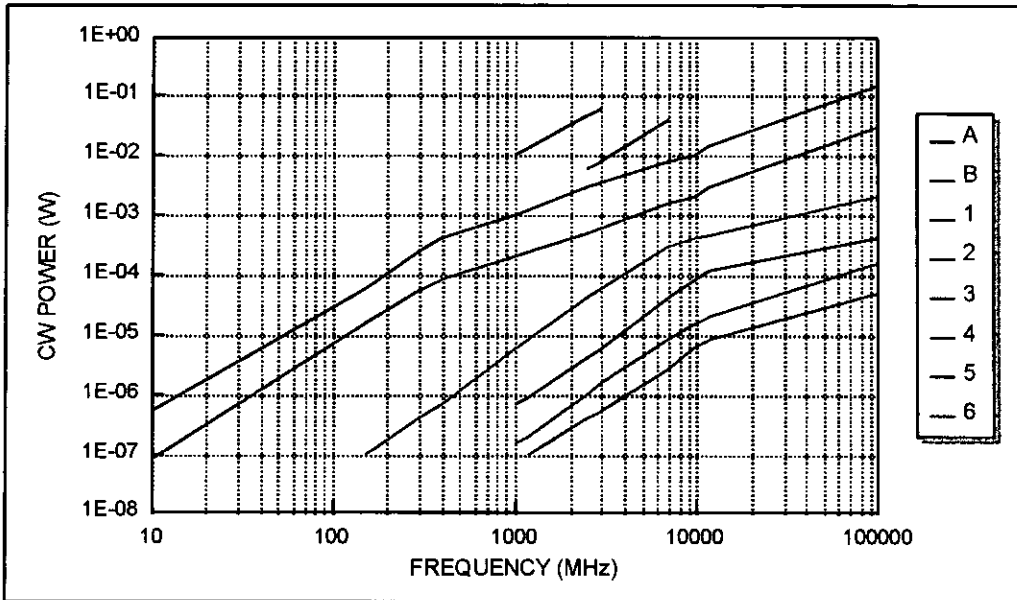
Since the late 1960s much component RFI and damage research has been conducted, primarily under the auspices of the U.S. Departments of Defense and Energy at the Harry Diamond, Lawrence Livermore National and various industry laboratories, under contract from the U.S. Air Force Wright Laboratories and the U.S. Naval Surface Weapons Centre - Dahlgren Laboratory. Much of the research results are now available and that of 2-18 GHz relevance was examined, [5-4], [7-34]-[7-36] and six references from [7-37], which between them cover RFI and HPM damage of various IC technologies and discrete components. Ref. [7-38] builds on the Harry Diamond laboratory's earlier work [7-34] to produce an empirically derived picture of IC pulsed-RF damage threshold at 3 and 10 GHz, see Fig.7.3, demonstrating the higher RFI sensitivity of ICs with smaller device sizes.

Figure 7.3: IC Damage Threshold for 0.1 $\mu$ s RF Pulses



Much of the research results of [5-4] and [7-35] are now presented as reference tables of susceptibility in Keiser [7-39] for TTL, CMOS, Line Drivers and Receivers, Operational Amplifiers, Comparators and Voltage Regulators. The susceptibility of VHSIC/VLSI was projected in [2-19] as needing over 100 dB of protection for 0.001-100 GHz. Fig.7.4, from [2-19], compares the CW RF power required to upset TTL and ECL ICs with those calculated for VHSIC, noting predictions of future device line widths at that time (1986) were 2-5  $\mu\text{m}$ . Widths <2  $\mu\text{m}$  are now common, see Section 7.2.1, with increased susceptibility implications.

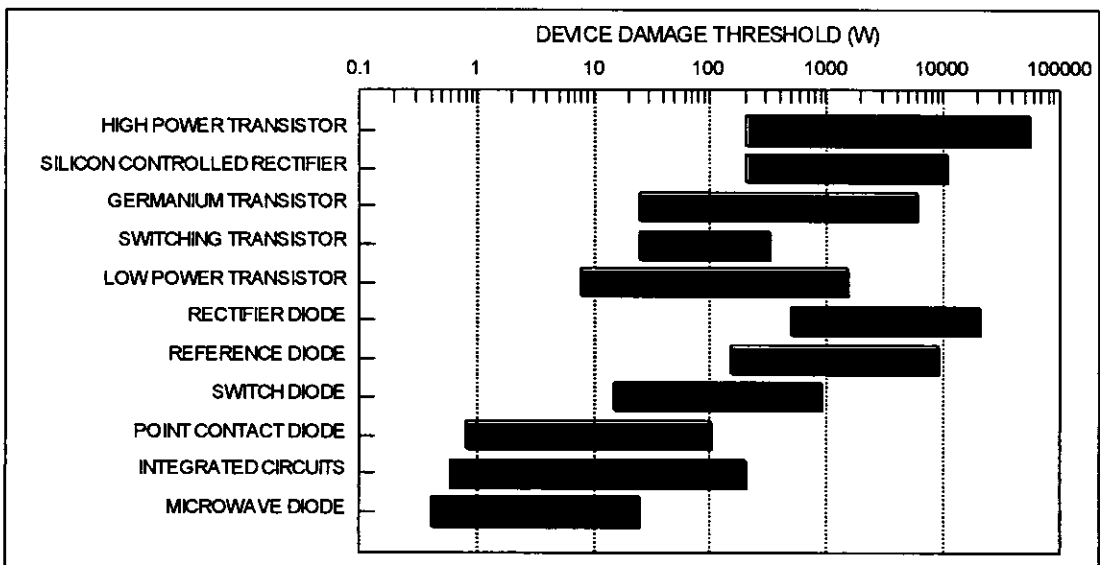
Figure 7.4: RFI Power Levels for Major IC Technologies



- |                                     |  |
|-------------------------------------|--|
| A - Measured TTL                    | 3 - Calculated VHSIC1 TTL, $F_T = 350$ MHz |
| B - Measured 10K ECL                | 4 - Calculated VHSIC1 TTL, $F_T = 5$ GHz   |
| 1 - Calculated TTL, $F_T = 350$ MHz | 5 - Calculated VHSIC1 ECL, $F_T = 5$ GHz   |
| 2 - Calculated ECL, $F_T = 350$ MHz | 6 - Calculated VHSIC2 ECL, $F_T = 5$ GHz   |

Fig.7.5, taken from [7-20], is based on much of the earlier referenced material in this Section and provides a summary of damage thresholds for a range of device types.

Figure 7.5: Typical Damage Threshold Levels for 1  $\mu$ s Pulses



Two other aspects are relevant; frequency dependency of RFI and RFI modes. Le Vine and Richardson [7-40] and [2-17] show device RFI sensitivity decreases at 15-20 dB/decade frequency, with occasional resonances linked to parasitic inductances and capacitances in the leads of typical 14-16 pin dual in line packages. Roach [7-41] noted that different RFI effects could be obtained dependent upon which IC pin had RF current injected into it and at what point in the read/write cycle the MOS memory IC the injection was initiated. This latter point has been identified by a number of subsequent authors, and suggests an important finding, that the pulse width, pulse repetition rate and frequency of a waveform may be as important as its peak power. This effect has been seen in BAe EMC laboratory tests [7-27] where a different RFI mode was seen when an electronic equipment was illuminated with different RF characteristics and lower power than the initially reported RFI incident.

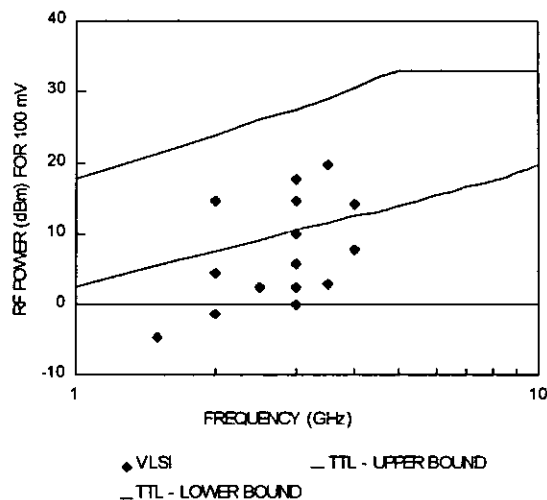
Antonone and Ng, in a recent openly published document [7-36] on HPM effects on components, conducted 0.1-5.0 GHz, 20  $\mu$ s pulse width, 1 kHz repetition frequency RFI tests and 1-2 GHz, 10  $\mu$ s pulse width, single shot component damage trend tests on analogue and digital ICs, infra-red detectors, CMOS digital ICs and hybrid amplifiers. The results showed that the microwave power for RFI in a digital device (15.8-79.4 mW) was more than that for an analogue one (0.04-39.8 mW), that the frequency dependence of the RFI was stronger for analogue devices, and that a maximum 7 dB (typical 5 dB) variation existed across a small number of samples of the same device. Of importance was the finding that damage power levels, which were similar for digital and analogue devices (at  $100 \pm 50$  W for 10  $\mu$ s pulse width), were 20-64 dB (100-2.5 million times) greater than those for causing RFI, concurring with Roe [4-20] who, on examining studies conducted by McDonnell Douglas Astronautics, showed a worst case RFI-to-damage margin for TTL ICs of 25 dB at 1 GHz, reducing to 10 dB at 10 GHz. The TTL RFI findings in [7-36] and [7-39] were expanded by Barber and Herke [6-6], who injected 1-18 GHz current into the input pin of one 7400 series IC and into the output pins of three each standard and Low Power Shottky (LS) 7400 ICs. The 1-10 GHz RFI signatures showed the LS series to be the more susceptible, agreeing with [7-36], with a decrease in sensitivity with frequency of 12-25 dB/decade, concurring with [7-40] (*'about 15 dB/decade'*) and [2-17] (*'in general by 20 dB/decade'*). Test jig effects above 10 GHz prevented useful observations.

### 7.3 IDENTIFICATION OF UPSET MECHANISM

The effects of HPM radiation on semiconductors, as noted in [2-21] by Dr. Hriar Cabayan, Program Manager of Lawrence Livermore Laboratory's HPM effects division, is governed by semiconductor physics equations. For electronics under illumination or with cable-borne RFI input signals, the principal mode by which the energy is coupled into the electronics is rectification. It occurs at diode and transistor p-n junctions, found in discrete components or within ICs. The phenomenon is explained in [7-20], [7-38] and [7-42]-[7-45]. The main effects of the demodulated RFI are operating voltage offsets for transistors and operational amplifiers, output state changes or latch-ups in logic devices and voltage comparators, and erroneous signals capable of inhibiting or upsetting data transmission and storage if the demodulated (wideband) RFI is within the circuit passband.

The relative susceptibility of devices to RFI is given by each device's Rectification Efficiency (RE). RE is defined as the ratio of the rectified DC voltage at the device output to the RF power level incident at the input. Richardson, in Ref.3 of [7-38], proposed that the absorbed power level that gives 100 mV be used as a standard for characterising the RE of a specific junction. The detected voltage rises rapidly for increasing RF power and, at the levels required to produce the 100 mV bias shift, Richardson observed that the difference between incident and absorbed power was insignificant. In practice most devices yield 100 mV at the 1-2 mW level, see Fig.7.6. Fig.7.6 also shows the increased susceptibility of VLSI, with its much smaller device size, compared with standard TTL.

Figure 7.6: Rectification Efficiencies of ICs



Richardson [7-44] used a RF rectification model of a diode to derive an equation for RE in a bipolar junction transistor, see Eqn.7.1, which enabled examination of the device size dependency of RE. The demodulation effect had already been shown (*via* calculations and measurements, [7-44]) to occur principally in the base-emitter junction of such transistors.

$$RE \cong \frac{1}{V_T} \left[ R_s \cdot \frac{A_E}{\omega C_\pi} \cdot \frac{1}{P_E^2} \right]^{\frac{1}{2}} VW^{-1} \quad \dots(7.1)$$

$R_s$  = Base sheet resistivity,  $\Omega$ /square, determined by base region  $\rho$ , base width and  $P_E$

$A_E$  = Emitter Area ( $m^2$ )

$P_E$  = Emitter perimeter (m)

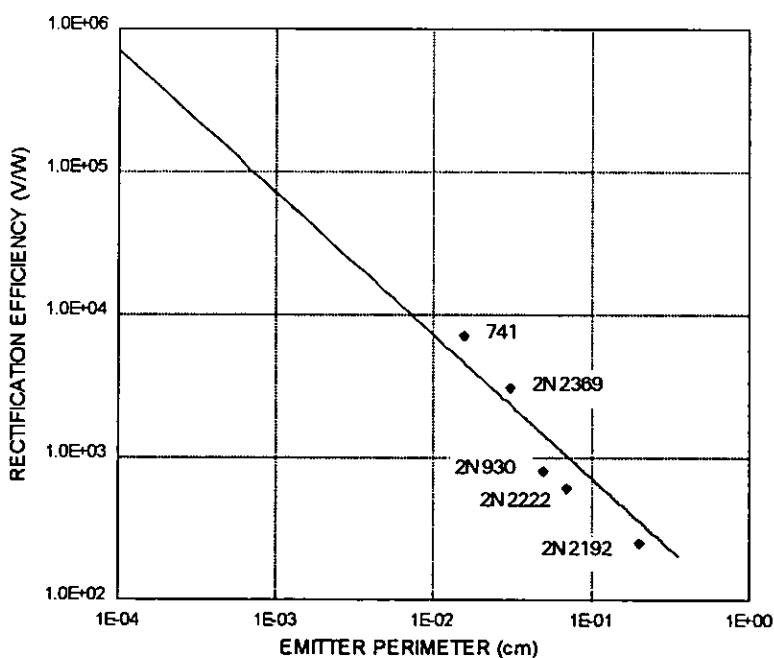
$C_\pi$  = Emitter-base capacitance (F)

$2L$  = Emitter width (m)

$V_T$  = 26 mV. The rectified offset voltage follows a square law [7-44] and is proportional to the absorbed power as long as the RF voltage at the junction does not exceed 26 mV.

For small transistors, *e.g.* those in the 741 operational amplifier, RE values of 3.1-5.0  $kVW^{-1}$  are calculated, indicating that micro-watts of RF energy are adequate to produce milli-volts of offset in these devices. Using Eqn.7.1, a graph of RE vs. emitter perimeter can be produced, see Fig.7.7. Fig.7.7 clearly shows that extrapolation of the equation to modern, high speed ICs using smaller transistor/FET sizes, leads to a prediction of increased RFI susceptibility.

Figure 7.7: Variation of Rectification Efficiency with Device Size

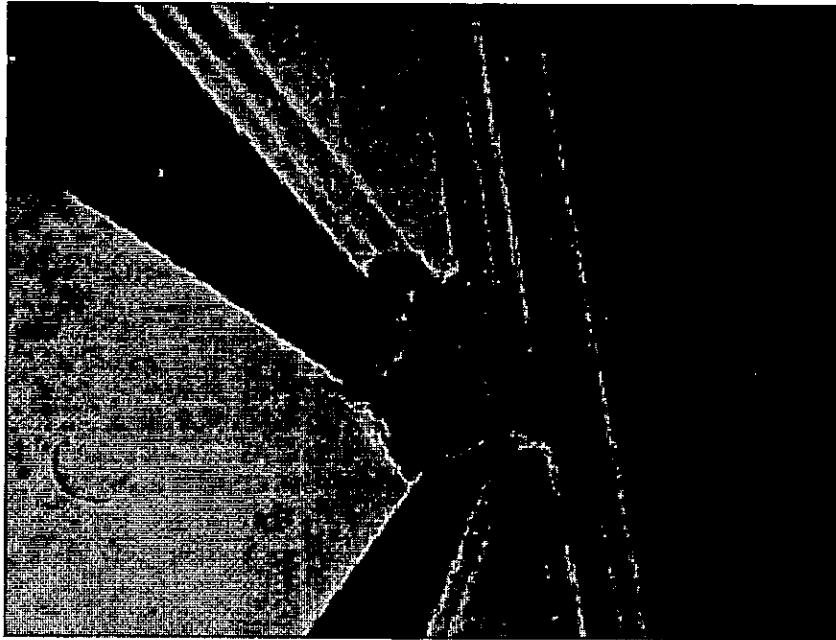


RE also differs between device types as the detection mechanisms are different [2-14]. In bipolar transistors it occurs at the emitter-base junction, whereas for MOS devices it occurs at the gate input. The effect in the former decreasing with  $\sqrt{f}$ , see Eqn.7.1, whilst for the latter the decrease is with  $\frac{1}{f^2}$  [7-43], explaining why bipolar transistors (and related ICs) are more sensitive at a given out-of-band frequency. This aspect is very noticeable for ICs with Schottky diodes on their inputs for electro-static protection. Due to their excellent rectification efficiency at microwave frequencies compared with ordinary diodes, they are very susceptible [7-36].

As suggested by Fig.7.7, VLSI circuits have much greater rectification efficiencies than standard TTL ICs [7-38], due to their small size, resulting in their predicted much higher susceptibility [7-20]. The reduction in gate size and increase in device density shown in Fig.7.1 in turn thus leads to a decrease in the amount of energy to cause upset or damage, *i.e.* to increased susceptibility to microwave and other frequency upset. This situation and its associated EMC implications was predicted by Audone [2-24].

Discussions with Prof. J.J. Whalen of the State University of Buffalo, New York, yielded references [7-46]-[7-50] which cover the mechanisms of pulsed microwave damage of semiconductor devices. Ref. [7-47] showed that at 9.3 GHz, GaAs 1  $\mu\text{m}$  MESFETs exhibit no degradation in performance, rather suffering catastrophic damage associated with metallic gate-source short circuit, see Fig.7.8. This photograph shows extensive damage which extends over a large area, including the entire metallisation path from the gate pad to the gate stripe, the gate pad metallisation, the source metallisation, and the gate stripe. The test data indicated an apparent incident power threshold, for both continuous wave and pulsed energy above 2  $\mu\text{s}$ . This level was 3-6 W for MESFETs with Titanium-Platinum- Gold gate metallisation, and 1.5-3 W for those with Aluminium gate metallisation.

Figure 7.8: Scanning Electron Micrograph of MESFET Damage



Tschursin [7-34] conducted 7-11 GHz irradiation testing of a number of samples of devices using a 10 W amplifier and with leads cut to form a quarter-wave dipole antenna, which was oriented parallel to the electric field for maximum coupling. Germanium diodes went short-circuit at  $23.8 \text{ kWm}^{-2}$  and Silicon ones went open-circuit at  $32.5 \text{ kWm}^{-2}$ . Both types of transistors sustained  $955 \text{ Wm}^{-2}$  for six minutes without damage. Current gain was permanently increased (up to 20%) in the Silicon transistors for power densities above  $717 \text{ Wm}^{-2}$ . Over 50% of the devices suffered catastrophic damage when subjected to  $2.15 \text{ kWm}^{-2}$  (Germanium) and  $2.65 \text{ kWm}^{-2}$  (Silicon), equating to a case temperature of  $115^\circ$  (Germanium) and  $180^\circ$  (Silicon). Forced air cooling of resistors in the range  $200\Omega$  -  $2 \text{ M}\Omega$  gave unchanged resistance beyond  $10.61 \text{ kWm}^{-2}$ , whereas convection-cooled items showed a permanent, up to three-fold increase in resistance, starting at  $4.5 \text{ kWm}^{-2}$ . In these items a sharp decrease in resistance was noted, to well below the original value, above  $10.61 \text{ kWm}^{-2}$ . The results showed that permanent changes in the component's electrical characteristics were predominantly thermally initiated with the electric field strength contributing little by itself. This, with research results from [5-4], led to the postulation that increasing or introducing forced-air cooling of components could lead to a decrease in susceptibility of Germanium and Silicon devices and resistors to microwave (and other) frequency upset. It was also thought that the careful choice of encapsulation type and better heat-sinking would also aid the heat transfer from junctions. This has been explored in the BAe EMC Laboratory and the results were inconclusive [7-27].

Semiconductor devices are thus damaged in three ways. Reverse bias of the junction causes avalanche breakdown and leads to open circuit, metal filamentation flows into the p-n junction material, which changes its characteristics leading eventually to severe junction damage or short-circuit, and electric field breakdown of the junction material, permanently changing the devices characteristics (*e.g.* transistor gain). In most cases the damage is thermal in nature rather than caused by high electric fields.

#### **7.4 CIRCUIT MODELS AS AN AID TO UPSET PREDICTION**

For frequencies below 100 MHz there are currently a number of electronic circuit analysis programmes, *e.g.* SPICE and variants IsSPICE, HSPICE Super-SPICE and SmartSPICE [7-51]-[7-56], which are appropriate for modelling RFI effects. They contain large-signal semiconductor device models and use time-domain techniques to predict RFI in linear and digital ICs. They are costly in run time for examination of the steady state response of devices to amplitude-modulated RF. Another programme, NCAP, which contains non-linear incremental (*i.e.* small signal) models and uses frequency domain techniques, has been successfully used to predict RFI at up to 100 MHz, though not of digital circuits. These programmes, though adequate for their intended purpose, *i.e.* the design of circuits to perform in-band, are limited by their basic device and circuit models [7-57]. To be of use above 10 MHz, parasitics need to be included and the situation becomes more complex as the microwave region is approached, where printed circuit tracks and IC pin inductances and pin-to-pin capacitances become appreciable. Modifications to the basic Ebers-Moll bipolar transistor model and Curtice and Statz FET models has enabled RFI prediction over the frequency range 50 kHz to 5 GHz using the SPICE and NCAP models [7-58]-[7-64].

The quality of the circuit simulation is highly dependent upon the individual device models. These are usually based on standard semiconductor physics equations, *e.g.* [7-65], and extensive parameter extraction measurements on real devices [7-66],[7-67]. This approach, particularly for microwave devices, is time consuming and the measurements difficult and a revised model, the Root FET model [7-68],[7-69], has superior performance than the earlier Curtice and Statz models. Data is fitted to physical effects, but only in as much as they appear in measurements. Thus a closer fit to reality is achieved without the time overhead of full physics-based models. Other aspects relevant to predicting RFI in electronics includes the ability to accurately model printed circuit boards, connectors

[7-70] and IC pin-to-chip interconnects [7-71] at microwave frequencies. Tools now exist, of which the Hewlett-Packard High-Frequency Design Software and the EEsof Series IV High Frequency Analog Design System are leading examples, [7-72], [7-73]. Continuing developments in device models and the wide availability of circuit simulation capabilities, as seen from RF and microwave CAD surveys [7-74]-[7-76], holds promise for the future of predicting microwave RFI of circuits. For the foreseeable future, however, the task of attempting to model RFI effects on the complex contents of a typical avionic box is still considered impractical. A probabilistic assessment of a database of statistically treated component RFI data and radiated susceptibility tests on exposed (*i.e.* with no covers) avionic circuitry offers a way ahead and this is discussed further in the following section.

## 7.5 PREDICTION OF UPSET AT MICROWAVE FREQUENCIES

### 7.5.1 Completion Of Ingress Equation

To predict  $P_{\text{CCT}}(f)$ , the microwave power delivered to the circuit element in the avionic box, the last term in Eqn.4.2,  $G_{\text{CCT}}(f)$ , must be evaluated. The maximum effective aperture,  $A_e$ , coupling the microwave energy within an avionic box to the circuitry has been equated to a half-wave dipole [4-21], [7-20], [7-38], [7-78]:

$$A_e = \frac{G_{\text{CCT}}(f)\lambda^2}{4\pi} \quad \dots(7.1)$$

where, as shown in Section 4.2,  $G_{\text{CCT}}(f)$  is the gain of the effective antenna connected to the device's leads. Ref.[7-39] gives an empirical equation based on Eqn.7.1 to predict the power delivered to the device through pick-up of fields by cables, wire and PCB traces within the box:

$$P_L \approx 0.13\lambda^2 P_d \text{ W, for } \lambda \leq 3.0 \text{ m} \quad \dots(7.2)$$

Where  $P_L$  is the power in the junction to which any conductor is connected, noting that at microwave frequencies parasitics may reduce the power actually dissipated in the junction. In reality  $P_L$  comprises two elements: cable-borne microwave current, as shown in Chapter 6, and pick-up of fields inside the box resulting from aperture ingress and re-radiation from the cable(s) carrying microwave current. The quantification of the relative contributions to  $P_L$  of cable-borne current and antenna pick-up within the box is suggested as a topic for further study.

Thus each term of Eqn.4.2 has been quantified.  $P_{ERP}(f)$  and  $FSL(f)$  are easily calculated as shown in Ch.2, to give the power density at the skin of the aircraft. Current and predicted future microwave environments are given in Figs.2.2 and 2.6. These represent the worst case, without atmospheric and illumination probability effects, both of which are highly mission scenario dependent and would reduce the actual power density vs. frequency vs. time profile to be encountered. A vehicle-independent predictor for  $A_A(f)$  has been developed, see Section 3.3.1 and Fig.3.11.  $A_{BOX}(f)$  was shown in Chapter 4 to comprise aperture ingress, for which equations exist which suffice for practical purposes, and cable ingress which is quantified in Ch.5 and 6. For typical avionic case thickness 1-18 GHz ingress through the material was shown to be negligible. Required protection levels against a given RF environment can then be determined from comparison of the  $P_{CCT}(f)$  profile vs. the circuit susceptibility profile, see Section 7.2.2.

To determine whether a real threat to avionic circuitry is posed by the current microwave environment, see Fig.2.2, it is necessary to insert appropriate data values into the overall ingress equation and compare the resultant  $P_{CCT}(f)$  with device RFI levels (Fig.7.4) and damage threshold levels (Fig. 7.5). Table 7.2 presents a worst case assessment at 1 GHz. It is important to note, as will be discussed in Section 7.5.2, that most of the equation's terms are highly dependent upon aircraft type and manufacture techniques, avionic box construction and device technology. Thus the output of Table 7.2 can only be expressed as there being a *high probability of upset* for the cases identified.

Table 7.2: Worst Case Assessment of Power in a Circuit Device

Ref.	Ch.2	Ch.3	Ch.4,5,6	-	Ch.7	Ch.7
Term	Incident $P_d$ (current Envt.)	Airframe Attenuation	Box Shielding	$P_d$ Inside the Box	Circuit Gain	Power in the Device
"	$(P_{ERP}(f)-FSL(f)) - A_{AIRFRAME}(f) - A_{BOX}(f)$				$+ G_{CCT}(f)$	$= P_{CCT}(f)$
Value	5kW/m <sup>2</sup> mean, 1MW/m <sup>2</sup> peak	+21±5.9 dB, Min. -3.2 dB	55 dB (Reqd. by [2-17])		0.13λ <sup>2</sup> Pd (Eqn.7.2)	
Set 1	10 <sup>6</sup> W/m <sup>2</sup>	-21.0 dB	-55 dB	0.025 W/m <sup>2</sup>		0.29 mW
Set 2	"	-15.1 dB	-55 dB	0.098 W/m <sup>2</sup>		1.15 mW
Set 3	"	+3.2 dB	-55 dB	5.248 W/m <sup>2</sup>		61.4 mW
Set 4	"	-15.1 dB	-30 dB	30 W/m <sup>2</sup>		362 mW
Set 5	"	+3.2 dB	-30 dB	2089 W/m <sup>2</sup>		24.4 W

The following notes should be read in conjunction with the table.

**Set 1:** 21 dB is the median of all the  $A_A$  measurements covered in Chapter 3. 55 dB is the box shielding required to ensure compliance with EUROCAE EMC qualification at 1 GHz. Careful design and construction techniques are required to guarantee this level of shielding, which is not commonly achieved in existing aircraft.

**Set 2:** 15.1 dB is the median minus one sigma of the Chapter 3  $A_A$  measurements and is considered a better prediction of airframe attenuation.

**Set 3:** Uses the worst case  $A_A$  from the Chapter 3 data, where a gain (rather than attenuation) of 3.2 dB was measured.

**Set 4:** Is the set thought most representative of existing aircraft, with 15.1 dB of airframe attenuation and (a practically achievable) 30 dB of avionic box shielding at 1 GHz. Actual values are highly dependent upon individual box construction and cabling.

**Set 5:** Is given as a demonstration of the absolute worst case envisaged, where there is no airframe shielding (using the same 3.2 dB gain as for set 3) in conjunction with 30 dB box shielding. The findings of this Thesis suggest that the probability of this being encountered is extremely low.

The more likely configuration to be encountered in existing aircraft will yield  $P_{ccr}(f)$  values at 1 GHz which lie between the 1.15 mW and 362 mW values in Table 7.2. By inspection of Fig.7.4 and the underlying data sets in Keiser [7-39], it can be seen that most device types can be upset by these levels of RF power dissipation. The upper end of this range also impinges on the damage threshold levels for some sensitive devices, see Fig.7.5. It is concluded, therefore, that a real threat exists to avionics from the current microwave environment, but which is highly dependent on the precise definition of that RF environment. This situation is exacerbated for the future environment, see Fig.2.6, where a maximum pulsed level of 15.3 GW/m<sup>2</sup> (41.8 dB higher than the current environment maximum) is predicted.

Pulse width is an important factor in determining circuit RFI or damage and much research has been performed on component damage by pulsed or CW microwave RF radiation, as discussed in Sections 7.2.2 and 7.3. Taylor and Younan [7-20] showed that the failure mechanism for thermal breakdown in discrete semiconductors can be described by

$$\frac{P_{DAMAGE}}{A_J} \sim K' \sqrt{A_J} \tau^{-1} + K \tau^{-0.5} + \frac{K''}{A_J} \tau^0 \quad \dots(7.3)$$

$P_{\text{DAMAGE}}$  = Damage threshold power (W)       $A_j$  = Junction area ( $\text{m}^2$ )

$K, K', K''$  = Device-specific proportionality constants, which can be computed from product data or can be measured.

Ref. [7-20] noted that tests had shown that Eqn.7.3 is valid for ICs for  $0.1\mu\text{s} < \tau < 100 \mu\text{s}$  and provided a table of fifteen devices tested, of which five failed at 35-90 W (100 ns pulse). Measurements by Antinone and Ng [7-36] indicate that device damage levels are typically 100W for 1  $\mu\text{s}$  pulses at 1-4 GHz. Using Eqn.7.3 to estimate the dependence on pulse width indicates power levels of 320 W are needed for 100 ns pulses, which is consistent with the IC damage power levels in [7-20]. Typical damage threshold ranges are shown in Fig.7.5.

It should be noted, however, that there is significant variation in  $K, K'$  and  $K''$  between device types because of the nature of the breakdown process. This is highlighted by the work of Whalen *et al.* [7-46] and [7-47] on 1  $\mu\text{m}$  GaAs MESFET pulsed RF damage at 9.3 GHz, where it was shown that the relationship between  $\tau$  and  $E_A$ , the absorbed pulse energy for damage, lay in the range 60-20 nJ for 1.5-10 ns pulse widths and could be described by:

$$E_A \text{ (in Joules)} = 2\tau \text{ (in seconds) for } 1 \mu\text{s} < \tau < 10 \text{ ms} \quad \dots(7.4)$$

### 7.5.2 Upset Prediction Models

No upset prediction models are currently available [7-79], but expressions by Ditton [4-21] and Garver and Tatum [7-38] using a Port of Entry (PoE) analysis technique are useful and are given in Eqns. 7.5 and 7.6.

$$\text{Garver and Tatum:} \quad S_f = \frac{P_f}{(A_e L)} \text{ (W)} \quad \dots(7.5)$$

$S_f$  = system failure power density ( $\text{Wm}^{-2}$ ),  $P_f$  = component upset level ( $\text{Wm}^{-2}$ ),  $A_e$  effective area of PoE ( $\text{m}^2$ ) and  $L_T$  = transmission loss (expressed as a ratio) from PoE to component.

$$\text{Ditton:} \quad P_L = P_d * A_e * SE_{\text{cable}} * SE_{\text{enclosure}} \text{ (W)} \quad \dots(7.6)$$

$P_L$  = power in the component,  $P_d$  = incident power density ( $\text{Wm}^{-2}$ ),  $A_e$  = PoE effective aperture ( $\text{m}^2$ ),  $SE_{\text{cable}}$  = cable shielding (dB) and  $SE_{\text{enclosure}}$  = box shielding (dB). In both cases the major problem in determining circuit RFI thresholds is that the terms in their expressions are each a function of a number of highly variable factors. Ref.[7-38] concurs

with the findings in Chapters 3 and 4 that the effective area of the PoE (*i.e.*  $A_A$  and  $A_{\text{BOX}}(f)$ ) depends on frequency, polarisation and angle of arrival of the RF energy, and that component susceptibility is a function of RF pulse width, rise time, repetition rate and frequency. Neither cover the important issue of probability of illumination, discussed in Ch.2. The findings reported in this thesis agree with the statement in Garver and Tatum [7-38] which states that *'Most of these factors are neither well controlled nor repeatable, but are relatively predictable when carefully analyzed (sic) statistically. As a result, the system susceptibility threshold is also somewhat random in nature and ideally should be treated as a probability of system failure rather than a fixed value.'*

It appears that statistical analyses of each of the variable factors using Cumulative Probability Functions (CPFs) may be the most suitable approach to solving the problem. By considering a given circuit technology type's susceptibility profile, a probability of failure CPF may be calculated. It may be noted that combination of CPFs with large uncertainties with those with smaller uncertainties tends to obscure the latter, this in effect substantiates the refinement of using only the larger ones, *e.g.*  $A_A$ . The approach is, however, limited in the area of circuit and component susceptibility where there is little data on which to conduct CPF analysis *vs.* circuit technology, although [7-38] notes that the uncertainty on this factor is not as large as that on the PoE. This suggests that further study of the dominant PoE coupling uncertainties may be more efficient than of electronic component CPFs. A further limitation of the approach is that avionic boxes contain complex combinations of circuit technologies, multi-layer printed circuit boards and wiring, suggesting that deterministic modelling may never be practical and that a probabilistic approach using the susceptibility CPFs of individual circuit elements and technologies may prove the only alternative to extensive and costly EMC tests on each avionic box type.

### 7.5.3 Protection Strategies Against Microwave Upset Of Avionics

Numerous publications, [2-17], [4-4,14,21,22], [7-20], and [7-80]-[7-84], describe design and protection methodologies necessary to ensure safe and correct operation of electronics, but are mostly applicable <1 GHz. Above 1 GHz EM energy can easily penetrate any enclosure unless great care is taken with respect to minimising apertures. Table 7.3 uses a schematic of coupling mechanisms and protection issues from [7-80] and shows a proposed protection regime additional to that outlined in Ref. [2-17]. The level of additional complexity and cost compared with current practice on BAe military aircraft is given, with an indication of the feasibility of protection benefits of modifying aircraft already in service. Emphasis is placed on first determining the actual microwave environment in which the aircraft must operate, then ascertaining system susceptibility and required safety margins, and finally deciding how the resulting protection requirement may be satisfied most cost-effectively. To date this route has rarely been followed and thus most aircraft are over-specified.

Two good design examples are a commercial aircraft fire and overheat detection system [4-4], and a U.S. Navy turbo-prop digital engine control unit [4-14]. These papers show that, by the careful application of existing design principles and practices, current civil [2-17] and military microwave EMC requirements can be met. Tests reported in [4-14] show that, using protection methods in Table 7.3, the unit operated correctly when irradiated at up to  $82 \text{ MWm}^{-2}$  at 2.85 GHz, with continual one inch arcing observed between the connector backshell and the overbraid shield at  $P_d > 4 \text{ MWm}^{-2}$ .

Table 7.3: Microwave Upset Protection Regime

ISSUE	PROPOSAL	COST*	MOD?
<b>EM THREAT</b>			
<i>Environment Definition</i>	Determine actual threat ( $P_d$ vs. time) by modelling precise environment, see Chapter 2	L/M	Y
<i>Safety Margins</i>	Using above, determine adequate SM vs. frequency based on probability of encountering power densities	L/L	Y
<b>HAZARD ASSESSMENT</b>			
<i>Modelling</i>	Conduct early modelling, to determine field ingress and power delivered to proposed avionics, using models described herein.	M/M	Y
<i>Databases</i>	Construct statistical databases of airframe attenuation and circuit, equipment and aircraft susceptibility to augment the modelling. Use this to arrive at a cost-effective recipe of protection elements from the following, for aircraft type vs. RF environment.	M/M	N/A
<b>AIRFRAME PROTECTION</b>			
<i>Material and Bonding</i>	Use high conductivity skin material and gaskets, with minimum and smallest individual apertures possible	M/M	N
<i>Screened Bays</i>	Cluster avionics in small number of screened/filtered bays with finger-stock doors, e.g. F-18 and SAAB Gripen, and RAM-line or RAM-paint internal surfaces of avionics bays.	H/H	N
<b>CABLE PROTECTION</b>			
<i>Cable Routing</i>	Route sensitive cables in aperture-less metal conduit, bonded at both ends.	M/H	N
<i>Cable Screening</i>	Shield cables and, of necessary, looms with 360° shield termination at each end and any interconnectors. No 'pigtailed' as they negate screening >1 GHz [4-21].	M/H	Y
<b>SYSTEM PROTECTION</b>			
<i>Inter-box Links</i>	Use fibre-optic links between avionic equipments.	M/M	N
<i>Filtering</i>	Use all-pin filtered and gasketed plugs on avionic equipment: >40dB attenuation >1GHz can be achieved [7-83].	L/H	Y
<i>Box Construction</i>	Use cast material cases, with minimum apertures and high conductivity gaskets.	L/M	N
<i>Architectures</i>	Reduce number of individual boxes and circuits whilst maintaining redundancy. Convert to digital at the sensor then use signal processing, fault-tolerant software and data coherence checking.	H/H	N
<i>Circuits</i>	Use less susceptible semiconductor technologies and/or on-pcb low pass absorber chips [7-84].	M/H	N

\* 'COST' column is Complexity/Cost, e.g. L/H = low complexity, high cost.

## 7.6 CONCLUDING REMARKS

The research has demonstrated that there is a real threat to electronic systems from the current microwave environment, but that the threat level is highly dependent upon the precise definition of that environment. Greater demands are placed on circuit protection as a result of both the changing environment (including speculative HPM weapons) and increasing susceptibility of circuitry with reducing device size. The research suggests that appropriate levels of protection will be difficult to meet for the worst case environment. It is shown that probabilistic approaches using statistical databases may be the only practical solution to many aspects of the upset equation. Further significant research effort in this area is required. An upset protection regime has been proposed which offers potential solutions for new aircraft designs. For existing aircraft which are required to operate in microwave environments harsher than those they are specified to, ingress modelling and equipment upset statistics are required to quantify the minimum extra required protection, thus minimising implementation costs. Further airframe attenuation measurements are required on different BAe aircraft types, preferably in an anechoic environment, with exploration of the effect of elevation angle of incidence of impinging EM radiation.

In the light of the current/future environment predictions reported in Chapter 2, it is recommended that future aircraft be specified to at least the latest UK military aircraft EMC specification levels. These are  $1 \text{ kWm}^{-2}$  mean and  $265.3 \text{ kWm}^{-2}$  peak pulse. The earlier specifications,  $66 \text{ mWm}^{-2}$  ( $5 \text{ Vm}^{-1}$ ) mean and peak, fall well short of even current international definitions of the mean microwave environment. It is suggested that additional radiated susceptibility tests are conducted using the *actual* modulations of off-board transmitters, particularly those on formation flying aircraft. The dependency of component, circuit and equipment upset of the pulsed RF parameters of frequency, pulse width and repetition frequency should also be investigated.

# *Chapter 8*

---

## **CONCLUSIONS AND SUGGESTIONS FOR FURTHER WORK**

## 8.1 INTRODUCTION

This chapter discusses the conclusions of the research and suggests further areas of research which would extend the understanding of mechanisms contributing to the microwave upset of avionics. The discussion is presented by the major topic areas of the thesis.

## 8.2 RF ENVIRONMENT PREDICTION

### 8.2.1 Conclusions

It is concluded that the precise definition of the external microwave environment level is a key factor in determining whether microwave upset of circuitry will occur, but that no definition of that level of quality is currently available.

Consequently it is also concluded that the EMC clearance power density profiles specified for U.K. military aircraft and, to a lesser extent, European-built civil aircraft are unduly harsh. This lack of precise environment definition has also resulted in equipment and aircraft EMC test safety margins which are pessimistic.

It is further concluded that the use of computer-based environment modelling tools, *e.g.* BAe's EW Evaluation System, could enable the required prediction of the *realistic* environment. This could lead to a reduction in the EMC qualification requirements of avionics and aircraft, with the potential for reduction in aircraft test timescales and costs.

### 8.2.2 Suggested Further Research Areas

*RF Environment Prediction* techniques need to be studied if the potential for reduced design and test timescales and costs are to be realised. The precise RF environments aircraft are subjected to should be determined, with a quantitative assessment of the probability of illumination for a given set of flight profiles. An estimation of probability of upset of avionics can be superimposed on this to yield higher quality EMC specifications, with more realistic, frequency dependent, safety margins than at present. This research should examine the possible need for extra EMC qualification tests to address specific modulations to be encountered (especially relevant for formation flying, where high power radiation by adjacent aircraft's radars and jammers is possible). Revised EMC qualification techniques should be researched to minimise over-test, possibly by driving the RF amplifiers used with signal generators capable of producing adequate representations of the RF scenarios to be encountered, *e.g.* EW RF threat simulators.

## **8.3 AIRFRAME ENERGY INGRESS**

### **8.3.1 Conclusions**

It is concluded that there are very few occasions where the airframe attenuation values measured on in-service aircraft approach the minimum required to prevent 1970's and 1980's avionics from being subjected to levels of power density approaching their qualified level. However, there is not thought to be a problem at this time for reasons stated in Chapter 3, which include the paucity of reported microwave upset occurrences, EMC-determined flying restrictions in the U.K., and the use of more appropriate levels in the latest aircraft EMC specification.

It is also concluded that the frequency-independent values of airframe attenuation assumed in the military and civil aircraft and avionic equipment design process are unduly severe in the microwave band. A possible and novel vehicle-independent correlation between cumulative probability functions of data measured on different aircraft has been demonstrated, which represents a step improvement in the ability to estimate microwave airframe attenuation for a given aircraft type. If ratified it offers the potential for supporting aircraft EMC design and qualification without aircraft tests.

### **8.3.2 Suggested Further Research Areas**

*Airframe Attenuation Predictor, Theoretical Study:* To determine the worth of the proposed predictor, an expansion of the cumulative probability function (CPF) study reported in Chapter 3 is required. The research should first examine the CPFs of the available measured data (from 6 aircraft specimens) by frequency sub-band to determine whether the predictor remains valid, and an initial sub-banding of 1 GHz is recommended. The theoretical aspect of this study should conclude with a wider statistical survey of such data from non-BAe aircraft types and result in an attenuation characteristics database.

*Airframe Attenuation Predictor, Empirical Investigations:* Further airframe attenuation data should then be gathered, from BAe military aircraft not yet examined, and similar 1-18 GHz and 1 GHz sub-banded CPF analyses performed. The attenuation measurements should cover full azimuth and elevation illumination, as the existing data sets cover only a limited number of azimuth angles of incidence of EM radiation of the aircraft. The optimum trade-off between test time and frequency resolution should be examined, with a minimum resolution of 10 MHz and an initial target of 1 MHz. To minimise ground and other reflections and obviate interference from other RF transmitters, the tests should

preferably be conducted in an anechoic environment. The results of these analyses should be compared with the existing data sets and conclusions drawn on the predictor's extent of validity. If appropriate, further research would be required to extend the predictor's validity to civil aircraft types.

***Avionic Bay Resonance Damping:*** The Chapter 3 results suggest that selective RAM placement within bays can considerably reduce the bay's internal field amplitude, thus offering a potentially low cost safety margin against the risk of avionic upset. A materials study is suggested, to examine the possible use of various absorber materials (including RAM paint) inside aircraft bays. The potential of this RAM lining for aiding low radar cross-section by minimising re-radiation of energy from the aircraft via apertures should be examined. The study should also address the possible application and benefits of such materials to the insides of avionic boxes containing particularly susceptible circuitry.

## **8.4 AVIONIC EQUIPMENT ENERGY INGRESS**

### **8.4.1 Conclusions**

From the Chapter 4 consideration of an overall equation developed to describe energy ingress to circuit device level, it is concluded that ingress through the case material of avionic boxes is negligible  $>1$  GHz, but that cable pick-up may not be as relatively insignificant  $>1$  GHz as previously thought by the international EMC community. Due to the significant variation in box construction in practice, it is not possible to conclude which ingress route, aperture or cable, is dominant at microwave frequencies. The airframe and box attenuation terms of the equation pose complex and time consuming modelling problems on even the most powerful computers available and, it is concluded, may thus lend themselves only to probabilistic determination. Ingress *via* regular shaped apertures, *e.g.* circular or slot, can be reasonably well predicted for most cases and it is concluded that careful application of existing EMC design rules can afford  $>55$  dB of box shielding  $>1$  GHz, adequate protection for most current avionics.

It is concluded that a significant part of the overall circuit protection required can be afforded at the box rather than airframe level by the use of appropriate box construction, application of conductive gasketing and good EMC design of ventilating and other apertures. Under these conditions the primary microwave ingress path is *via* the cable and connector route, where previously no adequate models existed to describe energy coupling from an incident field.

## 8.5 INGRESS VIA CABLE AND CONNECTOR COMBINATIONS

### 8.5.1 Conclusions

It is concluded from Chapters 5 and 6 that validated transmission line-based models can be used to predict the upper bound of voltage developed across a load in an avionic box, vs. incident power density on a wire entering it, in the range 2-18 GHz. Key enabling factors are precise knowledge of the line termination impedances, cable construction characteristics and use of modelling and measurement resolution of at worst 10 MHz.

It is also concluded that measurable pick-up does in fact occur for line illumination at distances much higher than the half-wavelength previously accepted value. The research did not investigate *per se* the furthest distance from the load that measurable voltage occurred, but the highest figure established was 3.05m. The transmission-line models require an extra term to describe the reduction in load voltage with cable length and illuminating antenna distance from the load. A postulation of re-radiation of energy from the wire as the cause was inconclusively examined, however an empirical equation describing the dependency was developed.

It is concluded that point-to-point agreement of modelled and measured data does not exist and will never be possible due to the high dependency on small features of the measured data and thus it is also concluded that coupling to a cable is best predicted on a statistical basis.

### 8.5.2 Suggested Further Research Areas

**Measurement Resolution:** Further practical examination of the smallest resolution required for complete characterisation of microwave field coupling to cables is suggested, to minimise the error bound on the measured load voltage. The investigation, covering the resolution range 10-0.1 MHz, should also address the results' applicability to airframe attenuation measurements. The trade-off of measurement time vs. error bound should be examined to determine the optimum resolution for practical laboratory and aircraft use.

**Cable Length and Antenna Position Dependency:** To fully understand this dependency further laboratory investigations are suggested to enable refinement of the empirical equation developed and explore the frequency range over which it is valid. It is suggested that these investigations should be conducted on a 4 m length of cable of the same type examined during this research and that smaller antenna position steps along the cable are

used. The frequency range suggested is 0.4-18 GHz, the lower frequency being the upper limit of the existing Conducted Susceptibility qualification tests and arguably the frequency at which the primary mode of energy coupling on aircraft commences the transition from cable-borne to *via* apertures.

The research work should include modelling partial illumination of a cable at various distances from the load and further laboratory investigations to examine this length dependency in more detail, using a greater number of cable lengths and antenna positions than before. The illuminating antenna for this work requires development, as a much smaller 'footprint' on the cable is required than was achieved in this research. Modification of the model could then follow, possibly based upon modelling footprint illumination by voltage source phase change over a given length of the cable. Finally, the possible need for Conducted Susceptibility tests above the current frequency limit of 0.4 GHz (for equipment which are neither RF transmitters nor receivers) should be investigated.

***Other Cable Coupling Model Issues:*** Dependent upon the outcome of the two previous suggested research topics, the study of two further aspects may be worthwhile. Further examination of the modelled *vs.* measured load voltage profile as a function of height above ground plane, using the high resolution measured data gathered during that research. The second aspect concerns the use of different materials in practical cables used on aircraft: further measurements on different cable types and sizes may lead to better understanding of the 'form factor' applicable to stranded conductor cables.

## **8.6 EFFECTS ON ELECTRONICS**

### **8.6.1 Conclusions**

Chapter 7 concludes that a real threat to airborne electronic systems is posed by the current microwave environment, but that the level of threat is highly dependent on the precise definition of the RF environment. Increasing susceptibility of circuitry with reducing device size and changing environment, including speculative HPM weapons, places greater demands on circuit protection and suggests that appropriate levels of protection will be difficult to meet for the predicted worst case environment. In the light of the Chapter 2 environment predictions and with the current lack of scenario-driven power density levels and safety margins, it is concluded that future and upgraded avionics need to be specified to at least the latest U.K. military aircraft EMC specification levels. A microwave upset protection regime is proposed which offers potential solutions for new aircraft designs.

Two important conclusions are that deterministic modelling of avionic boxes will never be practical and that a probabilistic approach using the susceptibility CPFs of individual circuit elements and technologies may prove the only alternative to extensive and costly EMC tests on each avionic box type, as conducted at present.

### **8.6.2 Suggested Further Research Areas**

***Effects of Modulation Parameters on Upset Potential:*** The possible need to conduct Radiated Susceptibility EMC qualification using the *actual* modulations of off-board transmitters, particularly those on formation flying aircraft, should be studied. This should include examination of the dependency of component, circuit and equipment upset on the pulsed RF parameters of frequency, pulse width and repetition frequency. The output is envisaged as a dependency surface, where the contours show the probability of upset for a given combination of these parameters. The use of EW RF threat simulators as signal sources to drive high power test amplifiers in support of this work is suggested. To support this investigation there may be a need to conduct tests on a sample avionic equipment with its panels removed to more readily be able to induce upset.

***Equipment Failure Modes:*** An investigation of electronic equipment failure modes is required to enable the understanding and prevention of the rarely encountered cases where incorrect (and thus potentially dangerous) information is generated and/or displayed by electronics when irradiated by even modest microwave power density levels.

***Aircraft Microwave Susceptibility Profiles:*** A statistical study of the component parts of the overall ingress equation per aircraft type is suggested, using the outputs of a number of the topics suggested earlier in this chapter. The study should include the examination of the potential to use these susceptibility profiles vs. RF scenarios to identify potential problem areas early in the aircraft development cycle and be able to propose minimum cost protection measures.

***Degradation of Microwave Protection Strategies:*** A study is suggested of the degradation of the protection methods, identified in Table 7.2, over the life-cycle of an aircraft. Cabayan [2-25], for example, shows that sequential salt spray and temperature/humidity cycling can lead to a 40 dB reduction in gasket shielding performance and suggests a need for a hardening database which would enable identification of minimal cost improvements and enable the trade-off of protection improvement vs. cost, degradation, weight penalty, and ease of installation. The suggested study should examine these aspects.

---

## REFERENCES

## Chapter 2

- [2-1] **Birken, J.A., Wallenberg, R.F. and Milton, O.** Advanced Composite Aircraft Electromagnetic Design and Synthesis. IEEE Symposium on EMC, Colorado, U.S.A., August 1981.
- [2-2] **Allen, S.G. and Harlen, F.** Sources of Exposure to Radio frequency and Microwave Radiations in the UK. NRPB-R144, March 1983.
- [2-3] The calculation of aircraft radio frequency hazard safe distances for the definition of **High Intensity Radio Transmission Areas (HIRTA)** in the U.K. BAe: ES/CISG 502 Issue 1, May 1987.
- [2-4] **Elton, L.D.** RF Environment External to Aircraft. Volume 1: The Calculation of Aircraft Safe Distances for the Definition of High Intensity Radio Transmission Areas in the United Kingdom. BAeSEMA report MNC 00220, Issue 2a, September 1992.
- [2-5] **Elton, L.D.** RF Environment External to Aircraft. Volume 2: Ship and Aircraft based Transmitters. BAeSEMA report MNC 00220, March 1992.
- [2-6] **Taylor, R.E. and Hill, J.S.** Airborne microwave measurements of Western U.S.A. urban areas. August 1981.
- [2-7] **Pywell, M.** The Control and Assessment of Non-Ionising Radiation Hazards within the Warton Unit. BAe-WAD-RP-GEN-EMC-057/1, February 1988.
- [2-8] **Woolnough, R.C.N. and Pywell, M.** The Control of RF Radiation Hazards in an Industrial and Airfield Environment. Presented by Pywell at IEE 9th Int. Conf. on EMC, Univ. of Manchester, U.K. 7 September 1994.
- [2-9] **NATO STANAG 4234 (Doct. AC/310-D/61):** EM Radiation (Radio frequency) - 200kHz to 40GHz Environment - Affecting the design of materials for use by NATO forces. Ed.1, Amdt.1, 1992.
- [2-10] **NATO STANAG 1307:** Maximum NATO Naval Operational EM Environment Produced by Radio and Radar. Ed.1, Amdt.3, 8 March 1993.
- [2-11] **NWS6:** U.K. Naval Weapons Specification 6 - 1978.
- [2-12] **NES 1006:** U.K. Naval Environment Specification 1006: 1991.
- [2-13] **Minimum Service External R.F. Environment:** Appendix 1 to Annex A to ARM1200/22, LR 61/85 dated 25 June 1986. Also contained in Annex F to Ordnance Board Proc. 42413 of 11 March 1986 (no change). Both superseded by OB Pillar Proc. 101 (Iss. 1), 28 August 1991, covering OB Memo. S/04/91 'Principles of Design and Use for Electrical Circuits Incorporating Explosive Components. Annex F field strengths/band breaks unchanged.
- [2-14] **Larsen, William E.** Digital Avionics Susceptibility to High Energy Radio Frequency Fields. FAA AMES Research Center, U.S.A. Proc. IEEE, 1988 Vol.3 pp 1098-107. Conference: NAECON 1988 (Dayton, Ohio, U.S.A.).
- [2-15] **NATO STANAG 3614AE** The Electromagnetic Compatibility (EMC) of Aircraft Systems. Ed.3, Amdt.0, 8 June 1989.
- [2-16] **MacDiarmid, I.P.** Civil Aircraft proposed external RF Environment levels. BAe-WAA-MM-GEN-EMC-2130, March 1988.
- [2-17] **EUROCAE USER'S GUIDE FOR AMJ No. XX.** Guidance to the Certification of Aircraft Electrical and Electronic Systems for Operation in the High Intensity Radiated Field (HIRF) Environment. (Certification Requirements and Procedures) EUROCAE WG33 Sub-Groups 2&3, Draft Version 2.2, 4 March 1993.
- [2-18] **Granatstein, V.L. and Alexoff, I. (Editors)** High Power Microwave Sources. 1987. Artech House, ISBN: 0-89006-241-2
- [2-19] **Denny, H.W.** Projected Susceptibilities of VHSIC/VLSI Devices to the Year 2000 Electromagnetic Environment. IEEE Int. Symposium on EMC, San Diego, California, U.S.A. September 1986.
- [2-20] **Denny, H.W.** Projected Trends in IC/EM Environment Interactions. SOUTHCON '87. Atlanta, Georgia, U.S.A. March 1987.
- [2-21] **Castro, C.** "Technology Update: The Evolution of High-Power Microwave." Defense Electronics, September 1990, pp.82-90.
- [2-22] **Benford, J. and Swegle, J.A.** "High Power Microwaves". 1992 Artech House ISBN 0-89006-415-6
- [2-23] **Green, G. (Washington Ed.)** 'SDI Identifies Science and Research Accomplishments.' Microwave Journal, April 1992, p.35.
- [2-24] **Audone, B.** "The EM Threat to Future Avionic Systems." AGARD Conf. Proc.417: "The Design, Development and Testing of Complex Avionic Systems," Las Vegas, U.S.A. 27 Apr. - 1 May, 1987.
- [2-25] **Cabayan, H.S.** "Current Status of High Power Microwave Effects and Simulation." High Power Microwave Systems for Defense Conference, Air Force Weapons Laboratory, Albuquerque, New Mexico, U.S.A., December 1-5, 1986
- [2-26] **Herskovitz, D.** "Killing Them Softly." J. Electronic Defense, August 1993, pp.41-46.
- [2-27] **Jaeger, D.** 'The Environment.' Seminar Proc. 'Aircraft and High Intensity Radiated Fields', ERA Report 90-0163, 18 April 1990. ISBN 0 7008 0402 1 (December 1990).

- [2-28] **Electronic Warfare Evaluation System (EWES): Product Description**, Ref. EWES/PD 2.0, June 1991. Data Sciences (U.K.) Ltd.
- [2-29] **Schleher, D.C.** 'Introduction to Electronic Warfare' Fig.2-5, p.57. Artech House, 1990 Printing. ISBN 0-89006-142-4
- [2-30] **Pywell, M. and Stubbley, N.** "Environment Models and Threat Simulators - High Quality and Lower Cost Validation of EW Systems" 3rd AGARD Sensor and Propagation Panel Symp. on Environmental Factors in EW Related to Aerospace Systems. Practica di Mare Air Force Base, Rome, Italy, 8-11 May 1995.

### **Chapter 3**

- [3-1] **Johns, P.B., Akhtarzad, K., and Rahhal, Y.** Numerical simulation of interference in aircraft due to electromagnetic fields. I.E.R.E. Conference on EMC, Southampton. September 1980.
- [3-2] **Breakall, J.K., Burke, G.J., and Miller, E.K.** The Numerical Electromagnetic Code (NEC). 6th Symposium and Technical Exhibition on EMC, Zurich, March 1985.
- [3-3] **Loller, C.P.** Ph.D. Thesis: An investigation into the electromagnetic properties of large scale Carbon Fibre Composite structures. 1987.
- [3-4] **Wang, J.H.H.** 'Generalised Moment Methods in Electromagnetics', 1991, J. Wiley and Sons, Inc.
- [3-5] **Yee, K.S.** 'Numerical solution of initial boundary value problems involving Maxwell's equations in isotropic media.' IEEE Trans. Antennas and Propagation, Vol. AP-14, pp.301-307, May 1966.
- [3-6] **Porter, S.J., Dawson, J.F. and Marvin, A.C.** Using integral equation methods to incorporate open-area test site effects in finite modelling techniques. 9th IEE Int. Conf. on EMC, University of Manchester, 5-7 Sept. 1994. IEE Conf. Pub. No.396, pp.241-245.
- [3-7] Internal BAe communication between I.P. **MacDiarmid** and M. **Pywell**: Technical Exchange discussions: SAAB microwave modelling of panel joints at 40 GHz.
- [3-8] **DEF. STAN. 59-41.** EM Compatibility Part 3: Technical Requirements, Test Methods, and Limits. Iss.4, and Supplement V: Test Method DRS02 (Radiated Susceptibility-18 GHz), both 9 July 1993.
- [3-9] **European Fighter Aircraft: EMC Specification for Equipment.** SPE-J-000-E-1000 (EFA-SP-J-000-2032), Issue 1 August 1991.
- [3-10] The **CATIA** Application Architecture Overview. SH52-0598-00, 1st Ed., November 1993.
- [3-11] **Pywell, M.** "Sowerby" Phase 2 Microwave Investigations BAe-WAD-RP-RES-EMC-099, Jan. 1990
- [3-12] **Loller, C.P.** (BAe) A Proposal for Future Topics of Research into the effects of NEMP and RF Weapons on aircraft systems. BAe-WAA-PL-RES-EMC-076, July 1987.
- [3-13] **Price, M.J.S. and Pywell, M.** "Sowerby" Microwave electromagnetic investigations on the Jaguar Fly-By-Wire aircraft: a test schedule. BAe-WAD-TS-RES-EMC-047, January 1988.
- [3-14] **Price, M.J.S.** (BAe) "Sowerby" microwave electromagnetic investigations on the Jaguar Fly-By-Wire aircraft: an Interim Report. BAe-WAD-RP-RES-EMC-085, March 1988.
- [3-15] **Price, M.J.S.** Investigations of the microwave penetration of aircraft: a Proposal for further studies and improved measurement techniques. BAe-WAA-PL-RES-EMC-099, April 1988.
- [3-16] **Pywell, M.** "Sowerby" Phase 2 Microwave EM Investigations: Test Schedule. BAe-WAD-TS-RES-EMC-054, July 1988.
- [3-17] **Pywell, M.** "Sowerby" Phase 2 microwave investigations: BAe-WAD-RP-RES-EMC-093 Oct. 1988
- [3-18] **Pywell, M.** Airframe Attenuation measurements between 12-17 GHz, taken on the Jaguar Fly-By-Wire EMC demonstrator. BAe-WAD-AR-RES-EMC-0136. September 1989.
- [3-19] 'Terrain Data and Multipath': Multipath analysis notes (16 March 1991) & presentation material (13 Mar. 1990). Simulator information pack provided to researcher by Amherst Inc., Buffalo, U.S.
- [3-20] **Willis, P.E.** Microwave Attenuation/Induced voltage at microwave/ TWT power for TM510. ERA Report 4000/5/04/1, March 1987.
- [3-21] **Carter, N.J., Stevens, E.G. and Watkins, P.** Initial Study for Airframe Attenuation Measurement Techniques from 1-18 GHz. Task 78404B. REC/02/91/R/17 (draft 1.070) 16 February 1991.
- [3-22] **Baden-Fuller, A.J.** Microwaves, 2nd Ed. An Introduction to Microwave Theory and Techniques. pp.104-105. Pergamon, ISBN 0-08-024228-6.
- [3-23] **Carter, R.G.** Electromagnetic Waves: Microwave Components and Devices. pp.168-171. Chapman & Hall, ISBN 0-412-34190-5.
- [3-24] **Ramo, S., Whinnery, J.R. and Van Duzer, T.** Fields and Waves in Communication Electronics, 2nd Ed., John Wiley and Sons.
- [3-25] **Crawford, M.L. and Koepke, G.H.** Design, Evaluation, and Use of a Reverberation Chamber for Performing EM Susceptibility/ Vulnerability Measurements. U.S. Dept. of Commerce, National Bureau of Standards, Technical Note 1092, April 1986.
- [3-26] **Pywell, M.** 'Ex-SRC Microwave Research Proposed for Cavalier Funding 1991.' BAe-WAD-MM-RES-EMC-331.

- [3-27] **Pywell, M. and Price, M.J.S.** 'Airframe Attenuation Measurements at Microwave Frequencies.' 7th Int. Conf. on EMC, Univ. of York, U.K., August 1990.
- [3-28] **Davenport, E.M., McQuilton, D. and Bowly, T.R.** Development of a Mode Stirred EMC Facility. 9th Int. Conf. on EMC, Univ. of Manchester, 5-7 September 1994. Conf. Proc. No. 396, pp.266-273
- [3-29] **Walker, W.F.W. and Heintz, R.E.H.** Conductivity Measurements of Graphite/Epoxy Composite Laminates at UHF Frequencies. pp.410-413, IEEE Symposium on EMC, 1977.
- [3-30] **Wellington, A.M. (BAe)** An investigation into the leakage of microwave radiation through aluminium and CFC panels. BAe-WES-RP-RES-EMC-0249, November 1991.
- [3-31] **MIL-STD-285 (Military Standard 285):** Standard for Measurement of the Attenuation Characteristics of EM Shielding Enclosures (100kHz - 10 GHz)
- [3-32] **Chromerics, Inc.** 'P1 and P2 Composite panels MIL-STD-285 Test Report.' Report 3028R, 3-5-90.
- [3-33] **Chromerics, Inc.** 'Composite panels MIL-STD-285 MOD Test Report.' Report No. 3131R, 31-07-90

#### **Chapter 4**

- [4-1] **Birken, J.A., Wallenberg, R.F. and Milton, O.** Advanced Composite Aircraft Electromagnetic Design and Synthesis. IEEE Symposium on EMC, Colorado, U.S.A., August 1981.
- [4-2] **King, R.J. and Hudson, H.G.** Experimental Data for EM Coupling through Slots. UCID-20842. Lawrence Livermore National Laboratory, U.S.A. July 1986.
- [4-3] **King, R.J., Ludwigsen, A.P. and Kunz, K.S.** Phenomenology of Electromagnetic Coupling, Part II. UCID-20215 Part 2. Lawrence Livermore National Laboratory, U.S.A. August 1985.
- [4-4] **Weekley, C.A.** Case History: Meeting HIRF Requirements. EMC Test & Design, April 1994, Vol.5, No.4, pp.14-19. ISSN 1054-5816
- [4-5] **Bethe, H.A.** Physics Review, Vol.66 p.166, 1944
- [4-6] **Collin, R.E.** Field Theory of Guided Waves. New York: McGraw-Hill 1960.
- [4-7] **Gluckstern, R.L. and Diamond, J.A.** Penetration of Fields Through a Circular Hole in a Wall of Finite Thickness. IEEE Trans. on Microwave Theory and Techniques Vol.39 No.2, February 1991.
- [4-8] **Butler, C.M., Rahmat-Samii, Y. and Mittra, R.** Electromagnetic penetration through apertures in conducting surfaces. IEEE Trans. Antennas and Propagation, Vol. AP-26, p.82, January 1978.
- [4-9] **Vance, E.F.** Shielding Effectiveness of Braided-Wire Shields. IEEE Trans. on EMC, Vol. EMC-17, No.2, pp.71-77, May 1975.
- [4-10] **Taylor, C.D. and Harrison, C.W. Jr.** On the Excitation of a Coaxial Line by an Incident Field Propagating Through a Small Aperture in the Sheath. IEEE Trans. on EMC, Vol. EMC-15, No.3.
- [4-11] **Schelkunkoff, S.** Electromagnetic Waves. D. Van Nostrand, Inc. January 1943.
- [4-12] **Grant, P.M.** Part 2 of Design Feature on EMI Shielding: Emitter/Susceptor Profiles Predict Proper Shielding. MICROWAVES (USA), 1986, Vol. 21, Part 7, pp. 79-81, 83-4,6.
- [4-13] **Molyneux-Child, J.W.** EMC Update: An Overview of Gaskets for Connector Shielding. pp.19-23, Electronic Engineering, Oct. 1993.
- [4-14] **Becker, P.E. and Kazmierczak, R.S.** High Power Microwave Test Results on a Digital Electronic Engine Control. Presented at NAECON '87, Dayton, Ohio, 18-22 May 1987: Proc. IEEE, Vol.4.
- [4-15] **Bates, R. Spence, S. Rowan, J. and Hanrahan, J. (W.L. Gore & Associates, U.K./U.S.A.)** EMI Gaskets - Dispelling the Technology Folklore. 8th IEE Int. Conf. on EMC, Edinburgh Sept. 21-24, 1992. IEE Conf. Pub. No.362, pp.246-250.
- [4-16] **Grant, P.M.** High Performance EMC Windows. IERE Conference on EMC. Univ. of Southampton, September 1980. Conf. Proc. pp.273-284.
- [4-17] **Molyneux-Child, J.W.** Radio-proof windows. IEE J. Electronics & Communications: EMC Supplement, July 1993. pp.S-11/S-12.
- [4-18] **Screening for Displays. Electronic Engineering, May 1991, p.21.**
- [4-19] **Mason, J.** Transparent conductive coat for RFI/EMI and ESD shielding. New Electronics, March 1993, p.57.
- [4-20] **Roe, J.M.** Protecting Digital Avionics Systems from High Power Radar Interference. 2nd Digital Avionics Conference. Los Angeles, USA. November 1977.
- [4-21] **Ditton, V.R. (McDonnell Douglas Astronautics)** Coupling to Aerospace cables at microwave frequencies. Int. Symp. on EMC, San Antonio, Texas, U.S.A. 7-9 October 1975.
- [4-22] **Butler, R.J.** Practical Design Considerations - Equipment Protection: The effects of introducing the requirements to meet the high intensity radio frequency environment (HIRF). Section 3.2, Proc. Seminar on Aircraft and High Intensity Radiated Fields. 18 April 1990. ISBN 0-7008-0402-1

#### **Chapter 5**

- [5-1] **Smith, Albert A. Jr.** Coupling of External Electromagnetic Fields to Transmission Lines. Wiley-Interscience. ISBN 0-471-01995-X
- [5-2] **Lorrain, P. and Corson, D.** Electromagnetic Fields and Waves, 2nd Ed.-1970 W.H. Freeman and Coy. ISBN 0-7167-0331-9.

- [5-3] McDonnell Douglas Astronautics Company, 'Integrated Circuit EM Susceptibility Investigation: Phase II: Cable Coupling Study', MDC E0921, 8 Oct. 1973, Contract N00178-73-C-0362 P00002.
- [5-4] Roe, J.M. *et al.* IC EM Susceptibility Investigation - Phase II MOS/Hybrid Study. MDC-E1125, August 1974. McDonnell Douglas Astronautics Company - East: Contract N00178-73-C-0362 US Naval Surface Weapons Center, Dahlgren, VA.

#### **Chapter 6**

- [6-1] **Panavia Standard 75.6411**: Electrical Single Wire. p.1 Iss.p, p.2 Iss.h (8/91).
- [6-2] **Anderson, M.K.** Field-to-Wire Coupling 1 to 18 GHz. Proc. 1988 Int. Symp. on EMC, Seattle, WA. August 1988.
- [6-3] **Brock, G., McMahon, A., Salazar, J., Griffin, P., Capraro, G., Drozd, A. and Pesta, A.** An SHF/EHF Field-to-Wire Coupling Model Enhancement to IEMCAP. Proc. 1989 IEEE Nat. Symp. on EMC, Denver, Colorado, May 1989. pp.131-136.
- [6-4] **Taylor, C.D. and Harrison, C.W.** On the Coupling of Microwave Radiation to Wire Structures. IEEE Trans. on EMC, Vol.34 No.3, August 1992, pp.183-188.
- [6-5] **Pywell, M.** 'IEE Colloquium on *EM Hazards to Active Electronic Components* and Publications by Dr. J. Whalen, State University of New York, Buffalo' Communication to Barber (DRA Farnborough) and Rayment (GEC-Marconi Defence Systems). 3 February 1994.
- [6-6] **Barber, G.D.M. and Hercke, D.L.** Conducted Susceptibility Measurements on Integrated Circuits. IEE Colloq. on 'EM Hazards to Active Electronic Components' London, 14 January 1994.
- [6-7] **Rayment, P.A.** Radiated Susceptibility Measurements on Integrated Circuits. IEE Colloq. on 'EM Hazards to Active Electronic Components' London, 14 January 1994.
- [6-8] **Dummer, G.W.A. and Blackband, W.T.** Wires & RF Cables. *Radio and Electronic Components: Volume Five*. Pitman & Sons. 1961. Chapter 11.
- [6-9] **Connor, F.R.** Antennas, 2nd Ed. (1989) ISBN 0-7131-3680-4
- [6-10] **Adams, A.T., Perini, J., Miyabayashi, M., Shau, D.H. and Heidary, K.** Electromagnetics Field-to-Wire Coupling in the SHF Frequency Range and Beyond. IEEE Trans. on EMC, Vol. EMC-29, No.2, May 1987, pp.126-131.

#### **Chapter 7**

- [7-1] **Wallace, D.** Microelectronics the Next Fifteen Years. AGARD CP417, Las Vegas, U.S., May 1987.
- [7-2] **Rawles, J.W.** VHSIC Technology Comes On Line. Defense Electronics, August 1987, pp.38-47
- [7-3] **Rawles, J.W.** VHSIC Forges Ahead. Defense Electronics, January 1989, pp.61-74.
- [7-4] High Performance IC Memories. **Hitachi Report** July 1989, pp.4-5.
- [7-5] **Liechti, C.A.** High Speed Transistors: Directions for the 1990s. Feature article, Microwave J., '1989 State of the Art Reference'.
- [7-6] **Flaherty, N.** Readout: Int. Solid State Circuits Conf. (ISSC) 1991 - San Fransisco. Electronic Engineering, March 1991, pp.9-12.
- [7-7] **Ball, S.** FPGA's - How the Products Fit. Electronics Times, 25 July 1991.
- [7-8] **Clarke, P.** Working Together in a Time of Change. [Notes from In-Stat's 1st European Forum, Florence, Italy] Electronics Times, 24 October 1991.
- [7-9] **Stiglitz, M.R. and Blanchard, C.** Phase II, DoD MIMIC Program: A Status Report. Microwave Journal, January 1992, pp.90-100.
- [7-10] Sony Accelerates Semiconductor Developments. **Electronics Times**, 31 March 1994.
- [7-11] **Rubenstein, R.H.** Sub-0.5 $\mu$ m Processes for Brilliant Systems. New Electronics, April 1994
- [7-12] **MacLeod, A.** Covering all the options: the RISC, the CISC and the Embedded. New Electronics, May 1994, p.7.
- [7-13] **Collins, L. and Flaherty, N.** RISC Processors: Analysis of latest Alpha, MIPS, Sparc and PowerPC Architectures. Electronics Times, 20 October, 1994, pp.22-23.
- [7-14] **Collins, L.** Sacred Cows are Led to the Slaughter. Electronics Times, 2 February 1995, p.12.
- [7-15] **Walko, J.** The Next Generation Lithography Steps Up. Electronics Times, 2 February 1995 p.20
- [7-16] **Flaherty, N.** Intel Plans Faster P6 and Pentium in CMOS, [report on 42nd IEEE/Univ. of Pennsylvania ISSC, San Francisco] Electronics Times, 23 February 1995, p.60.
- [7-17] **Takada, Dr. M.** Five Years to 1 GHz Processors. [report on 42nd IEEE/Univ. of Pennsylvania ISSC, San Francisco] Electronics Times, 23 February 1995, p.60.
- [7-18] **Hartnagel, H.L., Richter, R. and Grüb, A.** Nanoelectronics. Electronics & Communication Eng. J., June 1991, pp.119-128.
- [7-19] **Costanzo, L.** The Incredible Shrinking System. Electronics Times, 8 November 1990, p.11.
- [7-20] **Taylor, C.D. and Younan, N.H.** Effects from HPM Illumination. Microwave J., June 1992.
- [7-21] **Florig, H.K.** The Future Battlefield: A Blast of Gigawatts? IEEE Spectrum, Vol.25 No.3, Mar. 1988
- [7-22] Flight Safety Reminder. **BAe Weekly News Brief**, 1 Mar.1995, p.1.

- [7-23] **High Intensity Radio Transmission.** U.K. Civil Aviation Authority R&AD Occurrence List, August 1995, Item 12, p.7.
- [7-24] **Pankhurst, R.V.** The Coupling of EMI into Aircraft Systems. IERE Conf. on EMC, Southampton Univ., 16-18 September 1980.
- [7-25] **MacDiarmid, I.P.** Internal BAe report, November 1989.
- [7-26] **Ritchie, N.R.M. and Pywell, M.** Internal BAe report, February 1991
- [7-27] **Ritchie, N.R.M.** Internal BAe report, July 1991.
- [7-28] **Pywell, M.** Internal BAe Report, December 1992
- [7-29] **Hall, S.D.** Investigation into the Susceptibility of a Personal Computer to Pulsed Microwave Radiation. BAe-WES-RP-RES- EMC-0281, 11 November 1991.
- [7-30] **Pywell, M. and Woolnough, R.C.N.** Test Schedule for Computer Upset Tests at Microwave Frequencies. BAe-WSD-TS-GEN-RAD -0117, 2 December 1992.
- [7-31] **Sarti, E.J.** Microwave Upset Testing of a Personal Computer. BAe-WSD-RP-RES-EMC-0151, Issue 1. December 1992.
- [7-32] **Everett, W.W. III and Everett, W.W. Jr.** Microprocessor Susceptibility to RF Signals - Experimental Results. IEEE Proc. SouthEastCon, April 1984. pp.512-516.
- [7-33] **Braun, C., Guidi, P. and Schmidt, H.U.** Susceptibility Measurements on GPS Receivers. NATO AGARD 3rd Symp. of Sensor & Propagation Panel on 'Environmental Factors in Electronic Warfare related to Aerospace Systems', Practica di Mare Air Force Base, Rome, Italy, 8-11 May 1995.
- [7-34] **Tschursin, N.** Experimental Investigation of the Permanent Effects of RF Radiation in X-Band on Electronic Components. TR-1399. AMCS Code 5023.11.18400 DA-1N022601A093. Harry Diamond Laboratories, Washington D.C., Project 24600, June 1968.
- [7-35] **Roe, J.M. et al.** IC EM Susceptibility Investigation, Phase III. Report NSWC/DL TR-79-14 (MDC E1999), 5 January 1979.
- [7-36] **Antonone, R. and Ng, W.C.** HPM Testing of Electronic Components. UCID-21687, DE89 016682, 10 May 1989.
- [7-37] **Whalen, Dr. J.J. (Prof.)** Communication to M. Pywell with 24 Whalen (*et al.*) refs. 6 Sept. 1990.
- [7-38] **Garver, R.V. and Tatum, J.T.** Assessment Methodology for Radio Frequency Effects (RFE). IEEE National Symp. on EMC, Denver, Colorado, May 23-25 1989. pp.137-142.
- [7-39] **Keiser, B.** Principles of EMC, 3rd Ed., 1987. Artech House. Ch.10.9 IC Susceptibility, pp.178-180.
- [7-40] **Le Vine, S.D. and Richardson, R.E. Jr.** Measurement Techniques and Instrumentation for Determining Sensitivity of Digital IC's to RFI. IEEE Instrumentation and Measurement Technology Conf. IMTC/86 Boulder. Colorado, U.S. March 25-27, 1986, pp.62-64.
- [7-41] **Roach, J.N.** The Susceptibility of a 1k NMOS Memory to Conducted Electromagnetic Interference. IEEE Int. Symp. on EMC. Colorado, U.S., 18-20 August, 1981.
- [7-42] **Larson, C.E. and Roe, J.M.** Modified Ebers-Moll Transistor Model for RFI Analysis. IEEE Trans. Vol. EMC-21, No.4, November 1979.
- [7-43] **Forcier, M.L. and Richardson, R.E. Jr.** Microwave- Rectification RFI Response in Field-Effect Transistors. IEEE Trans. on EMC, Vol. EMC-21, No.4, November 1979, pp.312-315.
- [7-44] **Richardson, Dr. R.E. (Jr.)** Modeling (sic) of Low-Level Rectification RFI in Bipolar Circuitry. IEEE Trans. on EMC, Vol. EMC-21, No.4, November 1979, pp.307-311. (First presented at IEEE Int. Symp. on EMC, Atlanta, U.S.A. June 1978.)
- [7-45] **Sutu, Y-H and Whalen, J.J.** Demodulation RFI in Inverting and Non-Inverting Operational Amplifier Circuits. 6th Symp. and Tech. Exhibition on EMC, Zurich, 5-7 March 1985.
- [7-46] **Whalen, Dr. J.J., Calcaterra, M.C., and Thorn, M.L.** Microwave Nanosecond Pulse Burnout Properties of GaAs MESFET's. IEEE Trans. on Microwave Theory and Techniques, Vol. MTT-27, No. 12, December 1979.
- [7-47] **Whalen, Dr. J.J., Kemerley, R.T. and Rastefano, E.** X-Band Burnout Characteristics of GaAs MESFET's. IEEE Trans. on Microwave Theory and Techniques, Vol. MTT-30, No. 12, Dec. 1982.
- [7-48] **Darweesh, M.N. and Whalen, J.J.** Failure Analysis of GaAs MESFETs Overstressed with Microwave Signals. AFWAL-TR-85-1101, September 1985.
- [7-49] **Rastefano, E. and Whalen, J.J.** Failure Analysis of Half Micron Gate Metal-Semiconductor FETs Overstressed with 5 $\mu$ s X-Band Pulses. AFWAL-TR-86-1090, January 1987.
- [7-50] **Whalen, Dr. J.J.** Microwave Overstress Results for Half-Micron Metal-Semiconductor Field-Effect Transistors Overstressed with 5 $\mu$ s and 3 $\mu$ s X-Band Pulses. AFWAL-TR-87-1066, August 1987.
- [7-51] **Antognetti, P. and Massobrio, G.** Semiconductor Modelling with SPICE. McGraw-Hill Inc., 1988.
- [7-52] **PSPICE User Guide and Design Centre Brochure**, MicroSim Corporation.
- [7-53] **ICAP/4 (including IsSPICE)**, Circuit Design Tools, Intusoft 1993.
- [7-54] **HSPICE**, Brochure. 7225/6.93/5M Meta-Software Inc. 1993
- [7-55] **Super-SPICE**, Compact Software advertisement, Microwave J.

- [7-56] **SmartSpice** booklet, Silvaco 1993.
- [7-57] **Whalen, J.J.** Guest Editorial - Predicting RFI effects in semiconductor devices at frequencies above 100MHz. *IEEE Trans. on EMC*, Vol. EMC-21, No.4, November 1979.
- [7-58] **Tront, J.G., Whalen, J.J., Larson, C.E. and Roe, J.M.** Computer-Aided Analysis of RFI Effects in Operational Amplifiers. *IEEE Trans. on EMC*, Vol. EMC-21, No.4, November 1979, pp.297-306.
- [7-59] **Chen, G.K.C. and Whalen, J.J.** Macromodel Predictions for EMI in Bipolar Operational Amplifiers. *IEEE Trans. on EMC*, Vol. EMC-22, No.4, November 1980, pp.262-265.
- [7-60] **Fang, T.F., Whalen, J.J. and Chen, G.K.C.** Using NCAP to Predict RFI Effects in Linear Bipolar Integrated Circuits. *IEEE Trans. on EMC*, Vol. EMC-22, No.4, November 1980, pp.256-262.
- [7-61] **Chen, K.N. and Whalen, J.J.** A Nonlinear Incremental Model for Predicting EMI in MOS Transistors and ICs. *Proc. Int. Conf. on EMC*, Univ. of Surrey, 21-23 September 1982. pp.113-130.
- [7-62] **Whalen, J.J., Tront, J.G., Larson, C.E. and Roe, J.M.** Computer-aided analysis of RFI effects in Digital ICs. *IEEE Trans. on EMC*, Vol. EMC-21, No.4, November 1979, pp.291-297.
- [7-63] **McCarnant, A.J., McCormack, G.D. and Smith, D.H.** Improved GaAs MESFET Model for SPICE. *IEEE Trans. on Microwave Theory and Techniques*, Vol. 38, No. 6, June 1990, pp.822-824.
- [7-64] **Berroth, M. and Bosch, R.** Broad-Band Determination of the FET Small-Signal Equivalent Circuit. *IEEE Trans. on Microwave Theory and Techniques*, Vol. 38, No. 7, July 1990.
- [7-65] **Snowden, C.M.** Semiconductor Device Modelling. *IEE Materials & Devices Series 5*, 1988. Peter Peregrinus, ISBN 0-86341-130-4
- [7-66] **Golio, M., Miller, M. and Beckwith, W.** Software Provides Accurate and Versatile Parameter Extraction for Large Signal Modeling. *Microwave Journal*, July 1992, pp.121-135.
- [7-67] **Whitefield, D.S., Wei, C.J. and Hwang, J.C.M.** Large Signal Characterization and Modeling of Heterojunction Bipolar Transistors. *Annual Technical Report*, 31 May 1992.
- [7-68] **Root, D.E.** A Measurement-Based FET Model Improves CAE Accuracy. *Microwave Journal*, September 1991, pp.126-139.
- [7-69] A Faster Route to This Year's [D. Root] FET Model. *Microwave Engineering Europe*, Oct. 1991
- [7-70] **Larner, D.** Library Models SPICE Up Simulation for the Designer. *Electronics Times*, 1994.
- [7-71] Focus on CAD: Interconnect Models Derived from TDR. *Microwave Engineering Europe*, May 1993, p.27.
- [7-72] **March, S.L.** Simple Equations Characterize Bond Wires. *Microwaves & RF*, November 1991, pp.105-110.
- [7-73] **HP High-Frequency CAE Design Forum**. 5091-5378E, Aug. '92
- [7-74] **EEsof Series IV: High Frequency Analog Design System**; product brochure. EEsof Inc., 1992.
- [7-75] **Pitzalis, O.** Microwave to mm-Wave CAE: Concept to Production, *Microwave J.* 1989 State of Art Reference, Sept. 1989. [Sampling in *EW Designers Handbook* pp.4-1 to 4-3 as 'Computer Programs for Microwave Circuit Analysis, Synthesis and Optimization'.]
- [7-76] Entry Level CAD/CAE: An Independent Review. *Microwave Engineering Europe*, November 1992, pp.11-19.
- [7-77] **Pengelly, R.S.** RF & Microwave CAD: A Review of Present Status. *Microwave Journal*, Jan. 1993
- [7-78] **Whalen, J.J.** Assessment Procedure Application Utilizing UHF Transistor RF Pulse Susceptibility Data. *Proc. 2nd Symp. and Technical Exhibition on EMC*, 28-30 June 1977, Montreux, Switzerland pp.317-322.
- [7-79] **Dawson, J.F. and Hagiwara, S.** Simulation of EMI in ICs Using the SPICE Circuit Modelling Package. *IEE Colloq. on 'EM Hazards to Active Electronic Components'* Digest 1994/008
- [7-80] **MacDiarmid, I.P.** Practical Design Considerations - Modelling and Analysis. Seminar (18 April 1990) *Proc. 'Aircraft and High Intensity radiated Fields'* ERA Report 90-0163, p.2.3.1-2.3.12.
- [7-81] **Moore, P.M.** Practical Design Consideration - Aircraft Protection. Seminar (18 April 1990) *Proc. 'Aircraft and High Intensity radiated Fields'* ERA Report 90-0163, pp.3.1.1-3.1.8.
- [7-82] **EMC Design Guidelines**. 9000AA000EMC Issue 1, Newport Components. 18 November 1993.
- [7-83] **Iticsohn, P.** Des Connecteurs à filtre incorporé pour protéger les équipement électroniques. *Electronique Industriels*, No.22, 15 October 1981. pp.31-34.
- [7-84] **Uchikoba, F., Nakajima, S., Ito, T., Kobayashi, M. and Miura, T.** Absorber Chip Provides RF EMI Filtering. *Microwaves & RF*, Vol. 34, No.2, February 1995. pp.69-70,72.
- [7-85] **Jennings, P.** Statistical Approach to System Level Radiated Susceptibility Testing. *IEE Colloq.* 1992/113 on 'Role of Statistics in EMC Specification, Design and Clearance', 13 May 1992.
- [7-86] **Whalen, J.J.** Determining EMI in microelectronics - a review of the past decade. 6th Symp. and Technical Exhibition on EMC. Zurich, 5-7 March 1985.

# *Appendices*

---

- A. Paper: 'The Control of RF Radiation Hazards in an Industrial and Airfield Environment.' (1994)
- B. EMC Qualification of Avionic Equipment and Aircraft.
- C. Paper: 'Environment Models and Threat Simulators - High Quality and Lower Cost Validation of EW Systems.' (1995)
- D. Prediction of Cut-Off Frequencies for Peripheral Slots and Bay Door/Panel Ingress Characteristics.
- E. Paper: 'Airframe Attenuation Measurements at Microwave Frequencies.' (1990)
- F. Calculation of frequency spacing of cavity resonances for Port Gun Bay and bays behind Panels 55 and 56
- G. Cable coupling model listing.
- H. I.E.E. Letters: 'Improved Analysis of Airframe Microwave Attenuation Measurement Data.' (1996)

## **APPENDIX A: THE CONTROL OF RF RADIATION HAZARDS IN AN INDUSTRIAL AND AIRFIELD ENVIRONMENT**

R.C.N. Woolnough and M. Pywell (BAe). Presented: M. Pywell at 9th Int. Conf. on EMC, Manchester University, 5-7 September 1994.

### **ABSTRACT**

Unnecessary concern is caused whenever non-ionising radiation (NIR) is mentioned in the media. The term 'non-ionising' adds to the public's confusion, with Radio/Radar Frequency (RF) and Laser radiation being assimilated to nuclear, i.e. ionising radiation. The scientific community thus has difficulty convincing the public that any form of NIR can be used safely. This paper aims to show that, given adequate Control and Assessment (C&A) Procedures, an appropriate level of RF safety can be assured in any situation. It addresses the types and quantities of fixed site and mobile RF emitters (RFE) that may be present, and details the risks they pose to humans, flammable atmospheres, electrically-initiated electro-explosive devices (EEDs) and electrical/ electronic equipment. The rationale behind C&A Procedures is then explained, including the need for Specialist support. The level of Control is shown to be commensurate with the level of Risk perceived. The paper draws on the experience of instigating such a RF Safety regime, gathered at British Aerospace Defence's Warton Unit in Lancashire - a multi-site facility comprising manufacturing facilities, offices and an operational airfield used by both military and civil aircraft. Finally data on over nearly two decades of operations are presented to underline the benefits of implementing such a C&A regime in ensuring the safety of both employee and public alike.

### **1 BACKGROUND**

British Aerospace Defence Limited's Military Aircraft Division (MAD) has many and varied electromagnetic (EM) sources covering much of the RF spectrum, both as part of its production and flight test facilities and on its products (military aircraft). These pose varying levels of risk to a variety of susceptible device types in the form of humans, weapon systems, electronics and flammable atmospheres. In four years MAD have gone from a loosely defined RF Radiation Hazard (RADHAZ) control structure aimed at specific potential problem areas, to a fully controlled regime to the best standards currently in place around the world.

Over recent years the health issues associated with EM fields have moved steadily into the limelight including the 'Killing Fields' articles (1,2). It is an unfortunate fact of life that the media across the world generally find negative issues to be more news-worthy. Largely as a result of media-promoted public concern, significant research has been and is being carried out across the whole field of the biological effects of EM radiation. Problems

with aspects of this research, in particular repeatability issues, when merged with the creative talent of the media results in wasted company, national and international effort in redressing the 'balance of truth' and allaying the fears of both employees and the public. The overall state of ensuing flux then leads to the formulation of new guide-lines and legislation such as the proposed European Physical Agents Directive (EPAD) (3) which requires protection methods that are believed to be unnecessary once an adequate risk assessment is carried out in accordance with the present legal requirements (4).

MAD implements a RF safety programme which is directed at ensuring a safe working environment for all persons to which it has a duty of care, both on and off of its premises. It takes a positive and pro-active approach to health and safety (H&S) issues including those related to the safety of EM fields and participates in the preparation of both national and international standards so as to ensure that a 'state of the art' RF safety programme is in place. This approach enables an adequate and cost effective response to the needs and concerns of its most valuable asset, the employees. Additionally this also minimises sickness rates due to accidents and possible exposure to H&S litigation. All of this is based upon a realistic common sense approach carried out through an understanding of the issues and risks involved.

### **2 SUSCEPTIBLE DEVICES**

Four categories of susceptible device exist: biological systems (i.e. humans in this context), EEDs, flammable atmospheres and electrical/ electronic apparatus. Each represents a different problem and is covered by separate legislation and standards, although experience has shown that all may be adequately controlled via one C&A regime. Susceptibility problems associated with each of the categories are now given:

#### **RADHAZ to Humans**

The most widely publicised of the 'susceptible devices' is the human. The majority of the world-wide standards follow a reasonably similar approach, although precise rationales are different. In the radio frequency and microwave region of the EM spectrum, the hazardous effects are considered to be primarily thermal in nature. Such alarmist press articles as Darby (5), which follows on from (1,2), suggest proven links between low level power line frequency EM radiation and various health problems. Unfortunately, although no substantive and repeatable supporting evidence is given, these

articles create a false impression of hazard and risk levels which is difficult (and time consuming) to allay - they unnecessarily generate real fears in the minds of employees, especially and understandably those of pregnant women. Although different mechanisms for interaction between EM fields and humans have been proposed, the body of argument at the present time is simplistically defined as there appears to be no biological evidence as to the ability of EM fields to initiate or promote cancers or cause birth defects or other reproductive problems, Doll (6,7) and Oak Ridge Associated Universities (8). Doll does, however, sensibly advocate urgent studies into the work done so far, particularly by the Nordic countries, which suggests some weak link may exist in which RADHAZ could be a co-promoter rather than a cause.

The bulk of public concern at this time centres on 'hazards' from power line frequency NIR and this is the concern Doll et al. have primarily been addressing. This is also reflected in E.C. concerns on irradiation of humans at low field levels for a long duration from a variety of equipment in common industrial and domestic use. At this time at MAD the Radiation Safety Officer is responsible for 3 kHz-300 GHz, with 50 Hz aspects covered under general H&S and Electricity at Work auspices. Discussions are ongoing with U.S. RADHAZ specialists to learn from their experiences in this band, aimed at possibly including 0-3 kHz in the terms of reference. In this way alignment with the frequency range of the latest U.K. biological RADHAZ guidelines will be achieved, making the Safety Officer more 'NIR' rather than just 'RF' as at present. It is apparent that the existing C&A procedures will require minimal change to more formally control this additional sub-band. It is believed that the U.K. and other countries' research into this topic, augmented by learning from the U.S. where a number of RADHAZ litigations have occurred in recent times, will enable a C&A regime consistent with the actual level of risk. In this way the employees can be adequately protected and it should prove unnecessary to enact the worst case scenario of having to assess, by measurement, all 50 Hz pieces of equipment at regular intervals.

Apart from the very widely publicised effects of EM Fields on humans in general, high levels of RF radiation may present a specific hazard via dysfunction or malfunction of prosthetic devices, such as cardiac pacemakers. This dysfunction is basically an EM Compatibility (EMC) problem caused by upset of the circuitry, rather than a biological RADHAZ *per se*. Generally modern pacemakers are tested to reasonably high levels of EM fields and they usually have reversionary modes in case of failure. Although such devices have been available for a significant number of years, occasional problems are noted - such as airport weapon detectors and medical diathermy equipment

(9) and the withdrawal of one U.S. firm's pacemakers from the market in Germany, after German laboratory tests proved that failure could be induced via mobile telephones (10), so particular care is required in any C&A procedure.

#### RADHAZ to Electrical/Electronic Systems

RADHAZ to these systems is identical to EMC and is treated by MAD as such. RADHAZ C&A therefore is limited to determining the RF environment in which MAD's products and other equipment assets have to operate and ensuring that appropriate control procedures are in place. For military products these include EMC design guides, specifications and aircraft test procedures and, along with all other EMC aspects, are covered by the Division's EM Hazards Specialist and EMC Controller in concert. For civil aircraft and ground-based electrical/electronic equipment the responsibilities are similar, with the EM Hazards Specialist taking the lead in such areas as computer systems operations in airfield buildings.

The hazards to be encountered range from minor display interference (as can be seen when Personal Computers are irradiated) to major upset of avionics - a number of spectacular examples have been published in the open press in recent years. EMC specification, design and test for civil and military airborne systems is a well covered topic and is not discussed further in this paper.

#### RADHAZ to Electro-Explosive Devices

RF radiation of sufficiently high levels can cause weapons to be fired or weapons/external stores ejected by the inadvertent initiation of EEDs whilst on aircraft in flight or transit, being handled or in storage. The worst case example of this was an incident on the U.S.S. Forrester during the Vietnam war, where the carrier's radar initiated an aircraft missile which resulted in the loss of 134 lives and numerous aircraft, with some \$72M of damage (11). It is worth noting that RADHAZ to EEDs includes both initiation of the bare EED and upset of the weapon system electronics (an EMC aspect) which can result in the EED being 'deliberately' initiated. EEDs are essentially explosive devices that are initiated by passing a current through a resistive wire ('Bridge-Wire' devices), or through a mixture of a primary explosive and graphite particles ('Conducting Composition' devices). Bridge-Wire devices are initiated when the primary explosive is ignited by the resistive wire heating up. In the case of Conducting composition devices, the graphite forms a conductor and power is dissipated at the junctions of the particles causing 'Hot Spots' which initiate the primary explosive.

#### Explosion/Ignition of Flammable Atmospheres

All conducting structures behave as receiving aerials and there is a risk that sufficient current may be induced which, if a structural discontinuity exists

and is surrounded by a flammable atmosphere, may cause a spark which in turn causes ignition or explosion. Whilst this mechanism appears to be unlikely - and the risks are usually small in reality - a number of instances of this type of accident have been reported (12). The hazards to flammable atmospheres and protective measures are described in BS6656 (13).

### 3 THE RF ENVIRONMENT

Adequate and accurate definition of the RF environment in the vicinity of susceptible devices is crucial to quantifying the operational risks involved. The definition of 'vicinity' for MAD extends to:

- Its headquarters at Warton (Lancashire), an operational civil/military airfield with aircraft design, production and ground/flight test facilities as well as commercial/other office buildings. A second site (Samlesbury), some miles away, has materials manufacturing facilities and various office/stores buildings.
- Actual/potential Export Customers' air bases, to date as far afield as Saudi Arabia and Malaysia.
- Any location, world-wide, where MAD personnel work. It should be noted however that, where in place, the local RADHAZ C&A procedures take precedence and are only augmented by the MAD ones when deficiencies in the local C&A regime are perceived.

The RF environment on and around the Warton site is typical of the most complex situation to be assessed and controlled, with EM fields ranging across the spectrum from Medium frequency (MF) to Extremely High Frequency (EHF). These fields are generated by both intentional and unintentional emitters. The primary emitters are emitted from radio/radar antennas and the secondary emitters are such things as induction welding machines.

#### Airfield/Aircraft Transmitters

Within the MF, HF, V/UHF bands reside aircraft and ground-based communications systems and EMC test facilities. Ground/aircraft radars systems operate in the SHF/EHF bands, whilst airborne jammers operate throughout the HF-SHF bands and are subject to military Jamming Control Authority clearance in addition to local RADHAZ C&A procedures. Table 1 shows typical installations which may be found operating on or from an establishment such as the Warton Airfield.

#### Manufacturing Facilities

The airfield/aircraft transmitters are referred to as 'intentional' RFE whereas 'unintentional' emitters, such as induction welders and dielectric heaters, are more commonly found in manufacturing areas. High power RF induction furnaces, although there are none on BAe's two Lancashire sites, are typically

the highest power 'unintentional' RFE to be encountered in the industrial environment.

#### Design/Commercial/Airfield Support Facilities

Within the office a different environment has generally been created over the last ten years. This consists of attenuated fields from the airfield/aircraft transmitters and those from Cathode Ray Tubes in the large number of computer systems, portable and cellular telephones, lighting and dimmer circuits, heating and air conditioning. Other emitters include microwave security devices, microwave ovens, flight test RF telemetry links and portable V/UHF transmitters used by airfield Fire, Ambulance and Air Traffic Control services. RFE used by other industries and businesses include microwave communication links and radio telemetry links.

#### Accurate Quantification of the Environment

This is a complex task, even in the U.K. where a High Intensity Radio Transmission Area (HIRTA) scheme (14) is operated by the Ministry of Defence (MoD) to ensure the safe operation of military aircraft and helicopters with their weapon systems. This scheme comprises a database of emitters with Effective Radiated Power (ERP) above 500 W. An associated Flight Information Publication defines their geographical location and the safe vertical/horizontal spacing between each HIRTA (subdivided into four frequency sub-bands) and an aircraft with a given level of EMC clearance. Information published from the database covers primarily fixed location, high power ground transmitters, at frequencies mainly <5 GHz. More recently the database has been extended to include airborne and shipborne HIRTAs (15), but not yet for all nations' platforms. The U.K. HIRTA scheme is considered adequate for the task intended and can be considered a model scheme for the rest of the world, where such schemes do not yet exist. This causes particular problems when attempting to perform a RADHAZ assessment for BAe aircraft abroad.

The scheme has limitations in that, in conjunction with current EMC clearance methods (which include safety margins thought to be higher than necessary) it gives RADHAZ distances which are believed to be absolute worst case - higher than strictly necessary. In addition the scheme does not currently take into account probability and time of irradiation, or perform multi-emitter assessments as per (22). These aspects prevent an entirely accurate picture of the RF environment for RADHAZ purposes. These limitations can also adversely affect operational safety margins under certain conditions, particularly with respect to co-sited and/or co-frequency emitters where some or all have ERPs below the HIRTA minimum level, for example. Constructing a complete database of emitters is an unrealistic aim as, for example, the sheer numbers of emitters involved are enormous - for example it was estimated (16) that there were at least 0.5 million

microwave transmitters in the U.K. alone in November 1989. Of these 542 were high power systems covered by the HIRTA scheme, with an estimated rate of increase in transmitters (including transmitter 'retirements') of up to 100 per annum as communications systems migrated from the lower frequencies (e.g. HF band) to the microwave region, where the same data rate can be transmitted for a lower percentage of the available bandwidth.

#### **Environment Definition - RADHAZ Assessments**

Most RADHAZ assessments are still conducted using simple radio/radar system models and worst case RF parametrics, e.g. maximum ERP, antenna gain and beam coverage are generally used, with little or no consideration of probability or time of irradiation of the susceptible device. This historical situation is driven by the computationally intensive situation of trying to model an aircraft or aircraft formation, each one with multiple susceptible devices and device types, flying through a multi-emitter environment. The increased capability and performance of relational database technology and RF scenario generators (such as used by the Electronic Warfare fraternity), coupled with better antenna/radar system modelling promises substantial improvements in the quality of RADHAZ assessments. Rapid, low-cost and realistic RADHAZ assessment of any system on any vehicle, anywhere in the world appears now to be a realistic near term aim. To identify and understand any limitations of existing safety margins, C&A procedures and EMC clearance level requirements, research now targets: a) quantifying the time line profile of fields vs. frequency to be experienced by susceptible devices under various peace/war time conditions; and b) assessing any possible EED/electronic equipment safety margin degradation caused by dynamic flight through those multiple emitter environments, most of which have complex radar waveforms that are not yet fully addressed in U.K./U.S. standards.

Possible additional benefits of this research are the lowering of some civil/military equipment EMC requirement levels and safety margins, and a reduction of screening/siting requirements. This would be achieved through better definition of the environment, quantification of the probability of encountering high field levels in specified frequency sub-bands, and quantification of the risk of exposure to those fields for given time periods.

#### **4 SUSCEPTIBILITY ASSESSMENT**

The assessment of the susceptibility of devices is particularly difficult given the various frequencies that may be received by the device at any given instant. The complexity of the situation is significantly increased by the proximity of conducting objects and by the complex fields emitted by secondary emitters. This is exacerbated in the case of ground-based commercial electronics, such as computers, where there is very limited quantitative

(i.e. manufacturer-provided) susceptibility and safety margin data. Some computer manufacturers will only guarantee correct operation if field strengths are kept below 1-5 V/m for up to 1 GHz. Most will not guarantee operations for frequencies >1 GHz and will not state upset levels at any frequency. MAD and others have thus been forced to conduct some practical measurements in order to scope the safety margins in specific frequency bands of interest. Although the European Community (E.C.) EMC Directive (17) will assist in this area, such systems are likely to remain some of the most susceptible devices to RF radiation - increasingly so as their clock frequencies transit into the hundreds of MHz.

Assessments of susceptibility have traditionally been conducted on a single transmitter vs. a single susceptible device at a time. If an adequate safety margin can be theoretically demonstrated then neither multiple emitter assessments nor practical measurements are generally warranted. These are complex as they involve a number of generally dynamic fields in which phase changes, with relative position, can cause there to be a large margin of error due to signal phase summation when carrying out assessments based purely upon power or amplitude. Computers can ease the difficulty involved in carrying out the relatively simple but laborious field strength summation, but invariably a ratiometric summation of the relative effectiveness of the field to induce a harmful effect (a susceptibility ratio) is required in order to complete the RADHAZ assessment. Another significant problem is that susceptible devices and emitters may be mobile, e.g. vehicles and aircraft, which results in rapid variation of the components of the susceptibility ratio.

As the frequency of the field decreases the Rayleigh distance increases. Therefore at low frequencies it becomes increasingly more difficult to evaluate any potential hazard distances due to localised hot spots within the near-field of the emitter. Conducting media in the near-field will couple better into field and as such will significantly modify the field that would exist if the object were not there. These errors are particularly difficult to theoretically assess unless complex and expensive EM modelling is used.

ANSI-IEEE C95.3 (18) is the U.S. standard (no U.K./E.C. equivalent exists) for conducting measurements in order to establish whether a RADHAZ exists or not. However even within this standard there are acknowledged inconsistencies and errors, including the lack of a measurement quality factor to account for, or remove the inconsistencies that would occur between two or three sets of independently conducted surveys.

#### **5 RISK CONSIDERATIONS**

Risk assessment is a requirement of (4) although formal quantitative risk assessment plays little part in the present application of RF Safety Standards. However comparative risk assessment is an everyday

task in carrying out safety assessments. Relative risks due to a RFE installation have to be assessed. Woolnough (19) indicated the relative risks due to a typical radar system and, as with the system as a whole, the relative risk due to the presence of NIR have to be equally assessed. This initial risk assessment is used by MAD to determine how comprehensive a RADHAZ assessment needs to be carried out. This risk assessment considers both the likelihood of the different types of susceptible device being present and other emitters which may affect the validity of the emitter in isolation assessment. This initial assessment ensures a cost-effective approach to RADHAZ C&A is achieved, only necessitating field measurements to be taken when an inadequate level of safety margin can be established via physical or procedural constraints, or when a specific risk of concern is identified. In practice this cautious but effective approach to RADHAZ assessments rarely results in the need for extensive field measurements. The most important item to remember when carrying out a risk assessment is that the risk is the product of the severity of the hazard and the likelihood of exposure to that hazard. Table 2 shows a risk assessment matrix recently produced by the Engineering Employers Federation (20). This matrix is used to determine what action is taken to reduce high risk areas and the priority in dealing with them.

## 6 LEGAL REQUIREMENTS

At this point it is appropriate to outline the U.K. legal requirements for RADHAZ by topic. This section outlines present knowledge of the legal situation, however it is likely that other regulations may be found to be applicable. It is worthy of note that the standards/guidelines usually associated with RADHAZ C&A, listed below, are not *per se* legally enforceable unless included in contract documents. They can, however, be considered to be 'Codes of Practice' and thus enforceable via the Health and Safety at Work Act 1974 (HASAWA), which has a very broad base and a general duty of care is placed upon manufacturers, importers and suppliers of systems, employers, and employees to ensure, 'as far as reasonably practicable', the health, safety and welfare of others at work.

- National Radiological Protection Board (NRPB) 'Yellow Book' (21): RADHAZ to humans
- U.K. Ordnance Board Pillar Proc. P101 (22): RADHAZ to EEDs and firing circuits.
- BS6656(13):RADHAZ-Flammable Atmospheres
- BS6657 (23): RADHAZ to EEDs
- DEF. STAN. 05-74 (24): RADHAZ (in particular) to Humans
- U.K. HIRTA(14,15): military aircraft RADHAZ
- EUROpean Civil Aircraft Equipment (25)

Additionally there is a proposal by the E.C. for the EPAD (3) which will cover any mechanism for hazard which is governed by the laws of physics, e.g. Vibration, Non-optical Non-ionising Radiations and Optical Radiations. It should be noted that the EPAD is considered by some to be restrictive in its application. The main requirement is (4), which calls for a risk assessment of all situations to be carried out amongst other H&S management activities. This is applicable to all hazards to humans caused by RADHAZ, whether directly via irradiation or indirectly through RADHAZ to one or more of the other categories of susceptible device.

### RADHAZ to Humans

There are at present no explicit U.K. regulations defining exposure levels for workers or members of the public to EM fields <300 GHz. The H&S (Display Screen Equipment) Regulations (26) states that 'All radiation with the exception of the visible part of the EM spectrum shall be reduced to negligible levels from the point of view of the protection of operators' or users' health and safety.' Allen (27) indicates fields of 1-10 V/m and <1 micro-T at a distance of 30 cm from a computer cathode ray tube at 15 kHz, levels which are orders of magnitude below the investigation levels recommended by the NRPB. The Reporting of Injuries, Diseases and Dangerous Occurrences regulations 1985 (28) state that any incidence of cataract due to exposure to EM radiation shall be reported as a dangerous occurrence. While the application of this regulation relates mainly to optical radiations, causing such conditions as 'Glassblowers' eye', the wide scope includes those caused by RF and microwave exposure. Regulation 13 of the Provision and use of Work Equipment Regulations 1992 (29) states that 'Persons shall be protected from burns, scalds or sears from Work Equipment or its contents'. Although this does not apply to radiant heat this regulation could be applied to prevent RF burns from conducting objects in the fields of RFE.

### RADHAZ to Electrical/Electronic Equipment

There are currently no explicit national Regulations covering RADHAZ to electrical and electronic equipment although legal compliance in this area is implicitly linked to the relevant military/civil aircraft contract through EMC specifications. Eventual full implementation, from 1996, of (17) will form a legal requirement on all new electrical/electronic equipment for both RF susceptibility and emissions.

### RADHAZ to EEDs

The relevant Acts of Parliament that cover this field are the Explosives Act of 1875 and 1923. Regulation 12 of (29) states that 'Measures shall be taken as should prevent or adequately control risk to the H&S of users from the following hazards - ... unintended or premature discharges or explosions

(e.g. detonators). Regulation 3 of (28) defines any unintentional ignition or explosion of explosives to be a dangerous occurrence.

### **RADHAZ to Flammable Atmospheres**

Regulation 9 of the Highly Flammable Liquids and Liquefied Petroleum Gases Regulations (30) places a responsibility on occupier of any factory to prevent the presence of any means likely to ignite a flammable vapour where such a vapour may exist. Additionally the HASAWA may be considered to be applicable. Regulation 3 of (28) defines any explosion or fire involving process materials or products and resulting in 24 hours stoppage to be a dangerous occurrence.

## **7 FORMAL C&A REGIME CONSTRUCTION**

The construction of a full formal C&A regime is a costly and complicated task, with a balance needing to be drawn between the extent of the risk and the cost of reducing that risk to acceptable levels. It therefore follows that it would be most expedient to draw up a modular RF Safety programme from which compulsory and optional modules could be selected to optimise the control measures versus risk ratio for a given industrial situation. The basic modules of such a RF safety programme, as used by MAD, are described below. It is very important to remember that retrospective application of RF safety principles will be both more expensive and difficult to implement. Organisations which decide to implement RF Safety programmes should do so as early in the product/facility life-cycle as possible so as to ensure real financial gains in addition to improved safety.

### **7.1 Development Of Control Procedure**

When the development of a formal RF Safety programme was started at MAD the only parts of a programme that were in place were an airfield RF environment assessment report (comprising a theoretical assessment and some measurement data) and local procedures for some of the microwave systems that were in use on site. These documents, together with the site explosives and prohibited weapons safety manual (31), formed the total of RF protection in this area and had provided adequate levels of safety up to that time. An initial risk assessment was carried out (32) which, together with research into the basic problems associated with RADHAZ and the state of the art in international standards, allowed the development of a draft Control Procedure. This was discussed with a number of national and international experts to ensure that an adequate set of provisions had been incorporated and the document (33) has now been in use since early 1990. In the last year (33) has been taken up in the U.S. as one of the framework documents for a draft IEEE standard on practical RF safety.

### **7.2 RADHAZ Control Procedure Requirements**

This section covers the general requirements of the RF Safety Programme. It is based on (33) and work being carried out in the U.S.A. on a practical RF safety programme, which is utilising (33). The requirements of a RF safety programme are based upon both the individual level of risk posed by RFE and the total level of risk to susceptible devices located around the site under consideration. The following outline the elements of (33).

**Introduction to RADHAZ.** This is used to train personnel in the subject of RADHAZ. It is written so as to be informative and easily understood and covers policy position and statement, the EM spectrum, basic sources of RF radiation, the effects of RADHAZ and legal requirements.

**Introduction of Equipment.** This defines what equipment may not be brought on site; it is the first level of control and may be a total exclusion unless individual risk assessments are conducted.

**Registration and Assessment.** This defines the procedure to be carried out before the introduction of equipment onto the site or any modifications to existing systems. It includes sections on RFE registration and assessment and may actually include levels and techniques. At MAD the assessment procedure is maintained as a separate document (34).

**Training Requirements.** In general terms this describes the depth and scope of training to be given to different personnel, from the RFE operator to the personnel assessing RADHAZ.

**Auditing and Monitoring.** This is required under the Management of Health and Safety Regulations and is used to check systems of work and inspect equipment safety provisions and procedures.

**Medical Screening of Personnel.** Whilst medical screening for RF radiation is not generally necessary, MAD operate a medical screening programme that requires personnel to declare prosthetic devices to the Chief Medical Officer. A risk assessment is then carried out to evaluate whether the person is likely to suffer any harmful effects and to ensure any location/movement limitations are identified. Great care is required when instigating a medical screening programme. Boeing Inc. (U.S.A.) found out to their cost that a medical screening programme could actually be counter-productive. Their well-intentioned collaboration with a university and the method of screening used may have been seen as experimentation on personnel working within the EM pulse generator and led to an out of court settlement of \$500,000 (35).

**Appointment of a Radiation Safety Officer.** The appointment of a person to administer the application of the RF safety programme is considered essential. The duties and responsibilities of the Radiation Safety Officer (Non-Ionising)

[RSO(NI)] are covered below. The '(NI)' differentiates between this and the Ionising RSO, who covers nuclear aspects of the site's manufacturing and development operations.

**Accident and Incident Reporting.** This defines the duties of different levels of personnel involved in, or investigating an accident or incident.

**Responsibilities.** This defines specific responsibilities with respect of RADHAZ and includes the terms of reference of all personnel involved in the implementation of the Control plan.

**Safety Precautions for Specific Equipment.** This includes control methods for specific generic systems e.g. microwave ovens, induction heating devices and management radios. It may also include control methods related to specific susceptible devices.

## 8 ROLES OF RSO(NI) AND SPECIALIST

As a company with large numbers of emitters and susceptible devices, MAD have felt the need to appoint a full time specialist covering both RF and Laser Safety. In addition a RSO(NI) and Laser Safety Officer have been appointed to be responsible for the individual subjects. The role of a RSO(NI) is the same as for any safety related field, acting as a focal point for questions on RF Safety and responsible for the formulation and implementation of the RF Safety programme. A RSO(NI) does not necessarily have to be a technical specialist but must be technically competent, with a basic understanding of the effects and implications of RF radiation safety. It is also vital that the RSO(NI) has the authority to adequately control the hazards, including the power to close transmitters down under incident/accident conditions or where adherence to the C&A procedures is not demonstrated.

The role of a technical specialist is precisely that of a consultant. The technical specialist may or may not be the RSO(NI), but given the wide scope of the task a very detailed evaluation of whether organisations can afford to procure or train and maintain a technical specialist must be carried out. For facilities where the risk is assessed to be insufficient to support an employed specialist then there are a number of consultants and consultancy services available within the U.K.

For each company where RF Hazards may be present it appears reasonable to expect a person should be appointed as RSO(NI). As with any other safety issue, one person should be responsible for the RF safety of each system; often this can be satisfied by the system supervisor. If the evaluation of the risk is technically difficult or the output indicates that the risk is significant, then it would appear reasonable to consult a specialist. It would be wrong for this to be considered as appropriate for all companies as each organisation must evaluate its own levels of risk and operational methods.

## 9 HISTORICAL DATA

It is, as with other H&S areas, and probably always will be very difficult to measure the cost-effectiveness of RADHAZ C&A procedures. What is known is that failure to address and adequately control hazards to U.K. personnel from products or operations will, in the future, attract the attention of the law in the form of prison sentences and potentially unlimited fines (36). It is important therefore to be able to demonstrate, in the unfortunate case of incident or accident, that all sensible and reasonable precautions had been taken to prevent such an event. To this end MAD are also actively involved in the construction of international RF/laser incident/accident databases to enable preventative actions to be taken where appropriate.

In these ever more cost-conscious days, other cost/performance metrics need to be developed, rather than just the lack of incidents/accidents. Initial work has commenced on developing suitable metrics and, as an indication of the type of data which could be used, Table 3 gives some raw RADHAZ assessment statistics. The number of RADHAZ assessments for on- and off-site RFE and susceptible devices is given, with one column each covering new, changed or relocated transmitters and susceptible devices. The latter column also covers the case where changed standards and/or guidelines has required a re-assessment of the hazards posed to the devices. The table includes incident/accident numbers and it should be noted that, to date, none has resulted in any person sustaining physical damage or requiring medical treatment. Although a small number of incidents/accidents has occurred over the last two decades, procedures have been in place to contain them. Great care has been taken to learn from the experiences, modifying working practices and equipment wherever possible to prevent recurrence. One of the major limitations of this kind of data is that it gives little indication of the effort involved, e.g. the assessment of aircraft/weapons operations from a foreign air base involves substantially more effort than for the same aircraft/weapons from the Warton airfield where the RF parametrics and other features contributing to the RF environment are well known.

## 10 INTERNATIONAL COLLABORATION

In a relatively new scientific topic, where the first international protection limits were set in 1958, there is still much to be confirmed with respect to the safety of NIR. There is a large range of levels set as NIR protection standards ranging from the levels set by the Commonwealth of Independent States to the levels set by both the Americans and the U.K. NRPB. Those of the U.S and U.K., having a wealth of supporting research data acquired over the last few years, are acknowledged to represent the highest quality world-wide. Substantial research is still required to ensure a consistent approach across the

whole frequency spectrum. International research collaboration is highly desirable to: ensure coherence and qualification of research; optimise scientific expertise available per topic; improve the techniques used in the research; and ease the financial burden of the research.

This approach, coupled with the adoption of techniques used in other more established sciences, should enable an international consensus to be reached in all of the aspects of NIR Safety. This reasoning is further advanced by the emphasis for international standards to be developed to ease the financial burden of [exporting] companies' compliance with differing national standards.

Given the way that standards, particularly those related to safety, affect industry it must be considered important for U.K. Industry to have a direct voice into international and national standards setting so as to ensure that prohibitive standards are not unnecessarily set and, wherever possible, the needs of U.K. industry are adequately addressed. It is suggested that the only way for the cost-effective achievement of this objective is that Industry must have a select group of highly trained and internationally respected technical specialists. MAD supports this objective and has taken a forward looking approach in this area in the last four years and is seen to have paid dividends. The RADHAZ/Laser Safety Specialist provided detailed comments to the NRPB in the consultative stage of the development of their latest guidance and is a member of Sub-committee's 2 and 4 of the American Institute of Electrical and Electronic Engineers Standard Co-ordinating Committee 28 (IEEE SCC-28) who develop the U.S. standards in this area. IEEE SCC-28 are developing the new standard on a practical RF safety programme mentioned earlier in this paper. It is hoped that this evolving programme/standard will, in due course, be offered to the International Electro-Technical Committee for possible adoption as an international standard.

## 11 THE WAY AHEAD

Although work to date has enabled MAD to ensure the adequate control of hazards to its operations posed by RF radiation, there remains much to be done in the area of RF safety standards, control method and assessment techniques. The conduct of this further work is of great importance as non-compliance with recently introduced (U.K.) and pending (E.C.) legislation on H&S carries severe penalties. The prime elements of the way ahead are:

- International consensus (military and civil) is required within the topic matter of RF safety. Efforts towards this objective are being actively taken by a number of national and international organisations, with the development of such items as a revised NATO Standard for personnel exposure to RF Radiation, to which MAD have contributed.

- Realistic modelling of both the RF environment and susceptible devices is required. Research is being conducted in a number of areas in order to establish new methods and techniques in the definition of the RF environment. This is focussed on field mapping techniques rather than the wire line analysis approach. It is hoped that traditional EM modelling techniques, which are very computer intensive, may in due course be simplified and incorporated within the arsenal of RADHAZ assessment tools.

- Quantitative RADHAZ risk assessment techniques require development and international acceptance. Appropriate numerical techniques already exist but, at present, those techniques are not generally applied. Work now being conducted in this area strongly suggests that quantitative assessment of the likelihood of fields being present will play an important part within the assessment of RADHAZ.

- Databases of RADHAZ incidents/accidents are urgently required. The potential cost benefits to Industry and the Armed Services of learning from earlier experiences to prevent the 'many incidents precede an accident' syndrome cannot be over emphasised. Such preventative systems already pay dividends in other safety areas. MAD are actively involved with international organisations in such work, both on RF transmitters and lasers.

## 12 CONCLUSIONS

BAeDEF(MAD) has developed a RADHAZ Control and Assessment scheme of international calibre. This is currently being partly adopted as a U.S. standard and may in turn be adopted internationally. Such a scheme, having been operated successfully for some time, is believed to provide appropriate and cost-effective control of the risks associated with non-compliance with U.K. legal requirements, particularly in the area of human Health and Safety. It is probable that this scheme, or a sub-set thereof, would suffice for most industrial situations.

Co-operation and collaboration with national (NRPB/MoD *et al.*) and international agencies (primarily in the U.S.A.) enables industry to have a strong voice in standards setting. As much RADHAZ research still remains to be done, such work also ensures that the latest world-wide research ideas and information are available to assist in the timely identification of any additional precautions. Thus BAeDEF(MAD) continues to ensure the highest level of protection from RF hazards for employees, Customers and the public.

## 13 ACKNOWLEDGEMENTS

The authors wish to thank BAeDEF(MAD) for permission to publish and acknowledge comments provided by Mr. I.P. MacDiarmid (Divisional EM Hazards Specialist), Mr. B. Rylance (Divisional Health, Safety and the Environment Manager) and Prof. R.J. Simpson (University of Central Lancs.)

## 14 REFERENCES

1. Phillips A., Best S., 'Killing Fields', Electronics + Wireless World, Reed Publishing, February 1990, pp.96-117.
2. Coghill R., 1990, 'Killing Fields', Electronics + Wireless World, Reed Publishing, March 1990, pp.179-211.
3. Proposed European Community Directive on Physical Agents at Work. Official Journal, No. C 77, 18 March 1993, pp.12-29.
4. Management of Health and Safety at Work Regulations 1992 (Stat. Inst.1992 No. 2051).
5. Darby C., 1994, 'Are We all living with danger?' Womanpost, The Lancashire Evening Post, 5th April, pp.4-5
6. Doll et al., 1992, 'Electromagnetic Fields and the Risk of Cancer', Documents of the National Radiological Protection Board Volume 3 No. 1, NRPB, Didcot, UK.
7. Doll et al. Electromagnetic fields and the risk of cancer. Summary of the views of the Advisory Group on Non-ionising Radiation on epidemiological studies published since its 1992 report. Doc. NRPB, 5, No.2, April 1994.
8. Oak Ridge Associated Universities Panel, 1992, Health effects of Low Frequency Electric and Magnetic Fields, ORAU 92/F8, NTIS, Springfield, VA, USA.
9. Sowton, E. Environmental Hazards for Pacemaker Patients. J. Royal College of Physicians (London), Vol.16 No.3 July 1982
- 10 'Rubber Stamping EMC', What's New in Electronics, May/June 1994.
- 11 Taylor, C.D. and Younan, N.H. Effects from High Power Microwave Illumination. Microwave J., June 1992
- 12 Excell, P. Radio Frequency Ignition Hazards. Hazard Prevention, Vol.20 May/June 1984.
- 13 BS6656: 1991 Guide to Prevention of inadvertent ignition of flammable atmospheres by radio-frequency radiation.
- 14 Elton, L. RF Environment External to Aircraft, Vol. 1: The calculation of aircraft radio frequency hazard safe distances for the definition of HIRTAs in the United Kingdom. BAeSEMA MNC 00220, Sept. 1992.
- 15 Elton, L. RF Environment External to Aircraft, Vol. 1: Ship and Aircraft Based Transmitters. MNC 00220, Mar. 1992.
- 16 Pywell, M. An Investigation of the Microwave Upset of Avionic Circuitry. M.Phil.-Ph.D. Transfer Report, April 1992.
- 17 E.C. EMC Directive No.89/336/EEC.
- 18 ANSI-IEEE Recommended Practice for the Measurement of Potentially Hazardous EM Fields - RF and Microwave. C95.3-1991
- 19 Woolnough, R.C.N. Practical Control of Non-Ionizing Radiation Hazards. Radiofrequency Standards. Eds. D.N. Erwin, M. Grandolfo and B.J. Klaunenberg (1994)
- 20 EEF Health, Safety & Environment Newslines. No. 2, 1993.
- 21 Board Statement on Restrictions on Human Exposure to Static and Time Varying Electromagnetic Fields and Radiation. Documents of the NRPB, Vol.4, No.5 1993.
- 22 Principles of Design and Use for Electrical Circuits Incorporating Explosive Components. Ordnance Board Pillar Proceeding 101(Issue 1), 28 Aug. 1991
- 23 BS6657: 1986 Guide to Prevention of inadvertent initiation of electro-explosive devices by radio-frequency radiation.
- 24 DEFence STANdard 05-74/Issue 1. Guide to the Practical Safety Aspects of the Use of Radio Frequency Energy. 9 January 1989.
- 25 EUROpean Civil Aircraft Equipment User's Guide for AMJ. No. XX, December 1993.
- 26 Health and Safety (Display Screen Equipment) Regulations 1992 (S.I. 1992 No.2792)
- 27 Allen, S.G. RF field measurements and hazard assessment. J. Radiol. Prot. Vol.11 No.1 Tab.5, p.57
- 28 Reporting of injuries, diseases and dangerous occurrences Regulations '85 (No.2023), HMSO
- 29 Provision and Use of Work Equipment Regulations 1992 (S.I. 1992 No. 2932)
- 30 Highly Flammable Liquids and Liquefied Petroleum Gases Regulations made under the Factories Act 1961.
- 31 Moore, M.W. The Explosives and Prohibited Weapons Safety Manual. WMD1, Vols.1&2.
- 32 Pywell, M. The C&A of Non-Ionising Radiation Hazards within the Warton Unit. Feb. 1988. BAe-WAD-RP-GEN-EMC-057.
- 33 Woolnough, R.C.N. The Control of Non-Ionising RADHAZ in the Warton Unit. 15-12-92. BAe-WAD-RP-GEN-RAD-000140.
- 34 Jackson, M.A. The Assessment of RADHAZ within the Warton Unit. 19 Sept. 1991. BAe-WAD-RP-GEN-RAD-000345.
- 35 'Boeing Pays Worker With Cancer \$500,000' Washington Post, 17 August 1990
- 36 EEF Health, Safety & Environment Newslines. No. 8, 1992

**TABLE 1 - TYPICAL INTENTIONAL RF EMITTERS**

EMITTER	FREQUENCY (MHz)	PEAK POWER (kW)	MODULATION
ATC RADAR	600	500	4 μs Pulses
Air Surveillance Radar	2750-3050	58	Pulsed
Radar IFF/SSR	1000	1	Pulsed
Precision Approach Radar	9000-9200	320	Pulsed
HF Radio	2.8-23	0.4	Single Side band
VHF Radios	118-225	0.125	AM/FM
UHF Radios	225-400	0.125	AM/FM
Military Radar	9000-10000	2000	Pulsed
Radar/Comms. jammers	HF-SHF	(classified)	(various)
Medical Diathermy	27	0.1	CW
Cell-phones	900	0.013	AM/Digital

**TABLE 2 - RISK ASSESSMENT MATRIX**

Likelihood (Exposure)

Severity (Hazard)

	Minor	Up to 3 Days	3 Days +	Major	Death
	1	2	3	4	5
1 Extremely Unlikely	1	2	3	4	5
2 Unlikely	2	4	6	8	10
3 Likely	3	6	9	12	15
4 Very Likely	4	8	12	16	20
5 Certain	5	10	15	20	25
Insignificant - low priority		Importers within days	Prohibition Immediate		
p3		p2	p3		

**TABLE 3 - HISTORICAL DATA ON RADHAZ ASSESSMENTS**

YEAR	No. OF CHANGED RF TRANSMITTERS	CHANGED/RELOCATED SUSCEPTIBLE DEVICES	No. OF INCIDENTS	No. OF ACCIDENTS
1982	1	0	0	0
1983	0	0	0	0
1984	1	6	0	0
1985	3	1	0	0
1986	5	4	0	0
1987	13	6	2	1
1988	6	7	1	0
1989	9	12	2	1
1990	9	7	0	0
1991	7	3	1	0
1992	75	2	0	0
1993	17	6	3	0
1994	8 (to 19 July)	4 (to 19 July)	0	0

## **APPENDIX B: EMC QUALIFICATION OF MILITARY AVIONICS AND AIRCRAFT**

### **B1 INTRODUCTION**

This appendix covers the above and discusses the outcome of a review of EMC qualification standards for military avionics. It also addresses EMC test requirements and techniques applicable to whole aircraft.

### **B2 EMC QUALIFICATION OF AVIONICS EQUIPMENT**

Military avionics are subjected to numerous different tests prior to fitment to aircraft to ensure conformance to specification. An important area of these tests is the qualification of the equipment to function correctly when exposed to the aircraft's operational environment. This covers standard items, *e.g.* fluid contamination, salt, sand, altitude, temperature, rain and vibration, as well as more esoteric tests, *e.g.* EMC and fungus resistance. EMC tests cover many aspects, from conducted susceptibility and voltage transient resilience to compass safe distance, lightning strike and radiated emissions. The specific tests of relevance to this research programme are the Radiated Susceptibility (RS) tests, where each Unit Under Test (UUT) is irradiated at given microwave power density levels whilst its capability to continue operating correctly is examined. Applicable test standards and test techniques used are discussed.

#### **B2.1 STANDARDS**

All currently used microwave irradiation EMC qualification test specifications were reviewed and the relevant ones identified [B-1] to [B3], [3-8] and [3-9]. It was established that the latest UK military aircraft EMC specification [3-9], whilst based on earlier documents (mainly US MIL. STD. 461B/2 [B-2]), contains much higher test level requirements at microwave frequencies than any other specification, thus partially reflecting the anticipated worsening of the RF environment in that band. The prime changes to the RS test above 1 GHz in the transition from [B-2] through [B-3] and [3-8] to [3-9] are:

- upper limit lowered to 18 GHz, then later re-instated at 40 GHz,
- the requirement to measure power density at the Unit UUT,
- introduction of a restriction of the choice and modified use of transmitting antennae,
- new modulation requirements to simulate the effect of radars (*i.e.* high peak fields); with an additional double modulation test to simulate the effect of rotating radars.

#### **B2.2 TEST TECHNIQUES**

A review was carried out of the test techniques used in avionics EMC qualification >1 GHz for the [3-8] and [3-9] specifications, the only two directly applicable to this research programme.

##### **B2.2.1 The Eurofighter 2000 EMC Specification**

Tests above 1 GHz for the Eurofighter (EF2000, formerly known as EFA) are given below. Items a.-c. are only applicable to receivers and tuned amplifiers operating in the range 1 MHz to 40 GHz and are therefore not directly relevant to this research.

- a. CS-EFA-5: Conducted Susceptibility, Inter-modulation 30 Hz to 40 GHz, upper frequency to be defined by aircraft company's EMC specialist.
- b. CS-EFA-6: Conducted Susceptibility, undesirable signals rejection, 30 Hz to 40 GHz, upper frequency as above.
- c. CS-EFA-7: Conducted Susceptibility, Cross-Modulation, 30 Hz to 40 GHz, upper frequency as above.

d. RS-EFA-3: RS, Electric Field, 14 kHz to 40 GHz. Upper frequency "shall be defined by the aircraft manufacturer's EMC Specialist. Normally, for equipment with operating frequencies below 1 GHz, the upper test frequency shall be 18 GHz." The equipment has to operate up to specified interference limits without any degradation of performance; with swept frequency irradiation up to 18 GHz, and spot frequencies permissible for 18-40 GHz. Up to limits increased by 6 dB safety critical equipment must either perform satisfactorily or may go into fail safe conditions, returning to full performance when the interference signal is reduced to the un-enhanced limits. The r.m.s. CW field strength requirement for both externally mounted or in open EM areas equipment is  $955 \text{ Wm}^{-2}$  ( $600 \text{ Vm}^{-1}$ ), and for internally mounted equipment is  $26.5 \text{ Wm}^{-2}$  ( $100 \text{ Vm}^{-1}$ ). In addition the worst case modulation "shall be determined and used thereafter in the test". Also, as a minimum, the following is required to be used: A double modulation consisting of 100% pulse modulation with a pulse repetition frequency of 1 kHz ( $\pm 0.1 \text{ kHz}$ ) with a pulse duration of 1  $\mu\text{s}$  ( $\pm 0.1 \mu\text{s}$ ) together with a square wave modulation at 100% with a frequency of 0.5 ( $\pm 0.1$ ) Hz. Whilst the peak field strength under these conditions is to be specified by the aircraft manufacturer's EMC specialist, as a general rule that it will be equivalent to the CW requirement.

#### **B2.2.2 DEF. STAN. 59-41 (Part 3)**

A smaller, but similar list of tests as those above apply, with the equivalent to EFA-RS-3 being DRS02: RS for 0.79-18 GHz. Pulse modulated test levels of  $27 \text{ Wm}^{-2}$  ( $100 \text{ Vm}^{-1}$ ) are defined, plus 6 dB ( $=105.6 \text{ Wm}^{-2}$  or  $200 \text{ Vm}^{-1}$ ) for equipment generating drive signals to external stores, e.g. weapons and fuel tanks. CW test levels for 1-18 GHz are  $1.1 \text{ Wm}^{-2}$  ( $20 \text{ Vm}^{-1}$ ) and, as above, plus 6 dB ( $= 4.2 \text{ Wm}^{-2}$  or  $39.8 \text{ Vm}^{-1}$ ) for stores-driving circuits. This test, in common with EF-RS-3, is performed in a screened room, utilising RAM suitably positioned to minimise reflections. With the UUT on the ground plane, it is irradiated by a waveguide horn transmitting antenna spaced 1 m from each face of the UUT in turn. A field probe (also a waveguide horn at these frequencies) is used adjacent to the UUT to ratify the test power density level achieved. It is then irradiated with swept frequency RF energy whilst checking for malfunctions. Above 1 GHz any discontinuities in the UUT, i.e. potential energy ingress routes, are also presented perpendicularly to the linearly polarised transmitting antenna in turn and the test repeated. Limiting tests to only horizontal and vertical polarisations is driven by time and cost considerations.

#### **B2.3 DISCUSSION**

The radiated susceptibility test techniques of Sections B2.2.1 and B2.2.2 are equivalent, excepting the frequency range and absolute test levels difference, with the latter of [3-9] being 5-15 times higher than those of [3-8]. Ref. [3-9] contains a qualifier on the peak field strength requirement that "If investigations indicate that the equipment under test will be subjected to higher pulse field strength when used on the aircraft system (externally or internally mounted) these higher requirements apply." It was unclear how this would be effected in practice, but it is known that the maximum peak power density requirement is  $1 \text{ MWm}^{-2}$  ( $19.4 \text{ kVm}^{-1}$ ), to a MoD-defined frequency profile, but with mean power density not greater than  $1 \text{ kWm}^{-2}$ . These values ensure that equipment is qualified to levels much closer to the current and predicted future microwave environments in Chapter 2.

Conducting high power RS tests in a non-fully anechoic room leads to reflections, causing erroneous measurements of incident power density on the UUT and poor repeatability. The positioning of the measurement probe, which is usually specified as a double-ridged waveguide horn for 2-40 GHz, necessarily close to the UUT at these power density levels is also likely to lead to measurement errors due to field perturbation by the antenna itself. These measurement probes are calibrated by comparison against Standard Gain horn

antennas, used as a reference, whose performance is calculated using high accuracy mechanical details.

### B3 AIRCRAFT EMC QUALIFICATION

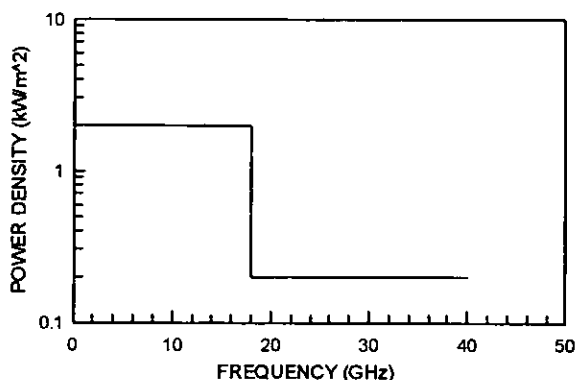
As discussed in Section 3.2 no other technique is available for whole aircraft EMC qualification and thus tests on aircraft, known as 'EMC clearance', are necessary to demonstrate adequate safety margins for safe and correct operation of systems when in the presence of both on-board generated and external EM fields. MoD and BAe research is targeted at the development of other techniques and tools which will reduce and eventually obviate the need for aircraft tests in the 1-40 GHz band. The cost and timescale benefits of obtaining EMC clearance without using the aircraft are substantial. For UK military aircraft any alternative clearance techniques must be acceptable to the clearance authority, the UK MoD, who have indicated willingness to consider such alternatives, if presented with supporting research evidence. This section outlines clearance requirements applicable to military aircraft and discusses how they are satisfied.

#### B3.1 CURRENT AND FUTURE TEST REQUIREMENTS

Microwave EMC clearance requirements for UK military aircraft currently in service are determined by the MoD's Technical Authority, the Armament and Aircraft Experimental Establishment, Boscombe Down. The techniques to be used, see Section B3.2, are researched and developed by the Defence Research Agency at Farnborough (DRA(F)). For export aircraft the Customer often mandates that the requirement and techniques are underwritten by the UK MoD, and thus the same procedures as for RAF aircraft are used. Even for Private Venture sales abroad, BAe normally use these established EMC clearance procedures as appropriate to the particular aircraft contract.

The current requirement for microwave EMC clearance of aircraft is to irradiate the aircraft under test with a series of high power (pulse) radar transmitters, whilst monitoring for upset. The test levels are generally as high as the transmitters, which are currently located at Boscombe Down, can attain. These mean levels (before [3-8] and [3-9] there was no peak pulse requirement for UK aircraft tests) are then translated, by subtracting the appropriate safety margin, into a HIRTA clearance for 'D' band (0.79-40 GHz), giving vertical and horizontal separation between the aircraft and high power transmitters in the UK. This requirement is intended to cover not only irradiation of the aircraft by ground based radars, but also, as noted by Audone [2-24], by radars and jammers on other aircraft, whether formation flying of the same type or on nearby aircraft.

Figure B1: Current Test Level Requirement For Unrestricted UK Flying



Current safety margin requirements for frequencies below 1 GHz, which are driven by the MoD, are 6 dB for flight safety and navigation/radio systems, and 15-20 dB for weapons systems. Fig. B1 depicts the current 0.79-40 GHz test level requirements, which have a

3 dB safety margin applied, for a military aircraft to fly anywhere in the UK, *i.e.* with a clearance to fly close to HIRTA zones (see Section 2.2). Future clearance requirements for new or updated UK military fighter aircraft involve the more rigorous demonstration by test of elevated clearance levels. Since the microwave clearance specifications for these and future aircraft reflect the worsening RF environment, realistic safety margins are required, based on the probability of actually encountering a given microwave power density, as discussed in Section 2.3.2. This in turn also relies on a better prediction of the environment to be encountered *vs.* geographical location.

### **B3.2 AIRCRAFT TEST TECHNIQUES**

The aircraft is irradiated and examined to ensure that no adverse effects are caused to avionics, primarily flight safety critical and weapons systems. These tests have been conducted for many years at MoD Armaments & Aircraft Evaluation (now Defence Evaluation & Research) Establishment, Boscombe Down, Wiltshire using high power radars operating at a few spot frequencies in the 1-10 GHz band. Because of the limited number of radars available, and the absence of reported avionic problems >1 GHz, it was considered adequate to extrapolate clearance levels from the few frequencies tested to 0.79-40 GHz. During 1989 another technique was re-introduced by using two other aircraft types as high power test transmitters. The test was not a formation flying test, although it is now also used for this purpose, rather being an additional microwave irradiation test adding more frequency points to the characterisation of the aircraft. Fig. B2 depicts the technique, with the aircraft under test in the background and the irradiating aircraft in the foreground. In order to satisfy the much elevated clearance test levels for the latest UK military aircraft it was necessary to develop new test techniques. Test techniques research at BAe, including that reported in Chapter 3, was conducted with a view to testing aircraft using a 'footprint' technique, where selected areas only of the aircraft are irradiated using high power RF sources, thus minimising free space losses incurred by the traditional method described in Section B3.2. The airframe attenuation research results were briefed to MoD (Ordnance Board and A&AEE) [B-4] in support of BAe's proposed use of the alternative clearance technique. In conjunction with avionics upset data also presented at the time, agreement in principle was achieved. Following further work by A&AEE and DRA(F) [2-17] the technique, in conjunction with avionics qualification evidence, is now a fully accepted EMC clearance technique for military and civil aircraft. An improvement to the technique for measuring airframe attenuation, mode stirring, was discussed in Chapter 3. High power commercial microwave amplifiers and antennas, recently acquired by A&AEE and BAe, now enable pseudo-swept clearance testing of aircraft, representing a significant improvement in the quality of EMC clearance testing of UK aircraft. This recent improved test capability will also enable better installed avionics susceptibility characterisation and could provide data to support the reduction of safety margins applicable to these tests.

### **B4 REFERENCES**

- [B-1]Carter, N.J. International EMC Co-operation in the Military Area. Paper presented at the IEEE Symposium on EMC in San Diego, CA, USA. 16-18 September 1986.
- [B-2][U.S.] MIL. STD. 461B/462 EMI Characteristics: Requirements for Equipment (1 April 1980), and EM Interference Characteristics: Measurement of (31 July 1967).
- [B-3]Carter, N.J. FS(F) 510 Issue 1. RAE Technical Memorandum: Recommended Technical Specification for the EMC of Aircraft Equipment.
- [B-4]Pywell, M. Microwave EMC Clearance of Military Aircraft, the New U.K. Ordnance Board-generated Safety Margin regime. BAe-WAD-VR-GEN-EMC-094, 20-06-1990

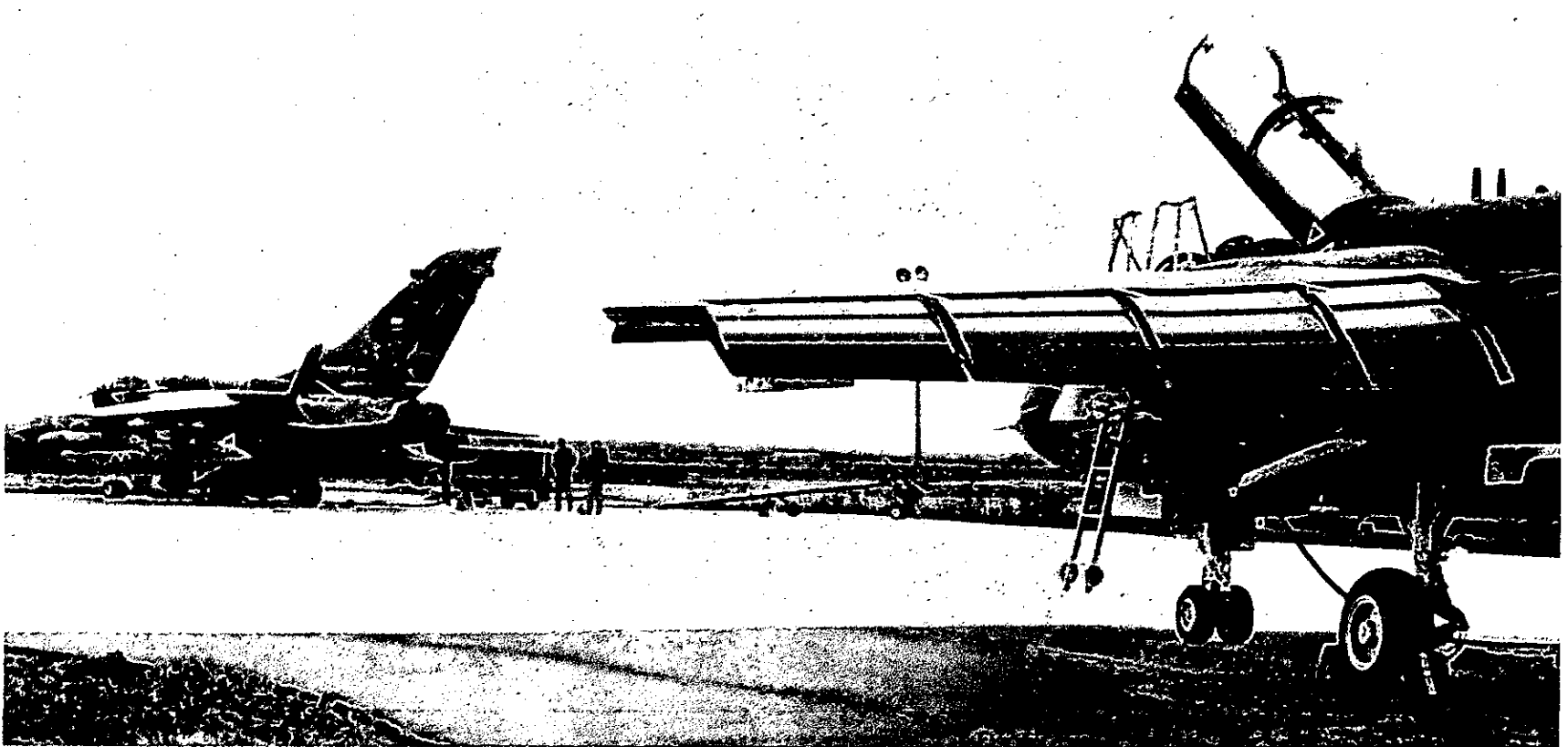


Figure B2: Microwave Irradiation Test Using Other Aircraft Type

## **APPENDIX C: ENVIRONMENT MODELLING AND THREAT SIMULATORS - HIGH QUALITY & LOWER COST VALIDATION OF EW SYSTEMS**

M.Pywell and N. Stuble (BAe). Presented at NATO AGARD 3rd Symposium of Sensor & Propagation Panel on 'Environmental Factors in Electronic Warfare related to Aerospace Systems', Practica di Mare Air Force Base, Rome, Italy, 8-11 May 1995.

### **SUMMARY:**

Recent conflicts such as the Falklands campaign, Gulf conflict and Bosnia have amply demonstrated the importance of EW to Mission Effectiveness and crew Survivability. In addition to this, since world-wide defence budgets are still reducing overall, the key driver for most Customers is Affordability. To a major aircraft prime contractor such as BAe Defence, these Customer requirements mean addressing a number of issues related to establishing the minimum necessary aircraft EW suite to satisfy those requirements. A key issue in this determination is a *precise* definition of the radar, RF and Electro-Optic (EO) electromagnetic environment that the aircraft must operate correctly in. This paper addresses this aspect and the tools and techniques necessary to produce aircraft EW systems that not only conform to specification, i.e. have no defects, but also have adequate performance, i.e. are 'fit for purpose'. It concentrates on the RF environment (modelling and threat simulators) as relevant to the testing of ESM/RWR/ELINT and ECM systems, although the principles are equally applicable to the EO, i.e. Infra-Red (IR) and Ultra-Violet (UV) regimes, and this is also discussed. It outlines EW System specification, describes EW environment modelling and its role in the design and validation process, covers EW Test and Evaluation (T&E) improvements, identifies shortfalls in current modelling capabilities, and gives major thrusts aimed at improving the EW development process. It addresses the issues above in the light of BAe Defence, Military Aircraft Division's experience in the field of both RF scenario modelling in support of a number of aircraft projects and planned ESM-ECM development work using scenario and equipment modelling, two world-class RF threat simulators, state-of-the-art ECM response measurement equipment and EW data analysis tools. It develops the argument that one of the main contributors to previous/current poor press on EW systems is believed to be the lack of *adequate* EW scenario definition at equipment/aircraft contract signature and that such definition should appear in specifications along side electromagnetic compatibility and other environmental issues.

### **1. INTRODUCTION**

Successful validation of complex EW systems prior to combat is a major technical goal of Industry, Government and Military Engineers alike. Adequate EW systems' performance is crucial to mission effectiveness and crew survivability and is likely to remain so for the foreseeable future. Even as current and future aircraft strive for ever lower multi-spectral signatures it is considered that a plateau will soon be reached at which point mission success and survivability will again depend largely on the capability of the vehicle's EW systems.

For a variety of reasons, EW systems world-wide have justifiably received bad publicity for many years - mainly through appearing to offer substantial technical promises which either have not been, or could not have been, realised. The methods of validating these systems, particularly ESM/ECM systems, have given cause for concern to the Customer and User alike. In particular there has appeared to be poor repeatability and substantial mismatch of results between laboratory tests and in-Service behaviour of EW equipment.

In addition, the traditional validation methods involving extensive flight trials can no longer be afforded in the light of shrinking defence budgets and there is a thrust both in the U.S.A. and Europe to move much of this work to the modelling and ground test phase, by aircraft testing in an anechoic chamber and a combination of avionic rig and threat simulator tests. This work, which includes extensive scenario modelling and the increasing use of EW equipment models, offers great promise in reducing not only the expensive flight testing phase, but also overall EW development timescales and costs. The affordability thrust also means that the following issues must be addressed, and this paper addresses primarily the last two:

- What is the minimum necessary EW suite to provide appropriate level of aircraft survivability?
- What are the trade-offs between various factors affecting the level of complexity of that suite and how are they related?
  - Radar Cross Section vs. Altitude vs. ECM capability
  - IR Signature vs. countermeasures capability, e.g. flares
  - Use of Stand-Off or Escort Jammers vs. fully capable Self-Protection Jammer
- What is the RF/EO environment (threat and other emitters) in which mission effectiveness and survivability are required?
- How to specify, design and validate the performance of an installed EW suite with highest quality and at minimum cost.

For EW systems validation to be achieved via this relatively new and more cost-effective route there is a need for better environment and emitter models, more capable and multi-spectral threat simulators for EW test and evaluation, realistic modelling of EW equipments and high power analysis capabilities. Although RF environment and threat simulation tools have existed for some time, it is only more recently that some of the more complex issues of environment modelling, such as terrain masking, have been addressed in any detail. Recent computing power increases now enable some of these computationally intensive tasks to be conducted in real time.

## 2. EW SYSTEMS

A typical modern aircraft EW suite is shown in Figure 1. Its prime objective is the immediate and unambiguous identification and classification of threat RF/EO emitters, and automatic engagement of countermeasures and/or timely set-on of own weapon systems, preferably via passive targeting. A factor in common between Radar Warning Receivers (RWR), EW Support Measures (ESM) and Electronic Intelligence (ELINT) is their function of detecting and processing radar signals. Although differences exist, in terms of this paper their main functions are effectively the same and thus hereafter the term ESM is taken to mean all three. Missile Warning (MW) systems are sub-divided into pulse doppler radar Missile Approach Warners (MAW) and passive (IR/UV) Missile Launch Warner (MLW).

## 3. SPECIFICATION OF EW SYSTEMS

Detailed knowledge of the following three items is crucial to the precise specification of EW suites, of whatever complexity:

- The RF/EO threat scenario(s), including geopolitical data to enable determination of non-military emitters in the theatre of operations for inclusion in the scenario(s),
- High quality RF/EO emitter parametric data, and
- Equally high quality operational analysis, covering tactics and the determination of Electronic Order of Battle.

This information is used to generate time ordered histories of engagements which form quantitative benchmarks of performance for the aircraft and its installed EW suite. Such benchmarks for ESM/ECM systems include pulse density (pulses per second) vs. frequency sub-bands vs. time, instantaneous dynamic range requirements vs. time, number of simultaneous pulsed and CW emitters vs. time, etc.

An ideal EW equipment specification is one where these time histories are included pre-contract, such that no ambiguity on performance issues can exist, and such that the aircraft and EW equipment suppliers can understand fully and concisely what is expected of their products, i.e. what is the definition of 'fit for purpose' for that aircraft when performing stated roles and missions. This level of specification, which requires significant modelling capability and effort, is rarely seen in specifications and less often, if ever, included pre-contract award. It is seen as an area where aircraft and EW equipment manufacturers, in concert with Defence Ministry and Air Force agencies, can enact major improvements in aircraft EW performance in terms of Affordability and reduced development timescales, balanced Survivability and Operational Effectiveness. Use of the modelling tools and techniques described later, during the Staff Target/Requirements phases of projects, is seen as a potential enabler of these major improvements.

## 4. EW ENVIRONMENT MODELLING AND ITS ROLE IN SPECIFICATION/VALIDATION PROCESS

### 4.1 Use of Modelling in the Specification/Validation Process

BAe Defence (Military Aircraft Division), in its role as a major aircraft manufacturer and systems integrator, has a suite of appropriate models and simulators to support the conceptualisation, design and development of whole aircraft and their systems. The two modelling tools of most relevance here are BAe's Airborne Weapon System Engagement Model (AWSEM) and the EW Evaluation System (EWES) by Data Sciences (U.K.) Ltd. AWSEM, which runs on an IBM Model 5 Mainframe, enables operational analysts to take a Customer's threat scenario and tactical information and create an Electronic Order of Battle for input to the EWES. Figure 2 gives a block diagram of the EWES suite of programmes and AWSEM as used by BAe. Figure 3 shows the considerable computing resources required to support such modelling capabilities as EWES. Slow run times for complex scenarios has, for example, led to a 1995 EWES upgrade, *inter alia*, to a DEC Alpha main host.

### 4.2 Use in Validation of ESM Systems

Figure 4 shows the typical arrangement and interaction of receiver model and EW receiver equipment in the validation process, whether at EW equipment supplier, ground avionic integration rig or aircraft ground/flight test stage. This shows how emitter and scenario data is input to both the EWES tool and RF threat simulator, and how the output of each is fed into the EWES or ESM Receiver Model and real avionic equipment respectively. The output of the Receiver model and real equipment, primarily in the form of time-ordered emitter track files with associated RF parametric and identification data, is correlated off-line via use of EW Analysis Post-Processor (EWAPP) and/or comprehensive EW [test] Data Merge, Analysis, Correlation and Statistics package (DMACS). By pre-determining allowable modelling and test error budgets and pass/fail criteria, a suitable regime for the quantitative demonstration of performance to specification can be determined through the comparison of modelled data with those acquired from rig or aircraft testing of the EW system. Where full ESM performance cannot be cost-effectively demonstrated via hardware tests, such as in the area of maximum pulse densities, it is necessary to use EWES and the receiver model as the verification tool. This requires that the receiver model is validated. This can be achieved by driving both real and modelled receivers with the same emitter scenarios and comparing their outputs. A typical EWES 'ESPRIT' (man/machine interface) tactical scenario page is given in Figures 5 and typical outputs of the EW Scenario Generator and Analysis Post-Processor are shown in Figures 6 (pulse descriptor file for input to Receiver Model) and 7 (two commonly used analysis pages) respectively.

#### **4.3 The Need for High Quality Emitter Parametric Data**

As stated in section 3, high quality emitter parametric data is crucial to precise specification of both RF and EO EW systems. The performance and effectiveness of EW systems in ensuring survivability and first time mission success is directly related to the quality of the emitter data used in the specification and design of, and subsequent programming into modern EW systems. This level of importance is recognised world-wide and most new EW equipments are now flight line re-programmable with the latest emitter data of the highest quality. Such parametrics include primary items such as frequency, pulse width, pulse repetition rate and scan parameters, and more difficult parameters to measure and/or determine, such as pulse jitter/stagger rate/pattern, frequency agility, and modulation on pulse.

Since many radar and RF emitters occupy a fairly small portion of the total electromagnetic spectrum it is hardly surprising that many emitters have broadly similar radar/RF parametrics. This in turn poses one of the most difficult tasks for an ESM system - that of unambiguously identifying a given emitter, often in the presence of many other emitters (including the aircraft's own transmissions). Quality and validated emitter parametrics used both in the specification and design stages, ensures that the ESM-ECM receiver has a measurement capability equal to (if not in excess of) the maximum range of each parametric it is specified to handle, but also that it can use the latest 'picture' of a given emitter to form a multi-parametric 'window' to aid in the identification/classification process within the ESM.

Parametric data on Red (potentially hostile), Blue (own/friendly) and Grey (neutral/other) emitters is collected through various intelligence gathering, including interception of actual transmissions by the threat radar - the ELINT mission. Data is analysed and collated into an Emitter Data Base (EDB). These are usually of the highest national and/or NATO security classification. The data gathering, analysis and database functions are complex and costly, yet essential [1].

Such data is only released to Industry on a project by project and strictly need-to-know basis, in relation to specific EW and aircraft contracts. This poses a problem to Industry where bid preparation and other pre-contract work often requires such data to enable the determination of the level of EW suite complexity and thus the level of test effort and resources/facilities required - both of which directly impact upon the bid price. It is therefore in the interest of Governments and Industry alike that suitably sanitised data is available during the bid and pre-contract phases of a programme. Although it is possible to construct unclassified emitter databases with a reasonable level of confidence in quality/fidelity of the data, a far better solution to enable a minimum of over-specification for Industry and Services alike is believed to be the production of down-graded versions of the national database(s). When using such data in support of EW system specification, design and validation, it is important to maintain adequate configuration control of the database. A method of assessing the impact of adding a new emitter, changed parametrics or behaviour of an emitter in a given scenario is required that gives confidence that the EW system still remains fit for purpose, as a change in parametric(s) can result in a significant change to the overall electromagnetic environment seen by the aircraft during a given mission.

#### **4.4 EO and Combined RF/EO Environment modelling**

To date most attention has been paid to radar/RF threat scenario definition, modelling and T&E facilities. The recognition that the majority of aircraft kills since the Vietnam war have been to IR-guided missiles, combined with the apparently ever-increasing use of lasers as primary or adjunct targeting systems, necessitates the development and use of EO modelling and test capabilities akin to those already well established for the radar/RF bands. Survivability in future conflicts is likely to be best ensured when aircraft and their EW systems have the scenarios described in section 3 defined in multi-spectral terms. Such scenarios would therefore fully describe the electromagnetic environment that the aircraft must operate correctly in and would include (as a minimum) the RF bands from HF, through the established microwave band (primarily C-J band with the more recent expansion of emitters into k-band), selected parts of the upper millimetre wave band (atmospheric windows in the 90-150 GHz area), various IR wavelengths (lasers, terrestrial heat sources, IR signatures of aircraft and inbound missiles) and UV wavelengths (lasers and missile motor plumes). Should such speculative directed energy weapons as High Power Microwave, Non-Nuclear Electromagnetic Pulse and laser dazzle/damage [2],[3],[4] prove to be viable, then these too would need to be included in the scenario specifications.

These multi-spectral scenarios will enable precise specification of not only ESM, but also Laser Warners and IR/UV Missile Launch/Approach Warners, and will enable appropriate specification of multi-spectral test equipment for T&E work, particularly in the area of sensor correlation, data fusion and crew situation awareness. Such scenario definition, modelling and T&E capabilities will become increasingly important for future aircraft where affordability, lethality, flexibility, availability and survivability considerations drive aircraft manufacturers toward much more highly integrated and covert sensors/systems, and faster reaction weapons systems than seen to date. Precise specification of systems of this level of capability, authority and probable automation - especially in the EW area - is seen as a prime requirement in minimising development costs/timescales and ensuring that the aircraft is fit for purpose. This argument is seen to be equally applicable to the upgrading of current aircraft, where increased EW capability and/or integration of EW elements is popular world-wide and predicted to remain so for the foreseeable future. To support the production of such EO scenarios the same fidelity level of data on EO sources is required as for the RF/radar emitter case, see section 4.3

#### **4.5 Modelling Shortfalls**

There are seen to be three main issues at present, which affect both environment/EW equipment models and simulators used for T&E and model validation:

**Emitter/threat system fidelity:** Somewhere between simple simulation and reverse engineering real equipment lies a cost effective 'simulation' of, for example, a threat radar system. For EW system performance specification and testing, a radar emitter needs much more than merely being modelled as a zero scan, fixed frequency/pulse width/pulse repetition rate isotropic point source. Levels of complexity of the simulation necessary, which in many cases approach *emulation* (i.e. an accurate representation of the emitter in *every* way the sensor/weapon system can determine), is largely limited by computing power, both in EWES-type tools and RF threat simulators. An example is the relatively small amount of data points which can be used to represent both emitter and own aircraft ESM antenna beam patterns. Typically large values are 500k points for a sensor antenna, split between the azimuth and elevation gains vs. frequency (i.e. a maximum resolution of 1 degree, 0.25dBi and 0.5 GHz), and 4k points per full beam pattern for each emitter in the scenario (i.e. maximum resolution of 0.5 degree, 0.1dBi and 0.5 GHz). In the U.S.A. the validation of threat simulators to be able to faithfully replicate a given threat is overseen by the CROSSBOW-S committee [5]. When extensive comparisons between the real threat and the simulator's version are complete (often >12 months per threat), they make recommendations for approval to the DoD Executive Committee on Threat Simulators, which manages and approves all DoD development of surrogate systems.

**Scenario fidelity:** Fidelity of the scenario is a trade-off of computing power vs. capability. To be truly representative all platforms must move correctly within the scenario, with such items as accurately modelled turn manoeuvres, 6-degrees of freedom on the own aircraft with at least 3 degrees of freedom for the 'enemy' airborne systems, terrain modelling/masking, missile fly-out models, etc. Ranges, resolutions and accuracies of all parameters within the scenario need to be at least equal to, or preferably better than those of the aircraft/EW system being modelled or tested. All engagements/tactics (which lead to EOB definition) and movement/manoeuvres of all players must be faithful representations of those contained in the specification. Current EW modelling tools and simulators cannot fully satisfy these requirements and those of emitter/threat system *emulation* in real time, although the ongoing vast increases in computing power and speeds now becoming available offer much promise.

**Modelling vs. Simulator Capabilities:** If the modelling system (e.g. EWES) and RF/EO threat simulator form an integral part of the specification, design and development process, then it is important, if not crucial, that their capabilities in a number of specific areas are very similar if not the same. Without this capability matching there is a real risk that correlation of results from the environment/EW equipment modelling and simulator/real EW equipment tests may not be possible without a substantial increase in the number of tests conducted or unnecessarily large error bounds and/or pass/fail criteria. This can come about, for example, if the emitters in the scenarios within the environment model and threat simulator start at different times and/or scan positions. When merged with the energy intercept algorithms for the sensor in the respective systems, it can easily be envisaged that the pulse descriptor time history from the environment model and simulator may well be different; possibly with marked differences (including missed pulses). Thus, if marginally or substantially different pulse descriptor files are presented to the ESM model and the real EW equipment via post-antenna injection or irradiation, then differences will result in the track file reports vs. time, making the correlation of modelled and test results difficult. This can also be exacerbated if the emitter and scenario processing within the simulator is not fully synchronised with its RF generation system. By careful consideration of these aspects it is possible to enhance repeatability, minimise these effects and thus enable an appropriate level of correlation between modelled and test results, leading to adequate validation of EW systems' performance.

**Modelling Enhancements Needed:** BAe has conducted extensive investigations into the requirements for modelling and T&E capabilities necessary to support the conceptualisation, specification, design and development of modern RF EW systems, and have extended some of these investigations, which are continuing, into the EO/laser arena. The items of particular interest in the RF area are listed below. Most have been taken into account in the specification of two world-class RF threat simulators, an ECM response measurement system and a comprehensive EW data analysis capability. In addition an upgrade to our EWES capability includes changes relating to modelling vs. simulator issues described above.

1. **Terrain modelling:** Various terrain types and surface cultures within scenario; including reflectivity aspects and sea states. *Vertical* as well as horizontal plane modelling. Grid size, terrain map input (e.g. DMA and DTED).
2. **Multipath:** Forward ground bounce, own transmitter vertical ground bounce. Specular/diffuse reflections = signal phase difference and thus changed amplitude at ESM. Own and other emitter multipath from aircraft in close proximity (includes need for some level of RCS modelling of aircraft involved - complex).
3. **Near field effects:** dependent on frequency, transmit/receive antenna size; more relevant to large aircraft or low flyers.
4. **Antenna patterns:** Better emitter/sensor antenna beam pattern modelling: i.e. more data points per pattern.
5. **Third party tracking:** irradiation of ESM by emitter which is tracking/locked on to another aircraft in the scenario.
6. **Atmospheric effects:** Attenuation varying representatively with frequency; rainfall rates; ducting.
7. **Chaff:** Eject/bloom times and stream/drop characteristics.
8. **Repeatability and Correlation:** Ability to specify emitter boresight start values (e.g. all North, centre of scan on velocity vector of aircraft, or random). Same/similar parameter ranges/resolutions/accuracies as threat simulators.
9. **Emitters/Sensors on platforms, particularly aircraft:** Current systems largely employ 'point' platforms, e.g. each aircraft's emitters/sensors exist at one point in space. Need for wire grid 'model' of (at least) own aircraft on which emitters and sensor antennas may be placed. Need substantial computing power increase to enable this.
10. **Improved Modulation on Pulse:** Improved fidelity needed.

11. ECM Effectiveness: Closed loop effects of own (and hostile) ECM on emitter behaviour and performance is required if quantitative metrics of survivability are to be specified and demonstrated in the future; cf. also 6.2
12. Missile Modelling: Adequate fly-out model needed for missiles with active seekers. Proportional navigation homing is suggested minimum. Model needs to be same as that used in threat simulator.

## 5. COMMONALITY OF EW AND EMC ENVIRONMENT PREDICTION NEEDS

### 5.1 Realistic Environment and Probability of Exposure

Specification of the minimum necessary RF environment(s) in which aircraft have to operate is also a key issue in the cost and development timescales of new and/or modified aircraft and their avionics [6]. Modern Electromagnetic Compatibility (EMC) specifications, which are most often based on a worst case consideration with additional safety margins, simulate conditions which rarely, if ever, occur in real life. A number contain single value field strength levels across significant parts of the RF and radar bands, even though in some sub-bands transmitters do not exist. Thus there appears the possibility for cost/timescale reductions, which could be applicable across all military platforms, if a better RF environment prediction were to exist or be developed. The time line field strength/power density vs. frequency profile the aircraft is subjected to during its various mission types and phases, for peace- and war-time conditions, also affects RADHAZ. This is required to be known to ensure that aircrew are not hazarded and that there is no unacceptable hazard posed to on-board fuel systems and weapons/systems containing electro-explosive devices. For both EMC and RADHAZ, the item requiring determination therefore is, as for EW, the profile of power density vs. frequency vs. exposure time, i.e. the *probability of exposure*, and, in the case of EMC, the consequent *probability of upset* of avionic circuitry when the aircraft is *actually* irradiated with such an exposure profile.

### 5.2 HIRTA/EUROCAE Prediction Methods/Limitations

Currently the RF environment drivers behind EMC specifications in the U.K. are the High Intensity Radio Transmission Area (HIRTA) scheme [7] for military aircraft and the European Civil Aircraft Equipment (EUROCAE) User's Guide [8] for civil aircraft. Of late the HIRTA scheme has assisted EUROCAE Working Group 33 in the definition of the European RF environment. In each of these schemes a worst case is statically modelled where transmitters are effectively assumed to be permanently pointing their boresights directly at the aircraft under consideration. Both use equations based on optical point source theory to give far field power density ( $P_d$ ):

$$P_d = \frac{\text{Antenna Gain} \times \text{Mean Transmitter Power}}{4\pi \times \text{Main Beam Slant Distance}^2}$$

with appropriate near field adaptations, particularly relevant for sub-GHz emitters, and antenna radiation patterns only for sub-0.6 GHz emitters where significant off-boresight elevation and azimuth sidelobes can be encountered.

Calculations, which take into account multi-transmitter sites, are translated into HIRTA exclusion zones which are simple geometric shapes (right-cylindrical for ground/shipborne emitters and spherical for airborne emitters). With the possible exception of hovering or slow moving helicopters at very low levels, this represents an extreme worst case assessment as military aircraft moving at over 300 knots above a few hundred feet altitude are unlikely to be irradiated at any appreciable level by ground emitters for more than a few seconds in reality. The two schemes therefore, although adequate for their intended purpose, i.e. ensuring safety when in proximity to high power RF/radar transmitters, are both considered very conservative, due to:

- no modelling of emitter/aircraft relative motion,
- no modelling of emitter scan patterns,
- inadequate transmit antenna modelling, and
- only using worst case RF parametrics rather than a realistic set vs. time (e.g. *constant* illumination by a CW source is unusual, whereas mode changes between search, track, lock and back to search are more realistic).
- other shortfalls, e.g. section 4.3: terrain, multipath, weather effects and modulation on pulse.

Since the EWES environment modelling capability addresses most of the shortfalls of these other tools/techniques, it is believed that there is significant scope for its use to develop *realistic* environment predictions upon which an estimation of probability of upset of avionics can be superimposed to yield higher quality EMC specifications. Aspects of BAe research are currently addressing this potential.

## 6. EW TEST AND EVALUATION IMPROVEMENTS

The development timescales of any avionic system is dominated by the T&E process, particularly so in the case of RF/EO EW systems. Table 1 shows the typical life cycle of aircraft EW systems prior to in-service use and shows T&E elements at the EW equipment supplier and the aircraft system integrator (avionic rig and aircraft ground/flight test). Operational Evaluation flying by Air Forces just prior to service use is a further T&E element. A major internal study of EW systems integration over many years and a number of aircraft types showed that many of the problems encountered, some 85%, could have been discovered much earlier in the development process, as shown in Table 2, by a combination of better T&E tools/techniques and specification/design methodologies. Although this underlined the possibility of verifying the majority of EW systems performance characteristics long before flight, through a combination of modelling, avionic rig and aircraft ground tests in anechoic chambers, it also showed that there would be a continued need for EW flight testing - albeit greatly reduced. Table 3 shows locations and techniques which can be used to support the development process. To minimise development costs and timescales it is necessary to push as much as possible of the T&E work to the top of the table. BAe Defence (Military Aircraft Division) is making much progress in enabling this by the provision of new/updated EW test and modelling capabilities.

## 6.1 Threat Simulators

The need for, use and availability of RF threat simulators for laboratory, chamber, flight line and test/training range is widely recognised and documented [9-13]. Such simulation ranges from signal generators, a number of which now have both very wide frequency range (e.g. 100 kHz - 40 GHz) and internal pulse/frequency modulation capability, to arguably the two most capable systems at this time - the Advanced Multiple Environment Simulator (AMES II) by Advanced Systems Development Inc., and the Combat Electromagnetic Environment Simulator (CEESIM) by Amherst Inc. Figures 8 and 9 are block diagrams of these two systems, showing the substantial complexity of the test tools required to adequately stimulate modern ESM and ECM systems. Having recognised the value of such simulators to the T&E process it is important from a cost standpoint, as world-class RF threat simulators are multi-million dollar items, to ensure that the simulator to be used at each point of the life cycle (see Table 3) is not over-specified. Here again is seen the importance of precise definition of the electromagnetic environment and scenarios, as the complexity and specification of the simulator required is directly driven by those items. From consideration of the scenarios and environment the key cost drivers of the simulator can be specified:

- Number and frequency sub-banding of RF channels, yielding the pulse density capability (of the order of 1-10 million pulses per second for modern ESM systems [14]).
- Number of simultaneous active emitters at any time.
- 'Concurrency' (how many of what type of emitter at any time) - a significant complexity/cost driver if a number of pulse doppler radars, CW emitters and lower pulse repetition frequency emitters need to be simulated simultaneously.
- Number of emitters and platforms per scenario.
- Pulse % drop-out tolerable by the EW equipment under test.
- Tolerable noise floor/bandwidth, intra-/inter-pulse noise levels, harmonics/spurious and inter-modulation signals.
- RF Output: 4, 6 or 8 port DOA; phase interferometer array.
- Power output, both for the post-antenna injection and (amplifier/transmission system) free space irradiation cases.

## 6.2 ECM Response Measurement

To evaluate ECM systems it is necessary to stimulate their receiver system, either ECM-specific or the ESM in the case of some modern ESM-ECM systems, and this is achieved by use of the simulators previously discussed. For high quality T&E work it is necessary to simultaneously stimulate ESM and ECM receiver elements for both post-antenna signal injection and irradiation cases. To enable this, special simulator frequency sub-banding, output power and combining arrangements may be required, especially if the simulator can combine other on-board aircraft transmitters and harmonics/intermodulation products thus caused into its outputs.

ECM response measurement can be achieved through use of spectrum analysers and, more recently, by comprehensive and easy to use pulse modulation analysers, e.g. Hewlett Packard 5373A. However such capability is only suitable for simple ECM engagements and is manually and experience intensive. To be able to sort and recognise an ECM technique from an RF environment containing many pulsed/CW emitters as well as transmissions from other aircraft emitters, then establish that the correct technique has been engaged spatially on the appropriate threat emitter is complex and well beyond the scope of such equipment. For this task a new generation of ECM Response Measurement System (RMS) has been specified and ordered by BAe which largely automates this task for laboratory and aircraft chamber/open air trials. Once again the environment and scenarios form the backbone of the specification of this equipment. By sampling the simulator output and the ambient RF environment, and through containing a pre-defined list of ECM techniques vs. their RF parametrics, the RMS is able to quickly identify ECM transmission by direction, time and emitter being jammed.

Currently the *effectiveness* of an ECM system is very difficult to measure absolutely. Survivability is a key issue in determining mission success and fleet affordability, but its quantification is made more difficult by the many interacting items affecting it (tactics, countermeasures engagement and/or deployment, SEAD/SOJ/ESJ support levels to the raid package, and so on). To quantify the survivability of an aircraft it is necessary to develop metrics which can be realistically specified and cost-effectively demonstrated with acceptable repeatability. Modelling has a role to play here [11],[15] but it is thought that a more realistic way forward, which would probably also achieve higher credibility with air crew, may be a statistical model determination based on chamber tests of a selected number of ECM types and technologies. Determination of the metrics and qualification/measurement of aircraft performance could be achieved via a modified threat simulator and RMS, where the threat simulator output is modified by the ECM transmitted from the aircraft. This topic of *Measures of Effectiveness* has attracted much attention in recent times, particularly in the U.S.A. where the Association of Old Crows has recently completed a study for the DoD on this topic [16].

## 6.3 EW Test Data Analysis

As discussed in section 4.2, a comprehensive tool is required for the parametric analysis of EW test data and its correlation with simulator and/or EW environment/equipment modelling outputs. The lack of such capabilities in the past is believed to have contributed much to the apparent differences between equipment and aircraft EW test results. Such a new tool has been specified and ordered by BAe which will enable, in addition to the near real-time correlation capability of the ECM RMS (cf. 6.2), post-test analysis of aircraft avionics/EW equipment data and threat simulator data. This includes correlation of simulator-generated data with that of the EW system under test and subsequent time history and statistical analysis. Multi-parametric comparison of test and simulator data against engineer-defined correlation 'windows' can also be carried out automatically.

In combination with precise scenario definitions, capable and realistic simulation, the ECM RMS, and a controlled, anechoic chamber electromagnetic environment, this new generation of EW analysis tool, enabled by computing advances in recent years, will enable quantitative and repeatable EW equipment, sub-system and on-aircraft tests.

#### **6.4 The Need for Correlated EO and RF Threat Simulation**

The importance of precise specification of the EO environment and scenarios is covered in section 4.4. For T&E of EO equipments there is a need therefore for the generation of appropriate stimulus for irradiation of sensors and post-sensor injection. In the case of lasers this is fairly straight forward for the post-sensor and direct irradiation of the sensor (via a closed 'hood') cases for un-installed equipment and avionics rig work. For the future, the use of multi-spectral sensors, data fusion, knowledge-based systems and fully integrated weapons systems on aircraft mean that it will be necessary to provide co-ordinated RF/EO stimulus to the EW system, particularly of IR/UV Missile/Laser Warners and ESM-ESM, and other aircraft RF/EO sensors. This poses a T&E problem as free space firing of lasers poses a safety hazard and there are no established IR/UV simulators akin to the well established radar/RF ones. Development work on such simulators is in progress in the U.S.A. and the Real-Time IR Scene Simulator (RISS) by Amherst Inc., which can also have UV capability, is believed to be the world leader at this time. Figure 10 gives a block diagram of the RISS. Use of such a system in conjunction with a RF threat simulator and laser irradiation and control system, will enable controlled and simultaneous multi-spectral stimulation of aircraft Forward Looking IR, IR Search & Track, passive Missile Warning Systems and Missile/Weapon Guidance Seekers. The use of such a comprehensive sensor stimulation suite in conjunction with an anechoic chamber may offer significant test quality and cost/timescale improvements on the combined aircraft ground and flight trials currently necessary to develop and clear such systems into service.

#### **7. IMPROVED EW DESIGN/T&E METHODOLOGY**

The thrusts of the previously described improved EW specification, design and T&E methodology are:

- Obtain the agreement of Government agencies on the principle of precise RF/EO EW scenarios pre-contract signature. Work with those agencies and EW equipment suppliers to support timely production of scenarios. Explore further the application of such methodology and tools to the EMC arena.
- Continue driving more of the EW system development process away from the highly expensive and time consuming flight test phase, through avionics rig, laboratory and aircraft in anechoic chamber trials, towards suitably validated modelling wherever possible.
- 1995 commissioning by BAe of EWES upgrade, transportable (1.0 MPPS) and (1.5 MPPS) RF threat simulators, transportable ECM Response Measurement System and comprehensive EW data analysis utility.
- Continue investigations of shortcomings of present modelling and T&E tools/techniques, particularly those identified herein and especially those in the area of EO threat simulation and ECM effectiveness modelling/test. Use this data to target improved capabilities to optimise development costs and timescales.
- Build on over 20 years of BAe experience of Operational Analysis, EW environment modelling and EW integration rig and aircraft trials work. Work with EW equipment suppliers to ensure affordable and mission effective EW system solutions for military aircraft, whether upgrades or on new airframes. Use of these Industry capabilities can lead, in co-operation with Government/Air Force agencies, to much increased quality specifications leading to aircraft weapon systems which are fully fit for purpose at the most affordable price.

#### **8. CONCLUSIONS**

BAe Defence Military Aircraft Division has learned many lessons from its 20+ years of involvement in EW equipment installed on its military aircraft. It has enacted most of the recommendations of internal study reports on its performance in this area and this year will augment upgraded EW environment and Operational Analysis modelling tools with major world-class EW test capabilities.

This paper has highlighted a number of the issues involved in the specification, design, development and test of EW systems and concludes that the dominant factor in many of the key areas of Affordability, Mission Effectiveness and Survivability is a precise definition of the electromagnetic environment in which the aircraft and its systems must operate correctly. A revised specification, design and development process has been described which can be used to provide evidence of performance at realistic cost and with maximum integrity. A number of potential enhancements to current generation modelling and test and evaluation tools are identified and BAe research and development work is ongoing in these areas.

With environment and scenario modelling tools and techniques in place, it is believed that Air Forces, Industry and Governments alike would all benefit from this precise and unambiguous definition of the radio/radar and electro-optic environments at the pre-contract stage for new or upgraded EW equipments.

#### **9. ACKNOWLEDGEMENTS**

The authors wish to thank BAe Defence (MAD) for permission to publish and acknowledge input/comment from: G. Slater (RMPA DASS Manager), C.D.Hinds (EF2000 DASS Manager), Dr. C.P. Loller (Head of EW & Stealth Facilities), K. Lawton (Specialist, EW Testing), K. Smith (Operational Analysis), I.P. MacDiarmid (EM Hazards Specialist) and Prof. R.J. Simpson (Univ. of Central Lancashire, U.K.). Acknowledgement is also made for material used in the paper/presentation to: Messrs. Peter Crouch, Data Sciences (U.K.) Ltd. [EWES], Larry Diamond & Joe Gorelick, Advanced Systems Development Inc. [AMES II] and Bob Cockrell & Larry Robinson, Amherst Systems Inc. [CEESIM and RISS].

**10. REFERENCES**

1. **Wade, L.** (Condor Systems) "The Significance of a Valid Threat Data Base to Effective Radar Warning Receivers." Presentation at Tutorial Session at 1994 Int. Symp. of the Association of Old Crows, Washington, D.C. October 1994.
2. **Audone, B.** "The Electromagnetic Threat to Future Avionic Systems." AGARD Conf. Proc. No. 417: "The Design, Development and Testing of Complex Avionic Systems," Las Vegas, U.S.A. 27 April - 1 May, 1987. [Unclassified]
3. **Cabayan, H.S.** "Current Status of High Power Microwave Effects and Simulation." High Power Microwave Systems for Defense Conference, Air Force Weapons Laboratory, Albuquerque, New Mexico, U.S.A., December 1-5, 1986 [Unclassified]
4. **Herskovitz, D.** "Killing Them Softly." J. Electronic Defense, August 1993, pp.41-46.
5. **Bolino, J.V. et al.** "Threat Simulator Validation", J. Electronic Defense, September 1991, p.40.
6. **Woolnough, R.C.N. and Pywell, M.** "The Control of RF Radiation Hazards in an Industrial and Airfield Environment." I.E.E. 9th Int. Conf. on EMC, Univ. of Manchester, U.K. , 5-7 September 1994.
7. **Elton, L.D.** RF Environment External to Aircraft. Vol.1, Issue 2a: "The Calculation of Aircraft Safe Distances for the Definition of High Intensity Radio Transmission Areas (HIRTA) in the United Kingdom." BAeSEMA report MNC 00220, September 1992. [Unclassified]. Vol.2: "Ship and Aircraft based Transmitters." March 1992. [Classified].
8. **EUROCAE USER'S GUIDE FOR AMJ No. XX.** Guidance to the Certification of Aircraft Electrical/ Electronic Systems for Operation in the High Intensity Radiated Field (HIRF) Environment. (Certification Requirements and Procedures) EUROCAE WG33 Sub-Groups 2&3. Draft Version 2.2, 4 March 1993.
9. **Fossier, P.** "MESA: Modular Interactive Electronic Warfare Simulator suited to the coverage of EW Equipment life cycle." Presented at AGARD Meeting on "Challenge of Future EW System Design," October 1993.
10. **Herskovitz, D.** "Technology Survey: A Sampling of Electronic Warfare Simulators." J. of Electronic Defense, December 1994, pp.56-66.
11. **Peccini, M., Veredice, A., Formica, A. and Conte, F.** "Real-Time E.W. Test Range Simulator." Presented at AGARD Meeting on "Challenge of Future EW System Design," October 1993.
12. **Stallard, R.** "Mobile EW Trials Facilities at DRA Farnborough." Presented at AGARD Meeting on "Challenge of Future EW System Design," October 1993.
13. **Hardy, S.M. and Lum, Z.A.** "Simulation Shadowland." J. Electronic Defense, November 1994, pp.38-47,67.
14. **Schleher, C.D.**, "Introduction to Electronic Warfare." Artech House (1990). ISBN 0-89006-142-4. p.38, Tab. 1-7.
15. **Teris, M.** "Current ECM Evaluation Methods." Article in J. Electronic Defense, January 1995 supplement; adapted from "Penetrator - An Integrated EW Encounter Simulation," Topics of Engineering, Vol.V, Pub.: AIL Systems, 1994.
16. **Porter, Rusty (AOC President):** "Taking the Measure of EW's Effectiveness". J. Electronic Defense, Vol.18, No.1, January 1995, p.12 and Vol.18, No.4, April 1995, p.10.

**Figure 1: Typical Aircraft EW Suite**

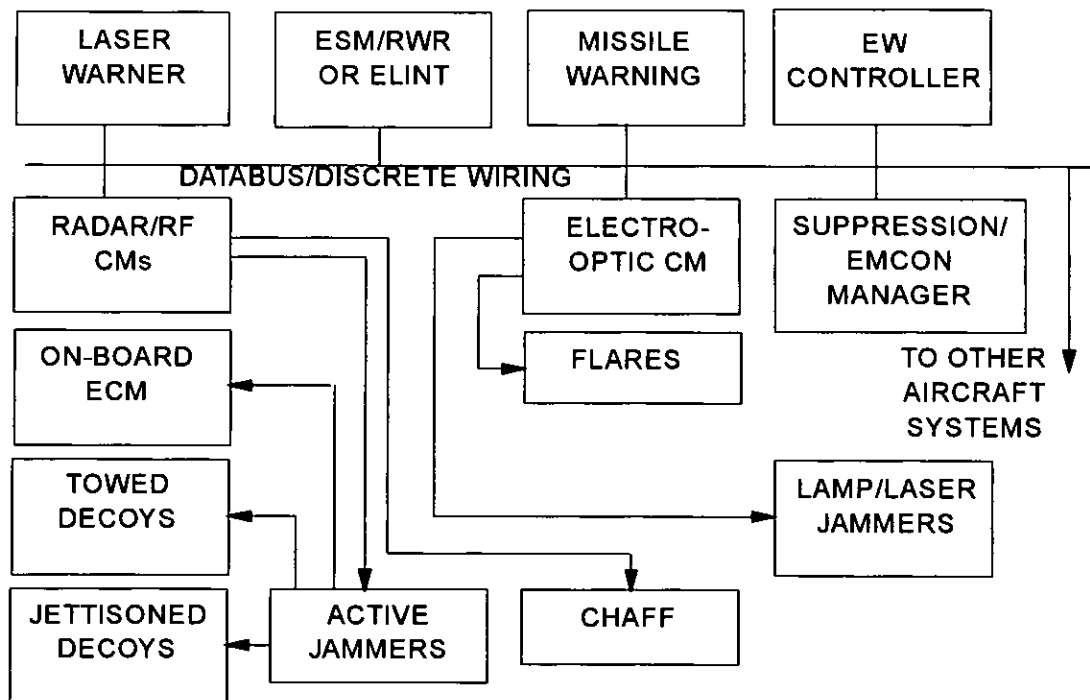
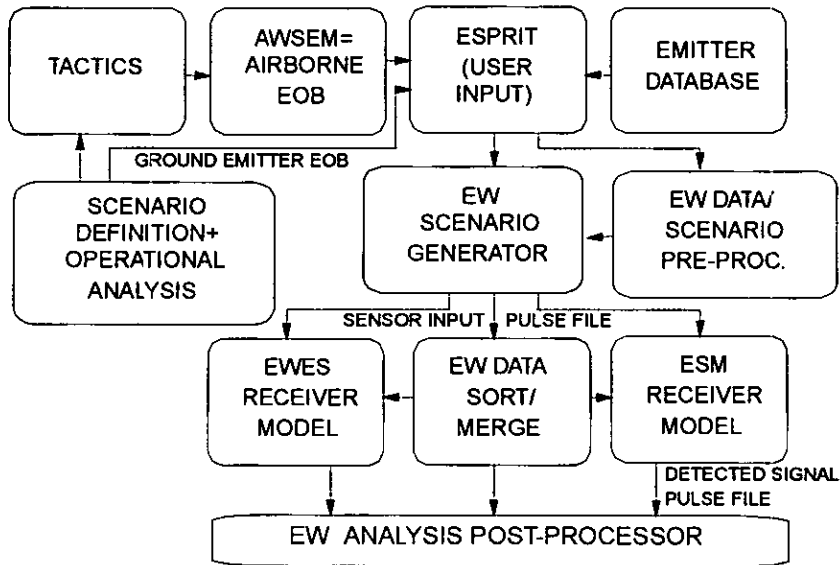


**Figure 2: Block Diagram of EWES and AWSEM**



**Key to Figure 2:**

- Threat Scenario Definition = descriptive + initial conditions
- Operation Analysis: Tactics and engagement rules into AWSEM = Electronic Order of Battle (EOB)
- EOB comprises platform manoeuvres and events plus emitter events (e.g. mode changes)
- Enhanced Scenario Preparation Interactive Tool (ESPRIT) is prime Graphical User Interface.
- ESPRIT output = full scenario manoeuvres and EOB list for input into Scenario Generator.
- EW Data and Scenario Pre-Processors are optional.
- EW Data Sort/Merge Utility, used for very large scenarios, is also optional.
- BAe currently have all but EWES Receiver Model and Scenario Pre-Processor.

**Figure 3: Computing Resources for EWES**

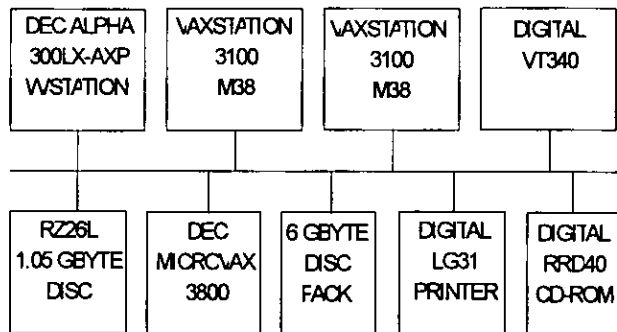


**Figure 4: Use of Modelling in Validation of ESM Performance**

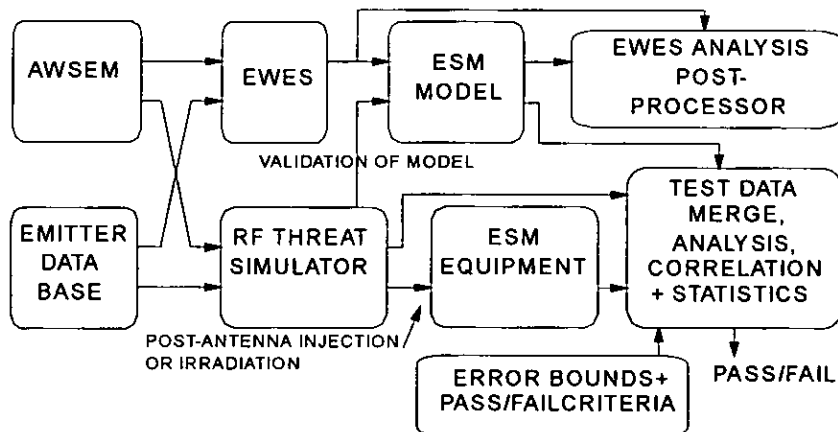


**Figure 5: Typical ESPRIT Tactical Scenario Display**



**Figure 6: Typical EW Scenario Generator Pulse Descriptor File Listing**

TYPE ID NAME	RF MHz	RFVAR %	LENGTH microsec	PLAT BRG degs	PLAT ELEVN degs	AMPLITUDE dBW/m <sup>2</sup>	RANGE km	INTERVAL ms	POL ANGLE degs	RATIO %	TIME hh:mm:ss
pulse 8 FIREX	2700.00	0.0	15.00	228.45	0.0	-84.871	100.00	0.234	0.0	100.00	00:00:00.000481411
pulse 8 FIREX	2700.00	0.0	15.00	230.14	0.0	-84.560	100.00	0.230	0.0	100.00	00:00:00.000604916
pulse 8 FIREX	2700.00	0.0	15.00	231.79	0.0	-84.255	100.00	0.226	0.0	100.00	00:00:00.000924869
pulse 8 FIREX	2700.00	0.0	15.00	233.42	0.0	-84.070	100.00	0.274	0.0	100.00	00:00:00.001150917
pulse 1 REDEW	3000.00	0.0	10.00	233.64	0.0	-85.514	300.11	0.200	0.0	100.00	00:00:00.001167467
pulse 6 DEWEW	7400.00	0.0	3.70	233.71	0.0	-81.633	288.47	0.420	0.0	100.00	00:00:00.001191417
pulse 5 SEATE	9350.00	0.0	20.00	234.07	0.0	-86.877	340.68	0.300	0.0	100.00	00:00:00.001241425
pulse 3 CANAB	9700.00	0.0	12.00	234.92	0.0	-88.508	200.01	2.000	0.0	100.00	00:00:00.001360138
pulse 7 VRA	15824.39	0.0	5.00	234.97	0.0	-86.671	384.73	0.650	0.0	100.00	00:00:00.001365903
pulse 1 REDEW	3000.00	0.0	10.00	234.98	0.0	-84.394	300.11	0.150	0.0	100.00	00:00:00.001367467
pulse 8 FIREX	2700.00	0.0	15.00	235.36	0.0	-84.42	100.00	0.230	0.0	100.00	00:00:00.001424470

**Figure 7: Commonly Used EW Graphical Analysis Pages**

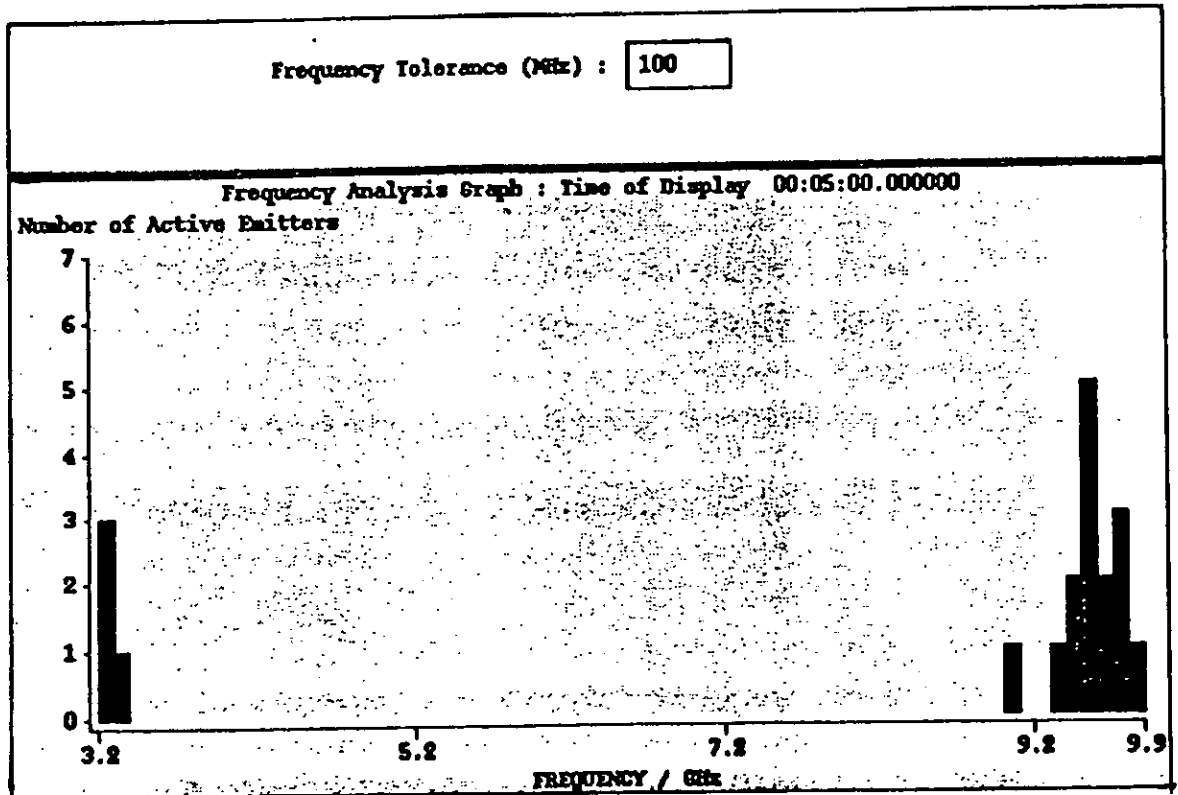
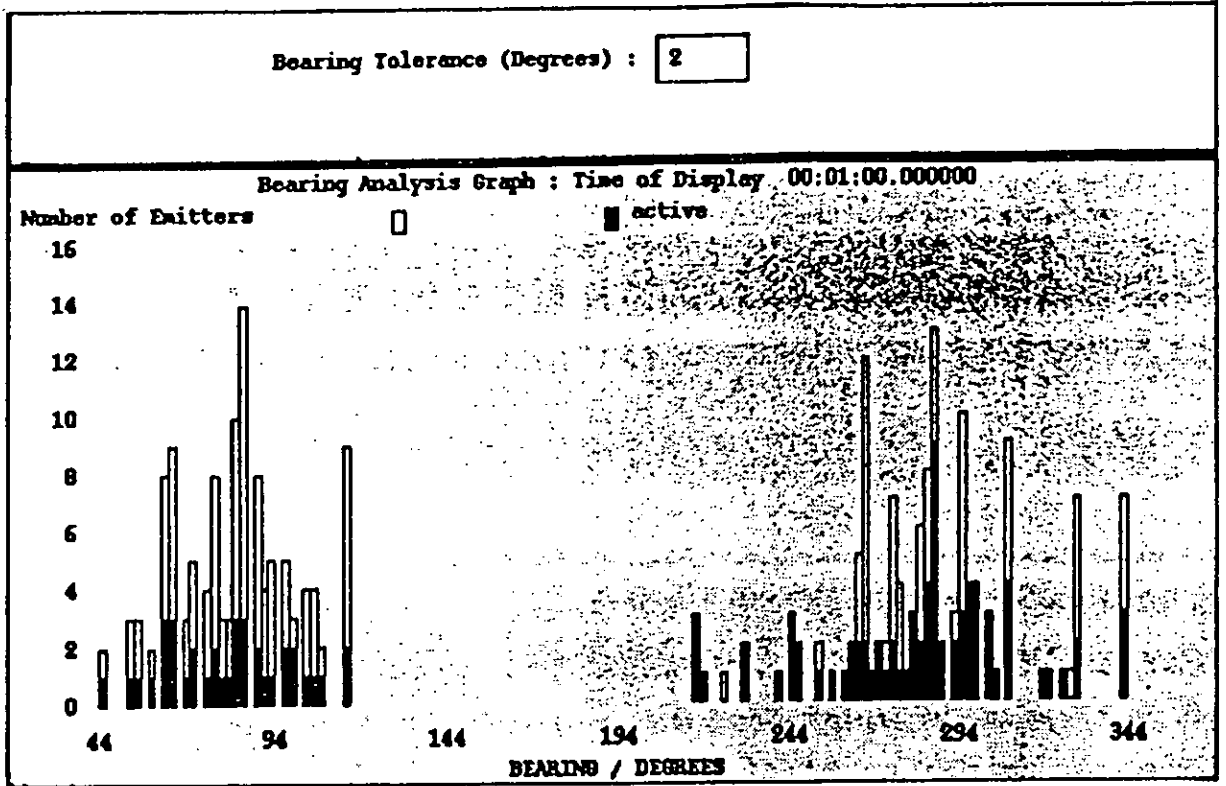


**Table 1: EW Development Life Cycle:**

Air Force/Government Agency	Operational Requirement
	Weapon System Specification
	Air Vehicle Specification
Aircraft Prime Contractor	System/Equipment Specifications
EW Equipment Manufacturer	Hardware/Software Specifications
	Design/Build/Code Hardware/Software
	Equipment and EW Sub-System test
Aircraft/Systems Integrator	Avionic integration rig tests; aircraft ground and flight tests.
	Corrections/Modifications and specification changes if necessary.
Air Force	Operational Evaluation leading to Initial Operational Clearance.
All parties	Changes/corrections leading to Final Operational Clearance.

**Table 2: Earlier Discovery of EW Systems Integration Problems**

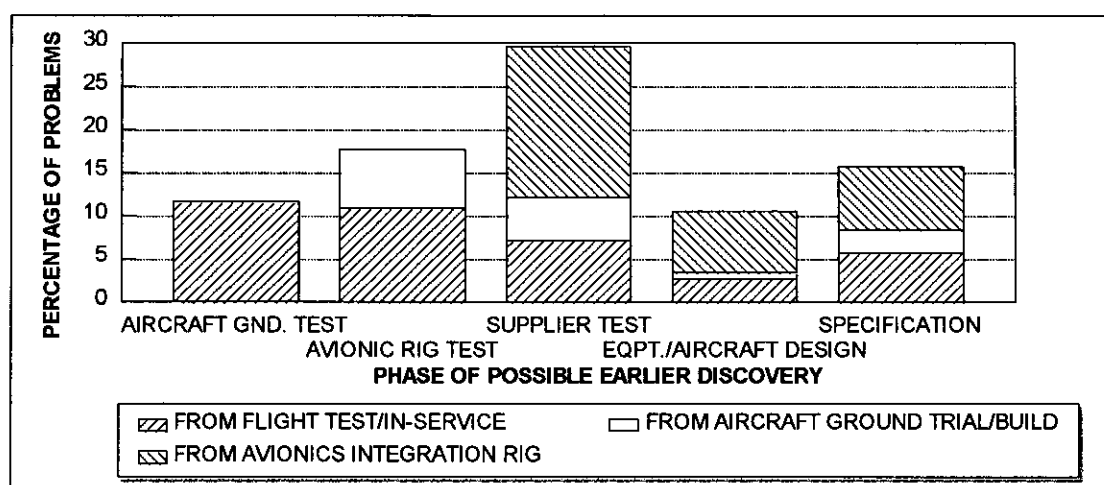


**Table 3: Development Test/Evaluation Locations and Technique**

Who/Where	What and How
<i>Aircraft &amp; EW manufacturers:</i> Own premises.	Environment/EW equipment modelling via use of EWES-type models and proprietary/generic equipment models
<i>EW equipment manufacturer:</i> Own premises.	Rig test: software, hardware, equipment, sub-system. Post-sensor injection; free space irradiation; anechoic chamber.
<i>Aircraft/Systems Integrator:</i> Sub-System Rig, Avionic Integration Rig	Progressive integration of equipment and sub-systems into full aircraft weapon system. Post-sensor injection and limited free space irradiation.
Airfield (e.g. Warton, U.K.)	Open air EW and EMC tests. RCS measurement, DOA measurements. Free space irradiation of installed EW equipments.
Anechoic chamber (U.K.)	Whole aircraft EW tests in secure and controlled electromagnetic environment. Irradiation using RF simulator and response measurement system for ESM/ECM.
Locally (North U.K.)	Local flight trials, covering test points now yet done + confirmation of selected items tested earlier. Signal generator(s)/threat simulator + amplifier/antenna.
e.g. RAF Spadeadam EW Training Range, Aberporth, BAe's North Sea Combat Range.	U.K. Flight trials: DOA, antenna coverage, EW performance demonstration. Irradiation by simulators/emulators, real radars; often involving other platforms.
U.S. anechoic chamber, e.g. Benefield Anechoic Facility, California.	Tests where either aircraft size or test requirements, e.g. multi-aircraft, dictate out-of-U.K. tests.
U.S. EW Flight test ranges: Nellis, Eglin, China Lake, Patuxent River.	Tests not possible with U.K./E.C. facilities, e.g. full aircraft in-flight RCS measurement & total weapon system performance in realistically dense RF environments. Free space irradiation + many emitter types/numbers.

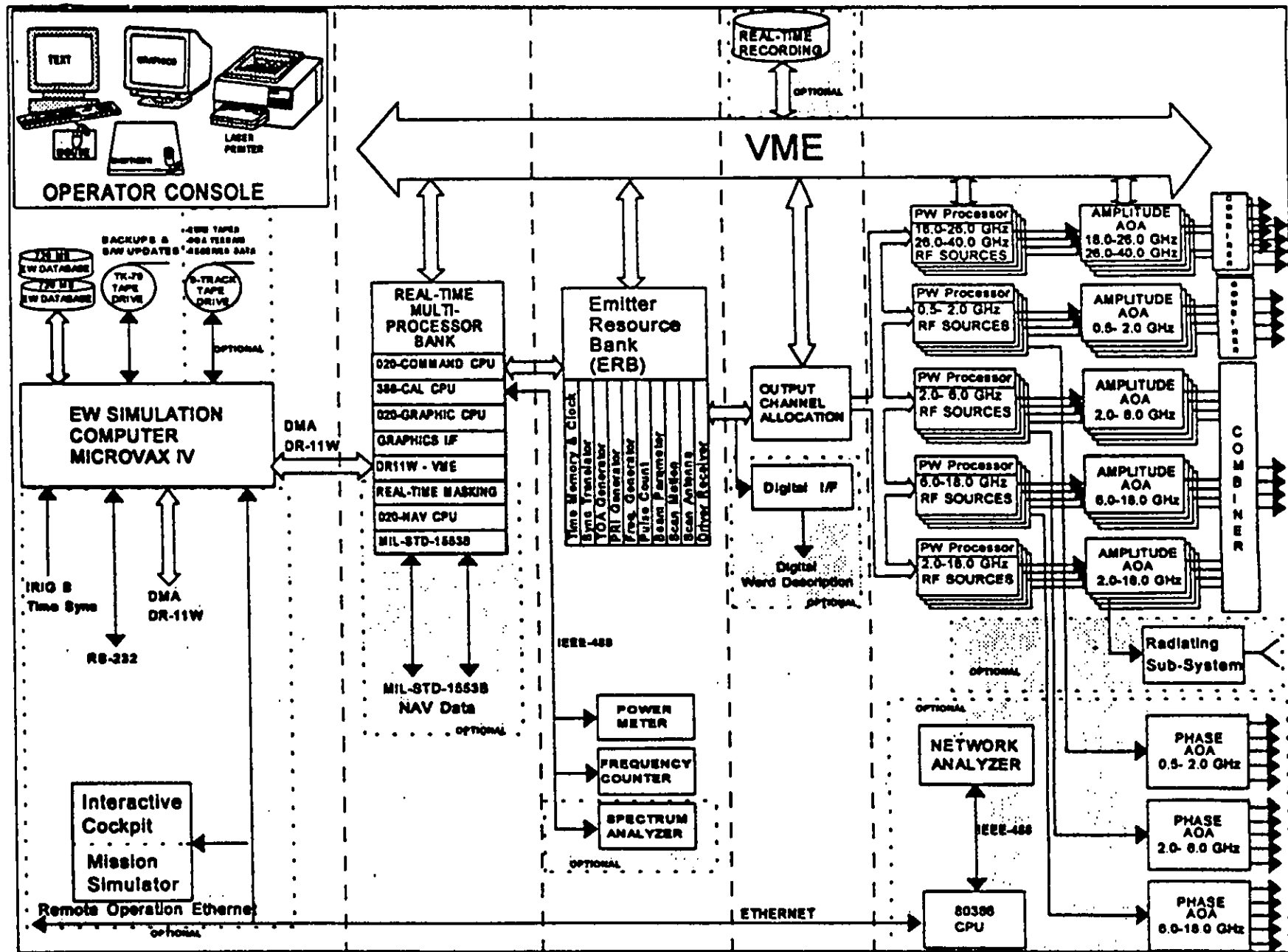
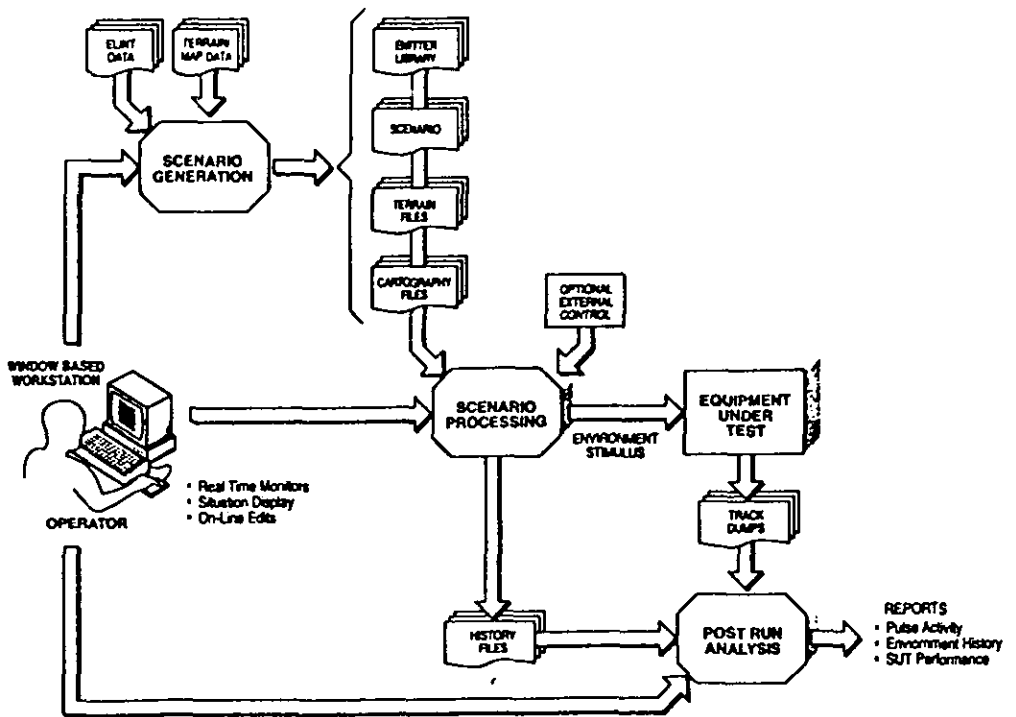
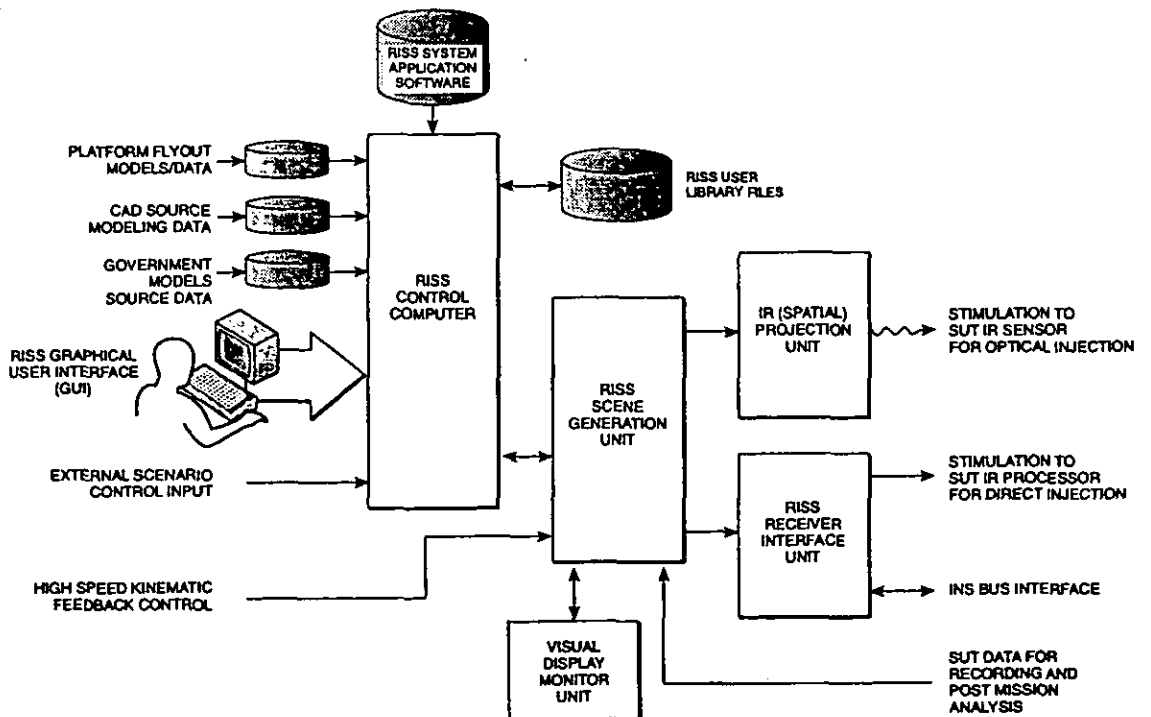


Figure 8: AMES II Block Diagram

**Figure 9: CEESIM Block Diagram**



**Figure 10: Real-Time Infra-Red Scene Simulation System**



**APPENDIX D: PREDICTION OF CUT-OFF FREQUENCY FOR PERIPHERAL SLOTS AND BAY DOOR/PANEL INGRESS CHARACTERISTICS**  
**ON JAGUAR FLY-BY-WIRE AIRCRAFT** (Appendix A of [3-11])

**D1 INTRODUCTION**

By considering that all panels/bay doors are perpendicular to the impinging wavefront, that they are not backed by cavities, and assuming that energy only enters the bays by the peripheral slots, some predictions may be made concerning cut-off frequencies and relative shielding performance of the four bay door/panels tested in Phases 2(a) and 2(b). Fig. D.1 is a scaled representation of the outlines of the bay door/panels tested during Phase 2(b), whilst Fig. D.2 is that for the Front Avionics Bay tested in Phase 2(a) of these investigations. The figures include the bolt positions and the lengths of the slots so formed.

**D2 SLOT CUT-OFF FREQUENCIES**

For a slot with a longest dimension  $d$ , EM radiation will pass freely through the slot with no attenuation if  $\lambda < 2d$ , where  $\lambda$  = the wavelength of the radiation [D-1]. When  $\lambda = 2d$  the shielding is zero. That is the cut-off frequency  $f_c$  is equal to  $\frac{c}{2d}$  where  $c$  is the propagation velocity of the wave. From equation (1) of [3-11], the attenuation  $R$ , for  $\lambda > 2d$ , may be expressed as  $R = 20 \log_{10}(\frac{\lambda}{2d})$  for  $\frac{\lambda}{2} > d > t$ , and  $t$  = thickness. That is, for frequencies below  $f_c$  the attenuation should increase at 20 dB per decade of decreasing frequency. Table D.1 gives the predicted cut-off frequencies for the various slots found on the bay doors/panel tested in the Phase 2 investigations. An example calculation is given here for the first bolt spacing in the table, along with an estimate of the error in the derived  $f_c$ .

Bolt spacing,  $d = 0.038 \pm 0.002\text{m}$  (i.e.  $\pm 5.3\%$ ), so  $2d = 0.076\text{m} \pm 5.3\%$

Thus  $f_c = \frac{c}{2d} = \frac{3 \times 10^8}{0.076} \text{ ms}^{-1} = 3.947 \text{ GHz} \pm 2.63\%$  (i.e.  $\pm 0.104 \text{ GHz}$ ).

**TABLE D.1**

Panel/Bay Door	(Local) Horiz./Vertical	d(m)	2d(m)	$f_c$ (GHz)
55	H	0.04	0.08	3.95
55	H	0.05	0.11	2.83
55	H	0.07	0.14	2.08
55 (13 different spacings)	$V_{\min.}$	0.03	0.05	6.00
"	$V_{\max.}$	0.07	0.13	2.31
56	H	0.04	0.08	3.95
56	H	0.04	0.08	3.85
56	H	0.20	0.41	0.74
56 (8 different spacings)	$V_{\min.}$	0.04	0.08	3.95
"	$V_{\max.}$	0.20	0.39	0.77
Front Avionics	V	0.86	1.72	0.17
Front Avionics	V	0.53	1.06	0.28
Front Avionics	H	0.82	1.64	0.18
Front Avionics	H	0.79	1.58	0.19
Port Gun Bay	V	0.39	0.74	0.41
Port Gun Bay	V	0.35	0.70	0.43
Port Gun Bay	H	0.96	1.92	0.16

From the above the following predictions can be made for each bay:-

### **D2.1 Port Gun Bay Door**

For vertically or horizontally polarised wavefront, no attenuation should be seen since in both cases the cut-off frequencies are well below the 2-12 GHz range under consideration.

### **D2.2 Front Avionics Bay Door**

As for the Port Gun Bay, no attenuation should be seen for either polarisation of impinging wavefront over the range 2-12 GHz.

### **D2.3 Panel 55 (Fully Bolted)**

For a horizontally polarised wavefront the lowest cut-off frequency should be 2.08 GHz, although the other two bolt spacings in this plane give  $f_c$  at 2.83 and 3.95 GHz, and so no attenuation should be seen in the range 3.95-18 GHz. For the range 2-3.95 GHz some attenuation may be visible but, since it will be very small, will almost certainly be swamped by measurement errors. For the vertically polarised case there are thirteen different bolt spacings, giving the situation overall that  $2.31 \text{ GHz} > f_c > 6.00 \text{ GHz}$ . Whilst this is obviously a complicated case, it can be said that:

- a) above 6.00 GHz there should be no attenuation,
- b) between 2 and 2.31 GHz there should be 0.6 dB attenuation, which will be swamped by measurement errors, and
- c) between 2.31 and 6 GHz there should be no more than 7.4 dB of attenuation.

### **D2.4 Panel 56 (Bolted And Hinged)**

For a horizontally polarised wavefront the lowest cut-off frequency is 0.74 GHz, whilst the other two bolt spacings in that plane give  $f_c$  values of 3.85 and 3.95 GHz. As for Panel 55 the maximum possible resultant attenuation would be less than 1 dB and will not be discernible. For the vertically polarised case there are eight different bolt spacings, giving  $0.77 \text{ GHz} < f_c < 3.95 \text{ GHz}$ . So for the frequency range of interest there should be no more than 3.9 dB of attenuation for 2-3.95 GHz and no attenuation for 3.95-12 GHz.

## **D3 BAY DOOR/PANEL INGRESS CHARACTERISTICS**

One of the characteristics of interest in the overall airframe ingress equation is whether horizontally or vertically polarised wave fronts are dominant components, or whether ingress is essentially independent of polarisation.

### **D3.1 Peripheral Slot Ratios**

A first pointer may be obtained by comparing the lengths of total horizontal (H) and vertical (V) lengths of the periphery of each panel/door considered. Since, in D.2 it was predicted that most cut-off frequencies of the peripheral slots are outside the 2-12 GHz range of interest, this ratio of H:V can be said to apply over that frequency range. Table D.2 gives the total H and V lengths along with the ratio of H:V for each bay door/panel investigated.

**TABLE D.2**

Bay Door/Panel	Total Length (mm)		Ratio H : V
	H	V	
Front Avionics	1610.00	1390.00	1.16:1
Port Gun	960.00	740.00	1.30:1
55.00	906.00	1130.00	0.80:1
56.00	300.00	849.00	0.35:1

From the table it can be seen that, for the Front Avionics Bay, Port Gun Bay doors and Panel 55, the ratios are close to 1:1, indicating there should be little difference between

polarisations of the impinging wavefront. Panel 56 results show a clear dominance of vertically polarised signal, since the ratio is close to 3:1.

### **D3.2 Irradiation 'Footprint'**

Part of the Phase 2(a) investigation showed the use of Tx antenna half-power beamwidth and Tx-to-aircraft spacing could be used to ensure a small irradiation 'footprint' on the aircraft for the 4m and 25 m Slide positions. These predictions, ratified by that work, hold for the Phase 2(b) work with the following additions. Since the bay doors/panels of this phase of the investigations are close to the air intake, and partially under the left hand wing root, greater shielding effects should be seen as the Tx is moved to the positions towards the rear of the aircraft.

## **D4 LIMITATIONS OF PREDICTIONS**

The preceding predictions are meant to give pointers to the absolute and relative ingress performance of each of the bay doors/panels tested. They are by no means comprehensive, as the treatment of such a system of multi-slots on a complex shaped airframe at any frequency is not trivial. At microwave frequencies no evidence has been found to suggest it has ever been attempted or achieved.

To aid the derivation of modelling for microwave ingress, the following is a short list of those areas where the above predictions are known to be limited.

### **1. Airframe Shape:**

A method needs to be developed to cater for the analysis of shaped panels. In particular, it needs to examine how the slots are angled in all axes to the impinging wavefront.

### **2. The Peripheral Slots:**

These are by no means simple slots. Each is like a section of rectangular waveguide with two 90° bends, and can be considered to be loaded by the primer/paint and any environmental gasketting. This will be the main reason why zero attenuation is unlikely to actually occur above the cut-off frequency. Due to the complex shape of the three dimensional slots formed at the panel periphery, it is possible that higher (than  $TE_{10}$ ) order transmission modes may occur. This may then lead to higher energy ingress through a given slot than otherwise be expected.

### **3. Bolt Spacings:**

Most panels do not have equal bolt spacings around their periphery. As a result the effective cut-off frequency in any axis will vary according to that spacing using this model. The implication of this is that an ingress model would have to address the bolt spacings for each panel on the aircraft, and would therefore be different for each aircraft considered. Some method of reducing this potentially huge analysis task needs to be developed, probably by consideration of the results of the planned panel ingress investigations in the EMC laboratory.

### **4. Corners of Rectangular Panels:**

A right-angled slot antenna is formed between the bolt nearest the corner on both the horizontal and vertical sides. It has been assumed for these predictions that the corner itself is a bolt and therefore forms two slots. The treatment of this aspect is likely to be complex.

### **5. Intra-Slot Resonances:**

The model used assumes each slot on the periphery is likened to a single slot on a thin, flat sheet of metal extending to infinity in each direction. This is unreal and it is highly likely that the slots resonate between each other in a highly complex fashion, somewhat akin to the slotted antennas on the dishes of some modern military radars. This factor will also lead to great difficulty in predicting accurately the energy entering the bays through the slots.

## 6. Cavity-Backed Slots:

No account has been taken of the fact that the panels/doors on the aircraft are backed by cavities in the forms of complex shaped bays with partial loading by cables, pipes, equipment and their racks. Although the treatment of simple rectangular cavities can be extended from microwave reference books, e.g. [D-2], no work had been found on either empty or loaded cavities of complex shapes such as those found on aircraft.

## 7. Slot Antenna "Pass-Band"

The model used merely treats the slot as having a value of  $f_c$  with zero attenuation above that frequency and 20 dB attenuation per decade decreasing frequency below  $f_c$ . In fact, a perfect slot behaves as a resonant slot antenna where  $f_c$  is the antenna resonant frequency. Theory and measurements for such an antenna agree below  $f_c$ , but above that frequency the picture is more complicated. Theory dictates that the antenna should then exhibit attenuation with increasing frequency, but with (lower amplitude) resonances at  $\frac{n\lambda}{2}$ , where  $n$  is an odd integer (1,3,5, etc.). It is highly probable that complex bay peripheral slots cause many resonances, some of which possibly lead to zero attenuation at many other frequencies above  $f_c$ . Some practical quantification of the performance above  $f_c$  will be required to establish how the model should be altered.

## D5 REFERENCES

- [D-1] Grant, Peter. Emitter/Susceptor Profiles Predict Proper Shielding: Part 2: EMI Shielding. Microwaves (USA), Vol.21, Part 7, pp.79-81,83,4. 1986.
- [D-2] Baden Fuller, A.J. Microwaves, 2nd. Ed. An Introduction to Microwave Theory and Techniques. ISBN 0-08-023227-8.

Figure D.1-1: Outline of Panels on EMC Demonstrator Aircraft

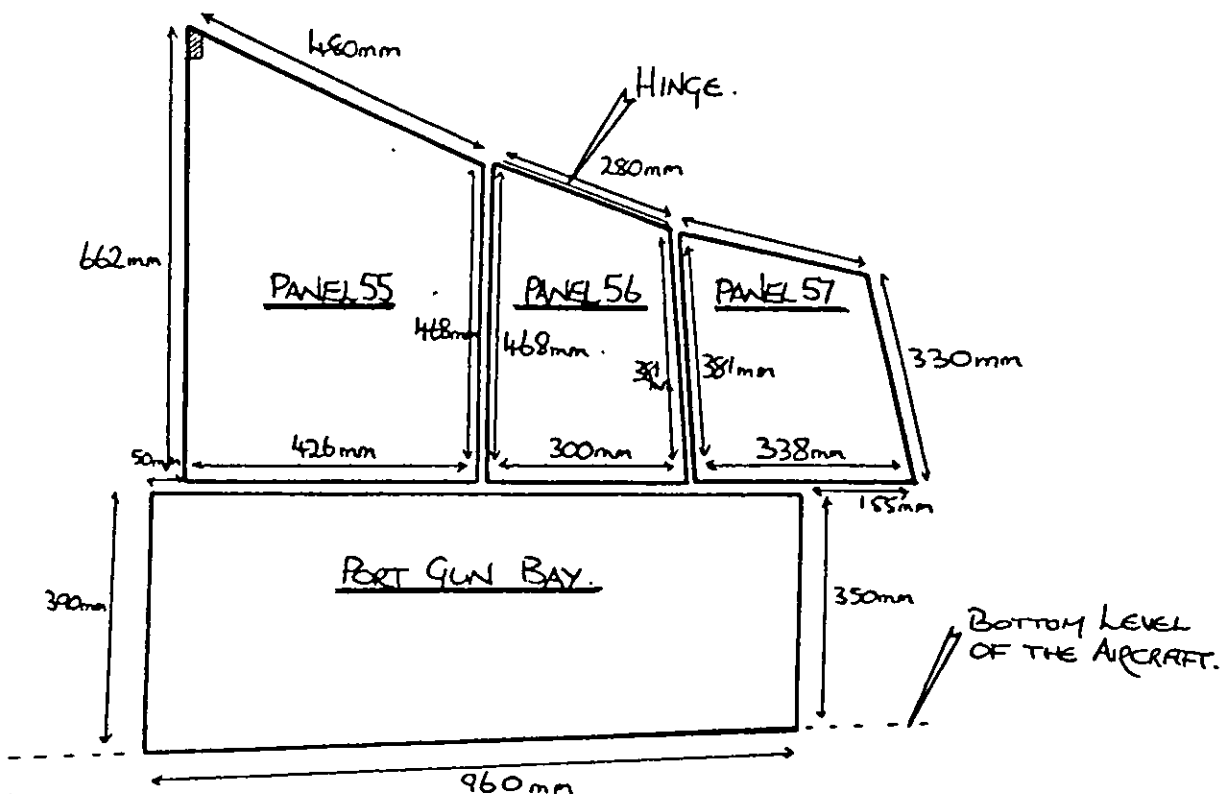


**Figure D.1-2: Panel 55 Bolt Spacings**  
(Scale 5:1)

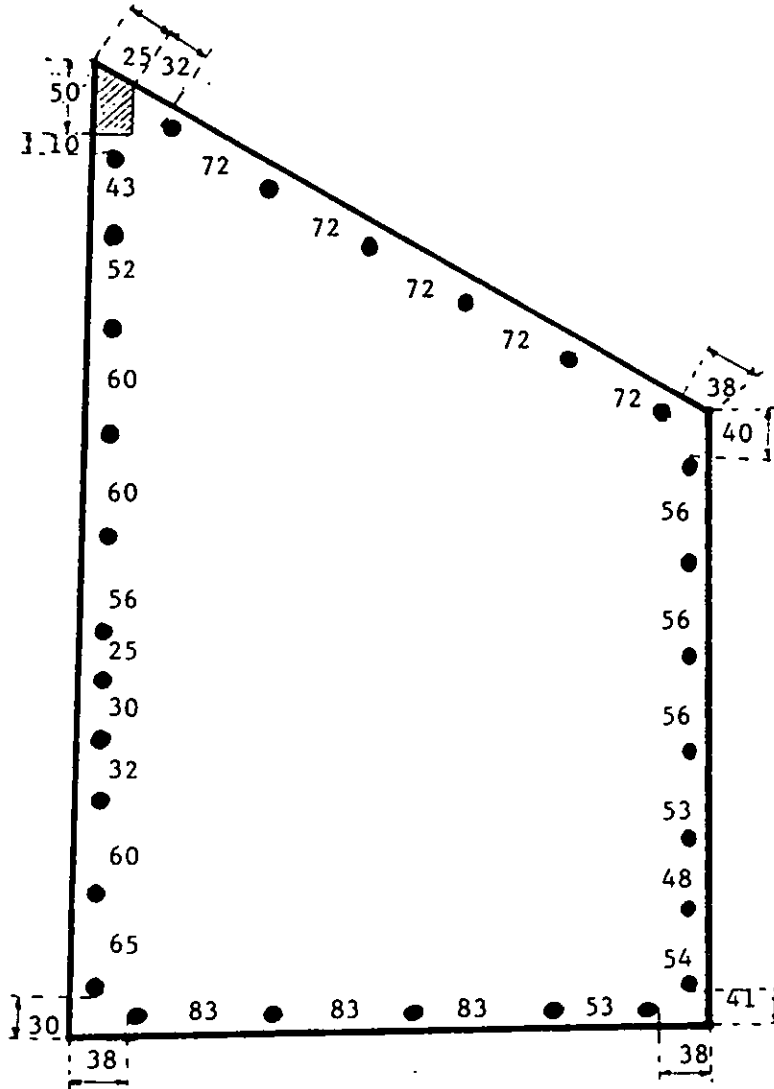


**Figure D.1-3: Panel 56/57 Bolt Spacings**  
(Scale 5:1)

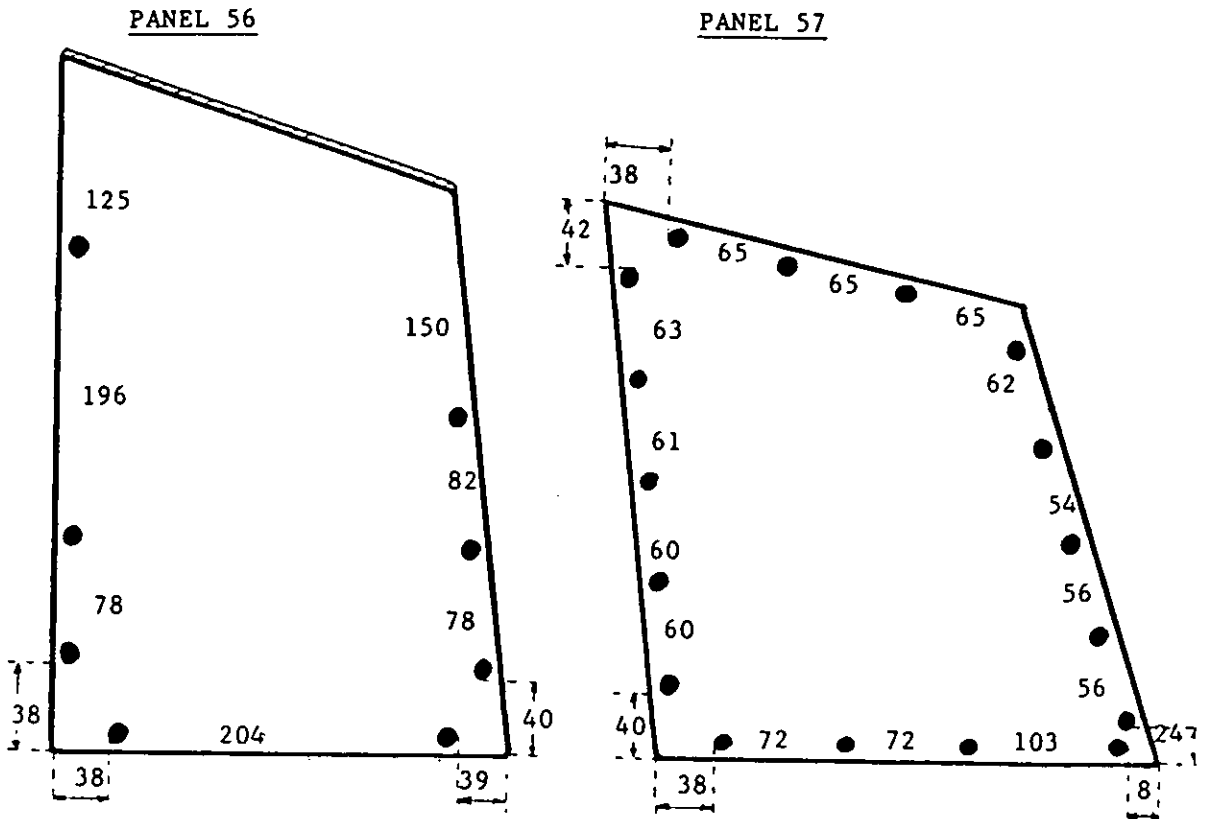


**Figure D.1-4: Port Gun Bay Bolt Spacings**  
(Scale 5:1)

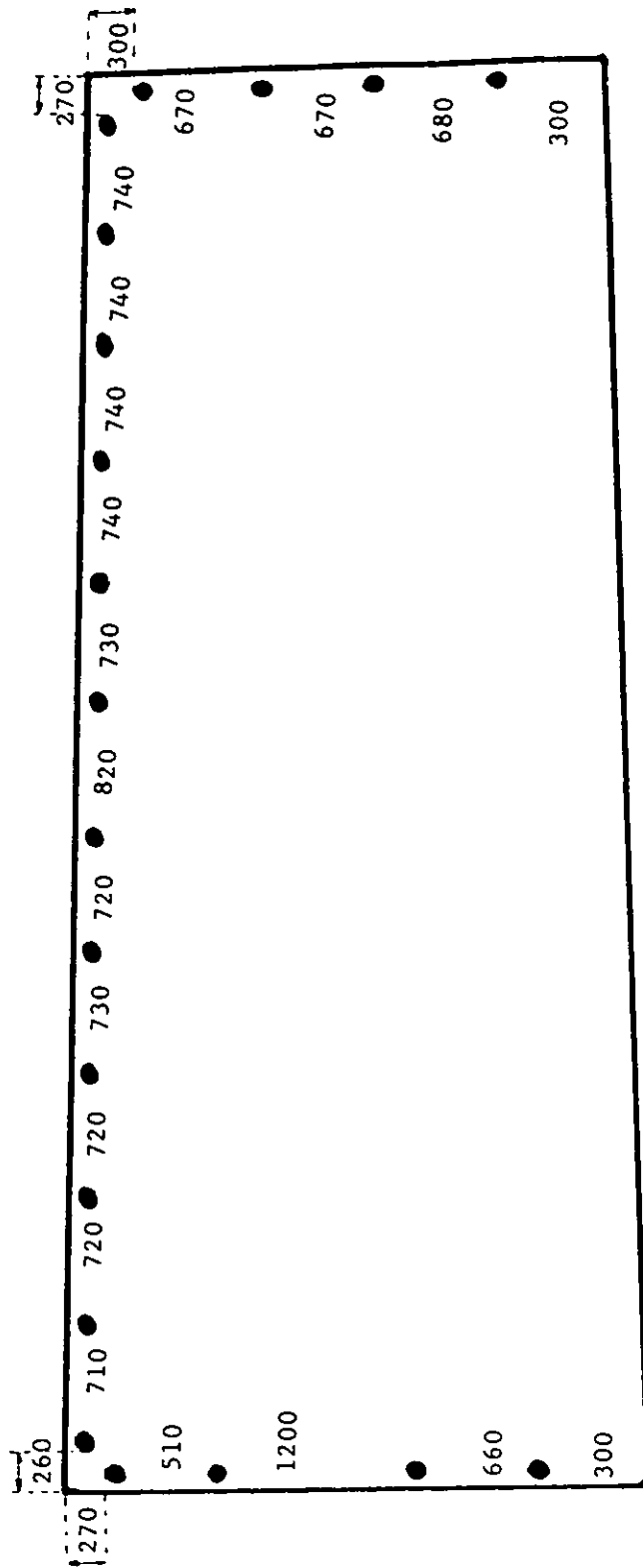
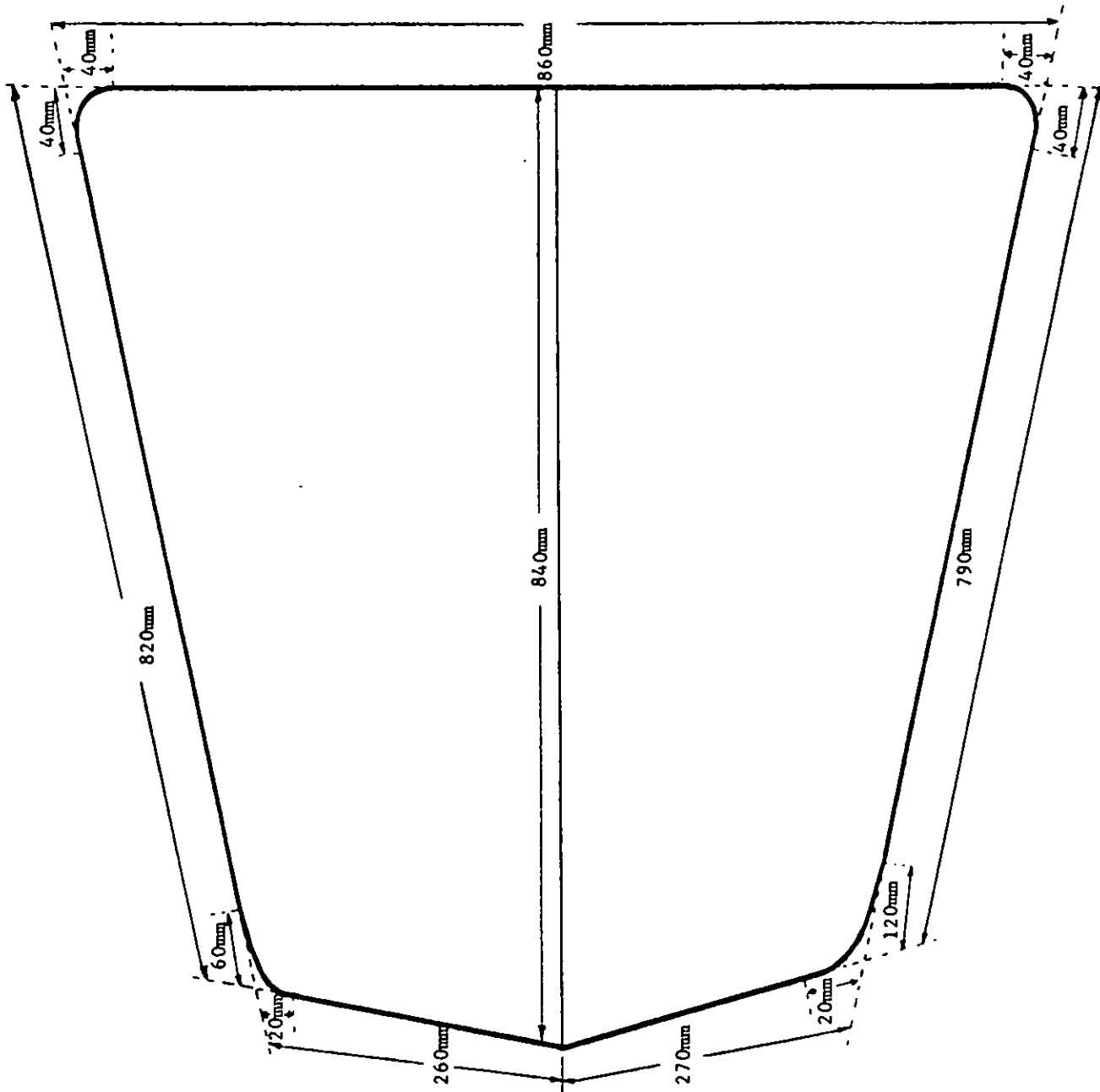


**Figure D.2: Outline of Front Avionics Bay Door**



## **APPENDIX E: AIRFRAME ATTENUATION AT MICROWAVE FREQUENCIES**

**Authors:** M. Pywell and M.J.S. Price, BAe. Presented by M. Pywell at I.E.E. 7th International Conference on EMC, University of York, 31 August 1990.

### **ABSTRACT**

Very few aircraft electromagnetic interference problems have been seen to date at microwave frequencies. However, with the worsening external RF environment and the growing use of more susceptible circuit technologies (e.g. VLSI, VHSIC) it is important to establish what level of protection is needed by avionics equipment. This level is determined by both the circuit's sensitivity and the frequency dependency of that sensitivity. To calculate the required level it is necessary to determine the protection afforded by the airframe. This information then leads to a better definition of the EMC Qualification test levels required. Since 1987 British Aerospace (BAe) has conducted research into the microwave energy ingress characteristics of a typical modern military aircraft, in order to provide answers to two questions: firstly, how much attenuation does the airframe present to microwave electromagnetic radiation; and secondly, how is the energy propagated within the aircraft. Research has included the development of techniques to investigate the dependency of energy penetration into a bay on angle of incidence, and the local ingress via a bay door's peripheral slot(s) using small irradiation 'footprints'. The research shows deterministic modelling of airframe ingress at microwave frequencies is likely to be impractical due to the complexity of the various coupling paths. Further laboratory research is required to generate even a stochastic model of these coupling mechanisms.

### **INTRODUCTION**

The combination of the following items points towards potential avionic equipment upset problems at some point in the future if adequate design measures are not adopted: ever smaller and higher density avionic circuit technologies, clock rates already in the lower Gbits/second, and the increasing external microwave environment, reference Larsen (1). Thus it has been postulated by Denny (2,3) and others that there may be problems caused by radio frequency interference (RFI) in the microwave (0.3-30 GHz) region of the electromagnetic spectrum. Against this background a BAe research programme was initiated in 1987 to examine the potential threat to avionics systems posed by the above combination of potential hazards. This paper describes the work carried out and addresses the findings of this research.

### **OBJECTIVES OF THE RESEARCH**

Prior to this research programme, the transfer function relating external electromagnetic fields to the microwave energy penetrating to the sites of avionic equipment was not known. The object of this research was therefore to establish this microwave transfer function for a typical military aircraft. More specifically, the objectives were to:

- i) establish the microwave attenuation,  $A_{\mu\text{wave}}$ , of the airframe by relating internal to external fields at a number of avionic equipment sites.
- ii) investigate the variation of microwave penetration as a function of variations in the relative position of the transmitter and aircraft.
- iii) investigate the transportation of microwave energy within the airframe.

In an attempt to meet these objectives experimental research work was conducted using a representative, metal bodied aircraft. A BAe demonstrator aircraft, although no longer flight-worthy and without much of its avionics equipment, has proved to be an excellent tool for the research of electromagnetic energy ingress and transportation mechanisms within airframes in a number of frequency bands.

### **TECHNIQUES USED ON AIRCRAFT**

The aircraft was used as an airframe only with both engines and all individual equipment cases removed but with the associated wiring looms left in place. In order to obtain meaningful results, interference fit light alloy plates were used to close off the engine outlets. These were electrically bonded to the inside of each outlet using metal loaded gasketing around each circumference. The airframe microwave attenuation factors were obtained by finding the difference between the power density measured inside an equipment bay and that measured at exactly the same position relative to the transmitter but with no airframe present. This assumes that the power density incident at the surface of the equipment bay with the door open is equal to that received at the site calibration point, 2m above the ground. To test this assumption, power density measurements were taken with the receiving antenna at the fuselage skin level with the bay door open and compared with those taken when no airframe was present (i.e. normal calibration). The results show good agreement between the skin level and the normal calibration results (figure 1). Placing a receiving antenna inside an enclosed space is likely to distort the radiation pattern of the antenna thereby

reducing repeatability and the accuracy of any comparative measurements. To minimise this distortion three steps were taken.

- i) The equipment bays tested were the largest ones available.
- ii) The receiving antenna was placed as far back in the bay as possible but away from nearby structures and with an unobstructed wide angle view of the transmitter.
- iii) A low gain planar log spiral antenna was used since high gain horns have significant sidelobes and both these and the main lobe can be distorted easily.

Using a spiral antenna has the disadvantage that higher transmitter powers are required to compensate for its low gain and the polarisation of the received signal cannot be determined. Airframe attenuation measurements were taken with the transmitting antenna positioned perpendicular to the centre line of the fuselage and directly opposite the receive point. The frequency range 2-18 GHz was swept to obtain the frequency response of the airframe attenuation. In addition to these measurements, two other techniques were used in an attempt to investigate how microwave energy penetrates and whether it is transported along the airframe.

### The ARC Technique

The ARC Technique was used to investigate the effect of phase variation in the illuminating field along the length of the aircraft. The transmitter was moved through different positions in an arc around the aircraft thereby measuring the airframe leakage as a function of the angle of incidence of the external radiation. By measuring the internal power densities and relating them to the calibrated power densities as before, the level of attenuation offered by the airframe for each position around the arc can be found. For this technique to be most effective the aircraft must be illuminated along its whole length with an external field of uniform magnitude. This is best achieved using a broad beamwidth transmit horn and a large separation between aircraft and transmitter. The minimum separation can be found from the following equations, reference Price (7):

$$i) \quad \text{In terms of antenna beamwidth } d_{\min} = 0.5L \left[ 0.5 + \sqrt{\frac{\sin^2 60}{\sin^2 \theta} - 0.75} \right] \quad \dots (1)$$

$$ii) \quad \text{For a 3 dB variation from freespace loss } d_{\min} \approx 0.5L \quad \dots (2)$$

$$iii) \quad \text{For a 1 dB variation from freespace loss } d_{\min} \approx 0.89L \quad \dots (3)$$

Where  $d_{\min}$  denotes the minimum separation between aircraft and transmitter,

$L$  denotes the length of the aircraft, and

$\theta$  denotes the half power beamwidth for the transmit antenna in the azimuth plane.

For an airframe of 14m, a transmitter maximum beamwidth of 35 degrees and a 1 dB freespace loss variation, the minimum separation was found to be 12m. This distance was therefore chosen as the approximate radius of the arc.

### The SLIDE Technique

The object of this technique was to establish how microwave energy penetrates the fuselage and whether it propagates inside the airframe. The transmitter is moved through a series of positions, parallel to the centre line of the airframe, termed the SLIDE. By using a narrow beamwidth antenna and a suitable separation between airframe and transmitter, the internal power density at one measurement point can be recorded as a function of the localised incident power density at a number of points along the length of the fuselage. A narrow beamwidth antenna is required to ensure that only a small "foot print" on the fuselage is illuminated and not the rest of the airframe including the equipment bay under investigation. The separation between airframe and transmitter is bounded by two requirements.

- i) The maximum distance is related to the number of transmitter positions required whose 3 dB "foot prints" do not overlap. This is given by:

$$d_{\max} \approx \frac{L}{2n \tan \theta} \quad \dots (4)$$

where  $n$  denotes the number of equally spaced transmitter positions along the SLIDE. (This assumes the SLIDE is the same length as the aircraft and the whole aircraft length is to be investigated.)

- ii) The minimum separation is limited by the radiation pattern distortion that occurs to the transmitting antenna when in close proximity to the airframe.

## **RESULTS OF ON-AIRCRAFT TESTS**

The experimental research work was conducted in two phases on the aircraft, with measurements being taken on the Warton Aerodrome test site. Initial feasibility work prior to the bulk of the investigations was helpful in defining the way the research should be carried out.

### **Instrumentation and Test Site Calibration**

The test instrumentation used is shown schematically in figure 2. A computer system controls a synthesised microwave signal generator transmitting, through appropriate Travelling Wave Tube Amplifiers, to a suitable antenna. The double-ridged waveguide antenna was used for the 2-18 GHz, 12m ARC work and 2-12 GHz SLIDE work 4m from the aircraft. A horn and parabolic reflector was used for the 12-18 GHz, 25m SLIDE work. At the receiver, energy is collected by a spiral antenna and passed down an ultra-low loss cable to the spectrum analyser. To prevent possible microwave currents on the screen of the receiving antenna cable entering the aircraft, two ferrite rings were placed around the cable at the skin of the fuselage. Figure 3 shows the aircraft test arrangement on the test site. As this was the first time such work had been conducted, much effort was expended characterising the test site and establishing the test technique in the frequency range 2-18 GHz. During calibration of the test site, consideration was given to the multipath phenomenon where reflections from the ground could have given rise to an interference pattern of the power density at the aircraft fuselage. Measurements showed that no discernable multipath effect was present for tests conducted over dry or wet asphalt and grass. Ground illumination was reduced by using directional transmitting antennae.

### **Initial Feasibility Work**

Initial feasibility work was conducted in order to:

- a) examine the relationship between power density measured without the aircraft present and that measured at the aircraft skin, for use as calibration data in the derivation of attenuation factors,
- b) examine the frequency resolution for adequate characterisation of the aircraft bays, and
- c) obtain some initial attenuation factors at five 2-18 GHz spot frequencies, for two bays on the aircraft.

Determination of  $A_{\mu\text{wave}}$  requires the measurement of power density in a bay and immediately outside the bay door. The time penalties of performing this calibration test for all relevant bays on an aircraft is large. An experiment was carried out to examine the difference in power density measured immediately outside bay doors and at corresponding points on the centre line of the aircraft with no aircraft present. The results showed little difference between the power densities measured. Hence all of the attenuation factors have been determined using centre line calibration data, with a few spot checks of the validity of the assumption being conducted throughout the investigation. An investigation of the necessary frequency resolution was carried out using 0.5, 0.1, 0.02 and 0.01 GHz steps between 2-4 GHz. The results gave an attenuation factor profile which became much more resonant the finer the frequency resolution, see figure 4. As a compromise between potential interference and adequate characterisation the majority of tests were carried out at 0.1 GHz intervals.

Internal field measurements were taken at five spot frequencies between 2 and 18 GHz for two locations; the Front Avionic and Port Gun Bays, (see figure 5). Results obtained gave a frequency independent airframe attenuation factor of 12-25 dB  $\pm$ 3.5 dB for 2-12 GHz, see figure 6. These results broadly agree with those of Willis (8) taken for two unspecified military aircraft in the U.K. in 1986. The results as a whole showed that microwave energy penetrated the airframe over the band, with variations of attenuation factor with aspect angle apparently illustrating shielding and scattering of energy by the aircraft wing and inboard pylon.

### **Attenuation Factor Investigations**

Following analysis of the above results a revised measurement technique was adopted for the majority of the microwave attenuation factor investigations. In addition, further research was to be carried out:

- i) Pseudo-Swept 2-18 GHz measurements were used, rather than five spot frequencies.
- ii) Measurement of attenuation factors in the 12-18 GHz band.
- iii) Examination of energy ingress through bay door/access panel peripheral slots.

The value of airframe attenuation factors (around 20 dB) found in the initial tests was confirmed, but with appreciable variation highly dependent on frequency when the pseudo-swept frequency test technique was used. No significant difference was seen between vertically or horizontally polarised transmitting antenna. The results of the SLIDE measurements, with their small irradiation 'footprint' on the aircraft, strongly suggested that the majority of ingress in the 2-12 GHz band occurred via the panel's peripheral slot(s). If

energy ingress was only via the bay door's peripheral slots then marked differences should occur between shoot-bolt (long slots), bolted and hinged, and fully bolted (many short slots) doors. Initial predictions were performed, using a  $20\log_{10}(\text{wavelength}/(2 \times \text{slot length}))$  consideration, and yielded relative and absolute ingress performance of examples of these three bay door types. It was predicted that for the long slot panels all energy above 0.5 GHz would penetrate the peripheral slots equally for each transmitter polarisation. For the short slot panels a cut-off frequency at about 6 GHz was predicted, as a result of the complex loaded waveguide formed by pairs of bolts around the panel periphery. For the hinged/ bolted panel with the hinge at the top, a hybrid result was predicted, with a clear difference between horizontally and vertically polarised incident wavefronts.

Thus the next set of tests covered 2-12 GHz internal field measurements in the Port Gun Bay, the bay behind the fully bolted Panel 55, and in the bay behind bolted/hinged Panel 56, see figure 4. Mean values were found of 20 dB for the frequency independent attenuation factor for the shoot-bolt type bays (Front Avionic and Port Gun) over the range 2-12 GHz. The predicted large difference in the hinged/bolted panel bay factors for the horizontally and vertically polarised incident wavefronts was not seen in the results. This is not fully understood but is thought to be a result of the complex loaded and stepped waveguide sections formed by the bay's peripheral slots, especially shaped ones such as corners. For the bays behind bolted and bolted/hinged Panels, and for both transmitting antenna polarisations, the results showed, see figure 7, that the attenuation decreased at 17 dB per decade of increasing frequency - comparing favourably with the 20 dB per decade predicted. However, the cut-off frequencies predicted for the bolted bays were not seen in the measured data. This is believed to be a result of the limitation of very simple model, but suggests that airframe ingress may be too complex to model directly, and that it may have to be derived by a probabilistic determination which may be based upon a model of empirical data:

- panel/door type and contouring,
- cavity resonance,
- airframe material,
- the coupling paths within the airframe.
- shape of peripheral slots,
- the characteristics of other apertures,
- paint/primer/gasketing materials in the slots, and

Of the total of four bays tested during this part of the research programme only two appeared to show any dependence of attenuation factor on aspect angle of incident wavefront. Attenuation factors for the Port Gun Bay illustrated some shielding and scattering effect of the wing and pylon. Similarly, factors for the bolted/hinged panel bay also showed marginally the same type of effect. The other two bays tested, unexpectedly, showed no evidence of aspect angle dependency. Energy may be entering these bays via routes other than their peripheral slots. One very interesting feature seen during the investigation was the low attenuation factors seen for the Front Avionics Bay, when irradiated from the tail-on position. The factors, 10-30 dB over the range 2-12 GHz, were as low as those found when irradiating the bay in direct line of sight. Since the bay is not visible from this position and the geometry does not allow that magnitude of specular reflection from the wing/pylon, it suggests some internal transport mechanism. This currently remains unexplained. Even when its resonant nature is taken into account, as seen in figure 4, the mean value of microwave attenuation for 2-12 GHz on this aircraft remains in the region of 20-25 dB  $\pm$  10 dB, independent of aspect angle and transmitting antenna polarisation. The pessimistically high error budget is as a result of the extrapolation of initial calibration data, which was taken in 0.5 GHz steps, for use with the 0.1 GHz steps of the attenuation factor measurements. The actual measurement error is thought to lie between the  $\pm$ 3.5 dB of the earlier work and  $\pm$ 6 dB.

An investigation of cavity resonances in aircraft bays was also carried out. By the judicious use of wide-band Radar Absorbent Material lining the bay it was shown that substantial cavity resonances, present within the bays, could be attenuated considerably, see figure 8. Consideration of these results against standard theory for empty rectangular cavities strongly suggests that multi-axis cavity excitation is present. During this phase of the research it was noted that there was appreciable (up to +16.5, -15 dB) difference in attenuation factors for the different transmitting antenna polarisations. The reason for this marked difference between these tests and the rest of the research results is not yet fully understood, but could possibly be due to the bay and door aspect ratio.

Further investigations on aircraft were carried out, this time in the 12-17 GHz band. These were not full characterisation tests, but merely to examine whether the zero attenuation factor effect apparent from the earlier bolted bay tests existed. The results showed an average of 22 dB of attenuation existed, again with a decreasing profile with increasing frequency at approximately 16 dB per decade, see figure 9. No firm conclusion could be made with the small amount of data to hand as to the real shape of the microwave attenuation profile. It was possible though to suggest that one of two conditions was present:

- a) a sharp resonance effect giving approximately zero attenuation at intervals of approximately 7 GHz, above the cut-off frequency; or,
- b) since the 2-12, 12-16, and 16-17 GHz results all have very similar gradients for the fully bolted bay, there is an as yet unexplained measurement problem. It is thought that this could be partly explained if the primer/paint within the slots prove to be significantly lossy at these higher frequencies.

### DISCUSSION

The results obtained from on-aircraft trials are complex and not particularly conclusive. The method of representing the results is a difficult choice and assessing the differences between a number of plots, i.e. as a function of angle of incidence, is not trivial. To assist in this task a method of calculating a "Figure of Merit" (FoM) has been devised. The FoM is useful for comparing similar situations. The larger the overall attenuation the larger the FoM. However, the quantitative measure of this FoM is not known so it is only used qualitatively. The accuracy of the FoM is greatest the larger the number of measurement points. The FoM is found from  $\text{Area} \times A_{\mu\text{wave}_{\text{max}}}$  ... (5)

where Area is found from figure 10. The equation derived is

$$A_{\mu\text{wave}_{\text{max}}} \left\{ A_{\mu\text{wave}_{\text{max}}} - d(A_{\mu\text{wave}}) \frac{\sum_{A_{\mu\text{wave}_{\text{min}}}^{A_{\mu\text{wave}_{\text{max}}}} p(A_{\mu\text{wave}})}{\sum_{A_{\mu\text{wave}_{\text{min}}}^{A_{\mu\text{wave}_{\text{max}}}} p(A_{\mu\text{wave}})} \right\} \quad \dots (6)$$

Figures 11 and 12 show the FoM values plotted as function of transmitter position on both the ARC and the SLIDE. For the Port Gun Bay, Panel 55 and Panel 56 there appears little difference between them or between the two senses of polarisation. The figures show interesting differences between the attenuations at different transmitter positions. These results, in the case of the ARC, are unexpected but in the case of the SLIDE the results confirm the intuitive belief that the attenuation should be lowest when the transmitter is directly opposite the receiver position. The FoM approach to data analysis needs to be extended to more of the trials data to be able to confirm these findings. It is not clear from the aircraft results whether energy is transported through the airframe. It would be very useful to be able to use time-gating techniques to study the various propagation delays experienced by the pulse. Unfortunately, restrictions on the minimum length of pulse for current equipment together with the dimensions of the aircraft suggests that all the delayed pulses will occur within a time span of about 35 ns making discrimination of the various propagation paths almost impossible. The pulse picture would be further confused by pulse ringing caused by the cavity resonances.

Computer modelling of airframe attenuation may become possible given more information about the mechanisms of propagation. However, such modelling is unlikely to be deterministic due to the complexities of the various coupling paths. An empirical approach seems more likely but expensive trials data would have to be gathered. This provides only part of the solution because the extent of coupling between the fields inside a bay and the circuitry within an equipment has still to be established.

### CONCLUSIONS

Investigations on a typical military aircraft have shown that incident microwave radiation in the range 2-18 GHz is attenuated (by approximately 20 dB) by the airframe in a complex fashion which does not lend itself to being modelled easily. During on-aircraft tests this value has been seen to approach zero, thus removing any shielding of avionics by the airframe. The attenuation factor has been found to behave counter-intuitively for various angles of incidence. Further research work is in hand to expand the knowledge of airframe attenuation, internal energy transportation mechanisms and methods of data analysis. Much of the next phase of research must be laboratory based, where more tightly controlled test specimens can be used.

### ACKNOWLEDGEMENTS

The authors would like to express their gratitude to British Aerospace for their permission to publish this paper and in particular the BAe Sowerby Research Centre, who funded the research work. This work has been carried out with the support of the Procurement Executive of the Ministry of Defence.

### REFERENCES

1. Larsen, W.E., 1988, "Digital Avionics Susceptibility to High Energy Radio Frequency Fields", Proc. IEEE NAECON, 3, 1098-1107.

2. Denny, H.W., 1986, "Projected Susceptibilities of VHSIC/VLSIC Devices to the Year 2000 Electromagnetic Environment", IEEE Intl. Symp. On EMC.
3. Denny, H.W., 1987, "Projected Trends in IC/EM Environment Interactions", SOUTHCON '87.
4. Audone, B., 1987, "The EM Threat to Future Avionic Systems", AGARD Conf. Proc., 417.
5. Kinney, C., 1983, "Directed Beam Weapons Open 21st Century Warfare", Mil. ECM, 26-30.
6. Granatstein, V.L. And Alexoff, I (Ed.), "High-Power Microwave Sources", Artech House.
7. Price, M.J.S., 1988, "Investigating the Microwave Penetration of Aircraft: A Proposal for Further Studies and Improved Measurement Techniques", BAe Internal Report WAA-PL-099.
8. Willis, P.E., 1987, "Microwave Attenuation /Induced Voltage at Microwave /TWT Power for TM510", ERA Technology Ltd, No. 4000/5/04/1.

Figure 1: Skin-Level vs. Normal Calibration Power Density Results

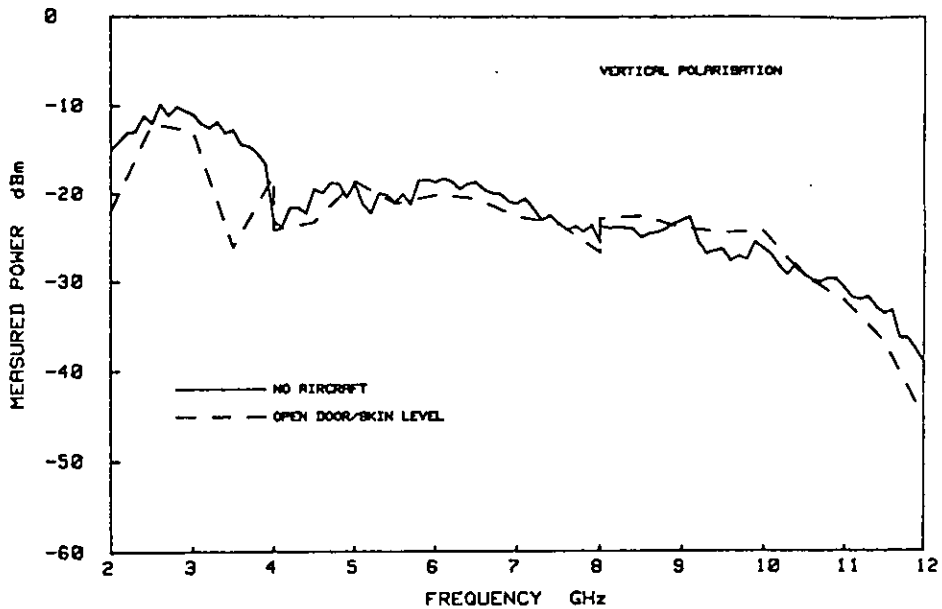


Figure 2: Test Instrumentation Schematic

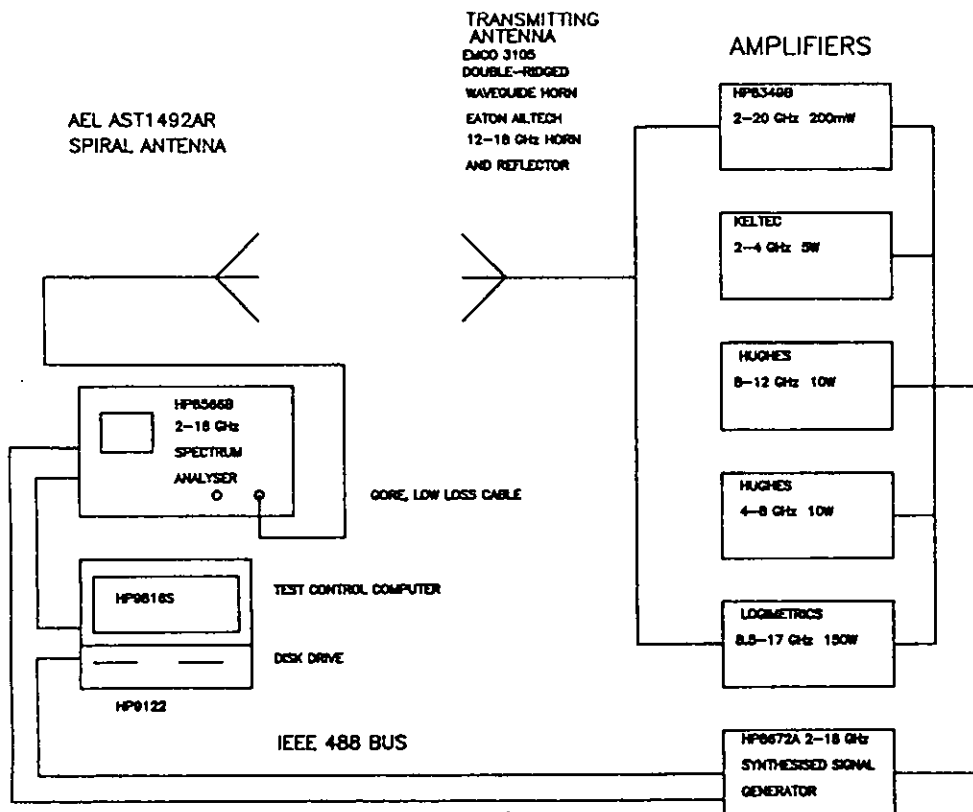


Figure 3: Aircraft Test Arrangement

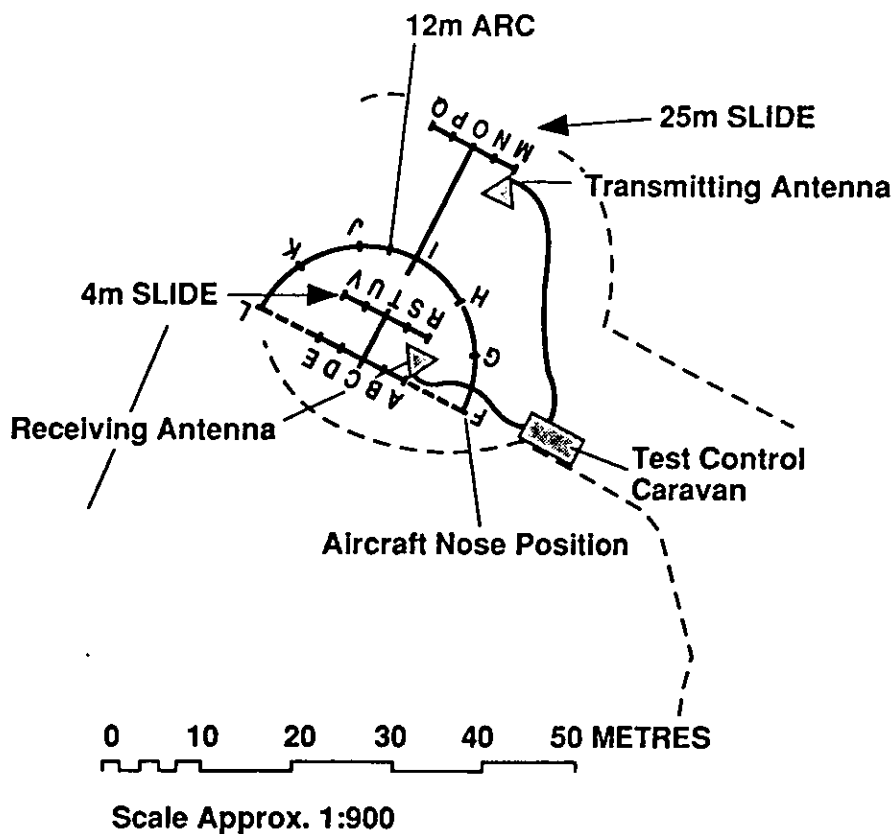


Figure 4: Test Frequency Step Resolution Investigation

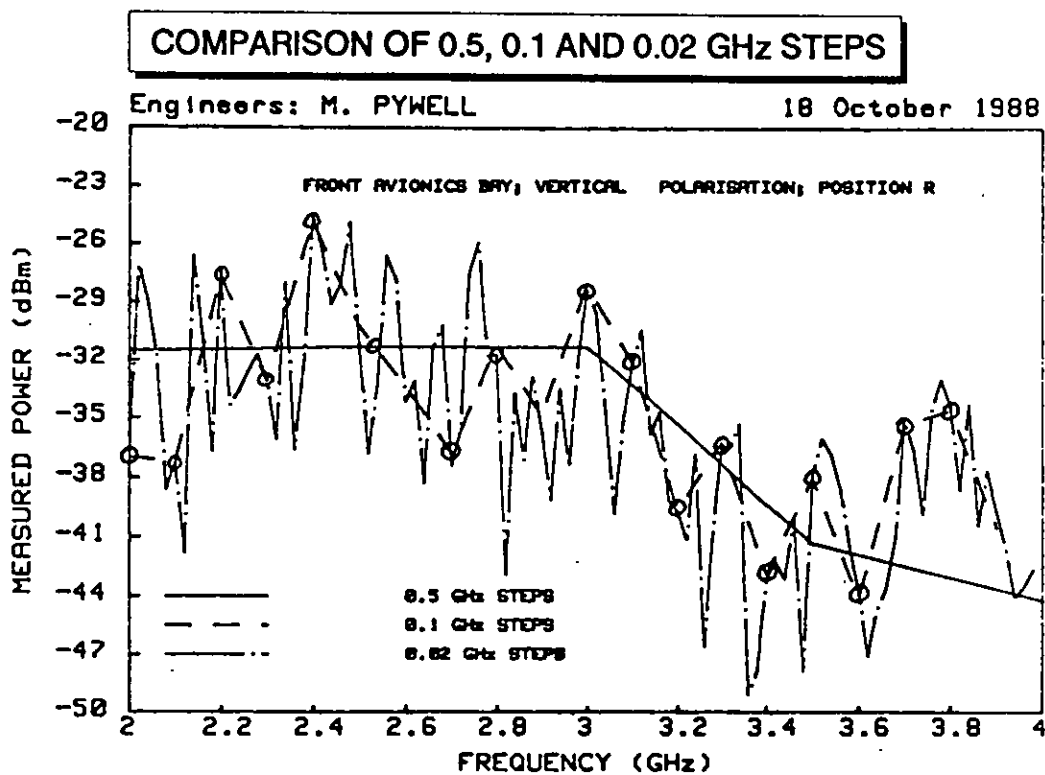


Figure 5: Location Of Bays Investigated

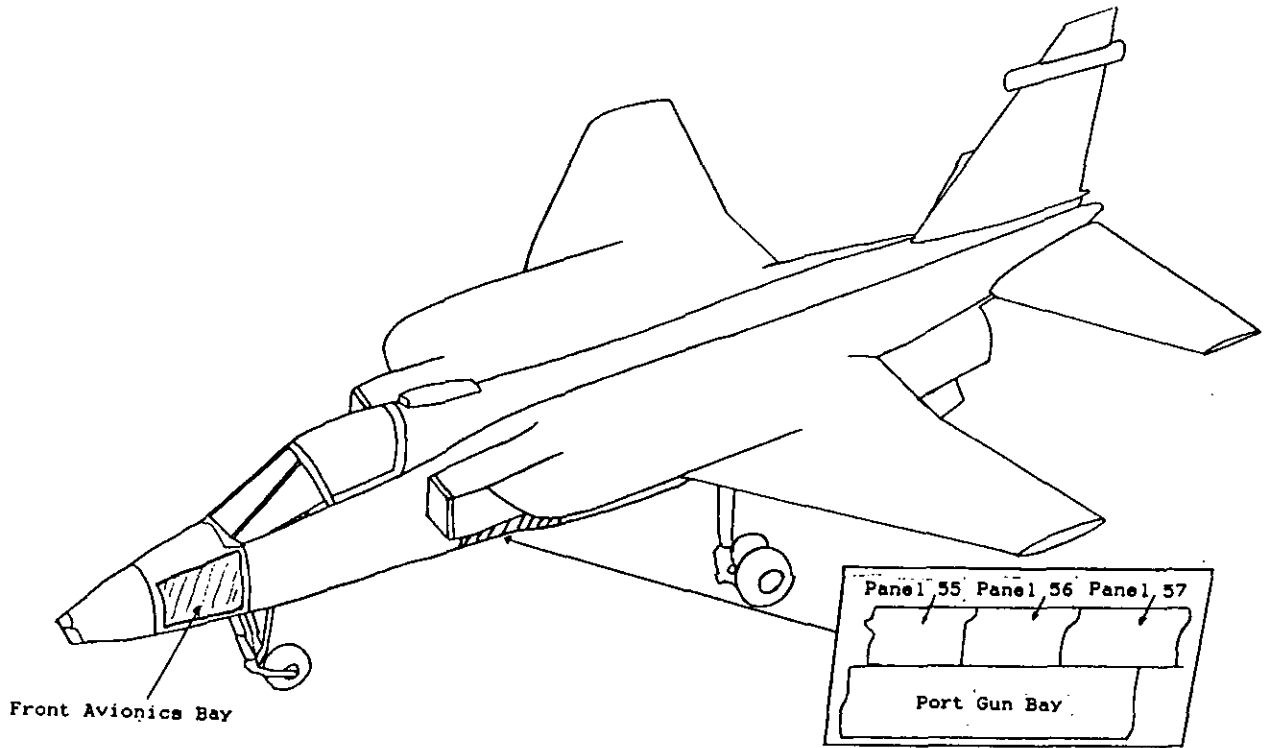


Figure 6: 2-12 GHz Airframe Attenuation Factor - Port Gun Bay

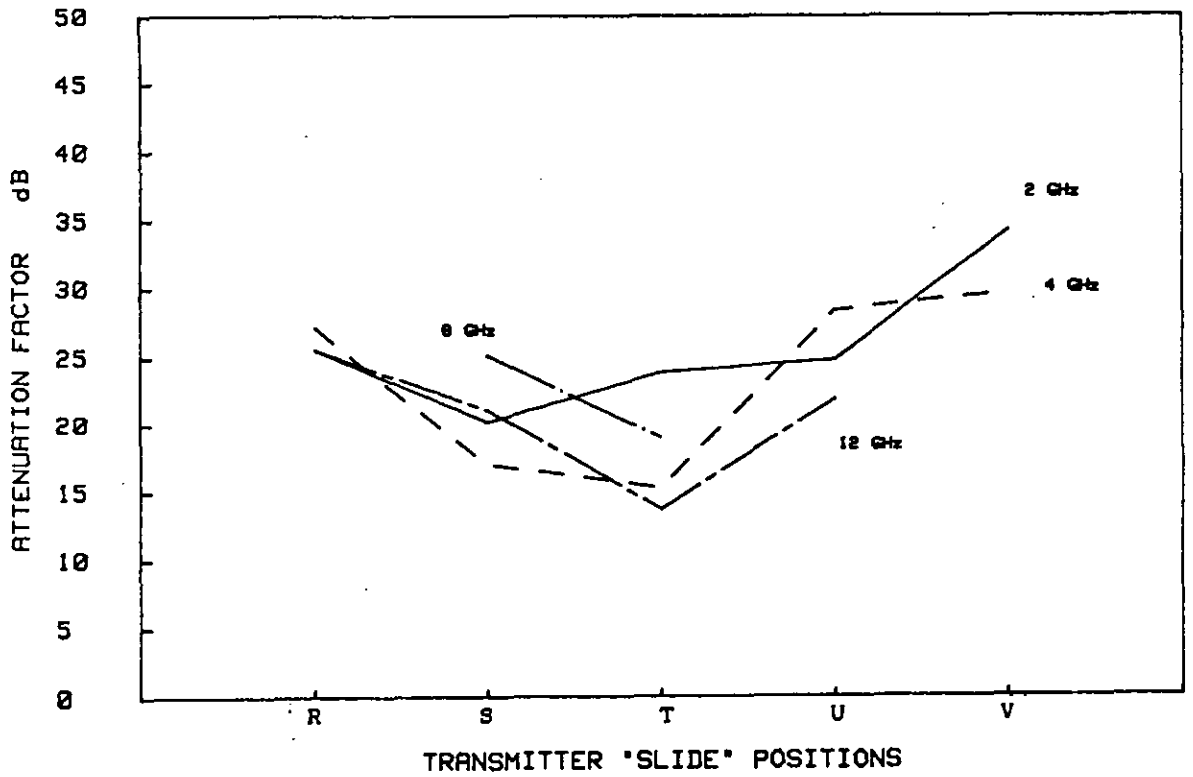


Figure 7: Frequency Dependence of Airframe Attenuation Factor - Panels 55/56 Bays

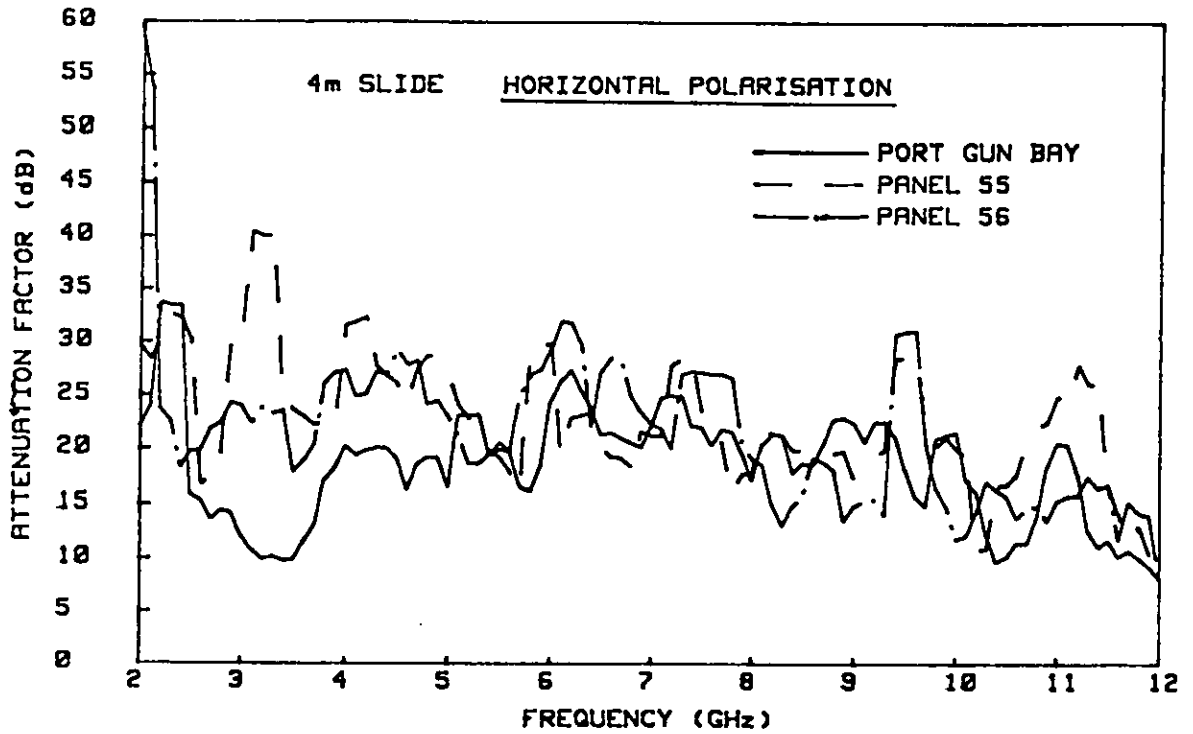


Figure 8: Damping of Panel 55 Bay Cavity Resonances

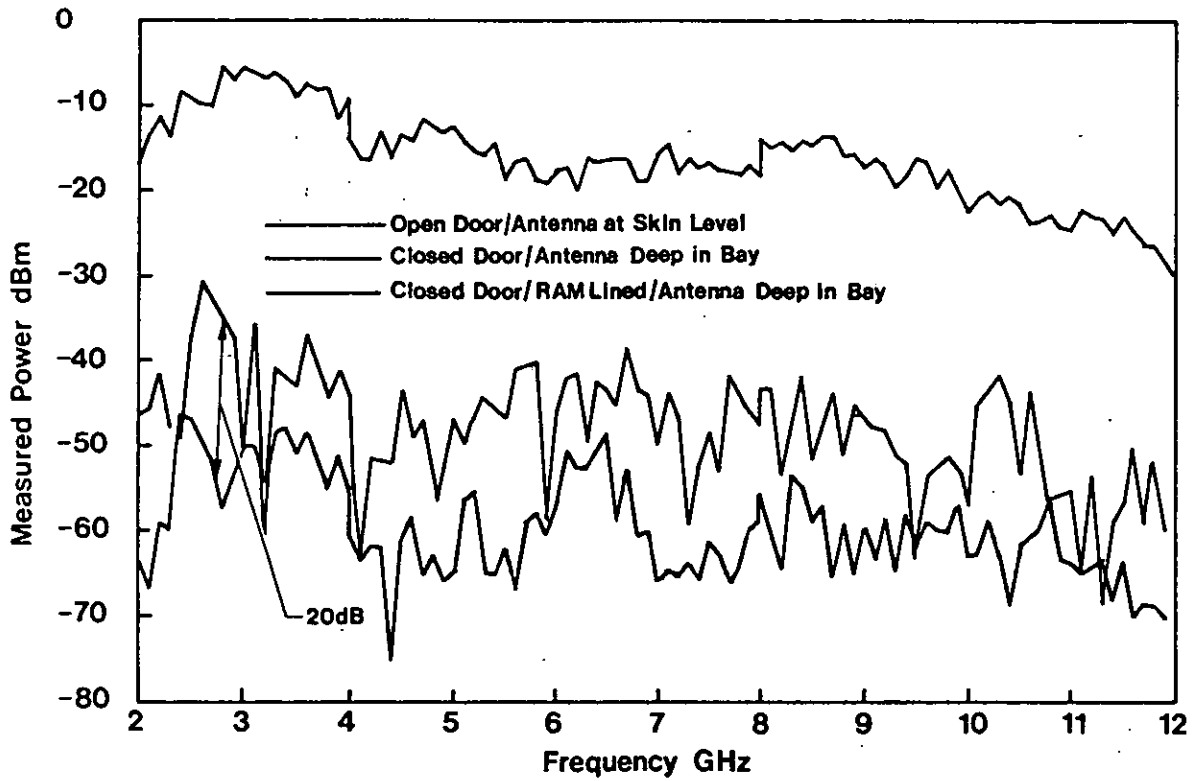


Figure 9: 12-17 GHz Airframe Attenuation Factors

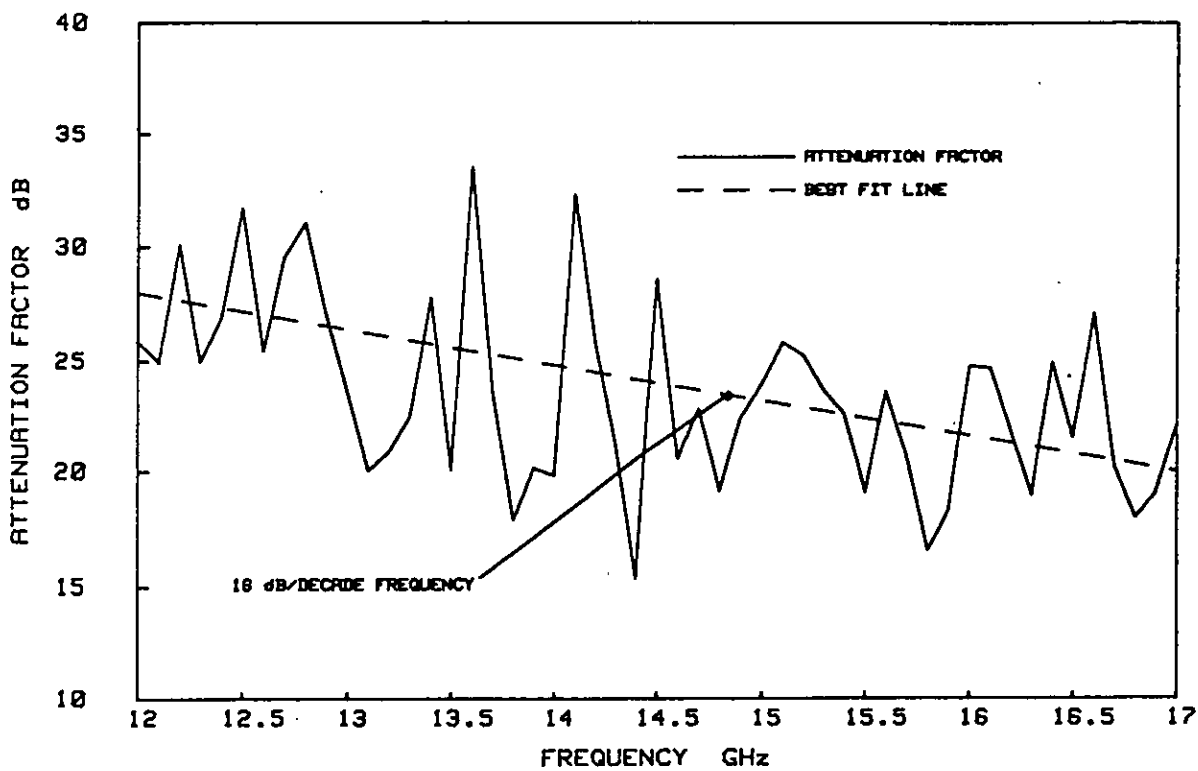


Figure 10: Derivation of 'Figure of Merit'

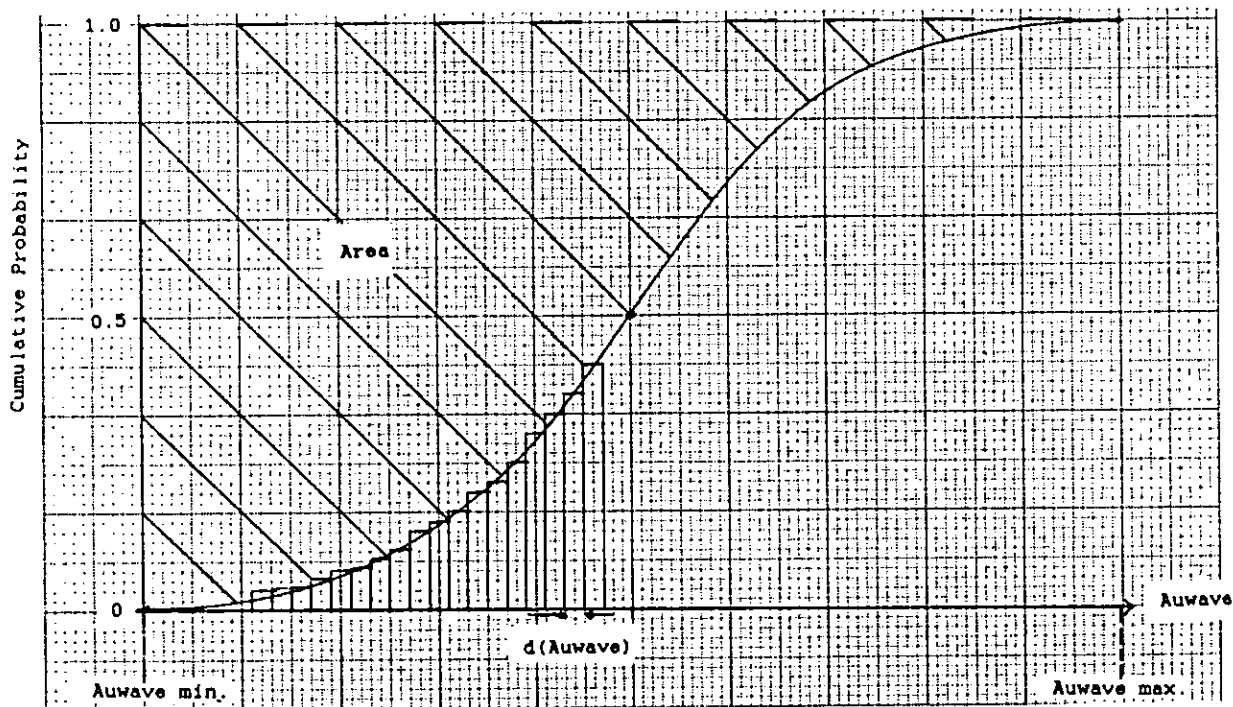


Figure 11: Arc 'Figures of Merit'

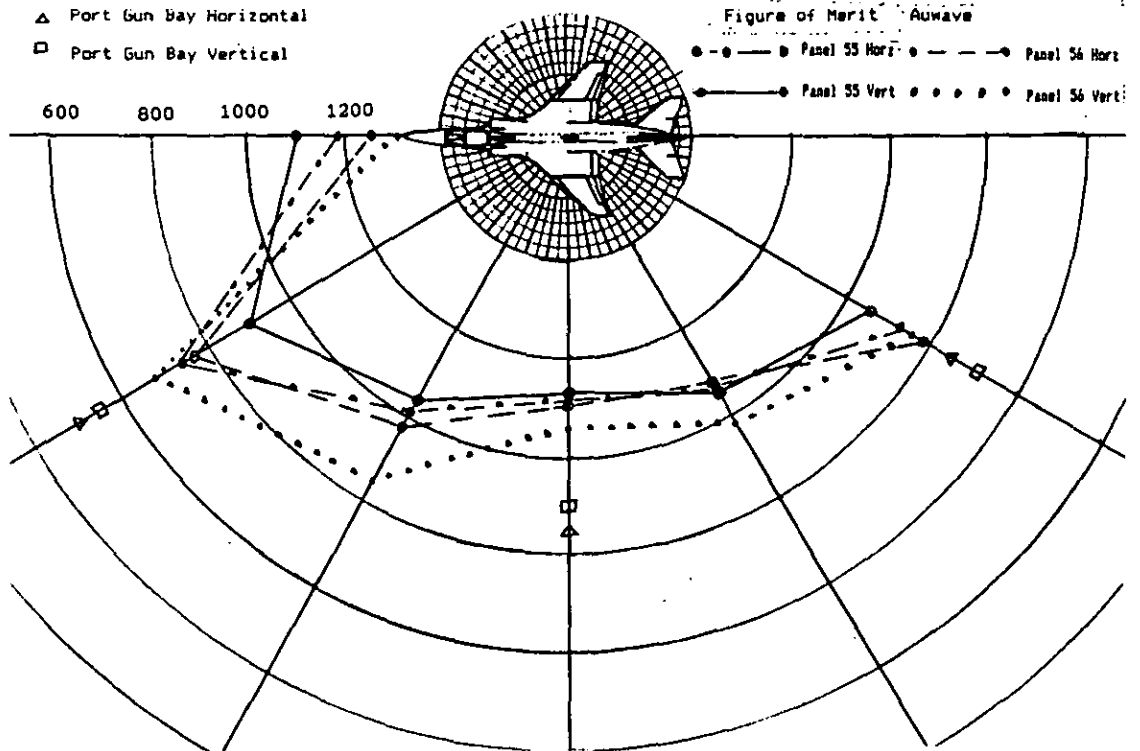
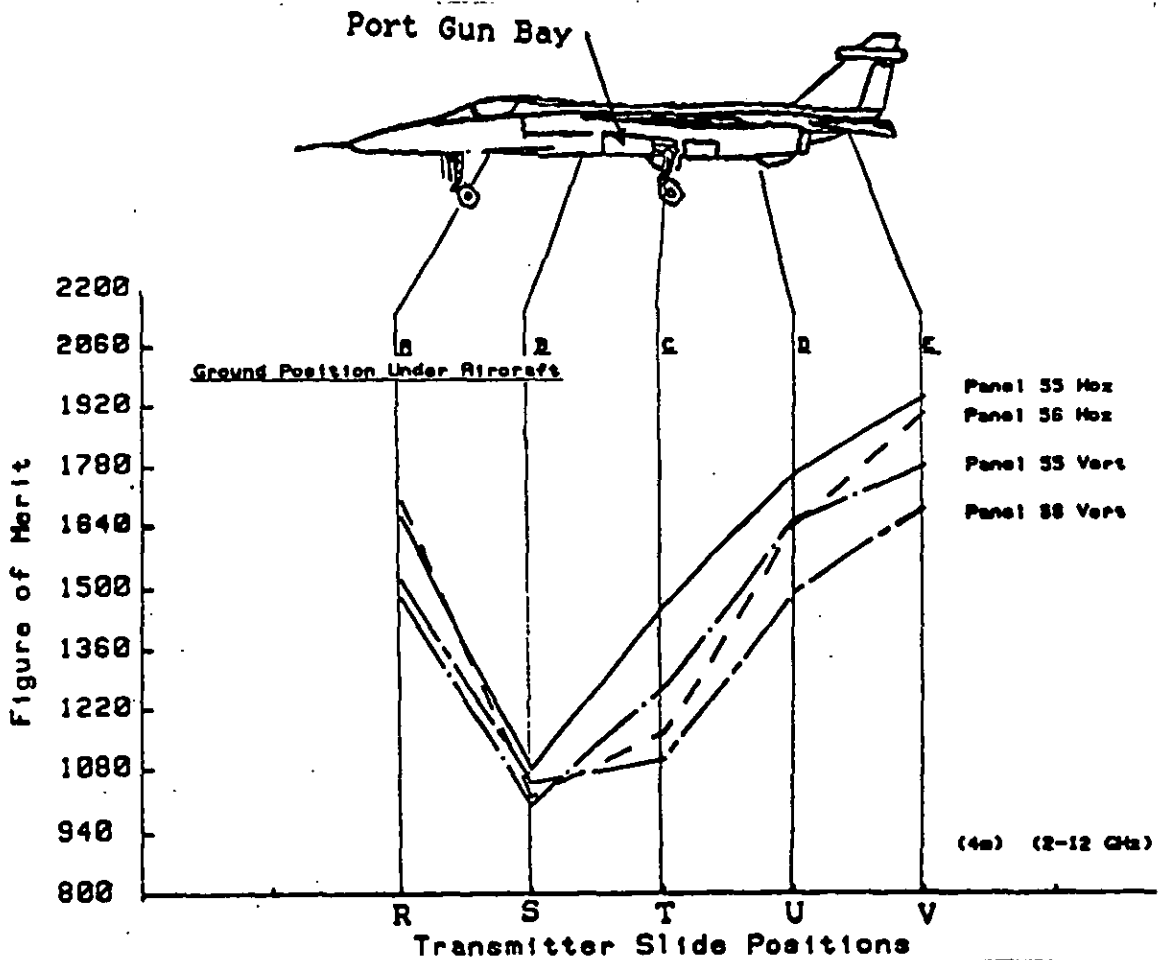


Figure 12: Slide 'Figures of Merit'



**APPENDIX F: FREQUENCY SPACING CALCULATIONS FOR CAVITY  
RESONANCES IN PANELS 55 & 56 BAYS**

To obtain an estimate of the resonant frequencies of the bays, they were treated as simple rectangular cavities of dimensions:

Bay (m)	Height (m)	Width (m)	Depth (m)
Panel 55	0.468	0.426	0.175
Panel 56	0.381	0.300	0.600

The theory of cavities, as given in [F-1] *et al.*, gives resonant frequencies:

$$f = \frac{c}{2} \sqrt{\left(\frac{l}{x}\right)^2 + \left(\frac{m}{y}\right)^2 + \left(\frac{n}{z}\right)^2} \quad \dots(\text{F.1})$$

where c is the velocity of light; x, y and z are the cavity dimensions in metres; and l, m and n are integers corresponding to the number of standing wave maxima across dimensions x, y and z. If it is assumed, for the sake of argument, that the method of driving the cavity will only excite modes in one of the dimensions, Eqn. F.1 simplifies to:

$$f = \frac{c}{2} \sqrt{\left(\frac{l}{x}\right)^2} = \frac{cl}{2x} \quad \dots(\text{F.2})$$

This leads to the following table, which shows the predicted frequency spacings of the resonances for each of the two bays, assuming only one axis in turn is excited. The lowest order mode is also given for a resonance within the 2-12 GHz range of interest.

Bay	Dimension (m)	Spacing (MHz)	Lowest Order Mode (TE <sub>lmn</sub> )
Panel 55	0.468	320.500	0,0,7
	0.426	352.100	6,0,0
	0.175	857.100	0,3,0
Panel 56	0.381	393.700	6,0,0
	0.300	500.000	0,4,0
	0.600	250.000	0,0,8

If resonance occurs across two dimensions then

$$f = \frac{c}{2} \sqrt{\left(\frac{l}{x}\right)^2 + \left(\frac{m}{y}\right)^2} \quad \dots(\text{F.3})$$

Thus for the Panel 55 and Panel 56 bays the resonances could be spaced apart by only 14 and 46 MHz respectively. If all three dimensions are involved, the frequency spacing would be an order of magnitude lower. However, this is considered unlikely because of the orthogonal orientation of the transmitting antenna and the panel edges to the cavity.

**Reference**

- [F-1] **Baden-Fuller, A.J.** An Introduction to Microwave Theory and Techniques, 2nd Ed., pp104-105, para. 4.13.

## APPENDIX G: CABLE COUPLING MODEL LISTING

```
' *****  
' * LOSSY LINE CABLE CURRENT MODEL *  
' * USING EQUATIONS DEVELOPED FROM A.A. SMITH, Jr. *  
' * Code designed and developed by M. Pywell *  
' * Translated to Q Basic and Optimised by D.A. Lee *  
' * ISSUE 1, VERSION r December 1995 *  
' *****
```

DEFDBL A-Z

DECLARE SUB complexmultiply (REAL, IMAG, REAL1, IMAG1, REAL2, IMAG2)

DECLARE SUB complexdivide (REAL, IMAG, REAL1, IMAG1, REAL2, IMAG2)

DECLARE SUB cosh (coshREAL, coshIMAG, alpha, beta, length)

DECLARE SUB sinh (sinhREAL, sinhIMAG, alpha, beta, length)

DECLARE SUB init (metal\$, diameter, length, height, Ra, Ca, Rb, Cb, Rcap, Lb, Pd, npts%, freq, freq1, freq2, k%, rhorel, murel)

DECLARE SUB outline (metal\$, diameter, length, height, Ra, Ca, Rb, Cb, Rcap, Lb, Pd, npts%, freq, freq1, freq2)

DECLARE SUB getdata (metal\$, diameter, length, height, Ra, Ca, Rb, Cb, Rcap, Lb, Pd, npts%, freq, freq1, freq2, k%, rhorel, murel)

DECLARE SUB prnt (length, height, diameter, metal\$, Ra, Ca, Rb, Cb, Rcap, Lb, Pd, Zo, x(), y(), npts%)

DECLARE SUB storedata (npts%, x(), y())

DECLARE SUB F1 (length)

DECLARE SUB F2 (height)

DECLARE SUB F3 (diameter)

DECLARE SUB F4 (metal\$, rhorel, murel)

DECLARE SUB F5 (Ra)

DECLARE SUB F6 (Ca)

DECLARE SUB F7 (Rb)

DECLARE SUB F8 (Cb)

DECLARE SUB F9 (Rcap)

DECLARE SUB F10 (Lb)

DECLARE SUB AF1 (Pd)

DECLARE SUB AF2 (k%, npts%, freq, freq1, freq2)

DECLARE SUB AF3 (npts%, freq, freq1, freq2)

DECLARE SUB AF4 (npts%, freq, freq1, freq2)

---

---

### MAIN PROGRAM

---

---

PI = 3.14159265358#

k% = 8001                   'Max number due to memory limits

DIM SHARED diskerr, diskerr\$

DIM x(k%), y(k%)

COLOR 2

CALL init(metal\$, diameter, length, height, Ra, Ca, Rb, Cb, Rcap, Lb, Pd, npts%, freq, freq1, freq2, k%, rhorel, murel)

quit = 0

DO

    CALL outline(metal\$, diameter, length, height, Ra, Ca, Rb, Cb, Rcap, Lb, Pd, npts%, freq, freq1, freq2)

    CALL getdata(metal\$, diameter, length, height, Ra, Ca, Rb, Cb, Rcap, Lb, Pd, npts%, freq, freq1, freq2, k%, rhorel, murel)

    GOSUB Calculate

    CALL prnt(length, height, diameter, metal\$, Ra, Ca, Rb, Cb, Rcap, Lb, Pd, Zo, x(), y(), npts%)

    CALL storedata(npts%, x(), y())

    CLS

    LOCATE 10, 1

    PRINT "                   +-----+"

    PRINT "                   | RUN AGAIN [Y/N] ? |"

    PRINT "                   +-----+"

    INPUT "                   ", yesno\$

    IF UCASE\$(MID\$(yesno\$, 1, 1)) <> "Y" THEN quit = 1

```

LOOP UNTIL quit
COLOR 7
CLS
STOP

```

---



---

===== CALCULATION SUBROUTINE =====

---



---

Calculate:

```

IF npts% > 1 THEN
  DO
    CLS
    LOCATE 10, 1
    PRINT "          +-----+"
    PRINT "          ! DO YOU WANT A LOG FREQUENCY SCALE [Y/N] ? !"
    PRINT "          +-----+"
    INPUT "          ", logs$
    logs$ = UCASE$(logs$)
    IF logs$ = "" THEN logs$ = "N"
    LOOP UNTIL logs$ = "Y" OR logs$ = "N"
  END IF
  CLS
  LOCATE 10, 10
  PRINT "Calculating..."
  LOCATE 12, 10
  PRINT "          "
  oldp = 0
  tstart = TIMER
  FOR a% = 1 TO npts%
    IF npts% = 1 THEN
      frequency = freq
    ELSE
      IF logs$ = "Y" THEN
        frequency = EXP(LOG(freq1) + ((a% - 1) * (LOG(freq2) - LOG(freq1)) / (npts% - 1)))
      ELSE
        frequency = freq1 + (a% - 1) * (freq2 - freq1) / (npts% - 1)
      END IF
    END IF
    x(a%) = frequency

```

---

----- IMPEDANCE -----

---

```

W = 2 * PI * frequency
Zo = 276 * LOG(4 * height / diameter) / LOG(10)
Z1REAL = 2 * (Ra / (1 + W ^ 2 * Ra ^ 2 * Ca ^ 2))
Z1IMAG = 2 * (-W * Ra ^ 2 * Ca / (1 + W ^ 2 * Ra ^ 2 * Ca ^ 2))
denominator = (Rcap + Rb) ^ 2 + (W * Lb - 1 / (W * Cb)) ^ 2
Z2REAL = 2 * ((Rb * (Rcap + 1 / (W ^ 2 * Cb ^ 2)) + Rcap * (Rcap + W ^ 2 * Lb ^ 2)) / denominator)
Z2IMAG = 2 * ((W * Rcap * (Rcap * Lb + Rb * Lb - Lb) + (Rcap - Rcap * Rb - Rb ^ 2 + Lb / Cb) / (W * Cb) - W * Lb ^ 2 / Cb) / denominator)

```

---

----- GAMMA S -----

---

```

alpha = 8.3 * 1E-08 * SQR(rhorel * murel * frequency) / (diameter * Zo)
' Below is the 'Re-Radiation' term of Eqns.6.8 and 6.9; disabled in this version.
' IF metal$ <> "Lossless" THEN
'   alpha = alpha + (39.728 * frequency / 1E+09 + 317.0781) / (2 * Zo)
' END IF
beta = 2 * PI * frequency / 3E+08

```

---

----- DENOMINATOR -----

---

```

temp1REAL = Zo * (Z1REAL + Z2REAL)
temp1IMAG = Zo * (Z1IMAG + Z2IMAG)
' {That was (Zo*Z1+Zo*Z2)}
CALL cosh(coshREAL, coshIMAG, alpha, beta, length)
CALL complexmultiply(temp3REAL, temp3IMAG, temp1REAL, temp1IMAG, coshREAL, coshIMAG)
' {That was (Zo*Z1+Zo*Z2)Cosh(Gamma*s)}
CALL complexmultiply(REAL, IMAG, Z1REAL, Z1IMAG, Z2REAL, Z2IMAG)

```

```

'{That was Z1*Z2}
  temp2REAL = (Zo ^ 2 + REAL)
  temp2IMAG = IMAG
'{That was (Zo^2+Z1*Z2)}
  CALL sinh(sinhREAL, sinhIMAG, alpha, beta, length)
  CALL complexmultiply(temp4REAL, temp4IMAG, temp2REAL, temp2IMAG, sinhREAL, sinhIMAG)
'{That was (Zo^2+Z1*Z2)Sinh(Gamma*s)}
  DREAL = temp3REAL + temp4REAL
  DIMAG = temp3IMAG + temp4IMAG
----- CURRENT -----
  Ez = SQR(Pd * 377)
'{Plane wave assumed; Ez in V/m}
  CALL complexmultiply(REAL, IMAG, Z1REAL, Z1IMAG, coshREAL, coshIMAG)
  numeratorREAL = -4 * Ez * (SIN(beta * height) + SGN(SIN(beta * height)) * .006#) * (Zo * sinhIMAG +
IMAG - Z1IMAG)
  numeratorIMAG = 4 * Ez * (SIN(beta * height) + SGN(SIN(beta * height)) * .006#) * (Zo * sinhREAL +
REAL - Z1REAL)
  CALL complexmultiply(temp2REAL, temp2IMAG, alpha, beta, DREAL, DIMAG)
'{This was Gamma*Denominator}
  CALL complexdivide(currentREAL, currentIMAG, numeratorREAL, numeratorIMAG, temp2REAL,
temp2IMAG)
----- VOLTAGE -----
  CALL complexmultiply(REAL, IMAG, currentREAL, currentIMAG, Z2REAL, Z2IMAG)
  ModulusV = SQR(REAL ^ 2 + IMAG ^ 2)
'{V in Volts}
  y(a%) = 20 * LOG(ModulusV / .000001) / LOG(10)
'{Voltage in dBuV}
----- BAR STRIP DISPLAY -----
  p = INT((a% / npts%) * 60 + .5)
  IF p > oldp THEN
    tleft = INT((TIMER - tstart) * (npts% - a%) / a%)
    tlh = INT(tleft / 3600)
    tlm = INT(tleft / 60 - tlh * 60)
    tls = INT(tleft + 1 - tlh * 3600 - tlm * 60)
    LOCATE 14, 28
    PRINT "Time Remaining: " + MID$(STR$(tlh), 2, 2) + ":" + MID$(STR$(tlm), 2, 2) + ":" +
MID$(STR$(tls), 2, 2) + " "
    LOCATE 12, 10
    PRINT MID$(" _____", 1, p)
    oldp = p
  END IF
NEXT a%
RETURN
===== FILE ERROR
HANDLER=====
diskerr: 'Called if error occurs during SUB Storedata
  diskerr = ERR
  diskerr$ = ERDEV$
  RESUME NEXT
END

SUB AF1 (Pd)
  LOCATE 17, 42
  PRINT " "
  DO
    LOCATE 23, 19
    INPUT "Power Density (W/m2) : ", Pd
    LOCATE 23, 10
    PRINT " "
  LOOP UNTIL Pd > 0 AND Pd <= 1000000!
  LOCATE 17, 42
  PRINT Pd;

```

END SUB

SUB AF2 (k%, npts%, freq, freq1, freq2)

LOCATE 19, 42

PRINT " "

oldnpts% = npts%

DO

LOCATE 23, 23

INPUT "Number of Points : ", npts%

LOCATE 23, 10

PRINT " "

LOOP UNTIL npts% > 0 AND npts% <= k%

LOCATE 19, 42

PRINT npts%;

IF (npts% = 1 AND oldnpts% > 1) OR (npts% > 1 AND oldnpts% = 1) THEN

LOCATE 21, 42

PRINT " ";

CALL AF3(npts%, freq, freq1, freq2)

END IF

END SUB

SUB AF3 (npts%, freq, freq1, freq2)

LOCATE 20, 42

PRINT " "

IF npts% = 1 THEN

freq1 = 0

freq2 = 0

DO

LOCATE 23, 24

INPUT "Frequency (GHz) : ", freq

LOCATE 23, 10

PRINT " "

LOOP UNTIL freq > 0 AND freq <= 30

freq = freq \* 1E+09

LOCATE 20, 42

PRINT USING "##.#####"; freq / 1E+09;

ELSE

freq = 0

DO

LOCATE 23, 18

INPUT "Start Frequency (GHz) : ", freq1

LOCATE 23, 10

PRINT " "

LOOP UNTIL freq1 > 0 AND freq1 < 30

freq1 = freq1 \* 1E+09

LOCATE 20, 42

PRINT USING "##.#####"; freq1 / 1E+09;

IF freq2 <= freq1 THEN CALL AF4(npts%, freq, freq1, freq2)

END IF

END SUB

SUB AF4 (npts%, freq, freq1, freq2)

LOCATE 21, 42

PRINT " "

IF npts% = 1 THEN

SOUND 2000, .4

ELSE

DO

LOCATE 23, 19

INPUT "Stop Frequency (GHz) : ", freq2

LOCATE 23, 10

PRINT " "

```

LOOP UNTIL freq2 > (freq1 / 1E+09) AND freq2 <= 30
freq2 = freq2 * 1E+09
LOCATE 21, 42
PRINT USING "##.#####"; freq2 / 1E+09;
END IF
END SUB

```

```

SUB complexdivide (REAL, IMAG, REAL1, IMAG1, REAL2, IMAG2)
REAL = (REAL1 * REAL2 + IMAG1 * IMAG2) / (REAL2 ^ 2 + IMAG2 ^ 2)
IMAG = (IMAG1 * REAL2 - REAL1 * IMAG2) / (REAL2 ^ 2 + IMAG2 ^ 2)
END SUB

```

```

SUB complexmultiply (REAL, IMAG, REAL1, IMAG1, REAL2, IMAG2)
REAL = REAL1 * REAL2 - IMAG1 * IMAG2
IMAG = IMAG1 * REAL2 + IMAG2 * REAL1
END SUB

```

```

SUB cosh (coshREAL, coshIMAG, alpha, beta, length)
coshREAL = .5 * (EXP(alpha * length) + 1 / EXP(alpha * length)) * COS(beta * length)
coshIMAG = .5 * (EXP(alpha * length) - 1 / EXP(alpha * length)) * SIN(beta * length)
END SUB

```

```

SUB F1 (length)
LOCATE 4, 42
PRINT " "
DO
LOCATE 23, 24
INPUT "Wire Length (m) : ", length
LOCATE 23, 10
PRINT " "
LOOP UNTIL length > 0 AND length <= 100
LOCATE 4, 42
PRINT length;
END SUB

```

```

SUB F10 (Lb)
LOCATE 15, 42
PRINT " "
DO
LOCATE 23, 14
INPUT "Load B Inductance Lb (nH) : ", Lb
LOCATE 23, 10
PRINT " "
LOOP UNTIL Lb >= 0 AND Lb <= 100
Lb = Lb * 1E-09
LOCATE 15, 42
PRINT CSNG(Lb * 1E+09);
END SUB

```

```

SUB F2 (height)
LOCATE 5, 42
PRINT " "
DO
LOCATE 23, 5
INPUT "Wire Height Above Ground Plane (m) : ", height
LOCATE 23, 4
PRINT " "
LOOP UNTIL height > 0 AND height <= 1D+200
LOCATE 5, 42
PRINT height;
END SUB

```

```

SUB F3 (diameter)
LOCATE 6, 42
PRINT "      "
DO
  LOCATE 23, 22
  INPUT "Wire Diameter (m) : ", diameter
  LOCATE 23, 10
  PRINT "      "
LOOP UNTIL diameter > 0 AND diameter <= .1
LOCATE 6, 42
PRINT diameter;
END SUB

```

```

SUB F4 (metal$, rhorel, murel)
DO
  LOCATE 7, 43
  PRINT "      ";
  LOCATE 23, 3
  INPUT "Metal Type (Lossless,Ag,Cu,Al,Brass,Nickel,Tin,Steel(max),Steel(min)) : ", metal$
  LOCATE 23, 1
  PRINT "      "
  SELECT CASE UCASE$(metal$)
    CASE "LOSSLESS"
      metal$ = "Lossless"
      rhorel = 0
      murel = 1
    CASE "AG"
      metal$ = "Silver"
      rhorel = .95
      murel = 1
    CASE "CU"
      metal$ = "Copper"
      rhorel = 1
      murel = 1
    CASE "AL"
      metal$ = "Aluminium"
      rhorel = 1.64
      murel = 1
    CASE "BRASS"
      metal$ = "Brass"
      rhorel = 3.9
      murel = 1
    CASE "NICKEL"
      metal$ = "Nickel"
      rhorel = 5.05
      murel = 1
    CASE "TIN"
      metal$ = "Tin"
      rhorel = 6.7
      murel = 1
    CASE "STEEL(MAX)"
      metal$ = "Steel (max)"
      rhorel = 12.7
      murel = 1
    CASE "STEEL(MIN)"
      metal$ = "Steel (min)"
      rhorel = 7.6
      murel = 1
    CASE ELSE
      metal$ = ""
  END SELECT
LOOP UNTIL metal$ <> ""

```

```
LOCATE 7, 43
PRINT metal$;
END SUB
```

```
SUB F5 (Ra)
LOCATE 9, 42
PRINT "      "
DO
  LOCATE 23, 12
  INPUT "Load A Resistance Ra (ohms) : ", Ra
  LOCATE 23, 10
  PRINT "                                "
LOOP UNTIL Ra > 0 AND Ra <= 1D+200
LOCATE 9, 42
PRINT Ra;
END SUB
```

```
SUB F6 (Ca)
LOCATE 10, 42
PRINT "      "
DO
  LOCATE 23, 13
  INPUT "Load A Capacitance Ca (pF) : ", Ca
  LOCATE 23, 10
  PRINT "                                "
LOOP UNTIL Ca >= 0 AND Ca <= 1000
Ca = Ca * 1E-12
LOCATE 10, 42
PRINT Ca * 1E+12;
END SUB
```

```
SUB F7 (Rb)
LOCATE 12, 42
PRINT "      "
DO
  LOCATE 23, 12
  INPUT "Load B Resistance Rb (ohms) : ", Rb
  LOCATE 23, 10
  PRINT "                                "
LOOP UNTIL Rb > 0 AND Rb <= 1D+200
LOCATE 12, 42
PRINT Rb;
END SUB
```

```
SUB F8 (Cb)
LOCATE 13, 42
PRINT "      "
DO
  LOCATE 23, 13
  INPUT "Load B Capacitance Cb (pF) : ", Cb
  LOCATE 23, 10
  PRINT "                                "
LOOP UNTIL Cb >= 0 AND Cb <= 1E+08
Cb = Cb * 1E-12
IF Cb = 0 THEN Cb = 9.809089E-45
LOCATE 13, 42
PRINT CSNG(Cb * 1E+12);
END SUB
```

```
SUB F9 (Rcap)
LOCATE 14, 42
PRINT "      "
```

```

DO
LOCATE 23, 10
INPUT "Load B Resistance Rcap (ohms) : ", Rcap
LOCATE 23, 9
PRINT "
LOOP UNTIL Rcap >= 0 AND Rcap <= 1D+200
LOCATE 14, 42
PRINT Rcap;
END SUB

```

SUB getdata (metal\$, diameter, length, height, Ra, Ca, Rb, Cb, Rcap, Lb, Pd, npts%, freq, freq1, freq2, k%, rhorel, murel)

```

DO
a$ = INKEY$
IF LEN(a$) = 2 THEN
Code = ASC(MID$(a$, 2, 1))
ELSE
IF a$ <> "" THEN SOUND 2000, .4
Code = 0
END IF
SELECT CASE Code
CASE 59
CALL F1(length)
CASE 60
CALL F2(height)
CASE 61
CALL F3(diameter)
CASE 62
CALL F4(metal$, rhorel, murel)
CASE 63
CALL F5(Ra)
CASE 64
CALL F6(Ca)
CASE 65
CALL F7(Rb)
CASE 66
CALL F8(Cb)
CASE 67
CALL F9(Rcap)
CASE 68
CALL F10(Lb)
CASE 104
CALL AF1(Pd)
CASE 105
CALL AF2(k%, npts%, freq, freq1, freq2)
CASE 106
CALL AF3(npts%, freq, freq1, freq2)
CASE 107
CALL AF4(npts%, freq, freq1, freq2)
CASE 0, 113
'Do nothing (Calculate option)
CASE ELSE
SOUND 2000, .4
END SELECT
LOOP UNTIL Code = 113
END SUB

```

SUB init (metal\$, diameter, length, height, Ra, Ca, Rb, Cb, Rcap, Lb, Pd, npts%, freq, freq1, freq2, k%, rhorel, murel)

```

length = 2#
height = .441#
diameter = .001319#

```



```

LOCATE 15, 42
PRINT CSNG(Lb * 1E+09);
LOCATE 17, 42
PRINT Pd;
LOCATE 19, 42
PRINT npts%;
IF npts% = 1 THEN
  LOCATE 20, 42
  PRINT USING "###.#####"; freq / 1E+09;
ELSE
  LOCATE 20, 42
  PRINT USING "###.#####"; freq1 / 1E+09;
  LOCATE 21, 42
  PRINT USING "###.#####"; freq2 / 1E+09;
END IF
END SUB

```

```

SUB prmt (length, height, diameter, metal$, Ra, Ca, Rb, Cb, Rcap, Lb, Pd, Zo, x(), y(), npts%)
PRINT
CLS
LOCATE 10, 1
PRINT "          +-----+"
PRINT "          | Output to printer as well as screen [Y/N] ? |"
PRINT "          +-----+"
INPUT "          ", Printquery$
CLS
PRINT "Cable length (m)      :"; length
PRINT "Height above ground plane (m) :"; height
PRINT "Wire diameter (m)       :"; diameter
PRINT "Metal type              :"; metal$
PRINT "Load A : R (Ohm), C (pF)   :"; Ra, ", ", "; INT(Ca * 1E+15 + .5) / 1000!
PRINT "Load B : R (Ohm), C (pF)   :"; Rb, ", ", "; INT(Cb * 1E+15 + .5) / 1000!
PRINT "Load B : Rcap (Ohm), L (nH) :"; Rcap, ", ", "; INT(Lb * 1E+12 + .5) / 1000!
PRINT "Power density (W/m^2)     :"; Pd
PRINT "Characteristic Impedance (Zo) :"; Zo
PRINT
PRINT "  FREQ (GHz)      LOAD VOLTAGE (dBuV)"
PRINT "  =====      ====="
IF UCASE$(Printquery$) = "Y" THEN
  LPRINT "Cable length (m)      :"; length
  LPRINT "Height above ground plane (m) :"; height
  LPRINT "Wire diameter (m)       :"; diameter
  LPRINT "Metal type              :"; metal$
  LPRINT "Load A : R (Ohm), C (pF)   :"; Ra, ", ", "; INT(Ca * 1E+15 + .5) / 1000!
  LPRINT "Load B : R (Ohm), C (pF)   :"; Rb, ", ", "; INT(Cb * 1E+15 + .5) / 1000!
  LPRINT "Load B : Rcap (Ohm), L (nH) :"; Rcap, ", ", "; INT(Lb * 1E+12 + .5) / 1000!
  LPRINT "Power density (W/m^2)     :"; Pd
  LPRINT "Characteristic Impedance (Zo) :"; Zo
  LPRINT
  LPRINT "  FREQ (GHz)      LOAD VOLTAGE (dBuV)"
  LPRINT "  =====      ====="
END IF
FOR a% = 1 TO npts%
  PRINT USING "#####.#####    ###.#####"; x(a%) / 1E+09; y(a%)
  IF UCASE$(Printquery$) = "Y" THEN LPRINT USING "#####.#####    ###.#####"; x(a%) /
1E+09; y(a%)
NEXT a%
IF UCASE$(Printquery$) = "Y" THEN LPRINT CHR$(12);
PRINT
END SUB

```

```

SUB sinh (sinhREAL, sinhIMAG, alpha, beta, length)

```

```

sinhREAL = .5 * COS(beta * length) * (EXP(alpha * length) - 1 / EXP(alpha * length))
sinhIMAG = .5 * SIN(beta * length) * (EXP(alpha * length) + 1 / EXP(alpha * length))
END SUB

```

```

SUB storedata (npts%, x(), y())

```

```

ON ERROR GOTO diskerr

```

```

PRINT

```

```

DO

```

```

PRINT "          +-----+"

```

```

PRINT "          ! Do you want to store data [Y/N] ? !"

```

```

PRINT "          +-----+"

```

```

INPUT "          ", Storequery$

```

```

LOOP UNTIL UCASE$(Storequery$) = "Y" OR UCASE$(Storequery$) = "N"

```

```

IF UCASE$(Storequery$) = "Y" THEN

```

```

DO

```

```

PRINT

```

```

PRINT "Enter Drive, Path and File name for storage (e.g. B:\data\test1.dat)"

```

```

INPUT "====>", filename$

```

```

diskerr = 0

```

```

OPEN filename$ FOR INPUT AS #1

```

```

IF diskerr = 53 THEN

```

```

    storeok = 1

```

```

ELSE

```

```

    IF diskerr = 0 THEN

```

```

        CLOSE #1

```

```

        DO

```

```

            PRINT

```

```

            PRINT "          +-----+"

```

```

            PRINT "          ! File Already Exists : Overwrite File [Y/N] ? !"

```

```

            PRINT "          +-----+"

```

```

            INPUT "          ", Storequery$

```

```

        LOOP UNTIL UCASE$(Storequery$) = "Y" OR UCASE$(Storequery$) = "N"

```

```

        IF UCASE$(Storequery$) = "Y" THEN

```

```

            storeok = 1

```

```

        ELSE

```

```

            storeok = 0

```

```

        END IF

```

```

    ELSE

```

```

        PRINT

```

```

        SELECT CASE diskerr

```

```

            CASE IS = 71

```

```

                PRINT "Drive "; diskerr$; " Not Ready"; " - Please Rectify"

```

```

            CASE IS = 76

```

```

                PRINT "Path Not Found - Please Select a Valid PATH"

```

```

            CASE ELSE

```

```

                PRINT "Error"; diskerr; "On Device "; diskerr$; " - Please Rectify"

```

```

        END SELECT

```

```

    END IF

```

```

END IF

```

```

LOOP UNTIL storeok = 1

```

```

DO

```

```

CLS

```

```

diskerr = 0

```

```

OPEN filename$ FOR OUTPUT AS #1

```

```

IF NOT diskerr THEN

```

```

    LOCATE 10, 10

```

```

    PRINT "Storing Data..."

```

```

    LOCATE 12, 10

```

```

    PRINT "          +-----+"

```

```

    oldp = 0

```

```

    FOR a% = 1 TO npts%

```

```

        IF NOT diskerr THEN

```

```

frequency = x(a%) / 1E+09
PRINT #1, CSNG(frequency); " "; CSNG(y(a%))
IF diskerr THEN a% = npts%
p = INT((a% / npts%) * 60 + .5)
IF p > oldp THEN
  LOCATE 12, 10
  PRINT MID$("_____", 1, p)
  oldp = p
END IF
END IF
NEXT a%
IF diskerr THEN
  IF diskerr = 61 THEN
    PRINT
    PRINT "Disk Full - Complete Data NOT STORED !"
  ELSE
    PRINT
    PRINT "Disk Error"; diskerr; "Data Not Stored"
  END IF
  INPUT "Please Rectify and press Return to Retry", dum$
END IF
ELSE
  SELECT CASE diskerr
  CASE IS = 70
    PRINT
    PRINT "Disk Write Protected : ";
  CASE IS = 71
    PRINT
    PRINT "Drive Not Ready : ";
  CASE ELSE
    PRINT
    PRINT "Error"; diskerr; "On Device "; diskerr$
  END SELECT
  INPUT "Please Rectify and Press Return to Continue", dum$
END IF
CLOSE #1
LOOP UNTIL diskerr = 0
END IF
END SUB

```

## **APPENDIX H: IMPROVED ANALYSIS OF AIRFRAME MICROWAVE ATTENUATION MEASUREMENT DATA: I.E.E. *Electronics Letters*, Vol.32, No.18, 29 August 1996.**

M. Pywell, I.P. MacDiarmid and R.J. Simpson

*Indexing terms:* Microwave attenuation, Aircraft, Shielding, EMC

Published data on 2-17 GHz airframe attenuation is augmented by measurement data from a total of six military aircraft, including helicopters. Analysis of the results provides a method of assessing 1-18 GHz airframe attenuation and opens up the possibility of aircraft microwave EMC clearance with minimal testing.

**Introduction:** The first line of defence against airborne electronics upset by the RF environment is the shielding afforded to the avionic circuitry by the airframe. At microwave frequencies of interest (>0.3-40 GHz), where apertures are the dominant method of energy ingress, aircraft construction techniques are important. Variations in both the build standard of individual aircraft and the angle of incidence of RF radiation impinging on the airframe can lead to significant variation in the internal fields to which avionic equipments are subjected.

With current limitations in energy ingress prediction methods at these frequencies, civil and military aircraft manufacturers are obliged to conduct costly and time consuming EMC tests on aircraft to ensure correct system operation with an adequate margin of safety. This letter briefly addresses the prediction issue, presents the results of analyses of measured airframe attenuation data from six fixed/rotary wing aircraft, and proposes a new method of assessing airframe attenuation which could minimise aircraft testing.

**Energy Ingress Prediction:** There is a lack of suitable analysis tools for the comprehensive modelling of energy ingress into whole airframes at frequencies >100 MHz. Derivation of values of airframe attenuation based upon practical measurements is thus likely to offer the best and most cost-effective solution to this problem at present. Military aircraft designers in the past have used arbitrary, frequency independent attenuations of between 6-20 dB as estimates for airframe attenuation since the early 1970's. Measurements taken across the band 1-18 GHz on a number of aircraft since the late 1980's have shown attenuation values to vary between aircraft types and between specimens of a given type, and to range between 59 dB and -3.2 dB (*i.e.* a field strength 'gain', resulting from standing waves within avionic bays).

**Practical Measurements:** A 1987-90 BAe research programme examined airframe attenuation on the metal-bodied Jaguar Fly-By-Wire demonstrator aircraft and provided a considerable measurement data set to support the study of microwave energy ingress and propagation in airframes. Absolute airframe attenuation values were determined, wavefront polarisation and angle of arrival dependency was observed, and it was established that energy ingress occurred predominantly *via* avionic bay door peripheral slots, rather than by some other, internal, energy transportation route. [1] describes the research results and measurement techniques used. The value of airframe attenuation,  $A_A$  at each frequency was calculated as follows:

$$A_A \text{ (dB)} = Pr_{\text{EXTERNAL}} \text{ (dBm)} - Pr_{\text{INTERNAL}} \text{ (dBm)} \quad \dots(1)$$

where  $Pr_{\text{EXTERNAL}}$  = power measured at the measurement location with no aircraft present, *i.e.* at open air test site calibration, and  $Pr_{\text{INTERNAL}}$  = power inside aircraft bay with door or panel closed. In each test case the power measured was normalised to remove the variation in transmitter amplifier output with frequency. Transmitter feeder and receiving antenna cable losses were also accounted for, as were the gain vs. frequency characteristics of the transmit and receive antennas used.

Other aircraft measurements, using similar techniques, were conducted by Willis on a prototype helicopter and two (unspecified, but certainly military) aircraft in 1986 [2], Carter, Stevens and Watkins on a Puma helicopter in 1991 [3], and at BAe on a modern military aircraft in 1992. All available data from the above aircraft investigations (either actual data files or reconstituted data *via* digitising  $A_A$  vs. frequency graphs) were analysed to produce a coherent data set per aircraft type and measurement location. The frequency steps used were: 500 MHz (one bay) and 100 MHz (three bays), with a short investigation using 20 MHz steps for the trials in [1]; 500 MHz for those in [2]; and 50 MHz for those in [3] and for the modern aircraft trial. Although these were the principal test resolutions, for those >50 MHz it is acknowledged that some individual tests were done with higher resolution.

**New Approach to Data Analysis:** For the discussions which follow on  $A_A$  trends by aircraft and bay type, and subsequent comparisons between them, it was necessary to arrive at some common attribute. A 'Figure of Merit' approach, as derived in Pywell and Price [1], cannot be used directly to quantify  $A_A$  or compare values of  $A_A$  between different bays and test configurations. To arrive at this common attribute, all the data sets for each bay were arranged as a function of frequency and the mean value determined at each frequency. For each aircraft the the mathematical average of the per-bay values was determined at each specific frequency. This was the attribute used and is referred to as the 'average'  $A_A$  value. To see whether any trends in  $A_A$  exist, either between the fixed wing aircraft investigated or between the fixed and rotary wing aircraft, the data sets from these trials were examined. Table 1 summarises the  $A_A$  data sets independent of frequency and measurement location within the aircraft, and gives the results of initial statistical treatment of each trial's data sets.

**Table 1: Summary of Trials and Initial Statistics**

AIRCRAFT TYPE	QTY. BAYS	DATA VALUES	AVG (dB)	MAX (dB)
DEVELOPMENT HELICOPTER	5	507	22.8	54
AIRCRAFT TYPE A	2	90	28.5	39
AIRCRAFT TYPE B	2	91	24.5	35
FLY-BY-WIRE JAGUAR	4	3800	18.6	59
PUMA HELICOPTER	2	306	10.3	26.9
MODERN FIGHTER	5	651	22	43.4

The table shows a wide range of  $A_A$  values for the different fixed wing aircraft types and helicopters investigated: maxima (32.1 dB), minima (17.2 dB) and average (18.2 dB). From the data examined there appeared little correlation between the data sets but it was observed that the bulk of many of the data sets lay within  $\pm 3$  dB of the set's median, particularly where measurements were taken with  $< 100$  MHz resolution. A further observation was that the median of the average values of  $A_A$  was 21.0 dB with a  $1\sigma$  of 5.9 dB. Together these observations suggested the possibility of a *generic* trend of airframe attenuation and to examine this possibility the data sets were subjected to further statistical treatment. The technique used was to determine the cumulative distribution of each data set, *i.e.* the percentage of each data set *vs.* increasing  $A_A$ . Fig. 1 shows the resultant distributions by aircraft type examined.

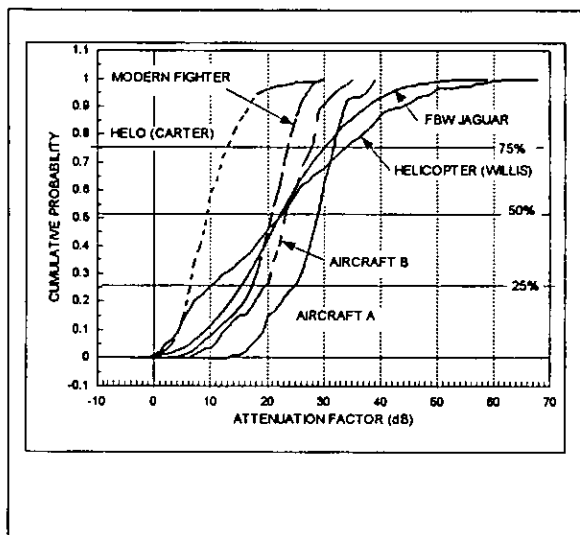


Fig. 1 Comparison Of Airframe Attenuation Statistics

These distributions are more useful than the rapidly changing  $A_A$  values with frequency in determining the contribution of  $A_A$  to the potential for avionic circuit upset. Slight variations in frequency, aspect angle, transmit polarisation and internal measurement location can each change the attenuations measured, whereas this statistical representation tends to show less variation with those individual parameters. The comparison of the EMC demonstrator and other data sets, each with a significantly lower number of data samples, suggests that the distributions would be closer to that of the EMC demonstrator if a matching number of samples were available from the other trials. With the exception of the Carter *et al.* helicopter line, where only one data set has been analysed and thus is thought to be of lower importance, Fig. 1 suggests that a probability of  $> 50\%$  exists of achieving an  $A_A$  of  $> 21$  dB and that this may also be independent of air vehicle type. Using airworthiness reliability figures and safety factors, higher values of probability may be required for a flight clearance basis.

These are important findings as, if true, it offers the potential for supporting the microwave EMC design and clearance of military and civil aircraft with minimal or no tests on aircraft. Appropriate confidence in safe and correct system operation could then be gained through equipment EMC qualification laboratory tests and consideration of the

contents of a database of equipment EMC results for a given aircraft.

Further research is required to explore this potential, which offers substantial time and cost savings to both the civil and military sectors of the aircraft industry. Initially all available measured data, including that from other sources, should be analysed by frequency sub-band to examine the validity of the  $A_A$  prediction, both by aircraft type and between individual aircraft of a given type. If the prediction is still deemed valid, further confidence should be attained by augmenting the existing data by selected measurements on other military aircraft types on which data does not yet exist.

**Conclusions:** The concept of statistical analysis of airframe attenuation, based on tests on multiple aircraft/bay types and numbers, has merit and is likely to offer the best and most cost-effective solution until maturation of rigorous computational EM modelling tools and techniques.

The research has shown that a significant spread of 1-18 GHz attenuation factors (-3.2 to 59 dB) can occur, although a possible vehicle-independent correlation has been demonstrated between the cumulative probability functions for the aircraft types examined. This represents a step improvement in the ability to estimate microwave airframe attenuation for a given aircraft type and offers the potential for supporting EMC design and qualification without the need for aircraft tests. Further study is recommended, commencing with a wider statistical survey of such data from other aircraft types.

**Acknowledgements:** The authors thank British Aerospace for permission to publish and Dr. A.G. Llewellyn (*EMC Controller, BAe*) for comment and assistance with aircraft trials data kindly provided by Dr. N.J. Carter (*Head of Electromagnetics, Defence and Evaluation Research Agency - Farnborough*).

M. Pywell and I.P. MacDiarmid (*BAe Defence, Military Aircraft Division, Warton Aerodrome, Warton, Lancashire, PR4 1AX*).

Prof. R.J. Simpson (*Univ. of Central Lancashire, Dept. of Electrical & Electronic Engineering, Preston, PR1 2HE*).

#### References:

- 1 Pywell, M. and Price, M.J.S. 'Airframe Attenuation Measurements at Microwave Frequencies.' 7th Int. Conf. on EMC, Univ. of York, U.K., August 1990.
- 2 Willis, P.E. Microwave Attenuation/Induced voltage at microwave/ TWT power for TM510. ERA Report 4000/5/04/1, March 1987.
- 3 Carter, N.J., Stevens, E.G. and Watkins, P. Initial Study for Airframe Attenuation Measurement Techniques from 1-18 GHz. Task 78404B. REC/02/91/R/17 (draft 1.070) 16 February 1991.